2011

A Methodology Towards Comprehensive Evaluation of Shape Memory Alloy Actuators for Prosthetic Finger Design

Kevin O'Toole
Technological University Dublin

A METHODOLOGY TOWARDS COMPREHENSIVE EVALUATION OF SHAPE MEMORY ALLOY ACTUATORS FOR PROSTHETIC FINGER DESIGN

Kevin O'Toole B.E.

Doctor of Philosophy (PhD)

Dublin Institute of Technology

Supervisors: Mr. Mark McGrath & Professor Eugene Coyle

School of Manufacturing & Design Engineering

2011

Dedicated to my late grandad, Thomas O'Keeffe, who first stirred my enduring captivation with science, engineering and mathematics.

"Learn from yesterday, live for today, hope for tomorrow.

The important thing is not to stop questioning"

~ Albert Einstein

ABSTRACT

Presently, DC motors are the actuator of choice within intelligent upper limb prostheses. However, the weight and dimensions associated with suitable DC motors are not always compatible with the geometric restrictions of a prosthetic hand; reducing available degrees of freedom and ultimately rendering the prosthesis uncomfortable for the end-user. As a result, the search is on-going to find a more appropriate actuation solution that is lightweight, noiseless, strong and cheap. Shape memory alloy (SMA) actuators offer the potential to meet these requirements. To date, no viable upper limb prosthesis using SMA actuators has been developed. The primary reasons lie in low force generation as a result of unsuitable actuator designs, and significant difficulties in control owing to the highly nonlinear response of SMAs when subjected to joule heating. This work presents a novel and comprehensive methodology to facilitate evaluation of SMA bundle actuators for prosthetic finger design. SMA bundle actuators feature multiple SMA wires in parallel. This allows for increased force generation without compromising on dynamic performance. The SMA bundle actuator is tasked with reproducing the typical forces and contractions associated with the human finger in a prosthetic finger design, whilst maintaining a high degree of energy efficiency. A novel approach to SMA control is employed, whereby an adaptive controller is developed and tuned using the underlying thermo-mechanical principles of operation of SMA wires. A mathematical simulation of the kinematics and dynamics of motion provides a platform for designing, optimizing and evaluating suitable SMA bundle actuators offline. This significantly reduces the time and cost involved in implementing an appropriate actuation solution. Experimental results show

that the performance of SMA bundle actuators is favourable for prosthesis applications. Phalangeal tip forces are shown to improve significantly through bundling of SMA wire actuators, while dynamic performance is maintained owing to the design and implementation of the selected control strategy. The work is intended to serve as a roadmap for fellow researchers seeking to design, implement and control SMA bundle actuators in a prosthesis design. Furthermore, the methodology can also be adopted to serve as a guide in the evaluation of other non-conventional actuation technologies in alternative applications.

ACKNOWLEDGEMENTS

Firstly, I would like to express my gratitude to my supervisors, Mr. Mark McGrath and Prof. Eugene Coyle for their expert guidance, continued interest, unparalleled assistance and patience throughout the course of this work. I am immensely indebted to both of them. This work could not have been completed without their valuable input and insights.

I am also grateful to the love and support shown by my parents throughout my time as both an undergraduate and postgraduate student. Their advice and interest in my work has led me to where I am today. I owe both a huge debt of gratitude.

I would also especially like to thank Dr. Marek Rebow, Head of Engineering Research at DIT, who has provided much support, enthusiasm and energy through his dedication to, and genuine interest in, all post-graduate students of the DIT engineering faculty.

I am indebted to the Head of the School of Manufacturing and Design Engineering at DIT, Mr. John Lawlor, and the previous Head of the Department of Manufacturing Engineering, Mr. Robert Simpson. Their willingness to assist and support the work by making available all the resources of DIT was tremendously helpful throughout the project.

Thanks to Mr. Derek McEvoy for his invaluable advice and experience during the design and build stages of my experimental systems and Mr. Frank Duignan for his expertise in electronic circuit design. Both have helped me overcome significant obstacles in the course of the work. I am also grateful to Professor

Annraoi de Paor, Professor Emeritus of Electrical Engineering at University College Dublin who provided me with invaluable advice during my transfer examination in 2008. Thanks also to the many other members of staff at DIT, too many to name here, but who have helped out in no small part during the course of the project.

Thanks also to all my fellow post graduate students in DIT. It is a privilege to work alongside such capable and helpful people. Thanks also to my extended family and friends for their on-going support, understanding and interest in my work.

Finally, I reserve my deepest gratitude for my partner, Agnieszka, for her love, support and devotion throughout the course of the work and who has shown incredible levels of tolerance of my late nights in the office, weekends lost to work and general behaviour unbecoming of a partner as a result of constantly elevated stress levels. I count myself lucky to have such a wonderful partner and will be forever grateful.

LIST OF KEY CONTRIBUTIONS

i. A comprehensive, focused methodology for utilization in the evaluation of SMA bundle actuators in prosthesis design.

ii. A nonlinear dynamic model of SMA bundle actuator behaviour comprising of stacked linear system models, based on a detailed characterisation of the mechanical and thermal response.

iii. A robust, adaptive control strategy featuring a feedforward inverse hysteresis model and optimized PID controller in feedback. The strategy is shown to be capable of accurately controlling SMA bundle response to a large range of input stimuli and disturbances.

iv. A novel design of a prosthetic hand and finger framework featuring SMA bundle actuators located in the palmar region of the hand.

v. An offline experimental procedure capable of determining optimum bundle size and carrying out performance verification of SMA bundle actuators for prosthesis design.

vi. A guideline for the utilization and implementation of non-conventional actuation technologies in diverse applications, intended for use as an aid to future researchers.

DECLARATION

I certify that this thesis, which I now submit for examination for the award of Doctor of Philosophy (PhD), is entirely my own work and has not been taken from the work of others, save and to the extent that such work has been cited and acknowledged within the text of my work.

This thesis was prepared according to the regulations for postgraduate study by research of the Dublin Institute of Technology and has not been submitted in whole or in part for another award in any institute.

The work reported on in this thesis conforms to the principles and requirements of the Institute's guidelines for ethics in research.

The Institute has permission to keep, lend or copy this thesis in whole or in part, on condition that any such use of the material of the thesis be duly acknowledged.

Signature _____ Date_____

Candidate

LIST OF ABBREVIATIONS AND SYMBOLS

Symbols

A_f	Austenite Finish Temperature (^oC)
A_s	Austenite Start Temperature (^oC)
circs	Circumference Segment (m)
C	Matrix of Christoffel Symbols
C_p	Specific Heat Capacity (J/kg.K)
c_s	Chord Segment (m)
D	Inertia Matrix
d	Diameter (m)
d_{t_c}	Cooling Time Delay (s)
d_{t_h}	Heating Time Delay (s)
$e(t)$	Error
E	Youngs Modulus of Elasticity (N/m^2)
E_a	Youngs Modulus of Elasticity – Austenite (N/m^2)
E_m	Youngs Modulus of Elasticity - Martensite (N/m^2)
F	Force (N)
g	Gravitational Acceleration (m/s^2)

h	Convection Coefficient (W/m^2.K)
H	Latent Heat of Transformation (J/kg.K)
i	Current (mA)
J	Jacobian Matrix
k	Stiffness (N/m)
k_c	Conductivity Coefficient (W/m.K)
K_d	Derivative Gain
K_i	Integral Gain
K_p	Proportional Gain
K_v	Variable Gain
l	Length (m)
L_c	Characteristic Length (m)
m	Mass (kg)
M_f	Martensite Finish Temperature (^{o}C)
m_k	Minimum Point of Input History
M_k	Maximum Point of Input History
m_n	Minimum Point of Input History - Final Link
M_n	Maximum Point of Input History - Final Link

M_s	Martensite Start Temperature (^oC)
Nu	Nusselt Number
P	Power (W)
Pr	Prandtl Number
$\dot{Q}$	Heat Transfer Rate (W)
Q_k	Discrete Trapezoid on Preisach Plane
R	Resistance (Ω)
r	Radius (m)
Ra	Rayleigh Number
S_s	System Sensitivity
t	Time (s)
T	Temperature (^oC or K)
T_m	Time Delay (s)
T_∞	Ambient Temperature (^oC or K)
u	System Input
V	Voltage (V)
W	Mechanical Work (Nm)
x	Displacement (m)

y	System Output
y_d	Desired Output
y_e	Modified Desired Output
y_h	Output due to System History

Greek

α	'Up' Switching System Input
β	'Down' Switching System Input
β_v	Volume Expansivity
ε	Strain
ξ_M	Martensitic Ratio
ξ_A	Austenitic Ratio
θ, q	Angular Displacement (deg)
τ	Torque (Nm)
τ_c	Time Constant (s)
υ	Kinematic Viscosity (m^2/s)
σ	Stress (N/m^2)
μ	Coefficient of Friction

Abbreviations

DEC	Decreasing
DIP	Distal Interphalangeal
E-S	Electro Strictive
FDP	Flexor Digitorum Profundus
FDS	Flexor Digitorum Superficialis
I-EAP	Ionic Electro Active Polymer
INC	Increasing
ITAE	Integral of Time-Weighted Absolute Error
MP	Metacarpo Interphalangeal
RMSE	Root Mean Square Error
PID	Proportional Integral Derivative
PIP	Proximal Interphalangeal
PTFE	Poly-Tetra-Flouro-Ethylene
SMA	Shape Memory Alloy
SMP	Shape Memory Polymer
SSE	Steady State Error
ua	Underactuation

TABLE OF CONTENTS

TABLE OF FIGURES

TABLE OF TABLES

1. INTRODUCTION

In their quest to find a cure for each ailment that affects mankind, humans have proved remarkably adept at developing sophisticated solutions that fit the task. Remarkably, prosthetic devices have existed for thousands of years, having first been documented in the literature in 1500 B.C. [1]. The first scientific approach to prosthesis development was pioneered in the 16th century by French surgeon, Ambrois Pare [2].

In the past, prosthetics were considered simply as replacements for missing limbs. However, thanks to recent technological progress, prosthetic solutions have become significantly more advanced than their ancient equivalents. These new intelligent prosthetic solutions replicate technology straight out of science fiction, featuring moving joints, 'thought based' controllability using bio-signals captured from remaining muscle tissue, and offering new hope for amputees in achieving full and active lives. However, despite the progress made, there still exists opportunities for improvement even with the most sophisticated solutions on the market to date.

The work described in the opening chapter of this report focuses on the key motivations and significance of the work. A brief review of the state of the art in intelligent prosthesis designs (those which can perceive and interact with their environment) and more specifically, prosthesis design using SMA actuation technology, allows for the identification of the primary aims and objectives of the work. Furthermore, a novel design methodology is presented which can

serve as a guide for researchers through each important step in the SMA actuated prosthesis design process.

1.1 Motivation and Significance of the Work

Amputation of an upper limb engenders many physical and psychological challenges including alterations to life-style and body image, changes in self-concept and impairments in physical functioning [3-5]. In the USA, reports indicate the total number of amputees is 350,000, with 35% experiencing upper limb amputation [6]. The Disability Federation of Ireland estimates that there are approximately 6000 people living with amputations in Ireland, however, in depth records are not maintained [7].

In spite of the technological progress achieved to date in the field of upper limb intelligent prosthetic solutions, various psychological and operational issues concerning their use have been reported. Studies have shown that the level of dissatisfaction with current prostheses is as high as 71.43% in terms of their functionality [3]. Patients have reported difficulties concerning the excessive weight of the devices, their unnatural response during prehensile activity, difficulties in controlling the devices and audible associated operational noise of approximately 50dB [8, 9].

A summary of commercial intelligent prosthetic solutions available on the market has shown that all are actuated via DC motors [9]. The problems associated with DC motors such as noise production, excessive size compared to non-conventional actuation technologies such as shape memory alloys (which limits possible degrees of freedom) and susceptibility to mechanical wear can

be linked to some of the noted problems experienced by the end-users. As such, there is an urgent need to investigate the possibility of integrating alternative actuators into functional prosthesis design which can deliver performance mimicking human capabilities and tendon-like actuation. Shape memory alloys (SMAs), owing to their unique properties, have attracted interest from researchers as potential candidates to fulfill the actuation requirements of the next generation of upper limb prosthetic solutions. Furthermore, the linear actuation of SMAs is similar to that of human muscle, thus outlining their appropriateness for the task.

1.2 Intelligent Upper Limb Prostheses – A Brief History

The current generation of intelligent upper limb prosthetic devices owe their development to research stretching back over forty years. Initially, the work focused specifically on the design of independent robotic hands. Examples such as the *Stanford/JPL* Hand [10], the *NTU* Hand [11], the *Utah/MIT* Hand [12], the *DLR I & II* Hands [13, 14] and the NASA designed *Robonaut* Hand [15], all actuated via DC motors, bear witness to this fact. The combination of sufficient miniaturisation and the implementation of human machine interfaces which facilitate direct control resulted in groups modifying their robotic hand concepts for use as wearable prosthetic solutions. This was accomplished by those developing the *Belgrade/USC* Hand [16] and the *Southampton-Remedi* Hand [17].

Noting the associated difficulties in using miniature DC motors as viable actuators for prosthesis design, other groups have experimented with pneumatic solutions, such as the *Shadow* Hand [18], the *Blackfingers* Hand [19]

and *RAPHaEL* [20] (Robotic Air Powered Hand with Elastic Ligaments). However, although *Blackfingers* and *RAPHaEL* were designed solely for prosthetic purposes, their drawback is their reliance on a compressed air supply. This effectively rules them out as viable alternatives to DC motor-actuated solutions.

Intelligent prosthetic solutions have been on the market since 2005, with the release of the Touch Bionics *iLimb* [21], the first commercially available prosthetic solution. The *iLimb* features miniature brushless DC motor actuation technology. In 2006, a rival to the *iLimb*, the Otto Bock *Michelangelo* hand was made commercially available. This myoelectrically-controlled prosthesis uses a single brushless DC motor and rigid fingers to produce grips with a separate linkage to the thumb to allow both tip and lateral opposition [22]. More recently, the *Fluidhand* [23], a hydraulically actuated solution, was released in 2008. Results have proved promising but clinical trials have yet to be completed. Work in SmartHand has recently gotten underway [24]. This is an on-going international collaboration lead by *Dr. Fredrik Sebelius* at Lund University with a goal of developing an intelligent artificial hand that looks and feels like a real hand.

To date, no prosthetic solution featuring SMA actuators has been released commercially. However, a significant body of work has been completed in this field with various prototypes being put forward for examination. A summary of these achievements is given in Section 1.3.

1.2.1 DC Motor Actuators – Disadvantages

DC motors are relatively heavy and bulky, resulting in prosthetic solutions exhibiting less degrees-of-freedom. Underactuated mechanisms can be implemented to overcome these disadvantages [25, 26]. However, the mechanical complexity can result in maintenance and repair issues in addition to a reduction in true degrees-of-freedom. DC motors commonly require complex transmission systems to operate [27]. These can be difficult to manufacture, difficult to assemble and difficult to maintain resulting in greater cost and development/production time per device manufactured. Furthermore, DC motors naturally produce undesirable levels of noise of up to 50dB whilst operating. Although this noise level is low, it remains audible to the human ear. True biomimetic actuators mimicking muscle movements should exhibit a silent drive technology for best results [28].

1.2.2 Pneumatic & Hydraulic Actuators – Disadvantages

Pneumatic actuators offer various advantages over conventional DC motor actuation technologies such as similarity to human muscle, high force production, and mechanical simplicity. However, critical factors in their design render them unsuitable for prosthetic applications such as reliance on a compressed air source, the requirement for bulky valves adding weight to the prosthesis, the compressible nature of gas leading to difficulties in control, large size, and high noise production during actuation [18]. The inherent dependence on compressed air also results in the end-user being required to carry the additional mass of an air cylinder to accompany the prosthesis. The size and

bulk exhibited when pneumatic actuators are arranged in parallel can render them unfeasible for a compact artificial hand design.

Hydraulic actuators result in additional mass due to the hydraulic fluid needed within the valving system. They are prone to suffer from fluid leakage which impacts on safe usage [29]. Furthermore, hydraulic actuators are rigid and inflexible, limiting the degrees-of-freedom of the prosthetic device whilst also exhibiting a low operating frequency [27].

1.3 Shape Memory Alloy Actuators – An Introduction

In the 1930's, *Arne Olander*, a Swedish physicist, discovered pseudoelastic behaviour in a gold-cadmium alloy [30]. He observed how the alloy could be plastically deformed when cool, but return to its original length when heated. Following on from this work, *Greniger and Mooradian*, when working with a copper-zinc alloy, noted the formation and disappearance of the martensitic phase by increasing and decreasing the temperature of the alloy [31]. A full understanding of the shape memory effect was put forward in 1949 by *Kurdjumov and Khandros* [32], and in 1951 by *Chang and Read* [33]. Both groups worked to form an understanding of the thermoelastic behaviour of the martensite phase. During the 1950's, similar effects were discovered in a host of other alloys such as copper-zinc and copper-aluminium-nickel. However, due to high cost, complex manufacturing technologies and undesirable mechanical properties, these materials were not selected for utilization in practical or industrial applications [34].

The discovery of a nickel-titanium alloy exhibiting the shape memory effect was made in the 1960's at the US Naval Ordnance Laboratory by a team led by *William Buehler* [35, 36]. This discovery sparked industrial interest in the alloys exhibiting the shape memory effect mainly due to the superior properties of nickel-titanium over alternate alloys in terms of mechanical behaviour and production costs. The alloy was termed Nitinol, an acronym of nickel (NI) titanium (TI) naval ordnance lab (NOL). In addition, the term 'shape memory effect' was first introduced to describe the shape recovery behaviour of the alloy.

The first commercially available application involved the use of Nitinol material for pipe coupling in F-14 fighter aircraft [37]. Nitinol has been widely used in biomedical applications due to its biocompatibility [38]. Some common areas of use are in medical stents, implants and orthodontics [39, 40]. However, it wasn't until the 1990's that research into the use of Nitinol SMAs as actuators in robotics and prosthetics began to take hold. Actuator applications include linear actuators, microswitches, robotic grippers and micro-electromechanical devices (MEMS) [41].

1.3.1 Advantages of SMAs

SMAs offer a range of advantages over conventional and unconventional actuators. These can be summarised as follows:

- *High Energy Density*. SMAs exhibit a specific actuation energy density of approximately 1000-2000 J/kg, far superior to other non-conventional actuators (Figure 1-1). This characteristic makes SMAs the most

appropriate choice in applications where size and weight are to be kept to a minimum [42].

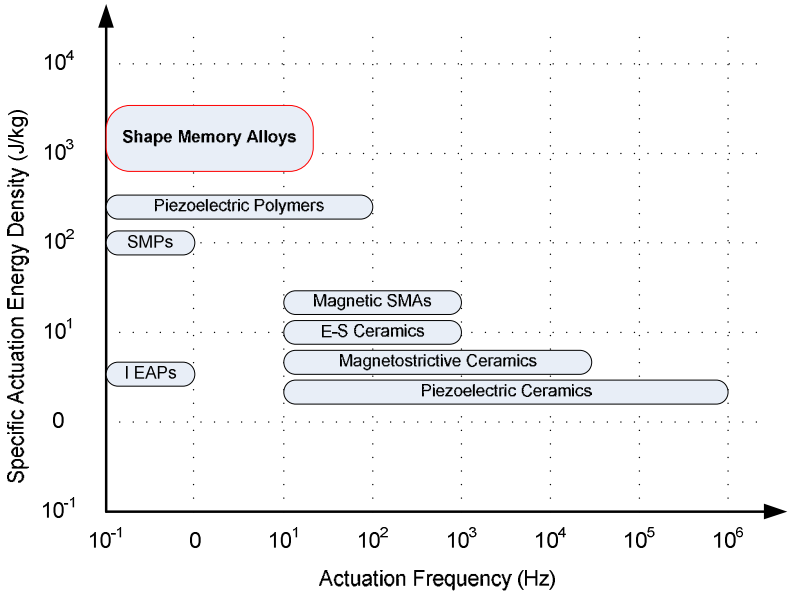

Figure 1-1. Energy densities of non-conventional actuation technologies

- *Quiet Operation*. Unlike conventional DC motor actuators which require moving parts to operate, SMA actuators actuate via a phase change which results in a reduction in overall length. The phase change is noise free, thus allowing for silent operation. This characteristic is important in biomedical and microelectronic applications.

- *Mechanically Simple*. SMAs undergo phase change, and hence dimensional changes under thermal excitation. The most common method of producing a suitable temperature rise is via joule heating. This simple approach requires no complex gearing mechanisms which is beneficial in terms of reduced production, maintenance and material costs.

- *Miniature Size & Low Cost*. SMAs are available in wire, tube, spring or sheet form, the most common of these being wire form. Typical diameters for SMA wires are found in the micron range, similar to the diameter of a human hair [42]. This compares favourably to relatively large conventional actuators such as DC motors which are considerably larger and bulkier. Their miniature size allows for SMA wires to be placed in areas unsuited to conventional DC actuation systems. Multiple SMAs can be deployed in parallel to increase actuation force where necessary. Furthermore, SMA wires are considerably cheaper than any other conventional actuator on the market presently.

1.3.2 Disadvantages of SMAs

While SMAs offer significant advantages in terms of actuation, there are certain disadvantages that must be taken into consideration. These are:

- *Nonlinear Characteristics*. SMAs exhibit significant nonlinear characteristics, specifically showing large hysteresis during the heating-cooling cycle and the loading-unloading cycle. These hysteretic effects can result in difficulties in terms of actuator modelling and control. A large percentage of current research is focused on overcoming these issues [34].

- *Low Efficiency*. It has been reported that the maximum theoretical efficiency of SMAs is on the order of 10% [43]. In reality it is often less than 1% [41].

- *Slow Speed of Response*. SMAs are thermally responsive actuators and as such they are limited by heating and cooling restrictions. Thus, their actuation periods are relatively slow in comparison with conventional actuators and some non-conventional actuators (Figure 1-1). Attempts to increase the response rate can lead to overheating and actuator damage.

- *Fatigue Effects*. Temperature, stress and strain all play important roles in the determination of the long term performance of SMAs. The actuator must be operated within its recommended limits in order to preserve its reliability over millions of cycles [44].

Based on the noted advantages of SMA actuators outlined in Section 1.3.1, an investigation of a range of techniques to overcome the associated disadvantages is warranted.

1.4 Key Advances in SMA Actuated Hand & Finger Solutions

Throughout the last twenty five years, attempts have been made to utilise SMA actuators as the primary actuators in a range of prosthetic hand and finger solutions. SMAs are considered to be a natural actuation solution for many upper limb prosthetic solutions. This is due to the observed similarity between the contraction-based actuation of SMAs and that of human muscle and tendons. This similarity allows for a biomimetic approach to design to be employed.

The first attempt to develop an SMA actuated robotic hand was carried out in 1984 with the release of *Hitachi's Robot Hand* [45]. The Hitachi Hand included a forearm where the SMA wires were mounted, weighed 4.49kg and was 69.85cm long. It demonstrates a 20N gripping force. Each finger features a number of

0.2mm diameter SMA wires that are set around the tube housings of its spring actuators. The design employed was relatively primitive and not adoptable as a prosthetic solution. Following this brief foray into the utilization of SMA actuators in robotic technologies, the focus of researchers returned to the use of conventional actuators such as DC motors and pneumatic actuators for the remainder of the 20th century. SMA actuated hands would not be revisited until the beginning of the 21st century.

In 2002, *DeLaurentis and Mavroidis* of Rutgers University conceptualised an SMA actuated prosthetic hand solution [46, 47]. They favoured a five-fingered, twenty degree of freedom anthropomorphic dexterous hand design actuated by SMAs located in the forearm region. Rapid prototyping techniques were used to manufacture a single finger. The group estimated that a finger tip force of 6.67N could theoretically be achieved using the proposed design. Unfortunately, there are few experimental results available in the literature and no complete solution has been documented to date. By locating the SMAs in the forearm to allow for a larger displacement, the possibility of an independent prosthetic hand becomes unfeasible.

Around the same time period, *Yang and Gu* of the Huazhong University of Science and Technology proposed a three fingered robotic hand actuated by antagonistic SMA wire actuators [48]. The design is not human-like in appearance and thus could not be used as a feasible or aesthetically pleasing prosthetic solution. However, as a robotic hand solution, the group demonstrated some success. The finger design consists of two flexible 8mm rods and features SMA wire actuators of 0.5mm diameter. The contraction and

relaxation of the SMA wires under thermal excitation allows for a simple gripping action. The group applied a linear position control algorithm based on the estimated steady state wire temperature with some success. This resulted in finger motions that were considered flexible and lifelike, acting in a fast and precise manner. However, hysteresis was not explicitly accounted for in the control strategy. The group used the design to demonstrate a grasping action applied to a 30mm diameter sphere with a weight of 3N. The work showed, for the first time experimentally, the possible integrity of the SMA actuators in terms of their speed of action and their ability to produce fine manipulation similar to humans.

Roznowski & Drzewiecki of the Gdansk University of Technology subsequently proposed an approach to SMA actuated prosthetic index finger design in 2004 [49]. The anthropomorphic design features four degrees-of-freedom. The group employed five SMA wires in an antagonistic arrangement directly coupled to specially designed mechanisms which in turn provide finger torque. They reported some success in achieving two different manners of action which depended on the weight and size of the manipulated object, and the proximity of the object to the artificial finger. However, there are few definitive results available within the literature. It can be safely assumed that the use of a single SMA wire actuator severely limited the finger tip forces generated during gripping activity.

In 2005, *Loh, Yokai and Arai* of the University of Tokyo attempted to develop a new shape memory alloy actuator for finger actuation in a prosthetic hand design [50]. This antagonistic arrangement of two 0.3mm diameter SMA wires

was intended to replace the bulky, heavy DC motors that were employed in a prosthetic hand solution developed by the University of Tokyo [51]. The group used a fast acting PWM heating method in an attempt to control the SMA wire temperature and reduce the build-up of excess heat. No experimental results are available in the literature.

Also in 2005, *Bundhoo and Park* of the University of Victoria proposed a biomimetic prosthetic finger design for children [28]. The group produced a four degree-of-freedom finger actuated by SMA actuators which closely mimicked the size and kinematics of a human finger. The group used single SMA wire-driven tendons to produce finger torque, an approach based on natural muscles and tendons. They calculated, based on their proposed mechanical design and kinematic solution, that wires of between 0.5-0.7mm in diameter would be suitable in generating the targeted maximum phalangeal tip force of 2.85N. The group suggested the use of SMA bundle actuators could be a way to increase the force generated whilst maintaining the speed of response. Later in 2009, the group successfully applied PWM-PD control to their biomimetically designed finger with promising results in terms of position and tracking ability. However, phalangeal tip force is observed to be low due to the utilization of single wire SMA actuators in the solution [52].

Maeno and Hino of Keio University in Yokohama proposed a miniature five fingered robot hand driven by forty SMA wire actuators in 2006 [53]. The hand exhibited twenty degrees-of-freedom. The SMA wires chosen were 0.5mm in diameter and mounted antagonistically. The recorded rise time was 0.2 seconds which is comparable to human performance. The device is not intended as a

prosthetic solution, but rather as a manipulator for use in remote operation tasks by humans. Experimental results showed a maximum finger tip force generated of 75mN, which would not be acceptable for full sized prosthetic applications. The miniature robotic hand demonstrated good grasping abilities with particular emphasis on three power grip and three precision grip postures.

A novel approach to SMA actuated robotic hand development was put forward by *Cho, Rosmarin and Asada* of the Massachusetts Institute of Technology in 2007 [54]. The group designed a robotic hand exhibiting thirty-two independent axes controlled using segmented binary control. This novel idea involves the division of the SMA actuators into several segments, controlling each segment with a simple on-off heater. The proposed design is unfeasible for use as a prosthetic solution largely due to the weight and bulk of the segmented binary control (SBC) heating system. The arrangement provides for a demonstration of SBC only. However, the robotic hand produced a notable range of human-like grasps under experimental testing.

Price, Jnifene and Naguib of the University of Toronto investigated the design, instrumentation and control issues surrounding the practical application of SMAs as artificial muscles in a three fingered robot hand [55, 56]. A sample finger developed by the group offered three degrees-of-freedom and had a mass of 91g, suggesting that the total hand mass would be significantly lower than conventional artificial hands. The group identified performance limitations such as slow cooling time. They proposed and evaluated a PWM sigmoid-based control algorithm for position control. This algorithm is intended to minimize

overshoot during heating, thus minimizing effects of the slow response time on cooling.

Most recently, in 2008, *Andrianesis and Tzes* of the University of Patras, Greece, unveiled the mechanical design of a five fingered, SMA actuated, biologically inspired, ultra lightweight hand for prosthetic purposes [57]. The group used 0.2mm diameter SMA wires mounted in the forearm region of the prosthesis. A sliding plate scheme, combined with artificial tendons and relaxation springs completes the mechanical design of the actuation system. The presence of a forearm section rules out use as a stand-alone hand prosthesis. This is considered unavoidable due to nature of the actuation mechanism employed. Locking mechanisms have been designed to fit into the palmar area to hold grip poses when no actuation is provided. These novel components prevent energy loss and heat build up in the actuators. It is estimated that the completed prosthesis will have a mass of less than 250g, which is considerably lower than the human hand and any prosthesis design to date using conventional actuation technology. This, however, can lead to other problems such as user confidence in the device. Presently, there are no experimental results available from the group to describe the grip forces or dynamic response achievable using the prosthetic solution.

1.4.1 Limitations of Current SMA Actuated Designs

A number of key functional limitations in current SMA actuated prosthetic hand and finger designs have been identified based on the review in Section 1.4.

i. *Low finger/phalangeal tip forces*. The force produced at the tip of the prosthetic finger, or any individual phalanx within the finger, is vital to the generation of successful gripping actions. Current SMA actuated finger designs cannot produce adequate force generation to be utilised as a feasible prosthetic solution owing to their reliance on single wire SMA actuators. A maximum of 6.67N is recorded in the literature [46].

ii. *Dependence on a forearm section*. Current SMA actuated prosthesis designs feature SMA wires located in a forearm region. This ensures that the SMA contractile strain is sufficient to allow adequate joint rotation and hence facilitate the production of desired finger postures. However, the dependence on a forearm region renders them of somewhat little use to those suffering from below-the-elbow amputations.

iii. *Sluggish responsiveness*. Designers to date have attempted to utilise large diameter SMA wires to improve phalangeal tip forces. However, responsiveness, particularly during the cooling phase, is reduced as SMA diameter increases owing to the reduced wire surface area to volume ratio. A realistic prosthetic solution should be able to compete with the responsiveness of the human hand to allow ease of adaption for the end-user.

By addressing these limitations, a more universal and useful prosthetic solution catering for a broad range of end-users can be realized.

1.4.2 Opportunities for Enhanced SMA Actuated Prosthesis Design

The overview of the literature available on SMA actuated prosthesis design outlined in Section 1.4 has highlighted a lack of clarity in the approach taken by researchers to address some of the problems associated with implementation. In order to further enhance SMA actuated prosthesis design, it is required to

i. Carry out a more complete analysis of mechanical and thermal behaviour of the SMA wires during actuation. This can lead to new opportunities for enhanced control based on a greater appreciation of the behaviour of the SMA wires.

ii. Determine the most suitable hysteresis compensation method which can be applied to SMA actuators in prosthesis design.

iii. Develop a technique capable of sizing appropriate SMA actuators for the task in terms of the SMA wire diameter, the number of wires required in parallel, the geometry, the length, the volume required by the actuator and the power requirements.

iv. Improve efficiency. Maintaining a high efficiency is crucial in a portable prosthetic device due to the reliance on battery power. It is necessary to establish a technique which can be adopted at the design phase that ensures maximum efficiency is guaranteed.

1.5 Main Aim & Objectives

SMA actuators have been heralded as revolutionary actuators for a broad range of applications including advanced prosthesis design. This is due to their many

favorable properties. However, the associated disadvantages in terms of their responsiveness and controllability have acted as significant barriers to their application in fully functional prosthetic solutions. As a result, SMA actuated prosthetic applications have suffered from design simplicity or require large actuator lengths to produce adequate displacement. Furthermore, it can be seen in Section 1.4 that research to date in the development of SMA actuated prostheses follows no identifiable core methodology. An appropriate methodology must be capable of guiding the researcher through all of the required phases in the production of a suitable solution involving SMA actuators. Research to date can be viewed as relatively sporadic and incomplete, resulting in unfeasible designs featuring SMA actuators that are sluggish in response, or exhibit low finger tip forces. This lack of clarity in a range of key areas (Section 1.4.2) has demonstrated the urgent need for a more comprehensive methodology capable of progressing SMA actuated prosthesis design.

The primary *aim* of this work is therefore **to develop and implement a suitable methodology which facilitates the full design and assessment of SMA bundle actuators in prosthetic finger design**

The integrity of the SMA bundle actuators is measured in terms of their capacity to replicate the functionality of the human muscle & tendon system which produces human finger movement. The SMA bundle actuators are designed for a novel mechanical prosthetic finger design which should be capable of mimicking the movement of the human finger for a range of prehensile activities and postures.

The *objectives* of the work in achieving the aforementioned aim can therefore be summarized as follows:

i. To determine a comprehensive design methodology for the determination of optimized SMA actuation in prosthesis design.

ii. To characterise the geometry, motion and force production of the human index finger phalanges during a series of prehensile activities for comparative use during the work

iii. To develop a precision experimental test bed capable of measuring SMA contraction, relaxation, wire temperature, ambient temperature and input power to a high level of precision.

iv. To characterize the mechanical capacities of various SMA bundle actuator arrangements in terms of force generation and contraction capacity owing to Joule heating and natural convection cooling.

v. To determine the optimum SMA bundle configuration for prosthetic finger actuation.

vi. To investigate the thermal behaviour of the SMA bundle actuators through analysis of transient wire temperature response profiles. Furthermore, an accurate determination of the convection coefficient is required for accurate modelling.

vii. To develop a dynamic model of SMA response to applied current and natural convection cooling based on the mechanical and thermal response data gathered.

viii. To prepare a critical review of current SMA control strategies employed by other researchers in order to identify the architecture of the best controller strategy.

ix. To develop a fast-acting, robust, optimised and accurate adaptive controller solution capable of precise position and tracking control of SMA bundle actuators.

x. To design an appropriate prosthetic finger solution upon which the proposed actuator can be implemented.

xi. To validate an appropriately sized and controlled SMA bundle actuation solution by demonstrating their capacity to replicate the work and movements required at each joint of the human finger during a variety of prehensile activities and postures.

It is envisaged that the results herein will furnish prospective researchers with the necessary tools to design and produce more advanced prosthetic solutions which offer a greater level of functionality, comfort and responsiveness than currently employed actuation technologies permit.

There are many associated secondary benefits of the work. Applications of the findings are directly relevant to a number of other fields. For example, rehabilitation engineering, specifically to post stroke rehabilitation endeavors and novel assistive technologies where SMA bundle actuators have the potential to be the primary actuation solution employed. In addition, the lightweight and simple characteristics of a SMA actuator makes them ideal for applications such as in space technologies owing to the minimal weight criteria of space missions.

Furthermore, the reduced maintenance demands due to the simplicity of the actuator provides a more reliable and longer lasting actuation source.

1.6 Novelty of the Research

There are many novel aspects of the work described within this report. It is evident, based on the review carried out in Section 1.4 that any approach to selecting, implementing and assessing the best SMA actuator solution for the role of primary actuator in prosthesis design, although highly desirable, does not currently exist. Therefore, the major novel contribution of this work is the development and utilization of a systematic evaluation procedure for the application of SMA actuators in prosthesis design (See Section 1.7).

A further major novelty of the work is the development of a dynamic response model describing the behavior of an SMA actuator (See Section 4.7, 5.6 and 5.7). This is arrived at following a detailed characterisation of SMA actuators (See Chapter 4 and 5). The data collected facilitates the development of a control strategy and appropriate tuning methodology for the first time (See Chapter 6). The highly novel control strategy evolves out of a detailed, categorized review of existing control strategies for SMA actuators employed by other groups (See Section 2.9) and the novel dynamic model of SMA response. Validation of the work is carried out using a novel experimental procedure (See Chapter 8)

It is also apparent that the key to addressing the limitations identified in Section 1.4.1 is to focus on improving the SMA actuation technology typically utilised in novel prosthesis designs. A novel approach featuring SMA bundle actuators in

conjunction with the selected control strategy developed is used to overcome these limitations.

The following features of the work can also be considered to be novel (See Chapter 7):

i. The design of a suitable SMA actuator and tendon network arrangement which provides increased phalangeal tip forces, thus allowing for a more functional prosthetic solution.

ii. The location of compact SMA actuators within the palmar area of a prosthetic hand solution, thus facilitating prosthetic solutions that are independent of the lower arm region.

iii. The design and optimization of an SMA actuated prosthetic solution to mimic the response of the human index finger.

1.7 Design Methodology

Previous SMA actuated prosthesis designs have been unsuccessful as a result of failure to account for the many nonlinearities and complexity of SMAs (See Section 1.4 and 1.4.2). It is therefore a necessity to produce a comprehensive methodology that ensures full consideration is given to all important steps within the process.

Puig et al have presented a detailed design methodology aimed at robotic hand development [58] (Figure 1-2). The *Puig* methodology is generic in nature and focuses the design problem by referring to both technological and market requirements. However, it is not possible to apply the *Puig* methodology to a

design problem featuring SMA bundle actuators as it does not specifically outline the actuator evaluation procedure. The outline of a more comprehensive design methodology has been developed based on the work of *Puig* to facilitate the adoption of any type of actuator, to allow for offline testing of the actuator, and to ensure energy efficiency is a focus of the design phase (Figure 1-3).

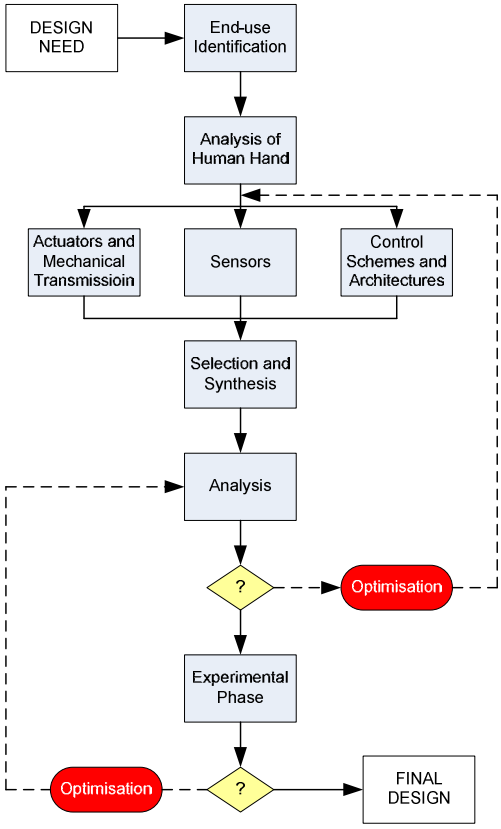

Figure 1-2. Puig Robotic Hand Development Methodology [58]

The *Generic Actuator and System Design* methodology outlined addresses the shortfalls of the *Puig* methodology by placing a focus on the modeling, control strategy development & tuning of the chosen actuator. The work can be divided into two parallel flows, one focusing on the characterisation, modeling and control of the actuator, and the other focusing on the design of the simulated environment for testing the actuator. The strategy allows for offline testing of

the actuation solution within a mechanical structure by incorporating a simulation routine. This is significant as it allows for the completion of the design and modification procedure of the full integrated mechanical system without prior need of manufacture.

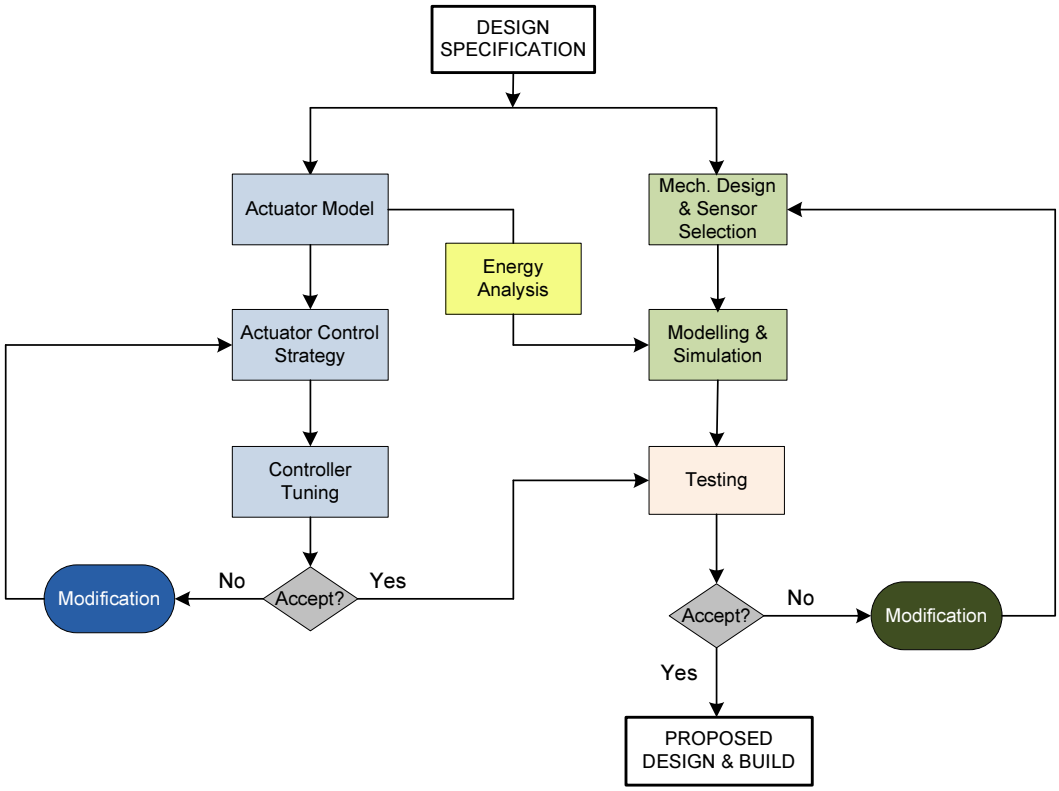

Figure 1-3. Generic Actuator and System Design Methodology

The *Generic Actuator and System Design* methodology must be specifically adapted for use in order to account for the nonlinearities and phenomena associated with SMAs. An effective SMA bundle actuator design methodology must allow for the unique and highly nonlinear actuation capabilities of SMA bundle actuators to be accounted for. Furthermore, the SMA design methodology must link all aspects of the work and serve as a reference guide for

any prospective researchers. Therefore, the principal components of the comprehensive design methodology for use with SMA actuators can be identified in order to determine the best possible work-flow:

i. *Analysis of the human hand*. An analysis of the mechanical capabilities of the human hand and finger is necessary. This acts as a comparative reference point for any new design proposals. Typical finger joint motion trajectories can be generated for a range of prehensile postures and movements, facilitating the selection of target objectives.

ii. *Design specification*. A design need must be identified for which the work is being carried out. Formalization of the aims and objectives of the work to satisfy the identified need is carried out at this stage. Parameters of the problem are identified.

iii. *SMA mechanical and thermal characterisation*. A complete characterisation of the mechanical and thermal response of SMA actuators to applied input current must be completed. The mechanical characterisation primarily focuses on SMA strain, force generation and relaxation of SMAs in bundle formation. The thermal characterisation focuses on the changes in SMA wire temperature during heating and cooling activity. Both the mechanical and thermal responses are interlinked.

iv. *Dynamic model of SMA strain*. The development of an accurate dynamic model of SMA strain is fundamental in allowing for accurate controller

design and tuning. The dynamic model can be generated using the data gathered during the SMA characterisation stage of the work.

v. *SMA control strategy design*. A suitable control strategy must be developed and implemented which provides fast and accurate control of SMA actuators. The control solution must account for the nonlinearities associated with SMA actuators.

vi. *Tuning Rule Implementation*. Appropriate tuning rules must be chosen to complement the control strategy selected.

vii. *Experimental Validation*. A series of experiments are required to validate the selected control strategy and tuning rules. In the event of unsatisfactory performance, a modification to the control strategy or tuning rules must be completed.

viii. *Prosthetic Finger Design*. The mechanical design of a prosthetic finger featuring SMA actuators is carried out. The finger must exhibit comparative geometry to the human finger to facilitate similar operational characteristics.

ix. *Kinematic analysis & Joint trajectory identification*. A kinematic analysis of the prosthetic finger design must be completed. The kinematic analysis ties together the finger joint rotation with SMA actuator contraction. This facilitates the derivation of optimum bundle lengths and any necessary gearing required to fulfill these needs. Suitable trajectories in terms of SMA contraction can be derived to achieve similar movement to that of the human finger.

x. *Dynamics analysis & SMA bundle sizing*. Dynamics plays an important role in determining the role played by external forces acting on the prosthetic finger during rotation. A complete dynamics model facilitates the sizing of SMA bundles to produce adequate force for rotation and gripping tasks.

xi. *Energy efficiency*. The efficiency of the proposed system is investigated based on the data gathered from the thermal response. Energy efficiency plays a vital role in prosthesis design owing to the reliance on batteries for power.

xii. *System analysis and experimentation*. An experimental procedure must be designed to assess the performance of SMA actuators in prosthesis design. The experimental procedure utilises the control strategy previously developed in conjunction with the dynamics and kinematics models produced. An optimization cycle can be conducted in the event of unsatisfactory results.

Based on the individual block requirements outlined, the flow of the methodology can be established (Figure 1-4). The SMA bundle actuator design methodology maintains the division of work in two parallel flows. The SMA bundle actuator is subject to characterisation, and modeling leading to the development of a suitable control strategy prior to implementation into a mechanical framework. Experimental validation of the controller is carried out. If the error is maintained below a preselected maximum value, the control strategy is accepted. If this is not the case, modifications to enhance control are carried out at this stage. In parallel, the prosthetic finger framework is fully

designed. Upon satisfaction with the design, a kinematic and dynamic model of the finger is carried out, allowing for a simulation of the finger during rotation. The sizing of an energy-efficient SMA bundle actuator is done by taking into consideration the findings from the characterisation phase of the work and the physical constraints of the mechanical framework.

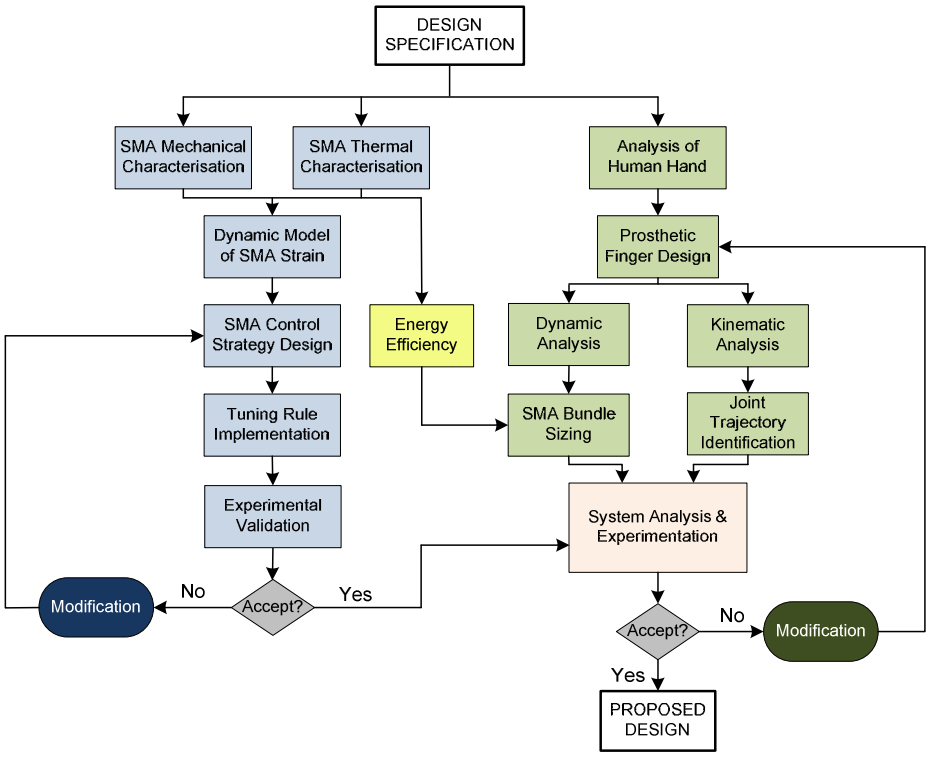

Figure 1-4. SMA Bundle Actuator Design Methodology for Prosthesis Design

The two parallel flows merge at the system analysis and experimentation point. The force and displacement requirements presented by the kinematic and dynamic models of the prosthetic finger are taken into account and applied to a suitably sized SMA bundle actuator. Testing is required to validate the complete design. Unsatisfactory results outside of the acceptable region set out at the design specification stage require design modifications to be carried out. The

steps thereafter must be repeated. A successful design is achieved when results fall within the selected acceptable region.

1.7.1 Proposed Finger Design Specification

The proposed methodology outlines a route to successful development of a viable prosthetic finger solution. The proposed design must meet or exceed a series of key values in order to improve on the current state-of-the-art designs which utilise SMA actuation technology:

i. In Section 1.4.1, it can be seen that a major concern involving SMA actuated prosthetic finger designs is low phalangeal tip forces. The maximum phalangeal tip force recorded in the literature of a workable design is 6.67N [46]. This is low in comparison with miniature DC motor actuated designs, which can achieve up to 30N finger tip force [13]. It is therefore considered as reasonable to set a target minimum phalangeal tip force of at least 10N at the tip of the distal joint in an energy efficient design. 10N of phalangeal tip force is suitable to allow a wide range of typical gripping and holding tasks to be accomplished by the end user. This is approximately 1/5 of the maximum human phalangeal tip force (See Section 3.4) and greater than the forces produced by previous SMA actuated designs.

ii. Portable operation is a key consideration in the design of any prosthetic device. The reliance on battery power means that the actuation system must be as efficient as possible. Available power limits are set by the limitations of current battery technology and the ergonomic

considerations for the end-user who must carry the battery throughout the lifetime of the prosthesis. A maximum allowable power of 45W for full finger operation (15W per joint) is sought, which is in line with typical miniature DC motors utilised in prosthesis design at present (See Section 8.5.3).

iii. The speed of response of the prosthesis is important from an ease-of-use perspective. It is intended that the prosthesis should be capable of forming any typical prehensile posture in less than 2 seconds. Furthermore, the dynamic posture formation should track human finger posture formation accurately.

1.8 Thesis Outline

The thesis is organised in a manner which follows the structure and flow of the proposed SMA bundle actuator design methodology outlined in Section 1.7. Chapter 2 provides the relevant technical background information on SMAs in terms of observed phenomenology and characteristic behaviour. A detailed review of hysteresis modelling and applied SMA control strategies is included.

Chapter 3 discusses the investigations carried out on the human finger and characteristic movements, postures, forces generated and functions. A series of parameters relevant to prosthesis design are identified and catalogued for biomimetic design and comparative performance investigations later in the work.

Chapters 4 & 5 focus on the characterisation and modeling of SMA bundle actuators. Within these chapters, the SMA bundle actuators are fully

characterized in terms of their mechanical capabilities and thermal behaviours. The characterisation is divided into two chapters owing to the large scope of the work. Chapter 4 focuses primarily on characterizing the SMA bundle actuator strain and force generation, while Chapter 5 focuses on characterizing the SMA wire temperature relationship with applied input current. It is noted that both chapters are inter-related. From the information gathered, a dynamic model of SMA strain response to applied input current is developed. Furthermore, the performance capacity and associated limitations of SMA bundle actuators can be determined.

Chapter 6 features the design, implementation and optimisation of a robust, accurate and fast control strategy capable of optimizing SMA bundle actuator performance. A robust tuning methodology based on the dynamic model outlined in Chapters 4 & 5 is implemented. Experimental testing and optimization of the selected control strategy is detailed.

Chapter 7 features the design, kinematic analysis and modeling of the dynamics of an optimised prosthetic finger design suited for use with SMA bundle actuators. The design is driven by a requirement to find the balance between the human finger aesthetics and the necessary components required to facilitate SMA bundle actuation.

Analyses of the full prosthetic finger design solution forms the basis for the work carried out in Chapter 8. A suitable evaluation procedure is described and applied to SMA bundle actuators for utilization in prosthetic finger design. The SMA bundle actuator is sized based on the data gathered during

characterisation in the previous chapters. A range of experiments are carried out and results can be assessed to evaluate the performance of the prosthesis.

Finally, in Chapter 9, the conclusions are drawn and a future work direction is outlined. A summary of a suitable implementation strategy for unconventional nonlinear actuation technologies is appended to provide future researchers with a tool to enhance their work.

****Note**** In order to maintain clarity throughout the work, a convention permitting the differentation between thermally induced effects on the SMA wires and load/stress induced effects is established for the benefit of the reader. The contraction of the SMA wires due to heating will be referred to as SMA *'strain'* activity, whilst relaxation of the SMA wires due to cooling will be referred to as SMA *'relaxation'* activity. Furthermore, the addition of loads to the wires will result in SMA *'extension'* activity.

2. SHAPE MEMORY ALLOYS – LITERATURE REVIEW

2.1 Introduction

Shape memory alloys exhibit a highly complex relationship between temperature, stress and strain. Much work has been carried out by researchers in the past in an attempt to understand the phenomenology of SMAs, and by others in an attempt to develop the best possible control strategy. This chapter presents a detailed background on the advances in SMA research to date. Furthermore, a detailed, categorized review of existing control strategies applied to SMAs by various researchers is included. The information found in this chapter is intended to provide the reader with the background information necessary to follow the flow of the work described herein.

2.2 Background to Shape Memory Alloys

Shape memory alloys consist of a group of metallic materials that demonstrate the ability to return to some previously defined shape or size when subjected to an appropriate thermal procedure [47]. The phenomenon was first discovered in the 1930s in brass alloys and since then a number of material systems have been shown to exhibit shape memory properties (Table 2-1) [34]. The shape memory effect is particularly pronounced in certain nickel-titanium (NiTi) alloys. These alloys, commonly referred to as Nitinol to reflect their discovery at the Naval Ordinance Laboratory [36], exhibit properties which are favourable to many engineering applications. Presently, NiTi is the most successfully applied shape memory alloy [41].

Table 2-1. Material systems with shape memory properties [41]

Metals	NiTi Based alloys (NiTi, NiTiCu, NiTiFe…) Cu Based Alloys (CuZn, CuZnAl, CuAlNiMn…) Fe Based Alloys (FePt, FeMnSi, FeNiC…)
Polymers	e.g. Polytetraflouroethylene
Ceramics	e.g. Zirconium Oxide
Biological Systems	e.g. Bacteriophages

2.3 Phenomenology of Shape Memory Alloys

The shape memory mechanism is based on a martensitic transformation; a reversible, solid-state phase transformation between the high temperature austenite phase and the low temperature martensite phase [41]. When the material is in its martensite form, it exhibits properties such as low ductility and malleability, allowing for easy deformation. When in its austenite form, the material exhibits substantially different properties such as high strength and hardness [34].

The martensitic transformation cycle is a temperature-dependent cycle (Figure 2-1) [35]. The temperature at which this phenomenon begins is known as the austenite start temperature, A_s. As the temperature rises further, the percentage of Austenite in the SMA increases until the austenite finish temperature, A_f, is reached. At this point the SMA is 100% austenite. During cooling, the material begins to revert to its martensite phase when the martensite start temperature, M_s, is reached. As the temperature of the SMA falls further, the percentage of

martensite increases. This continues until the martensite finish temperature, M_f, is reached where the material is 100% martensite.

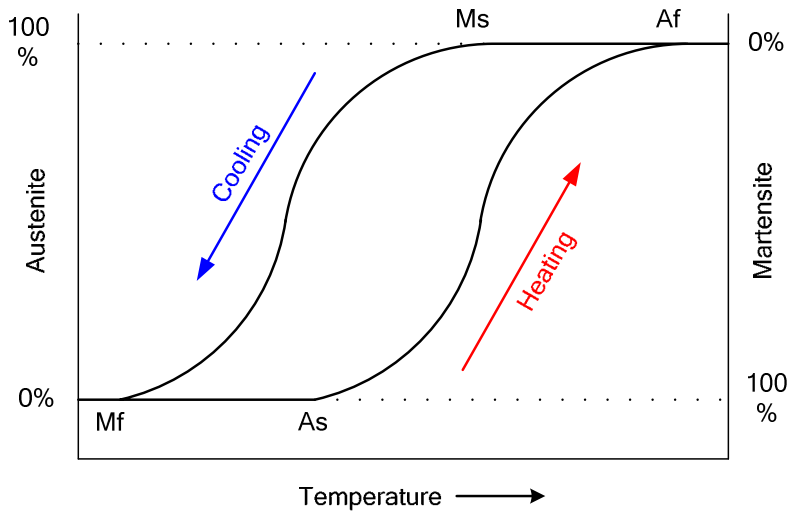

Figure 2-1. Temperature dependent martensitic transformation

It can be seen in Figure 2-1 that the martensitic transformation is characterised by a large hysteresis loop. The hysteresis is present due to the differences between the transition temperatures A_s and M_f, and A_f and M_s. During martensitic transformation, the physical properties of the SMA such as Young's modulus, heat capacity, thermal conductivity and electrical resistance vary. In the range where martensite and austenite exist simultaneously, nonlinearities and hysteresis exists. The size and characteristics of these nonlinear elements are a function of their constituents, the manufacturing processes applied and the cyclic history [59].

In addition to thermally-induced martensitic transformation, transformation can be induced by applying a sufficiently high mechanical load to the material in the austenite phase [60]. This loading results in the SMA material exhibiting partially martensitic characteristics such as reduction in ductility and

malleability. This is known as *stress-induced martensite*. Hence, this permits the SMA material to deform to a greater degree than would be possible if the material remained in the austenite phase. Upon release of the applied load, the material reverts back to its austenite phase. This phenomenon is known as pseudoelasticity [61].

2.3.1 Phenomenology of Phase Transitions in SMAs

Austenite exhibits a generally cubic crystal structure which is different to the tetragonal, orthorhombic or monoclinic crystal structure associated with martensite. The martensitic transformation does not occur by diffusion of atoms, but rather by shear lattice distortion. Martensitic crystals formed have different orientation directions known as variants. Twinned martensite is formed by a combination of self-accommodating martensitic variants, while detwinned martensite is formed when a specific variant is dominant. The phase transformation from austenite to martensite forms the basis of the behaviour of SMAs [60].

On the crystallographic plane, cooling from austenite to martensite under zero loading conditions results in fully twinned martensite (Figure 2-2). Similarly during the heating process, the reverse occurs. If a mechanical load is applied to the SMAs in the twinned martensitic phase, it is possible to detwin the martensite by re-orientating a certain number of variants. This results in an observable shape change which remains after the load is released.

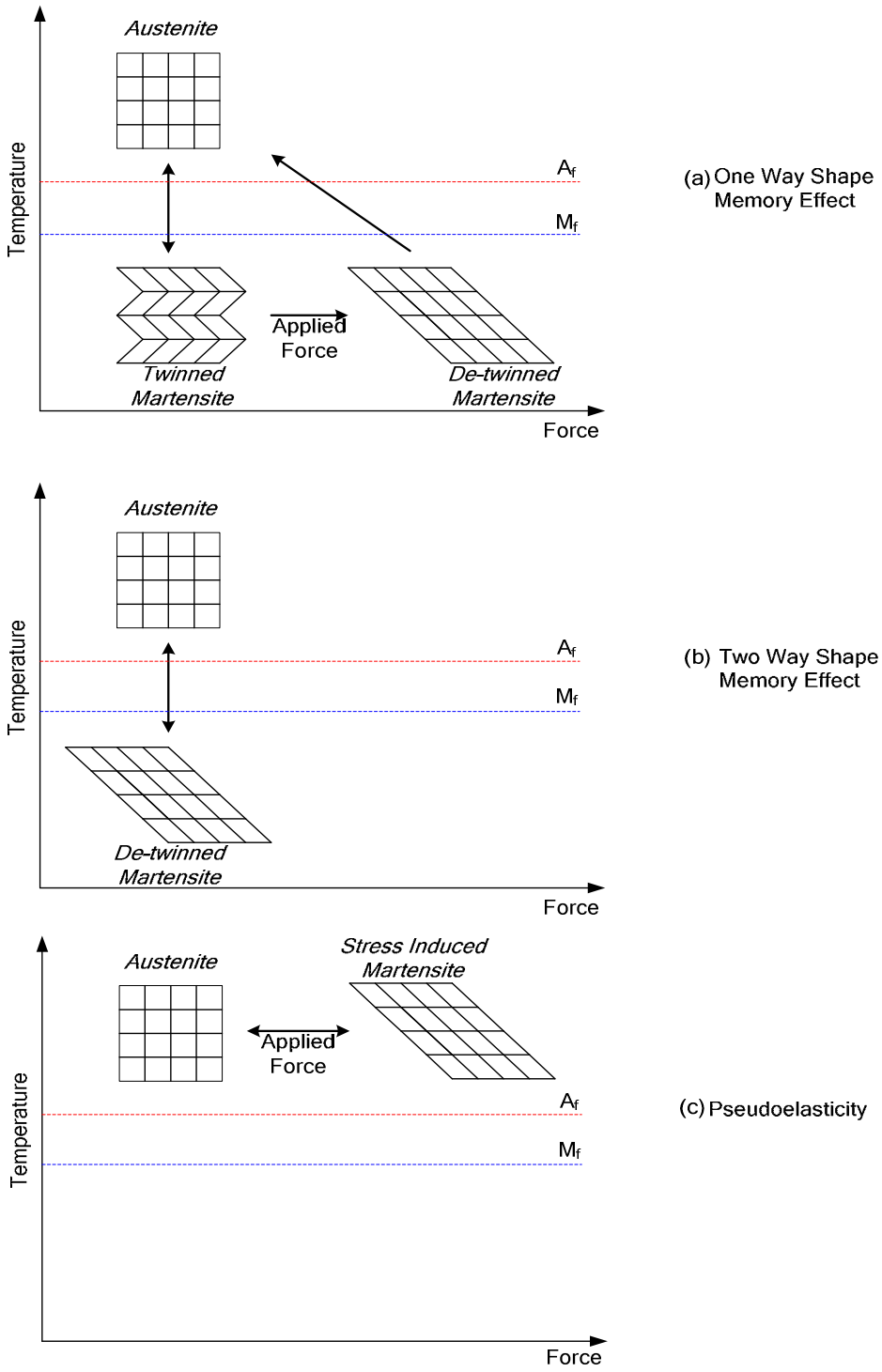

Figure 2-2. Crystallographic Plane View Models of various SMA effects

If the material is subsequently heated to its austenite phase, the reverse transformation will occur, leading to the complete shape recovery of the

material. Further cooling will form twinned martensite, with no observable shape change. This is known as the one way shape memory effect.

In the event of mechanically loading the SMAs in the austenitic phase and cooling them to the martensitic phase, the direct formation of detwinned martensite will occur, producing an observable shape change which can be recovered by heating the material back to the austenitic phase. This is referred to as the two-way shape memory effect [62].

The addition of a large mechanical load to the material while in the austenitic phase results in a stretching effect. The austenite initially displays an elastic behaviour. If the stress applied is sufficiently large, the material will transform into stress-induced martensite in a highly nonlinear manner. Unloading will result in the complete recovery of the strain via a hysteresis loop. This pseudoelastic process does not require a change in SMA temperature.

2.4 Implementations of SMA Actuators

SMA actuators can be classified into three categories depending on the characteristics of the SMA actuator [34]. This is illustrated further in Figure 2-3.

- *Free Recovery*. A deformed SMA component returns to its original shape under thermal excitation above the A_f temperature. Any further temperature changes following this do not cause any macroscopic shape changes.

- *Constrained Recovery (Force Generation)*. If a deformed SMA component is prevented from changing shape when heated above A_f, a large force is

exerted. This principle has been successfully applied to fastener rings or electric connectors.

- *Work Production.* If the SMA component overcomes an external rest force when heated above its A_f temperature, a motion is generated and work is produced. When cooled, the reset force causes a return motion to the initial position. Thus, repeated heating and cooling produces periodic actuation cycles.

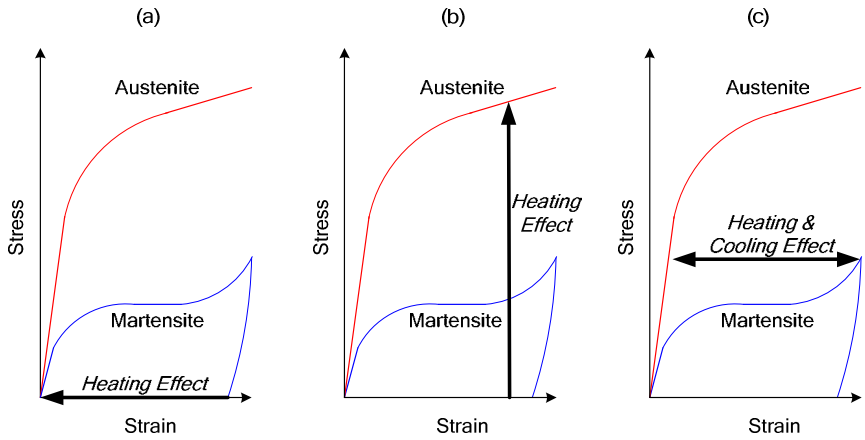

Figure 2-3. Function mechanisms of SMA actuators in the stress-strain diagram. (a) free recovery, (b) constrained recovery, (c) work production [34].

2.5 SMA Wire Actuator Layout

SMAs exist in single wire, multiple wire, spring, or strip form. For robotic and prosthetic gripper applications, SMA wire actuators are the most successfully implemented form and as such are the primary focus of this review. The selection of a particular form of SMA actuator depends on the intended task. Variables such as strain, bias force, torque generation and frequency of

operation play a key role in the selection. Some common layouts of SMA wire actuators are (Figure 2-4):

i. Single SMA Wire

ii. Bias Spring Assisted SMA Wire

iii. Antagonistic SMA wire

iv. SMA Bundle Actuator

v. Bias Spring Assisted SMA Bundle Actuator

vi. Equal Antagonistic SMA Bundle Actuator

vii. Non-equal Antagonistic SMA Bundle Actuator

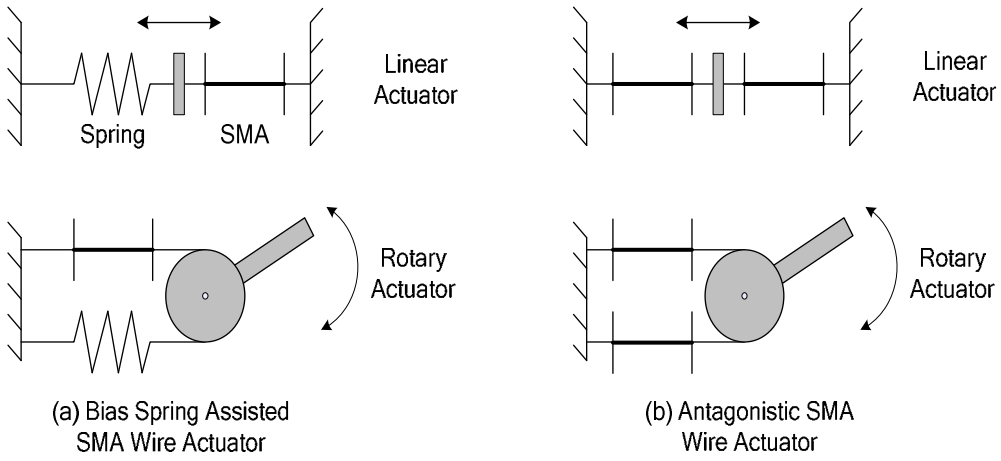

Figure 2-4. Common Single SMA Wire Actuator Layouts [41]

2.5.1 Bias Spring Assisted SMA Actuator

As an actuator, the SMA wire can only provide force or displacement in one direction under thermal excitation. A bias (return) mechanism is necessary in

order to return the actuator to its original shape after the heating phase. Biasing is usually implemented using a spring [63, 64]. The disadvantages of biasing lie in the additional space requirements, the increase in actuator complexity and the increase in actuator weight. In addition, the output force capability is reduced as the bias spring opposes the force of the SMA wire.

In dynamic loading activity, it is important to determine the correct spring stiffness required for the task. The spring must have the ability to return the SMA to its original length whilst permitting enough force or displacement action to take place in the actuator. An over-stiff spring will result in an actuator being unable to perform its required task. An under-stiff spring will result in not enough bias force available to return the actuator to its original position.

2.5.2 Antagonistic SMA Wire Actuator

An alternative method of producing a bias force is to implement SMA wires acting in opposite directions [65, 66]. This is referred to as an antagonistic layout and provides force in both directions of movement. When in its martensitic phase, the SMA actuator exhibits a greater degree of malleability. Thus, in antagonistic action, the SMA wire in its austenitic phase can apply a suitable biasing force to the opposing SMA wire in its martensitic phase resulting in the martensitic wire returning to its original shape. It is of critical importance to control the heating and cooling cycles for the opposing wires precisely in order to achieve maximum benefit from the arrangement. If heating and cooling cycles are not executed in the correct sequence, both wires can exist in their austenitic phase simultaneously leading to undesirable effects.

2.5.3 SMA Bundle Actuators

Bundling SMA actuators in parallel provides a means of magnifying the force generated by the actuator by up to a factor of approximately 20 whilst only doubling the size of the actuator [47].

A gap between the wires is required in order to reduce the possibility of heat transfer between the wires leading to undesirable effects such as slow cooling times. Placing the SMA wires too close to each other reduces convection cooling of the SMA wires, and hence reduces the overall effectiveness of the actuator.

Similar to single wire actuators, a bias force is required to return the SMAs to their original position. This required bias force is larger due to the increased number of SMA wires present in the bundle. The biasing force can be introduced by a spring element or by an antagonistic arrangement of SMA bundles. The antagonistic arrangement can have two forms, non-equal antagonistic arrangement, or equal antagonistic arrangement (Figure 2-5). The former is acceptable when the required force in one direction is greater than the return force. The latter is acceptable when the force required in both directions is approximately equal. Calculation of the required forces results in correct bundle sizing.

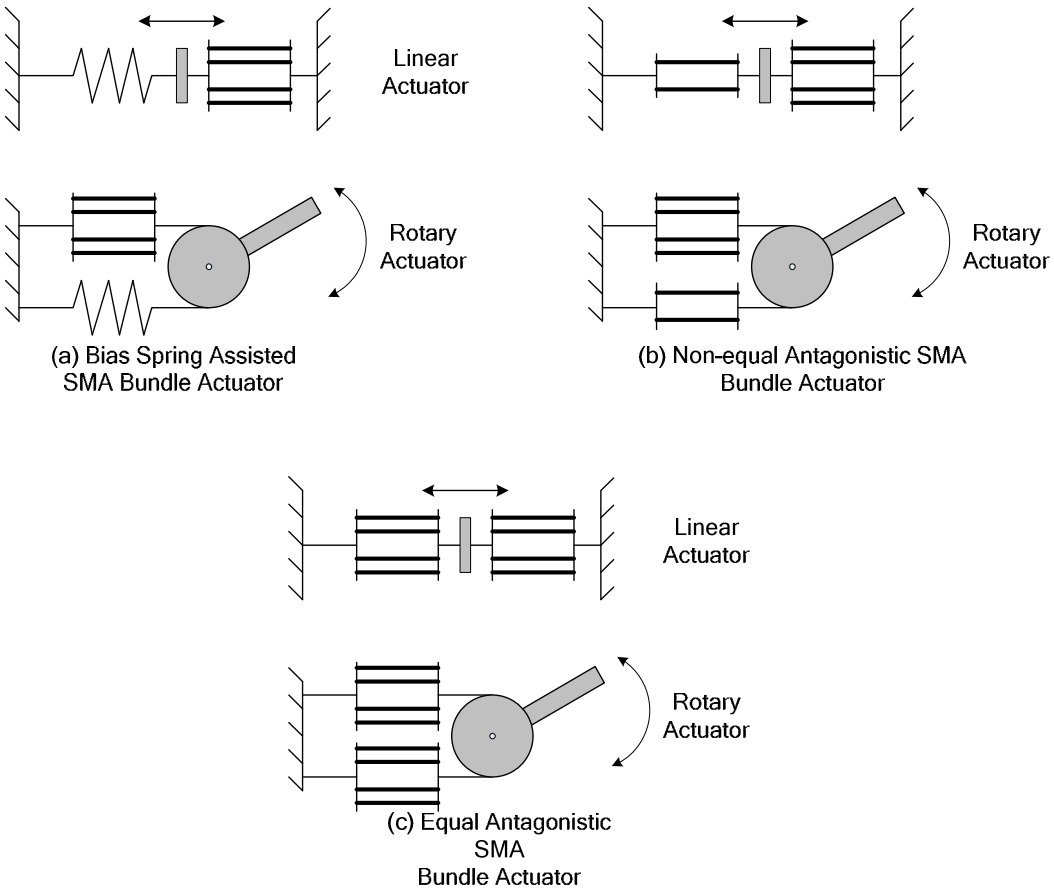

Figure 2-5. SMA Bundle Actuator Possible Arrangements

2.5.4 Heating & Cooling of SMA Actuator

SMA actuators rely on the addition of thermal energy to perform work. There are several methods available to raise or lower the temperature of the actuator. However not all are practical or allow for precise SMA temperature control. Precise control of temperature can lead to the production of precise forces and displacements of the actuator.

2.5.4.1 SMA Heating Methodologies

The heating of the SMA wire can be achieved by:

i. *Resistive/Joule heating* – Passing electric current through the SMA [67].

ii. *Ambient heating* – Increasing the ambient air temperature surrounding the SMA.

iii. *Peltier heating* – Invoking the Peltier effect to heat individual segments of the SMA [68].

Resistive/Joule heating is the best strategy available to increase the temperature of the wire in a prosthesis application. However, although this concept is relatively simple, there are associated disadvantages such as:

- *Large currents*. The resistance of the SMA is small and therefore a large current is required to provide effective heating. For example, a 150μm diameter SMA wire requires 400mA of current to heat to a temperature of 127^{o}C [42]. This is the highest rated current recommended by the manufacturers for wires of this diameter [69]. However, it should be noted that a wire temperature of 127^{o}C is considered unsafe in an open environment, and thus must be maintained in an enclosure. This can result in raised ambient temperature which negatively impacts on the performance of the SMA wire during the cooling phase if excess heat build-up is not adequately dissipated.

- *Electrical Isolation.* The heating current must flow through the SMA element, not through other conductive parts near or in contact with the SMA element. This results in special requirements for the components of the actuators.

- *Variable Resistance.* The electrical resistance of martensite and austenite differ slightly [70]. As a result, when applying current, the voltage must

vary to counteract this resistance change by means of a current regulation circuit (See Section 4.4.1). Omitting this regulator will result in changing currents leading to imprecise temperature control.

2.5.4.2 SMA Cooling Methodologies

The cooling of SMAs can be achieved naturally provided that the ambient temperature is lower than the M_s temperature of the SMA wire. This method is relatively slow (2-4 seconds) but is useful if the speed/bandwidth of the actuator is not critical. The rate of cooling is affected by the surface area of the SMA wire, the convection coefficient of the material and the difference between the SMA wire temperature, the ambient temperature of the environment and the properties of the surrounding fluid. The closer that the ambient temperature is to the transformation temperature, the slower the cooling rate is. Alternatively, by decreasing the diameter of the wires, the rate of cooling will improve. This owes to the greater the surface to mass ratio of the wire, the greater the rate of cooling for a particular actuator sizing. However, decreasing the diameter of the wire will adversely affect the force generation capacity of the actuator. There are several novel methods in the literature that have been employed to increase the rate of cooling further whilst not sacrificing force generation. These are:

- *Conduction.* Heat sinks have been successfully applied to SMA actuators in order to increase the rate of heat conduction away from the SMA wires [50, 71].

- *Convection.* Forced air or liquid cooling solutions have been successfully implemented previously [72, 73]. However, these methodologies require

a constant supply of compressed air, or liquid, for successful implementation. This adds to the size, complexity and weight of the actuator significantly, whilst also requiring additional energy to operate.

- *Peltier Cooling.* The Peltier effect has been used to forcefully cool SMA wire segments [74]. However, this requires a significant increase in the size of the actuator housing. This is due to the application of miniature heat sinks to each segment of a SMA wire.

A conduction cooling strategy is most suited to portable devices such as prosthesis as they do not rely on a compressed air/liquid cooling source (convection) and do not require a large actuator housing for implementation (Peltier Cooling).

2.6 Hysteresis in SMAs

Hysteresis is a strongly nonlinear phenomenon which occurs in many industrial, physical, and economic systems. In 1928 the phenomenon was defined by Scottish physicist Alfred Ewing as follows; “When there are two quantities, M and N, such that cyclic variation of N causes cyclic variation of M, then if the changes of M lag behind those of N, we may say that there is hysteresis in the relation of M and N.” [75].

In a deterministic system containing no hysteretic or dynamic effects, it is straight forward to predict the system’s output at any instant of time. In systems exhibiting hysteresis, it is not possible without knowing both the system’s state and the history of inputs (Figure 2-6) [76]. Hysteresis in systems is usually undesirable and can result in inaccuracies in modelling and control. Control

strategy effectiveness is undermined and, on occasion, the phenomenon can lead to instability in the system.

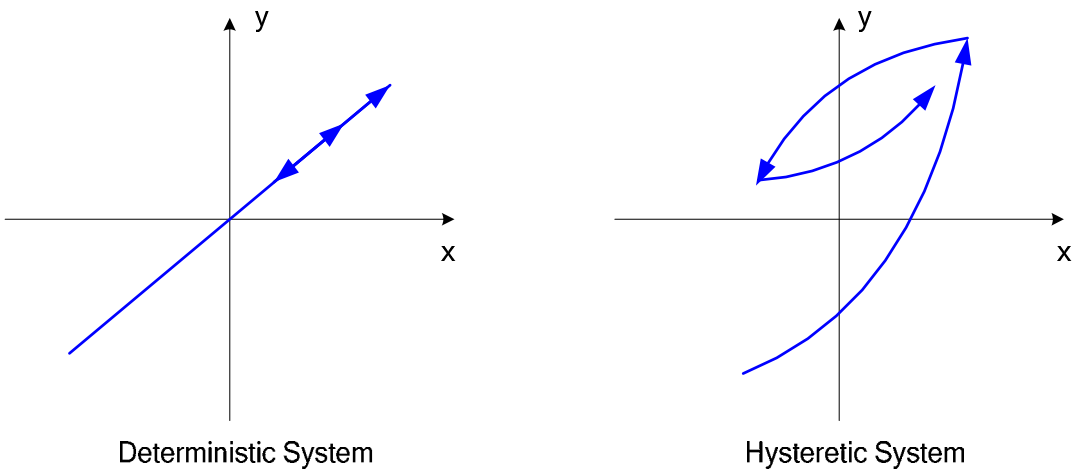

Figure 2-6. Input/Output Diagrams for Deterministic & Hysteretic Systems

SMAs exhibit severe hysteresis due to a complex thermomechanical relationship. An accurate model of SMA behaviour can play a vital role in the development of a mechanical system and/or a suitable control strategy involving the use of SMA actuators. The development of an SMA actuator model has been approached from numerous perspectives such as thermodynamics, micromechanics, thermomechanical, finite element and phenomenological [77]. Of these, phenomenological approaches are the most suited to engineering and control tasks as the parameters involved can be measured [41].

2.7 Phenomenological Modelling of SMAs – An Overview

Phenomenological models can be described by internal variables such as martensitic fraction, strain and temperature, or by utilising numerical techniques specifically to model the effects of hysteresis. *Tanaka* first described

a constitutive relationship between the three internal variables which describes the complex temperature-stress-strain behaviour of SMAs:

$$\dot{\sigma} = \mathrm{D}\dot{\varepsilon} + \Theta\dot{T} + \Omega\dot{\xi} \tag{2-1}$$

where D is the elastic modulus, Θ is the thermoelastic tensor, Ω is the transformation tensor, $\dot{\varepsilon}$ is the rate of change of SMA strain, $\dot{T}$ is the rate of change of SMA temperature, $\dot{\xi}$ is the rate of change of the martensitic ratio and $\dot{\sigma}$ is the rate of change of SMA stress [61]. The hysteresis behaviour can be described by the phase transformation component in the constitutive relationship. *Tanaka* proposed a kinetics equation describing the phase transformation as a function of stress and temperature. This was assumed to be an exponential relationship:

$$\begin{aligned} \xi_{M\to A} &= \exp[A_a(T_{SMA} - A_s) + B_a\sigma] \\ \xi_{A\to M} &= 1 - \exp[A_m(T_{SMA} - M_s) + B_m\sigma] \end{aligned} \tag{2-2}$$

where A_a, A_m, B_a, and B_m are material constants in terms of transition temperatures A_s, A_f, M_s, and M_f. *Liang and Rogers* adopted *Tanaka's* constitutive relationship (Eq. *(2-1)*), however, they proposed a cosine relationship for the phase transformation kinetics equation [78]. The phase transformation equations for heating and cooling are given by

$$\begin{aligned} \xi_{M\to A} &= \frac{\xi_M}{2}\cos[a_A(T - A_s) + b_A\sigma] + \frac{\xi_M}{2} \\ \xi_{A\to M} &= \frac{1 - \xi_A}{2}\cos\left[a_M\left(T - M_f\right) + b_M\sigma\right] + \frac{1 + \xi_A}{2} \end{aligned} \tag{2-3}$$

where $a_A = \pi/(A_f - A_s)$, $a_M = \pi/(M_s - M_f)$, $b_A = -(a_A/C_A)$ and $b_M = -(a_M/C_M)$. C_A and C_M specify the influence of stress on the four transformation temperatures, and ξ_M

and ξ_A are the martensite and austenite ratios respectively. *Brinson* improved on this by separating the martensitic fraction into that induced by stress and that induced by temperature [79]. The *Liang and Rogers* phase transformation equations were used in this model (Eq.(2-3)).

Ikuta developed a variable sublayer model and, similar to *Tanaka*, used an exponential term to describe phase transformation [80]. *Ikuta's* model described the major hysteresis loop behaviour of SMA actuators. This was further extended by *Madill and Wang* to include minor hysteresis loop behaviour [81].

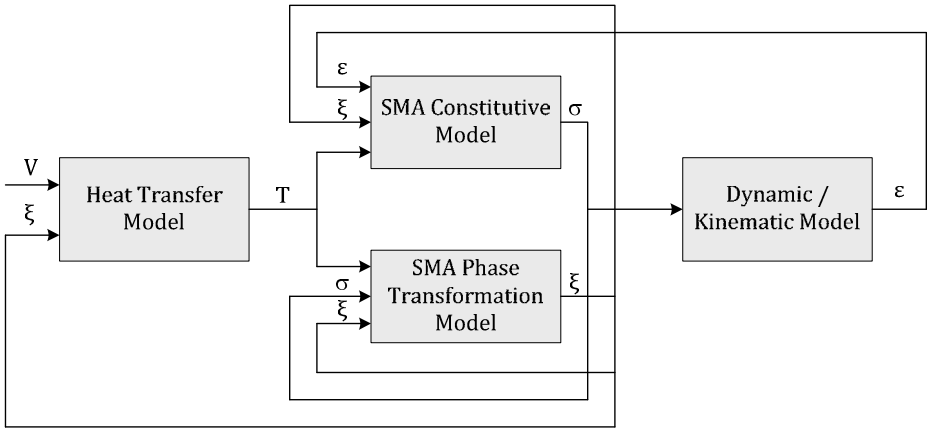

Figure 2-7. SMA Actuator Modelling – Elahinia's 4 Interconnected Sub-models [82]

Elahinia significantly advanced the modelling procedure by breaking the SMA model into four interconnected sub-models, a heat transfer model, a dynamic/kinematic model, a constitutive model and a phase transformation model [82] (Figure 2-7). The constitutive model of *Tanaka* and an enhanced phase transformation model based on the work of *Liang and Rogers* were utilised. The dynamic/kinematic model is system specific. The heat transfer

equation consists of joule heating and natural convection, and is based on the work of *Shahin* [83]

$$mc_p \frac{dT}{dt} - m\Delta H \frac{d\xi}{dt} = i^2 R - hA(T_{SMA} - T_\infty) \quad (2\text{-}4)$$

Furthermore, it has also been shown that the effect of increasing the stress applied to SMA wires results in a linear increase in phase transformation temperatures [82, 84].

The phenomenological models described thus far provide good estimations of the SMA actuator behaviour and are well suited to parametric studies. However, the practical usage of these models in a control system relies on accurate SMA wire temperature measurement combined with a high computational capacity to provide real-time data. This is not feasible in a portable system such as a prosthesis where computational power is limited, and accurate SMA wire temperature measurement is extremely difficult. As a result, it is necessary to investigate numerical modelling techniques which have the potential to overcome these issues.

Appropriate numerical modelling techniques are founded on work used to describe the hysteresis behaviour exhibited by nonlinear materials and actuators. There are various approaches such as the *Krasnosel'skii-Pokrovskii* model [85], the *Prandtl-Ishlinskii* [86, 87] model, the *Duham* hysteresis operator [88] and the *Preisach* independent domain model [89] amongst others.

The Preisach model is the most widely implemented numerical model for describing the hysteresis present in SMAs. This owes to the fact that the

Preisach model features the ability to model the major and minor loops of complex hysteresis, the wiping-out property (See Section 2.8.3), exhibits a well-defined identification algorithm, and convenient numerical simulation form [90]. In the nonlinear actuation field, the Preisach model has been used to successfully model the hysteresis phenomena associated with piezoelectric crystals, piezoceramics and SMAs [91, 92]. While notable disadvantages exist, such as large data collection requirements and a lack of robustness to disturbances, these can be tackled by implementing a suitable control strategy in conjunction with the model. The Preisach model is widely accepted as the best hysteresis model available presently [93]. Based on the advantages outlined, it is seen as the most appropriate approach for the work described herein. Implementation of the Preisach model must therefore be investigated.

2.8 SMA Preisach Model Implementation

Preisach modelling of hysteresis in SMAs has been on-going since the mid 1990's. *Hughes and Wen* verified that SMAs exhibit the wiping out property and minor loop congruence (See Section 2.8.3), two crucial properties that enables them to be modelled using the Preisach model [91]. *Gorbet and Wang* used the Preisach model to identify the hysteresis within a two-wire differential SMA actuator [94]. They demonstrated the potential to generate highly accurate models of the major and minor loops using a set of 'first order descending (FOD) curves' [76] (See Section 2.8.4). This identification technique has been criticized for its mathematical complexity and time consumption. As a result others have attempted to simplify the identification procedure by implementing simple parameter fitting techniques. This capitalizes on the proportional relationship

of the major loop of the hysteresis and obtaining weighting functions based on temperature-stress relationships within SMAs [95-98].

2.8.1 Mathematical Basis of the Preisach Model

The Preisach model was first suggested in the 1930's to describe ferromagnetism [89]. The main assumption made is that the system consists of a parallel summation of a continuum of weighted hysteresis operators $\gamma_{\alpha\beta}$ with α and β representing 'up' and 'down' switching values of input (Figure 2-8). In relation to SMA Preisach model identification, α refers to the turning on of a heating source (the heating stage), while β represents the switching off of the heating source (the cooling stage).

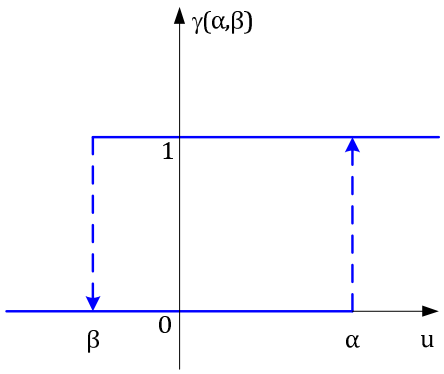

Figure 2-8. Non-Ideal Relay Hysteresis, γ(α,β)

As the input, u(t), varies in time, each individual non-ideal relay, P, adjusts its output in accordance with the current value and the weighted sum of these outputs provides the overall system output y(t) (Figure 2-9). The Preisach function is an arbitrary weight function $\mu(\alpha,\beta)$.

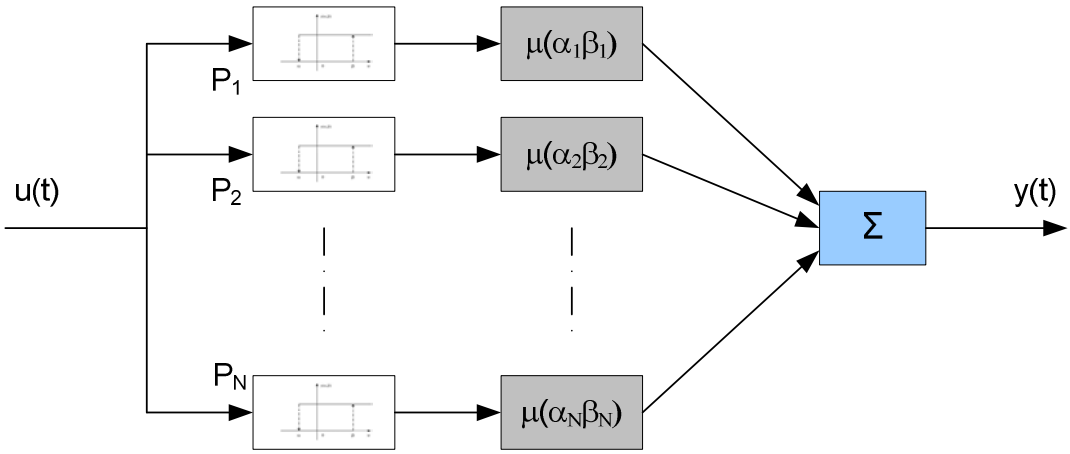

Figure 2-9. Weighted Parallel Connections of a Finite Number of Non Ideal Relays

Combining the Preisach functions and the hysteresis operators, the Preisach model can be written as

$$y(t) = \iint_{\alpha \geq \beta} \mu(\alpha, \beta)\left[\gamma_{\alpha\beta} u(t)\right] d\alpha d\beta \tag{2-5}$$

which describes the overall system output.

2.8.2 Geometrical Interpretation of Preisach Model

The Preisach plane is a plane of coordinates (α,β). The half-plane, where α > β is considered only as it has a physical equivalent in nature. Each point is mapped to a specific relay hysteron with values outside of the triangle Tr considered to be zero (Figure 2-10). The hypotenuse of Tr is the line α = β with the coordinates of the vertex representing the maximal value of the input being modelled [99].

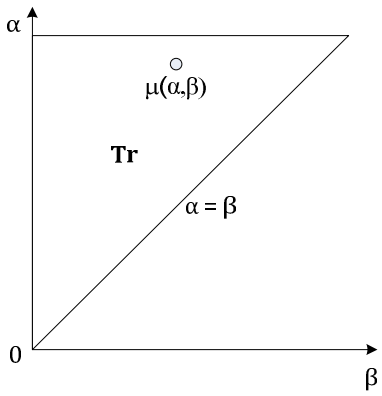

Figure 2-10. The Preisach Plane - Geometrical Interpretation

The relationship between the Preisach plane and the inputs to and outputs from a hysteretic system can be shown via an example: The inputs to the system are termed α when they are greater than the previous input and β when they are less. The sequence of the input values is critical in modelling systems with hysteresis owing to the hysteretic dependence on value history. The sequence of inputs is $\alpha_1 \rightarrow \beta_1 \rightarrow \alpha_2 \rightarrow \beta_2 \rightarrow \alpha_3$ (Figure 2-11).

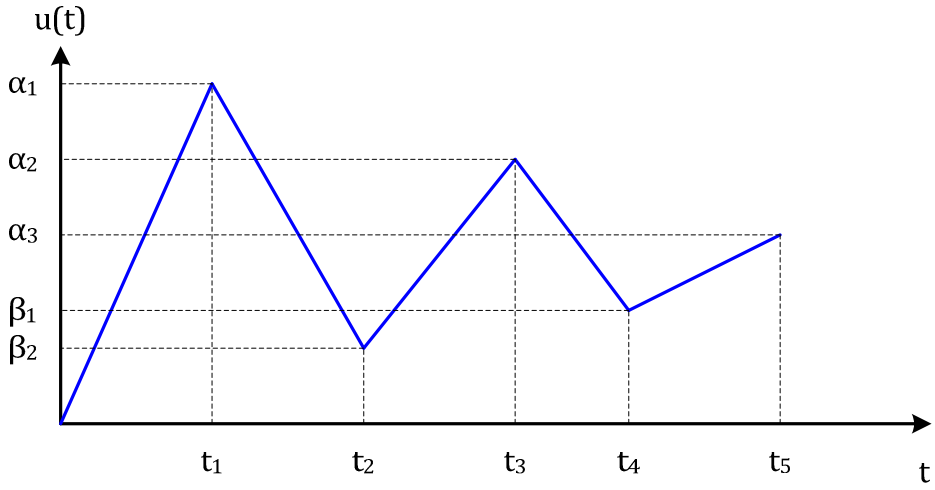

Figure 2-11. Sequence of Input Values ($\alpha_1 \rightarrow \beta_1 \rightarrow \alpha_2 \rightarrow \beta_2 \rightarrow \alpha_3$)

The initial step in the sequence, α_1, sees the input value increase relative to its previous position. This increase is represented geometrically on the Preisach plane by a horizontal line, $\alpha=u(t)$, moving upwards until it reaches α_1 (Figure 2-12). The triangle Tr is now subdivided into two regions, $S^1(t)$ and $S^0(t)$. All hysteresis operators in the $S^1(t)$ subset of Tr have their values changed to their 'up' position of 1. All hysteresis operators that remain in the $S^0(t)$ subset maintain their 'down' value of 0. The input is now reduced to β_1. This is represented geometrically on the Preisach plane by a vertical line, $\beta=u(t)$, moving from right to left. This has the effect of reducing the size of the $S^1(t)$ subset causing some of the hysteresis operators to return to their 'down' value of 0. However, as long as the β value does not decrease to zero, there will remain some unchanged hysteresis operators in their 'up' position of 1.

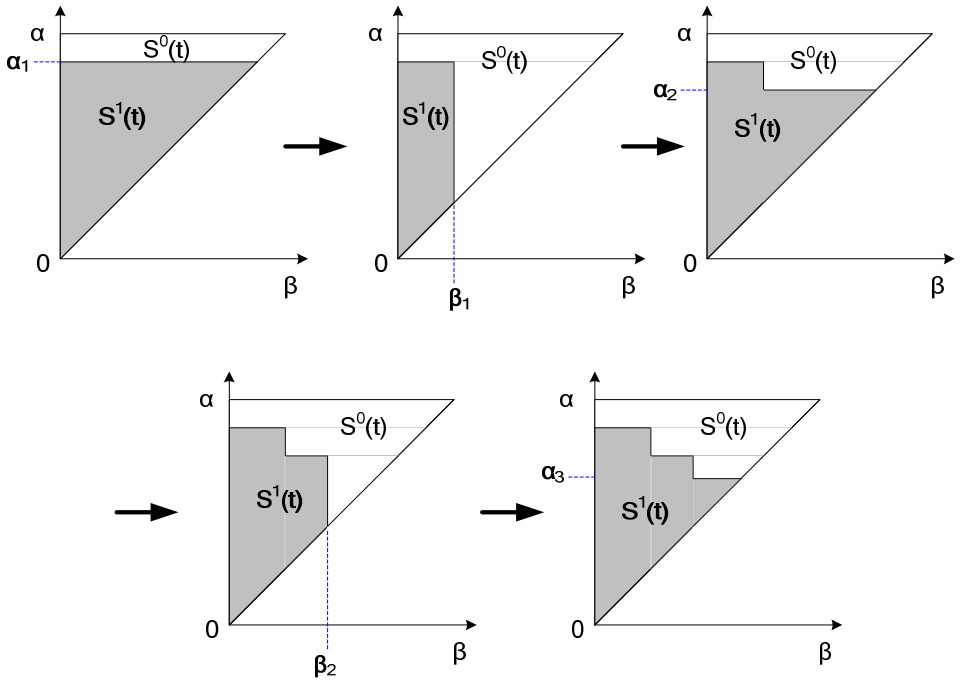

Figure 2-12. Evolution of triangle T division into Subsets $S^1(t)$ and $S^0(t)$

When the value of u(t) is increased to α_2, these unchanged operators will facilitate the calculation of a slightly different output result for α_2 as the third value in the sequence compared to the first value. In this particular example, the sequence continues in this fashion with hysteresis operators in their 'up' position of 1 accumulating as the sequence progresses. It can be surmised that Eq.(2-5) can be expressed as

$$y(t) = \iint_{S^1(t)} \mu(\alpha,\beta)\gamma_{(\alpha,\beta)}u(t)d\alpha d\beta + \iint_{S^0(t)} \mu(\alpha,\beta)\gamma_{(\alpha,\beta)}u(t)d\alpha d\beta \quad (2\text{-}6)$$

which can be reduced to

$$y(t) = \iint_{S^1(t)} \mu(\alpha,\beta)d\alpha d\beta \quad (2\text{-}7)$$

resulting in a straight forward computation of y(t).

2.8.3 Wiping out Property & Minor Loop Congruency

The wiping out property is defined as '*the constraint that the output be affected only by the current input and the alternating series of previous dominant input extrema, the effect of all others being wiped out*'. A dominant maximum is one that is greater than any subsequent u(t) value, while a dominant minimum is one less than any subsequent u(t) [91]. This wiping out property is so called as it is the equivalent of erasing the history associated with the vertices on the Preisach plane [76]. The wiping out property is demonstrated geometrically in (Figure 2-13) where the second α value is greater than the first. This results in the initial vertex value of (α_1,β_1) being covered by the horizontal line $u(t)=\alpha_2$, in effect 'wiping out' the (α_1,β_1) vertex value from the system.

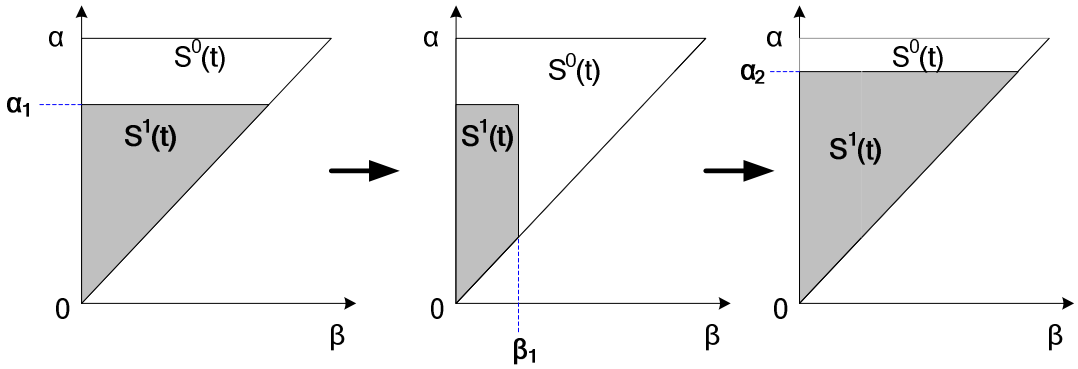

Figure 2-13. Wiping-out Property in Alpha

The wiping out property is not limited to the alpha cycle of the input. It can occur in the beta cycle in the similar fashion, whereby the new beta value is less than a previous beta value in the sequence. This is illustrated in (Figure 2-14) where partial wiping out is shown as the new beta value is greater than 0. A beta value of 0 would result in total wipeout, effectively resetting the system sequence to the beginning again.

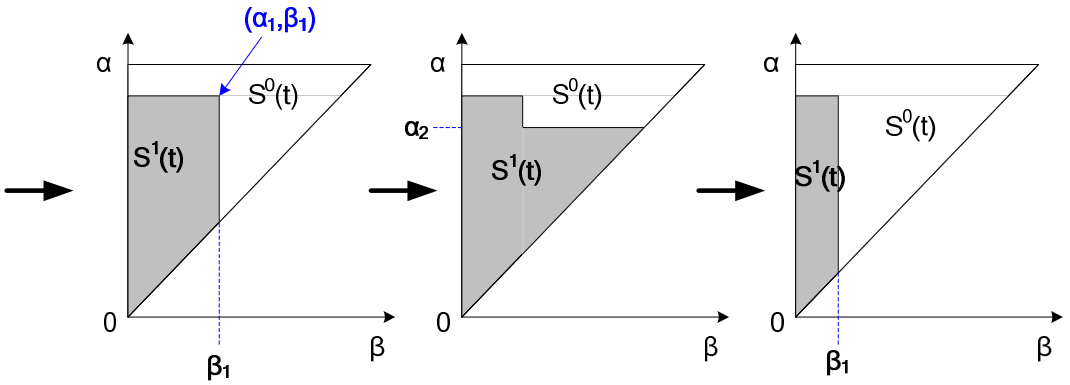

Figure 2-14. Wiping-out Property in Beta

The congruent minor loop property requires that all equivalent minor hysteresis loops be congruent. Two minor loops are considered equivalent if

they are generated by an input u(t) varying between the same two extrema. Congruency between minor loops means that one will exactly overlap the other if shifted by an appropriate vertical translation [91]. This property implies that the shape of a minor loop in the hysteresis depends only on the two extrema values of the input path used to generate the loop.

2.8.4 Discretisation of the Preisach Plane

There are many difficulties associated with the implementation of the Preisach model in its continuous form in practical applications, namely:

- The evaluation of double integrals can be time consuming and difficult
- The identification of an infinite number of hysteresis operators $\gamma_{\alpha\beta}$
- The calculation of associated Preisach functions $\mu(\alpha,\beta)$

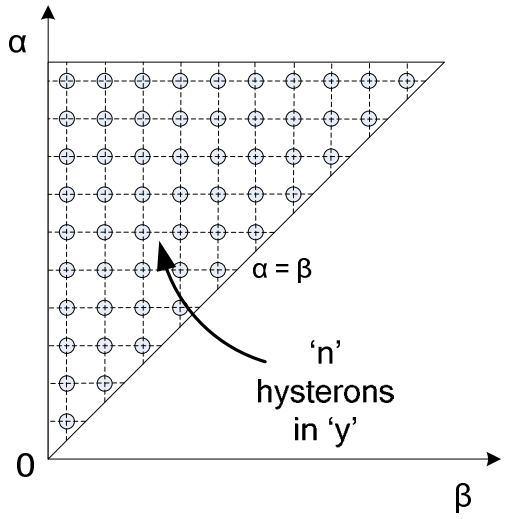

Figure 2-15. Discrete Representation of the Preisach Plane

As a result of these difficulties, a methodology involving the discretisation of the Preisach plane was developed [85]. This involves dividing up the Triangle T into

its discrete analogue with hysterons (relays) appearing at regular intervals on both the vertical and horizontal directions. If the number of hysterons on the vertical axis is *n*, then the total number of hysterons on the plane is *n(n+1)/2* (Figure 2-15).

Mayergoyz describes a technique known as 'first order descending (FOD) curves' to identify the weights, μ, of the discrete hysterons on the discrete Preisach plane [76]. A FOD curve is generated by first bringing the input value u(t) to its lowest possible value, increasing u(t) monotonically to value α, then decreasing u(t) to a value β. The measured values are labelled $y_{\alpha 1}$ at u(t)=α and $y_{\alpha 1 \beta 1}$ at u(t)=β (Figure 2-16).

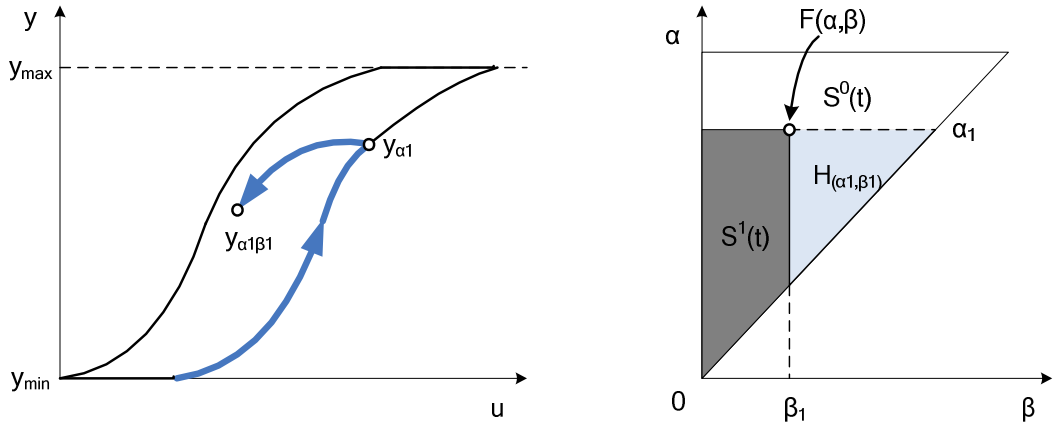

Figure 2-16. First Order Descending Curve Identification Procedure

This procedure is repeated for all hysterons on the discrete plane with a higher number of hysterons generating a more accurate map of the hysteresis present. Interpolation techniques can be used to calculate values in between the hysterons but this can lead to inaccuracies. A balance must be found between hysteron density and time consumption for optimal results. For example, too

few hysterons will result in inaccurate hysteresis modelling, while too many will require excessive experimental derivation time.

2.8.5 Numerical Implementation of the Forward Preisach Model

In order to numerically implement the Preisach model, a two parameter function, F(α,β) must be defined as follows:

$$F(\alpha,\beta) = y_\alpha - y_\beta \tag{2-8}$$

It can be shown that the integral over the area $H_{(\alpha1,\beta1)}$ in Figure 2-16 is equal to the difference between the output for α_1 and β_1.

$$\iint_{H_{(\alpha_1,\beta_1)}} \mu(\alpha,\beta)d\alpha d\beta = F(\alpha_1,\beta_1) \tag{2-9}$$

The set $S^1(t)$ can be subdivided into n trapezoids, Q_k, where n may vary with time.

$$\iint_{H_{(\alpha_1,\beta_1)}} \mu(\alpha,\beta)d\alpha d\beta = \sum_{k=1}^{n(t)} \iint_{Q_k(t)} \mu(\alpha,\beta)d\alpha d\beta \tag{2-10}$$

Each trapezoid Q_k can be represented as a difference of two triangles $H(M_k,m_{k-1})$ and $H(M_k,m_k)$ where M_k and m_k denote the maximum and minimum points of the input history (Figure 2-17).

Thus:

$$\iint_{Q_k(t)} \mu(\alpha,\beta)d\alpha d\beta = \iint_{H_{(M_k,m_{k-1})}} \mu(\alpha,\beta)d\alpha d\beta - \iint_{H_{(M_k,m_k)}} \mu(\alpha,\beta)d\alpha d\beta \tag{2-11}$$

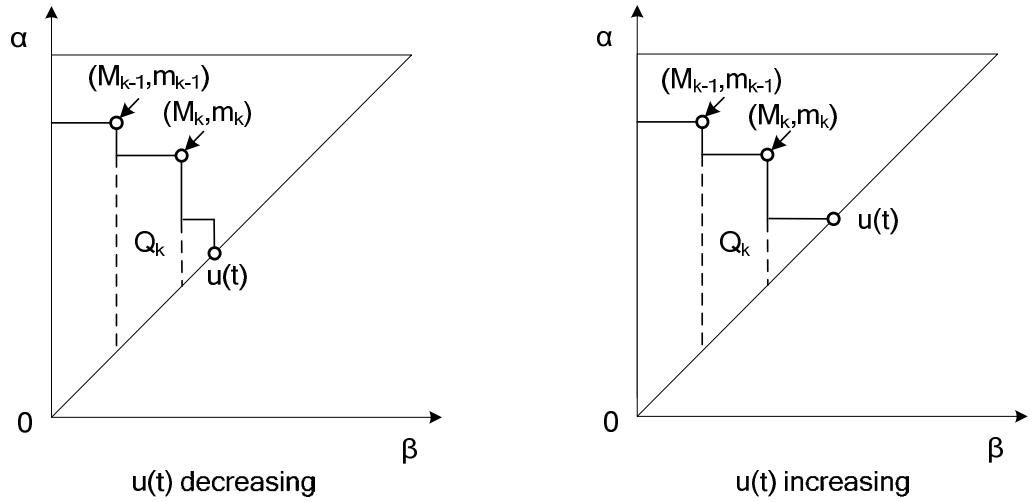

Figure 2-17. Discrete Points on the Preisach Plane

From Eq.(2-9), it can be seen that:

$$\iint_{H_{(M_k,m_{k-1})}} \mu(\alpha,\beta)d\alpha d\beta = F(M_k,m_{k-1}) \tag{2-12}$$

and

$$\iint_{H_{(M_k,m_k)}} \mu(\alpha,\beta)d\alpha d\beta = F(M_k,m_k) \tag{2-13}$$

Therefore, Eq.(2-11) can be rewritten as:

$$\iint_{Q_k(t)} \mu(\alpha,\beta)d\alpha d\beta = F(M_k,m_{k-1}) - F(M_k,m_k) \tag{2-14}$$

From Eq's *(2-7)*, *(2-10)* and (2-14), the output y(t) can be written as:

$$y(t) = \sum_{k=1}^{n(t)} F(M_k,m_{k-1}) - F(M_k,m_k) \tag{2-15}$$

In the case where the input is decreasing monotonically, the final link of the interface is vertical and m_n=u(t). If the input is increasing monotonically, the

final link is horizontal and $m_n = M_n(t) = u(t)$. Thus, Eq.(2-15) is slightly different for the decreasing and increasing cases:

u(t) decreasing monotonically:

$$y(t) = \sum_{k=1}^{n(t)-1} [F(M_k, m_{k-1}) - F(M_k, m_k)] + F(M_n, M_{n-1}) - F\big(M_n, u(t)\big) \tag{2-16}$$

u(t) *increasing monotonically*

$$y(t) = \sum_{k=1}^{n(t)-1} [F(M_k, m_{k-1}) - F(M_k, m_k)] + F(u(t), m_{n-1}) \tag{2-17}$$

The discrete Preisach model outlined is highly suitable for implementation in software using *state-machine* architecture owing to its iterative logic. A *state-machine* provides a means of programming a logical flow, with each state representing an event in the flow and executing in the millisecond range. The state-machine utilised in Section 4.7.1 takes approximately 10ms to execute one iteration of the inverse Preisach model encompassing 20 logical steps.

2.9 SMA Controller Strategies

The highly nonlinear response of SMA actuators has rendered the development of a successful controller strategy very difficult. Various groups have attempted to develop a wide variety of suitable controllers by using strategies ranging from the classical linear strategies to complex strategies featuring an inverse mathematical model of the hysteresis associated with SMAs. The following is a comprehensive review of the key developments to date in the area of SMA control.

2.9.1 Linear Control Strategies

Linear control strategies were amongst the first control strategies investigated for the control of SMA contraction owing to the relative ease of implementation. *Reynaerts and Van Brussel* studied the use of classical PID controllers in position control applications for SMA based robotic manipulators [73]. *Troisfontaine et al* experimented with a PI and PID controller for position and temperature control [100]. While this group used temperature feedback in their experiments, it must be noted that this is generally considered impractical owing to the difficultly of precisely measuring the SMA wire temperature in an open environment [71]. *Hashimoto et al* applied PD control to SMA wires on a walking biped robot [101], while *Ikuta et al* applied PID control to a segmented active endoscope consisting of SMA spring actuators using a novel approach that featured electrical resistance feedback in combination with position feedback [102]. However, the main drawback associated with linear P, PI, and PID controller strategies is that the controller performance deteriorates rapidly once outside the range of tuned gains due to the nonlinear characteristics of the SMA response [103]. *Teh and Featherstone* used antagonistic pairs of SMAs to significantly reduce any nonlinear hysteresis associated with SMAs and improved the positional speed and accuracy using a PID control strategy [41, 104]. However, this strategy relies on the use of antagonistic pairings which may not be practical in many applications.

2.9.2 Nonlinear Control Strategies

Nonlinear control strategies for SMA actuators have been attempted by various groups owing to the presence of nonlinear effects such as hysteresis in the

heating-cooling cycle and in the loading-unloading cycle. Various groups have approached the problem using a wide variety of nonlinear techniques to cancel out the negative effects of the nonlinearities. *Grant and Hayward* applied variable structure control (VSC) to a pair of antagonistic SMA actuators [105]. The controllers are based on the simple concept of switching the control input on the sign of the error. VSC requires infinitely fast switching in order for the state trajectory to follow the discontinuity surface exactly. Since infinitely fast switching is practically impossible, some level of chattering is unavoidable. *Song and Mukherjee* extended this approach by comparing two common robust compensators often used in VSC (bang-bang type and saturation type) with a smooth time varying type employing a hyperbolic tangent function [106]. The results illustrate the superiority of the smooth time varying compensator as chattering is reduced and stability is also guaranteed. However, the complex hysteretic behaviour associated with SMAs is not specifically addressed, resulting in increased error potential when applied to SMA actuator control.

Elahinia and Ashrafiuon also applied VSC in an attempt to achieve accurate positioning of a three degree of freedom combined SMA and DC motor driven robotic arm [107, 108]. Results demonstrated the possibility of effective and robust performance of the controller strategy despite significant modelling inaccuracies during controller parameter identification. However, the utilization of a DC motor in the actuator structure brings associated disadvantages (See Section 1.2.1). More recently, *Choi* attempted to demonstrate the feasibility of using a SMA spring mechanism for position control using sliding mode control [109]. Results showed good positional accuracy but with sluggish response. The

authors note that control accuracy can be further improved by using more advanced SMA materials with faster response times.

Shameli et al demonstrated that the use of a nonlinear PID-P^3 controller worked to reduce errors by modifying controller gains nonlinearly with respect to error size [110]. The cubic term within the controller works on the magnitude of the error, responding with a large additional control action to large errors while for smaller errors the cubic term tends towards zero. In comparison with nonlinear techniques which can introduce chattering into a system, the PID-P^3 approach results in a generally smooth, stable output. The group demonstrate the stability of the proposed controller, and tuning was restricted to trial-and-error only, hence replication of the results is considerably difficult.

Eren and Mavroidis developed b-spline based adaptive control (BAC) for SMA actuated robotic systems [103]. BAC is based on a hybrid of b-spline approximation, VSC, and integral control. Adaptive gain scheduling based on b-splines selects gains from a predetermined function according to the offset from the desired position and operating conditions, while an adaptive update enhances this further based on the controller performance. Experiments were carried out on a three degree of freedom robotic arm giving reasonable results. *Kumon et al* attempted to reduce computational needs of adaptive controllers by applying simple adaptive control (SAC) to an SMA actuator [111]. SAC works by tuning only one feedback gain value adaptively [112]. The controller was designed to be robust, but sufficiently simple to allow for implementation onto a microchip. Two SAC strategies were employed, one to control stiffness of the SMA based on the linear relationship between SMA stiffness and SMA electrical

resistance, the other to control positional accuracy. The position could be controlled to converge to the desired displacement, although, the authors note that the performance required further improvement in terms of speed of response.

It has been observed that the use of nonlinear control strategies which do not explicitly deal with the complex nonlinearities associated with hysteresis suffer from suboptimal SMA actuator performance. As described, some groups have attempted to account for the hysteresis by using a range of mathematical functions as compensating functions. However, the complex nature of both the major and minor loops within the hysteresis cannot be dealt with by one explicit function [76]. Hysteresis in SMAs is highly dependent on the SMA actuator historical cycles and any nonlinear strategy must be able to account for this to ensure maximum accuracy.

2.9.3 Inverse Model Based Control Strategies

The presence of hysteresis in SMA actuators, combined with the nonlinear dynamics of the response result in the need for complex controller strategies. Fortunately, methods to mathematically model hysteresis have existed since the early 20th century (See Section 2.6). This fact, combined with continual rapid developments in affordable computational processing capacity allows for the development and use of real-time enabled predictive models of hysteresis in model-based control strategies. Inverse model-based strategies utilise an inverse mathematical model of the nonlinearity to cancel out undesirable effects. These have been combined with a linear controller to increase the speed of response of the system [113].

Song et al, following on from their previous work with VSC control, developed active position control of an SMA actuated composite beam [114]. They employed a robust smooth compensator to compensate for SMA nonlinearity, to improve the transient performance and to improve stability of the system. The controller featured a feedforward term to preheat the SMAs and to compensate for environmental heat losses, and a PD controller in a feedback loop to eliminate steady state error and improve responsiveness of the system. A hyperbolic-tangent-function-based robust compensator was used to compensate for the associated hysteresis. The disadvantage of this approach lies in the fact that the compensator does not take the complex hysteretic effects such as minor loops into consideration. As a result, model accuracy is significantly reduced. They developed further upon this work by adding a feedforward neural network derived inverse hysteresis model in an attempt to further reduce the hysteretic effects [115]. A robust control strategy was used to compensate for typical uncertainties such as error in the models of the SMA hysteresis while attempting to ensure stability. However, the implementation of neural-network-derived models contain inherent drawbacks such as its "black box" nature, greater computational burden, susceptibility to over-fitting, and the empirical nature of model development [116].

Majima et al developed a control strategy consisting of a PID controller in a feedback loop combined with a feedforward element to compensate hysteresis effects [98]. The feedforward element consists of a controller input corresponding to the desired displacement which is obtained from the static phenomenological model of the SMA actuator. Results show a smooth motion over the desired displacement range with lower gains than standalone PID

control. The results are dependent on the accuracy of the mathematical model being utilised. The complex nature of SMA dynamics and the resultant complexity of the phenomenological models results in heavy computational power requirements. This is undesirable in portable devices such as prosthetics which rely on a battery source of power. Furthermore, minor hysteresis effects were ignored in this study leading to considerable inaccuracies with the model. Minor hysteresis effects must be considered in order to determine a fully accurate profile of the nonlinear response.

Briggs and Ostrowski attempted to formalise an approach for inverting out the hysteresis in SMA composites by using phenomenological models incorporated within the framework of homogenization [117]. This approach uses a modified mathematical model developed by the group to predict the SMA wire temperatures which result in a desired set of SMA contractile strain values. Results show that the overshoot is eliminated using the predictive hysteresis controller, but the rise time is greater than that associated with conventional closed-loop feedback control. Homogenization inherently compromises model accuracy which can result in increased controller effort. In addition, SMA wire temperature is extremely difficult to measure directly or to predict using analytical means due to the significant and complex influence of the surrounding environment on the SMA wire temperature [118]. The authors also note that the study did not focus on the speed of response of the system, a crucial factor for application in prosthetic devices.

More recently, *Nguyan and Ahn* used an inverse Preisach model in a feedforward loop to reduce the hysteresis effects combined with a PID

controller in a feedback loop. The PID controller works to compensate for any inaccuracies occurring as a result of limited or inaccurate data collected to populate the inverse Preisach model of hysteresis [113]. The group have also developed variations on this theme by introducing a fuzzy based inverse Preisach model to reduce modelling inaccuracies, and a fuzzy based PID tuning rule-base [113]. In other work, *Kha and Ahn* have also experimented with a similar inverse model in an Internal Model Control (IMC) strategy [99]. The values used within the proposed fuzzy system, although showing promise, were arrived at using a genetic algorithm tasked to find the optimum PID parameters. The group did not demonstrate any links to the phenomenological behaviour of the SMA actuators and relied fully on numerical results gathered using the genetic algorithm. Fuzzy rule generation appears to be based on the groups experience gained from working with SMA actuators utilising a trial-and-error approach only. Consequently, no defined methodology to optimise both the disturbance rejection and set-point tracking capability of the SMA actuator in the presence of external factors such as changes in ambient temperature or increased stress acting on the SMA wires is described.

Kumagai et al used a similar approach by adopting a neuro-fuzzy inference system to generate an SMA dynamic model used in a feedforward loop [119]. The system identification of the dynamic system is performed by observing the change of state variables when responding to a known input using ANFIS – 'Adaptive Neuro-Fuzzy Inference System'. While results show promise using ANFIS, the aforementioned disadvantages associated with neural networks still ring true.

2.9.4 Controller Review - Conclusions

A move towards inverse model based feedforward control systems combined with a PID controller in feedback (Figure 2-18) has been on-going in recent years.

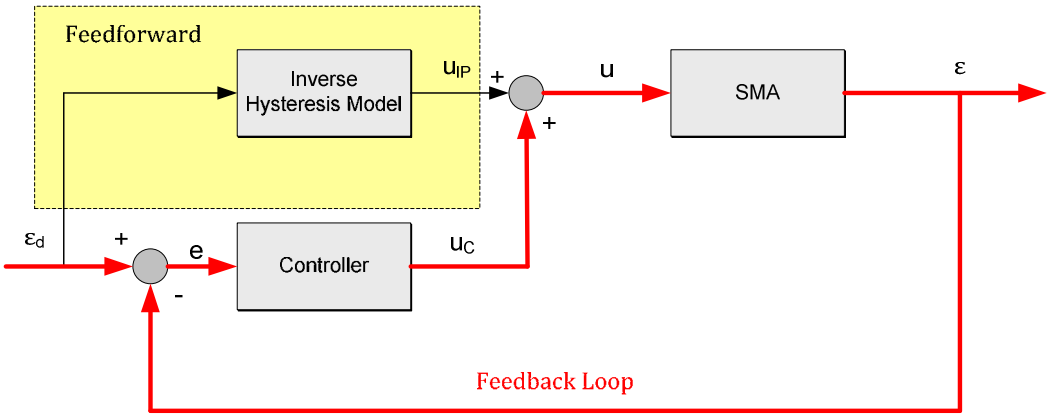

Figure 2-18. Architecture of an inverse model based feedforward control system combined with a PID controller in feedback

This is primarily due to favourable factors such as the increase in computational power available and the potential superior performance of the strategy compared to others in terms of system responsiveness (See Section 2.9.3). However, no formal tuning methodology has been identified or implemented to date for these control strategies in the literature available. Trial-and-error approaches are readily adopted, which prove difficult to replicate and leave room for improved performance. A suitable tuning methodology is vital in order to determine suitable controller values for good set-point tracking and good disturbance rejection (robustness). A series of performance criteria chosen for the specific application of SMA bundle actuators in prosthetic finger design can

be used to establish the acceptable level of set-point tracking accuracy and robustness required.

Furthermore, the proportional gain, integral time and derivative time values determined for a PID controller in the feedback loop using a tuning technique could be adapted to take into account the variation in SMA actuator response to changes in applied input current. By considering the complex thermo-mechanical behaviour of SMA actuators, it can be predicted that the response to different thermal stimuli will vary greatly. This allows for the possibility of an adaptive controller in the feedback loop charged with modifying the system PID gain values accordingly. These approaches will be presented in Chapter 6.

3. BIOMECHANICAL CHARACTERISATION OF THE HUMAN INDEX FINGER

3.1 Introduction

The human finger is a natural, complex manipulator capable of assisting in the delivery of a wide range of prehensile postures and activities [120]. The design of a functional finger prosthesis is rooted in the successful development of a suitable biomimetic mechanical system [28]. This system must be capable of mimicking human finger performance to as reasonable an extent as possible. This chapter focuses on the characterisation of the human index finger in terms of its physiology, biomechanical limits, typical angular motions and force generation capabilities exhibited during common prehensile postures. These parameters are considered to be the vital parameters required in the development of a viable prosthetic finger solution.

The values of the parameters determined can be utilised as targets for an ideal biomimetic solution. The index finger is chosen for examination as it plays a key role in all of the common prehensile postures, unlike any other finger of the human hand. Furthermore, the similarities between the movement of the index finger and the other fingers of the human hand with exception of the thumb mean that the results are easily transferrable. The work described in this chapter describes the 'analysis of human hand' section of the SMA bundle actuator design methodology adopted.

3.2 Anatomy & Physiology of the Human Index Finger

The human finger owes its structure to bones, its mobility to joints, its force generation capacity to muscles and its control to nerves [121]. The index finger consists of three small bones known as phalanges; namely the proximal, intermediate and distal phalanges. The proximal phalanx is located nearest to the hand and connected to the metacarpal bones within the palmar region of the hand. The distal phalanx is located at the tip of the finger and the intermediate phalanx is located between the proximal and distal phalanges (Figure 3-1).

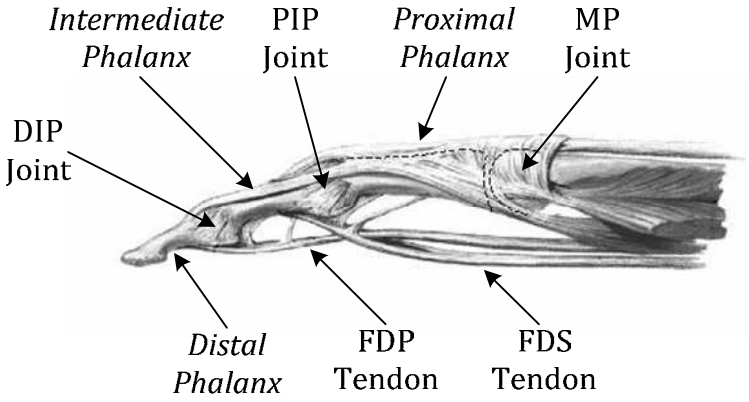

Figure 3-1. Anatomy & Physiology of the Human Index Finger [28]

The movements of the human finger can be classified in four directions; flexion (bending), extension (straightening), abduction (moving sideways away from the body), adduction (moving sideways towards the body) [122]. The scope of the current work focuses primarily on achieving flexion (and extension through antagonistic actuation) within a biomimetic mechanical finger.

The joints of the human finger are known as the MCP (metacarpo-phalangeal), PIP (proximal-interphalangeal) and DIP (distal-interphalangeal). The MCP joint

exhibits 2 degrees-of-freedom (DOF) and can be considered as a universal joint capable of all four directions of movement, while the PIP and DIP joints are 1 DOF revolute hinge joints capable of extension and flexion only [123].

Movement of the phalanges of the index finger is achieved by extrinsic muscles located within the forearm region for heavy lifting applications. Intrinsic muscles located within the palmar region of the hand and a complex tendon network exhibiting nonlinear stiffness characteristics are utilised for precision movements [52].

Finger flexion is attained by the actions of two extrinsic flexors; flexor digitorum superficialis (FDS) and flexor digitorum profundus (FDP). The anatomical arrangement of the tendons can be used to explain joint motion. The extrinsic flexors originate in the forearm, cross over multiple joints and insert into either the middle or distal phalanx. The FDP spans the MCP, PIP and DIP joints, connecting to the base of the distal phalanx, while the FDS spans the MCP and PIP joint, connecting to the base of the middle phalanx. As a result of this layout, the FDP generates motion at the MCP, PIP and DIP joints, while the FDS generates motion at the MCP and PIP joints [124].

Finger extension is achieved by extensor tendons. These extensor tendons pass over the MCP joint and branch off into medial, central, and lateral slips at the PIP joint. The central slip inserts into the base of the middle phalanx, while the medial and lateral slips pass on either side of the PIP joint, inserting into the distal phalanx [125]. The extensors mainly generate motion at the MCP and PIP joints, while extension of the DIP joint is mainly achieved by the activation of the intrinsic muscles through the extensor mechanisms [126, 127].

3.3 Prehensile Postures of the Human Hand

Prehension can be defined as "the application of functionally effective forces by the hand to an object for a task, given numerous constraints" [128]. The movements of the human hand can be divided into two main groups; prehensile movements, and non-prehensile movements [129]. Prehensile movements are those for which an object is seized or grasped and held within the compass of the hand. Non-prehensile movements do not involve grasping or seizing activity, but rather those movements whereby objects can be manipulated by pushing or lifting motions of the hand. Prehensile movements are examined within the scope of this work and as such the principal focus will remain on these.

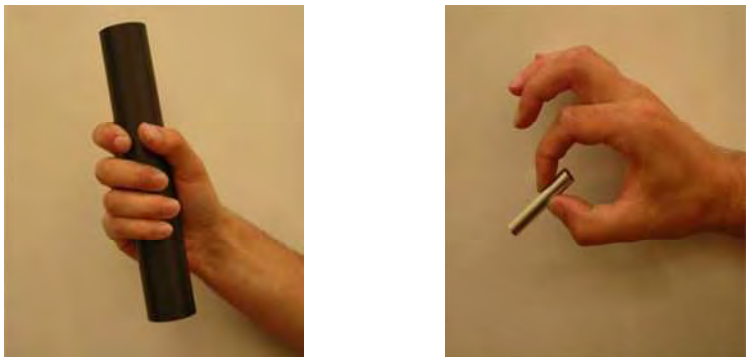

Power Grip Precision Grip

Figure 3-2. Power Grip & Precision Grip

Prehensile gripping activity has been subdivided into two broad categories referred to as the power grip, and the precision grip (Figure 3-2) [129]. The power grip clamps an object between partly flexed fingers and the palm, while the thumb applies a counter force. A precision grip pinches an object between the flexor aspects of the fingers and the opposing thumb.

Further subdivision of prehension activity into six common prehension postures includes cylindrical, tip, palmar, spherical, lateral and fully closed [130].

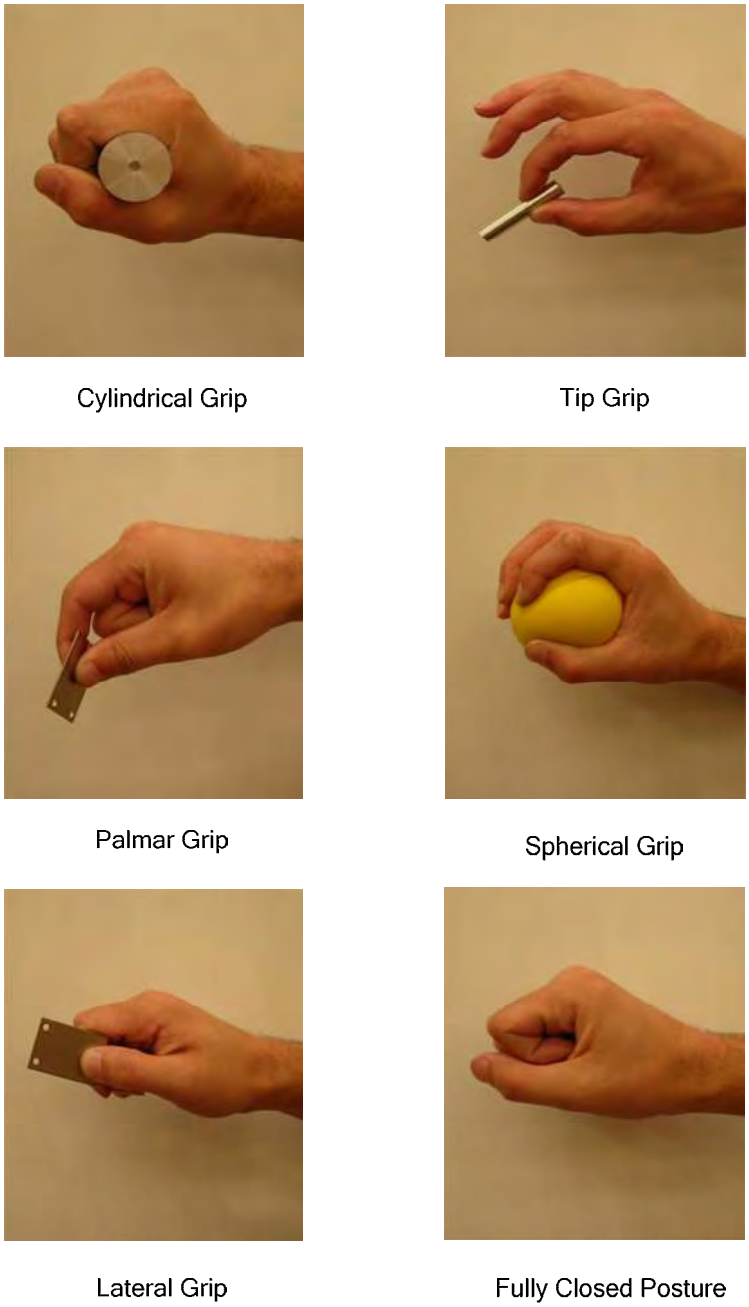

Figure 3-3. Prehension Activity Subdivision

These can be considered in order to identify common grip postures for everyday tasks (Figure 3-3). The highest prehension forces achievable are derived from a

cylindrical power grip around an object 31.7mm in diameter for the average human hand size [131]. Precision grip forces are lower due to the lower force generation capabilities of the intrinsic muscles involved in the prehensile activity.

3.3.1 The Role of the Index Finger in Identified Grip Postures

The index finger plays an important role in the formation of the six common prehension postures. The index finger and opposing thumb feature exclusively in three grip postures - the tip, palmar and lateral grip postures. The cylindrical and spherical power grips feature the index finger playing a role in conjunction with the other fingers within the hand and the opposing thumb. The fully closed grip features the index finger applying no phalanx tip forces.

It is necessary to quantify the forces and movements associated with the index finger in order to determine the required dynamic and steady state performance of the biomimetic system. Maximum force limits can be determined by examining data on cylindrical gripping activity found in the literature [131, 132]. However, the lack of available data on the index finger joints in the literature warrants further investigation into the force produced, the rotation rates, and the dynamic response of the individual joints.

3.4 Key Biomimetic Characteristics

The development of a biomimetic mechanical system relies on precise actuation capabilities in order to carry out everyday tasks successfully. Mechanical actuators produce rotation and phalanx tip force generation by actuating joints within an artificial finger which are rigidly linked to the structure of the

artificial finger. For an accurate representation of the human finger, the dynamics of each of the human finger joints must be closely mimicked by a suitably designed mechanical framework. The solution must be able to accurately reproduce the following physical actions:

i. The maximum angular displacement for each joint within the finger (degrees)
ii. The angular velocities associated with each joint within the finger (degrees/sec)
iii. The angular accelerations associated with each joint within the finger (degrees/sec^2)
iv. The maximum forces achievable within each finger joint (N)
v. The forces within each joint of the finger required for carrying out everyday activities (N)

It is therefore necessary to determine maximum values for the requirements outlined. It is also necessary to establish the physical actions associated with common prehensile movements in order to facilitate the development of a suitable controller. This controller must be capable of reproducing the movements and forces required for actions that do not require full movement and/or force generation.

3.4.1 Relevant Biomechanics of the Index Finger

The relevant biomechanics of the index finger for this work can be subdivided into phalanx forces generated and angular rotation capacity. Some of the required data, such as maximum force achievable by the complete finger and

maximum angles of rotation, has been gathered from previous work [131-134]. Data regarding angular velocity and angular acceleration associated with specific prehensile postures is unavailable within the literature. As such, experimentation to determine the necessary values is carried out. This is outlined further in Section 3.5.

3.4.1.1 Human Index Finger – Force Generation Capabilities

It has been shown by others that the average maximum force generation ability of the human hand is achieved during a cylindrical power grip posture on a 31.7mm diameter cylinder [131]. The results in terms of maximum forces applied by each phalanx in conjunction with the percentage contribution of the phalanx to the overall prehensile force are outlined in Table 3-1. As the presence of the thumb opposes the phalanx tip forces generated, based on the equilibrium of forces applied it is assumed that the finger joints produce half of the total force values recorded, whilst the thumb produces the remainder. This ensures a stable grip.

Table 3-1. Summary of maximum prehensile forces achievable in the human index finger [131, 132, 134]

Index Finger Joint	Max Force (N)	Percentage Contribution	Max Phalanx Tip Force(N)
Distal	*56.6*	*41.6*	*28.8*
Intermediate	*32.2*	*23.7*	*16.1*
Proximal	*25.8*	*19*	*12.9*
(Meta)	*(21.4)*	*(15.7)*	*(10.7)*

3.4.1.2 Human Index Finger – Angular Rotation Capacity

The maximum angular movement of each phalanx of the finger has been investigated. Previous work has shown that the maximum angle of movement of each joint in the hand does not vary much from finger to finger [132]. The angular movement of the distal interphalangeal (DIP) joints stay, on average, within 0 to 80^{o}. The proximal interphalangeal (PIP) joints stay, on average, within 0 to 100^{o} and the metacarpophalangeal (MP) joints stay, on average, within -20 to 90^{o} .

3.5 Experimental Requirements

Experiments are required to determine the angular velocities and angular accelerations associated with prehension postures. The prehensile activities are performed at a subjective medium pace. The maximum phalangeal forces associated with tip and palmar prehension postures must also be determined. Due to the differing nature of the two experiments, two separate testing setups and procedures were required.

3.5.1 Angular Motion Experimental Setup

An experimental test bed was developed featuring a National Instruments (NI) vision detection system setup capable of monitoring the movements of the human finger during a range of prehensile movements. The human finger has been outfitted with a series of white dots on black background material in order to allow for maximum contrast and ease of detection by the vision system. The dots are located on the MP, PIP and DIP joints, and on the finger tip. Each dot is partly different in shape in order to remove the possibility of crossover during

the detection process (Figure 3-4). Crossover can be defined as the system detecting a point and associating it with the incorrect joint.

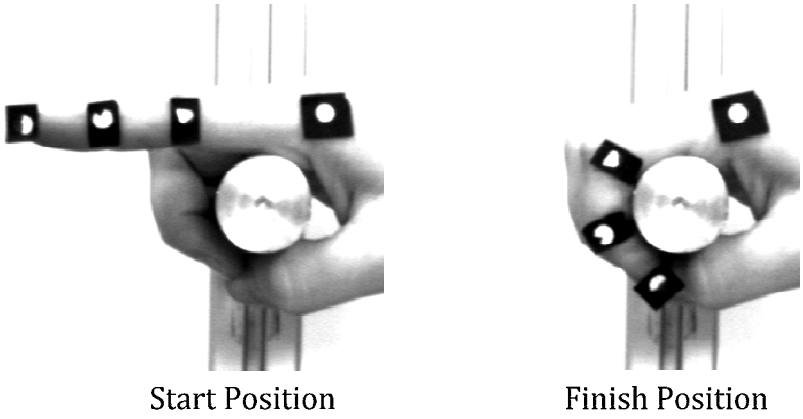

Figure 3-4. Finger Joint Detection Process – White Dots on Black Background

A rigid structure was developed providing a stable gripping point for the human hand which allows for natural and comfortable movement of the index finger. The 31.7mm cylinder is attached perpendicular to the camera, thus facilitating the centering of the camera whilst providing an optimal grip diameter for experimental work.

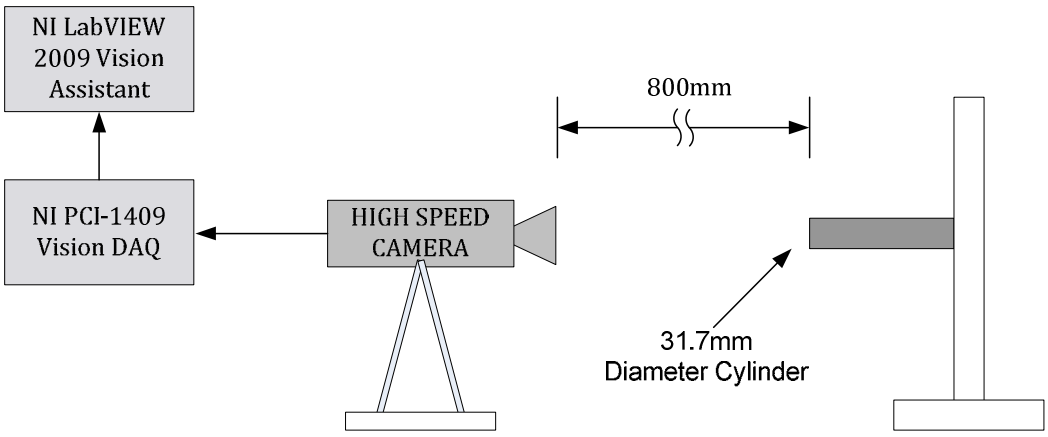

Figure 3-5. Schematic Diagram of Angular Motion Detection Test Bed

The rigid structure is located 800mm directly in front of the camera lens to aid detection of the maximum range of motion of the human finger (Figure 3-5). High speed image capturing is employed to allow for playback of the captured frames at different rates. This reduces the number of experiments required and eliminates large variations in subjective gripping rates that would be expected with a group of test subjects. All data is assimilated and compiled in NI LabVIEW 2009 via utilization of NI Vision Assistant software.

3.5.2 Angular Motion Experimental Procedure

Experimental work is required to detect the angular motion in terms of angular displacement, velocity and acceleration at each joint. The movements of the index finger during tip and palmar prehensile movements are closely matched with the only notable difference being the position of the thumb. Therefore tip and palmar prehension can be considered as one motion in terms of the movement of the index finger. The fully closed prehensile posture serves to allow experimentation featuring the maximum angular rotation at each joint.

3.5.3 Force Experimental Setup & Procedure

Measurement of prehensile force is carried out using a Vernier™ hand dynamometer capable of precisely measuring power grip and precision grip forces (Figure 3-6). The data is collected by a NI Compact-DAQ and compiled in LabVIEW 2009. The experiment is used to capture data pertaining to prehensile activities involving the direct application of force to an object. Experiments are not required for all prehensile types. Lateral grips rely on forces from the thumb acting perpendicular to the movement range of the finger.

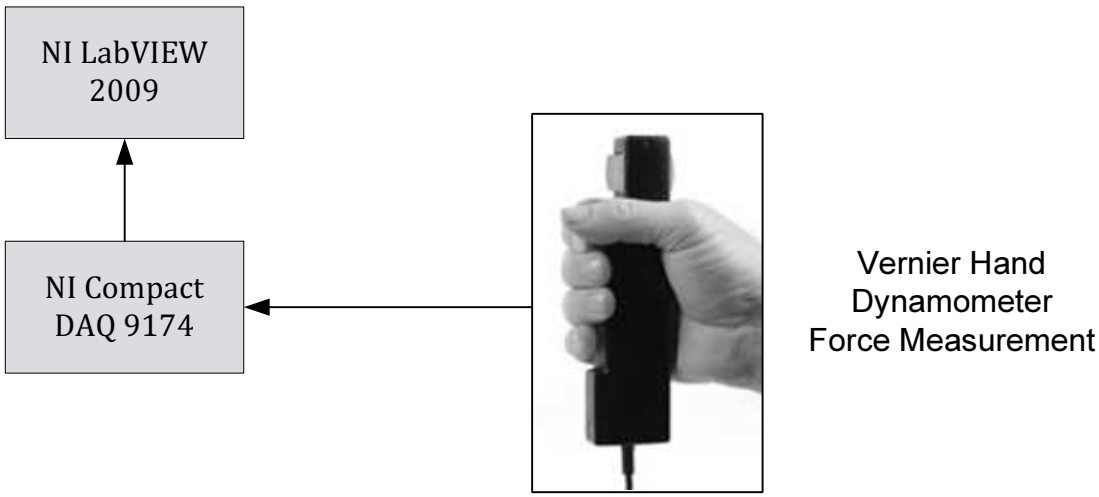

Figure 3-6. Vernier Hand Dynamometer for Grip Force Detection

The forces applied in this formation would therefore only be brought about by the rigid nature of the index finger designed without abduction or adduction capabilities. Spherical gripping relies heavily on the size and diameter of the spherical object under prehension. However, the nature of spherical prehension in terms of forces applied to the index finger is broadly similar to that of cylindrical gripping with smaller maximum forces achievable due to the offset nature of the grip forces. Therefore, the only forces required to be found explicitly from experimentation are that of tip and palmar prehensile activity.

3.5.4 Force Characterisation

The key measurand required from experimentation is steady state force. Prehensile activity during each experiment is carried out on a 20mm^2 section of the hand dynamometer. The test subject is requested to apply maximum force from the index finger of the subject's dominant hand onto the pressure pads of the hand dynamometer while being opposed by a counter pressure from the thumb. This is carried out for each predefined prehensile posture. The

experiment is divided into four sections which are conveyed to the test subject by a series of visual prompts.

i. Posture preparation – the test subject is allowed 5 seconds to prepare the correct posture on the hand dynamometer
ii. Initialization of force – the test subject is required to initialize the downward force onto the pressure pad until they reach a comfortable steady state within a 5 second window.
iii. Steady state capture – the test subject is required to hold the steady force for 15 seconds, with the average reading being taken.
iv. Release – The subject is required to fully release the hand dynamometer from their grip.

The test is carried out five times in succession in an attempt to capture the average grip force value.

3.6 Experimental Results & Discussion

The high-speed camera used to capture the various prehensile movements facilitates visual playback at different frame speeds mimicking different rates of prehensile activity. Ten subjects were used to subjectively categorize the gripping paces seen as a result of varying the frame speeds into what they would consider to be slow, medium and fast prehensile movements. All subjects were requested to eliminate movements which they considered very slow, or very fast. The results were compiled and used to establish the angular velocity and acceleration for different prehensile movements. Angular displacement limits are unaffected by different playback speeds and thus remain the same

throughout. The joint rotations can be mapped for each. The grip pace henceforth referred to as 'slow' takes between 2-4 seconds to form the desired postures (the 2 second range depends on the posture being formed as some postures require less movement and hence can be completed in shorter time periods), 'medium' pace requires 1-2 seconds to form the desired postures while 'fast' pace requires less than 1 second to form all postures.

3.6.1 Angular Motion

The angular displacement, velocity and acceleration for the MP, PIP and DIP joint of the index finger of the human hand was determined for cylindrical, fully closed, tip/palmar and lateral grip movements. Third order polynomial equations are selected by curve fitting, to approximate the path of each angular displacement at each pace.

The angular velocities and angular accelerations are derived from these polynomials resulting in the determination of all principal variables required to complete the dynamical equations of the human finger (See Section 7.9). The angular displacement profiles for the prehensile postures are outlined in Figure 3-7, Figure 3-8 and Figure 3-9. The angular displacement profiles show a max displacement occurring at the PIP joint during fully closed activity. The maximum displacement is in line with results from previous groups at approximately 90^{o} [132].

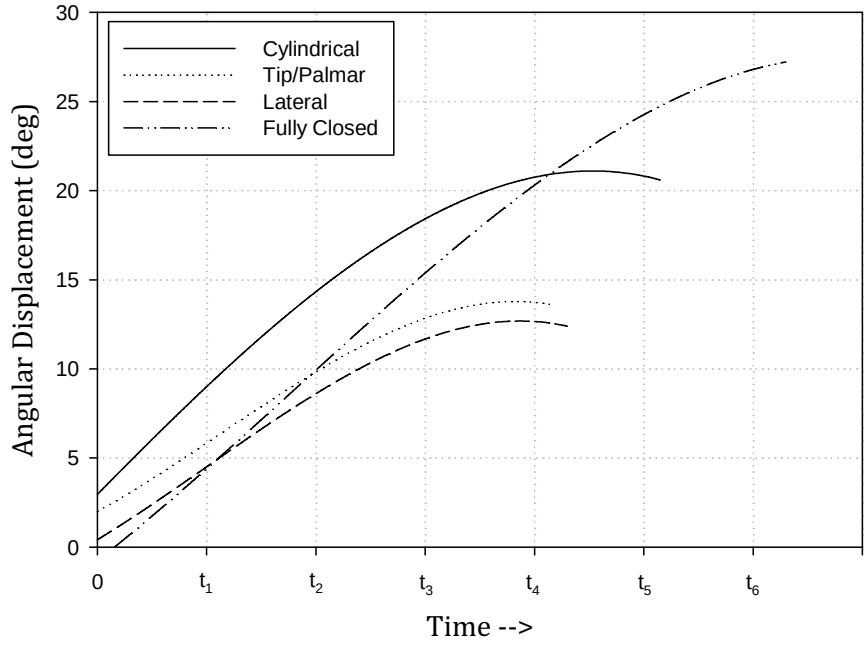

Figure 3-7. Prehensile Activities – Angular Displacement Profiles – MP Joint

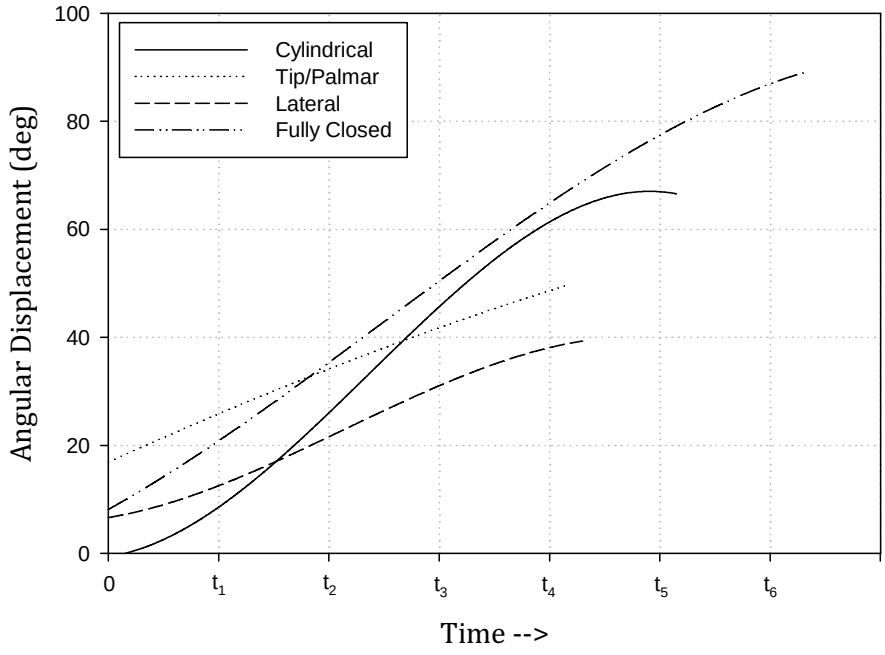

Figure 3-8. Prehensile Activities – Angular Displacement Profiles– PIP Joint

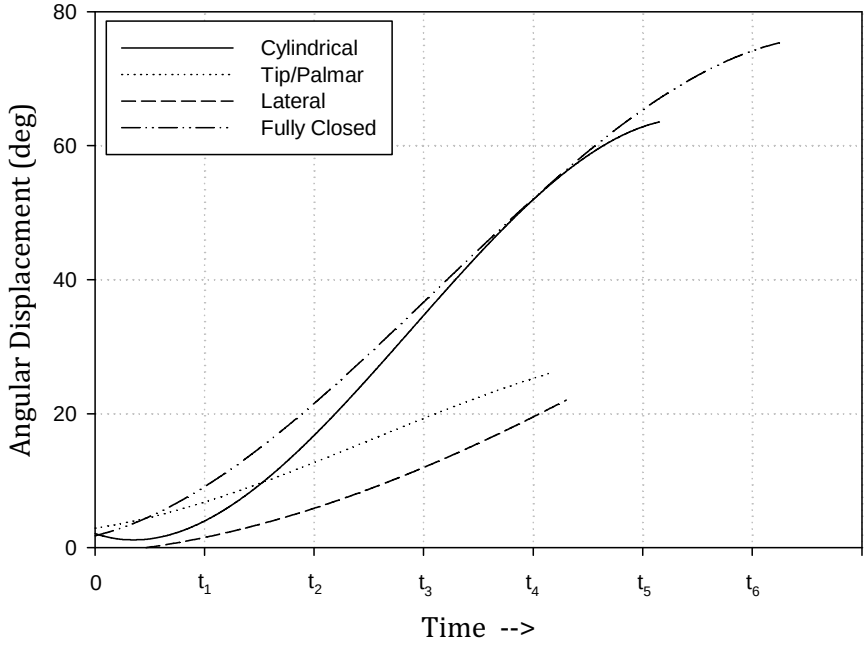

Figure 3-9. Prehensile Activities – Angular Displacement Profiles –DIP Joint

Maximum displacement values of 75.6^{o} and 27.3^{o} have been recorded at the DIP and MP joints respectively during fully closed prehensile activity (Figure 3-10). As would be expected, the faster the subjective rate of prehensile activity, the higher the angular velocity and acceleration values. The peak values for angular velocity are found in the MP joint during fully closed prehensile activity, while secondary maximum values are found at the MP and PIP joints during cylindrical prehensile movements (Figure 3-11). The maximum angular acceleration is found during cylindrical gripping activity in the PIP and DIP joints of the index finger (Figure 3-12).

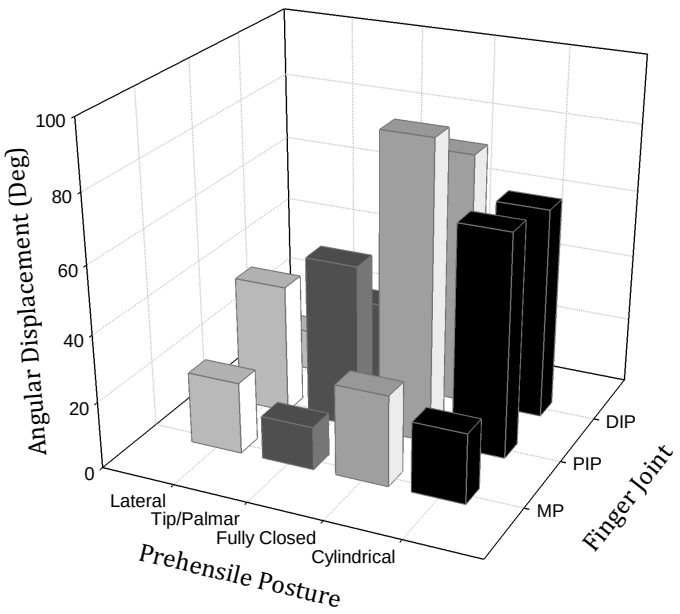

Figure 3-10. Prehensile Activities – Angular Velocity Profiles

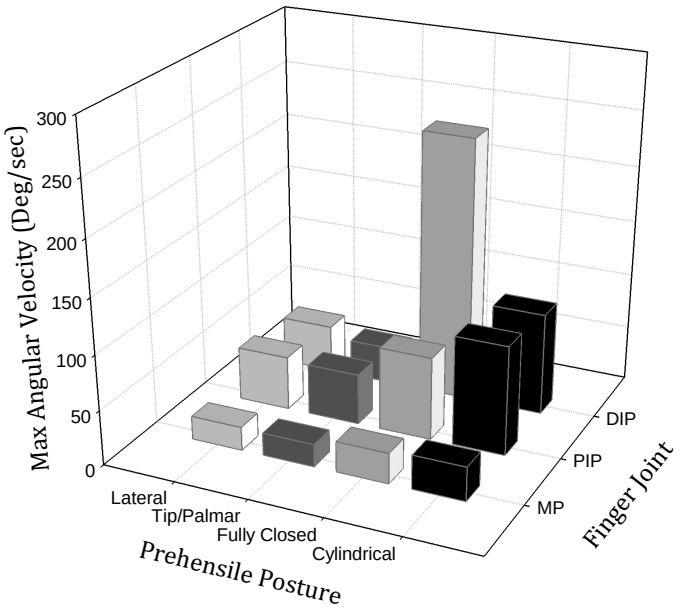

Figure 3-11. Prehensile Activities – Angular Acceleration Profiles

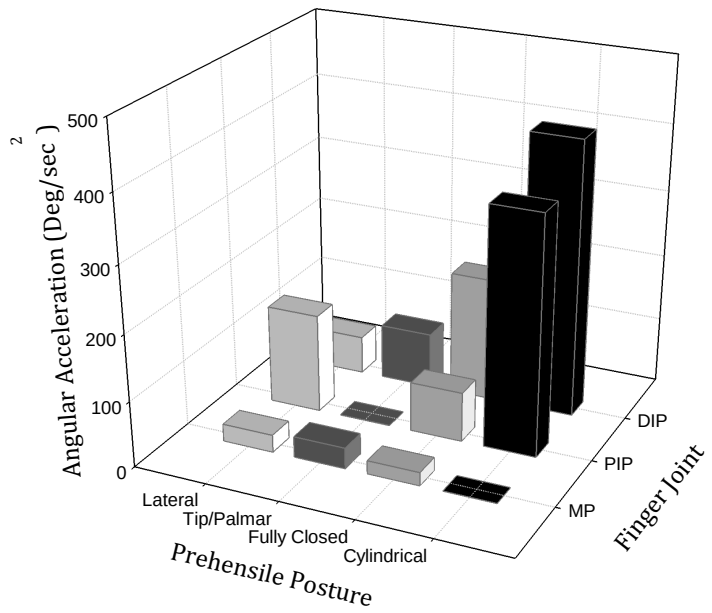

Figure 3-12. Prehensile Activities – Angular Displacement Profiles –DIP Joint

It is demonstrated that cylindrical prehensile activity demands a greater level of overall activity from the joints of the human finger. Fully closed activity places high demands on the finger joints. It can therefore be hypothesized that an artificial actuator, in a suitable mechanical prosthesis capable of mimicking the maximum angular displacement of the human finger, during fully closed posture formation, but with the ability to mimic the angular velocities and accelerations associated with cylindrical prehensile activity would suffice for all common prehensile postures and activities in terms of angular motion.

3.6.2 Force Results

The forces applied by tip and palmar prehensile postures are considerably smaller in magnitude in comparison with the forces applied during power grip postures such as the cylindrical grip. This is due to the use of smaller muscle groups within the hand for precision movements as opposed to the use of muscle groups within the forearm for power gripping activity.

It has been found that the weakest forces are delivered by the tip grip posture, with an average value of 13.26N. Palmar grip delivers a slightly larger prehensile force with an average value of 17.4N.

The precision gripping postures examined exhibit lower force generation capacities than the power gripping postures. However, within a prosthesis, the capacity to perform precision maneuvers is deemed more important than capacity to generate very large forces for power gripping activity. Successful actuator implementation involves a compromise between actuator power requirements, actuator size and acceptable force generation capacity to carry out most everyday tasks.

3.7 Conclusions

A comprehensive review of the movements and forces generated within the human index finger with relevance to prosthetic finger design has been carried out. Typical prehensile postures have been examined in order to collate data on the angular displacement, velocity and acceleration associated with each grip type. Force generation data has been collected for each grip posture from data available in the literature and through experimentation on the human index finger for forces generated during relevant prehensile postures. The data collected will be inserted into the dynamics equations of an artificial index finger to facilitate the calculation of joint torques required to mimic the behavior of the human index finger. The characterisation carried out in this chapter fulfills the analysis of the human finger and trajectory development phase of the adopted methodology.

4. MECHANICAL CHARACTERISATION OF SHAPE MEMORY ALLOY BUNDLE ACTUATORS

4.1 Chapter Introduction

An investigation into the dynamic and steady state response of SMA bundle actuators to applied input current is required. The relationships garnered during experimentation can be used in the selection and implementation of an optimal actuation solution. The vital characteristics, in relation to actuator design for prostheses, are SMA strain, SMA relaxation upon cooling and force generation capacity owing to their importance in joint rotation and phalanx tip force generation within an SMA actuated prosthetic finger solution. The mechanical characterisation phase is an important phase of the adopted design methodology. Experimental work is required to determine the optimum SMA bundle actuator make-up and response to applied input current. These outcomes play an important role in the development of a appropriate dynamic model which can be utilised in the implementation of a suitable control strategy.

4.2 Identification of Ideal Actuator Characteristics

The ideal actuator for use in prosthetic finger applications exhibits certain key characteristics as outlined in Table 4-1. At present, no actuator is known to exhibit all of these desired characteristics. As a result, efforts have been made to implement a wide range of solutions such as electromechanical actuation, pneumatic actuation, hydraulic actuation and single-wire SMA actuation with limited success (See Section 1.2.1 & 1.2.2). Single wire SMA actuators have been

shown to be inadequate owing to the low mechanical work capacity exhibited when applied to artificial joints [46]. Recently, basic investigations have been carried out using multiple parallel SMA wires acting together as a single actuator [47, 135]. These are commonly referred to as SMA bundle actuators, and have the potential to increase mechanical work at the joints dramatically. An in-depth assessment of their suitability in prosthetic finger joint actuation and their performance against other actuation solutions is required.

Table 4-1. Desirable Characteristics for an Ideal Actuator

Primary Ideal Characteristics	**Secondary Ideal Characteristics**
Ease of Integration	Small & Lightweight
Robust to Environmental Changes	Noiseless Operation
Durable over Millions of Cycles	Cheap & Abundant
High Mechanical Work Capacity	Fast Transient Response
Low Power Requirements	Controllable Response to Input
Minimum Time Delay	Minimum Moving Parts

The ideal actuator characteristics can be further classified as either primary or secondary. Primary characteristics are those that are important to the workings of the device. If the actuator performs poorly, or compensation cannot be applied to overcome associated problems, the actuator may be deemed unsuitable for the task and rejected. Secondary characteristics can be defined as those that increase the benefits and desirability of a particular form of actuator

specifically for prosthetic finger actuation. However, failure to meet or compensate for these would not immediately result in rejection of the actuation solution. In terms of prosthetic finger design, the mechanical work capabilities and transient response of ideal actuators must be able to mimic the performance of the human finger. Owing to the portable nature of a prosthetic device, low power requirements are desirable to ensure that the device can be used for long periods of time without the need for frequent battery replenishment. Prosthetics are commonly subjected to use in changing environmental conditions. It is crucial that these changing conditions do not severely impact on the integrity of the device. Information gathered has allowed for the cataloguing of key characteristics associated with human index finger performance (See Section 3.6). These are outlined in Table 4-2. An ideal actuator coupled with a suitable transmission system must closely replicate these characteristics.

Table 4-2. Key Characteristics of Human Index Finger Performance

Characteristic	**Value & Location**
Max Finger Tip Force	28.8N (Distal Joint – Cylindrical Grip)
Max Angular Displacement	90^{o} (PIP Joint)
Max Angular Velocity	≈240 deg/sec
Max Angular Acceleration	≈400 deg/sec^2
Rise Time	Fast Pace: <1s=;, Med. Pace: 1-2s; Slow Pace: 2-4s

4.3 Contrasting SMAs with Alternate Actuators

SMA bundle actuators have only emerged recently as a viable actuation technology for intelligent prosthesis design. As such, it is important to contrast their inherent characteristics with some of the more established actuation technologies for prosthetic applications (Table 4-3).

Table 4-3. Key Characteristics Actuation Comparison

Characteristic	**DC Motors**	**Pneumatic**	**SMA Bundles**
Controllable Response to Input	✓✓	×	**?**
Robust to Environmental Changes	✓✓	✓	**?**
Fast Transient Response	✓	✓	×
High Mechanical Work Capacity	✓	✓✓	**?**
Low Power Requirements	×	×	**?**
Minimum Dead Time	✓	✓	**?**
Small & Lightweight	✓	×	✓✓
Noiseless Operation	×	×	✓✓
Cheap & Abundant	×	×	✓
Durable over Millions of Cycles	×	✓	✓
Ease of Integration	×	×	✓
Minimum Moving Parts	×	×	✓
Table Key: ✓✓- *Excellent* ✓- *Good* × - *Poor* **?** – *Requires Investigation*			

DC motors offer many practical advantages such as their linear response to input, their robustness to environmental changes and their fast response to changing stimuli. However, disadvantages such as noisy operation, complex transmission systems, relative expense and durability issues can render them undesirable especially in prosthetic applications [29]. Pneumatic air muscles, such as the McKibbon muscle, have been the focus of experimental investigations as viable alternative actuators. However, they suffer from major disadvantages such as requiring a compressed air source to function and exhibiting dry friction thus making position control difficult [136]. This renders them unsuitable for portable applications such as prosthetics.

SMAs offer many advantages across the characteristic spectrum. Practically, they are the smallest and cheapest actuators offering the greatest force to weight ratio (See Section 2.3). They contain few moving parts and simple transmission systems in order to operate, resulting in lower maintenance costs. However, their nonlinear response and susceptibility to environmental temperature fluctuations can result in controllability issues which must be overcome for successful integration. Of crucial importance to prosthetic hand applications is the transient response, torque generation capabilities and power requirements of SMAs.

Provided that the unknown characteristics prove to be favorable and a suitable robust controller can be developed, SMAs offer the greatest potential for application as actuators in a prosthetic finger solution.

4.4 Identification of Key Parameters

Experimentation is required to determine the key parameters not yet available in the literature in terms of SMA bundle actuator technology. The key mechanical parameters that must be determined to facilitate successful SMA bundle actuator design for prosthetic finger applications are:

i. SMA bundle actuator steady state strain capacity

ii. SMA bundle actuator steady state force generation capacity

iii. SMA bundle actuator dynamic response to various applied input currents

iv. SMA bundle actuator response to loading

4.4.1 Experimental Test Bed Design

An experimental test bed was developed to facilitate testing of both single SMA wires and various SMA bundle sizes (Figure 4-1 & Figure 4-2). The key objective of the testing phase is to determine the unknown SMA characteristics as outlined in Table 4-3. The test bed is designed modularly to facilitate a range of experimentation. The test bed displays a highly accurate SMA strain measurement capability using a *Solartron™* LVDT. SMA force generation is carried out using a *Transducer Techniques™* 50N load cell. SMA wire temperature is measured using a 25μm k-type micro-thermocouple with a time constant of 0.1 seconds (Figure 4-3), while ambient temperature is measured using a 1mm k-type thermocouple. Voltage and current are also monitored. Data acquisition algorithms were developed in *NI LabVIEW* 9.0 to facilitate the real-time collection of data. All data is sampled at 100 samples per second. The

experimental test bed features a polycarbonate housing to ensure stable environmental conditions at room temperature (21°C).

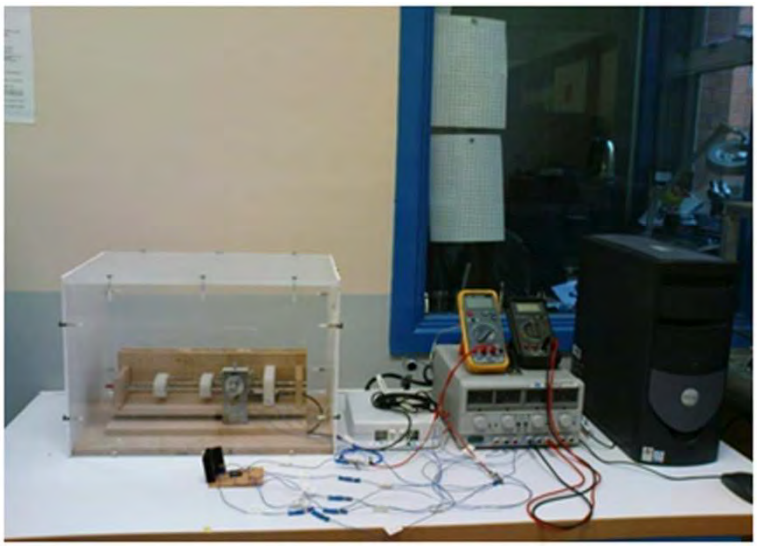

Figure 4-1. Experimental Characterisation Test-Bed

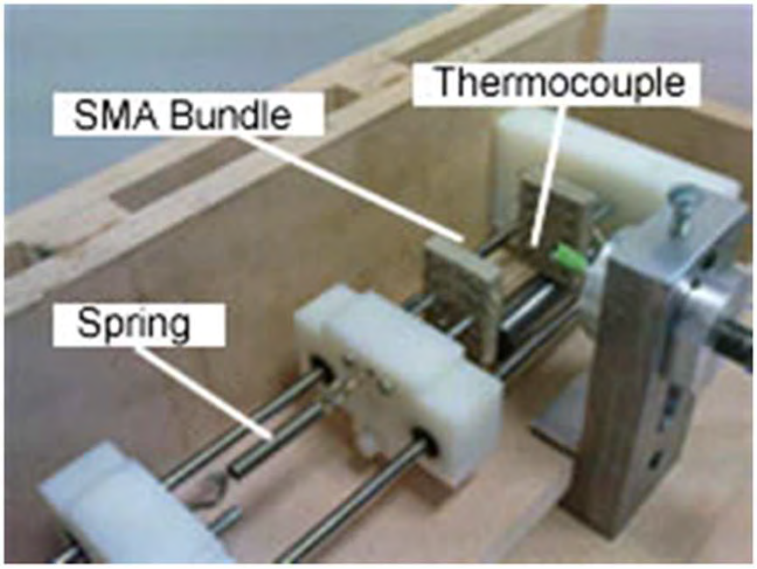

Figure 4-2. SMA Bundle and Spring Layout

The rig can be used in an open or enclosed state depending upon the nature and objectives of each individual experiment. Bundles of different sizes, and springs of different stiffness values (to provide the relaxation force required) can be

inserted to cater for a range of tests. A schematic diagram of the test bed is outlined in Figure 4-4.

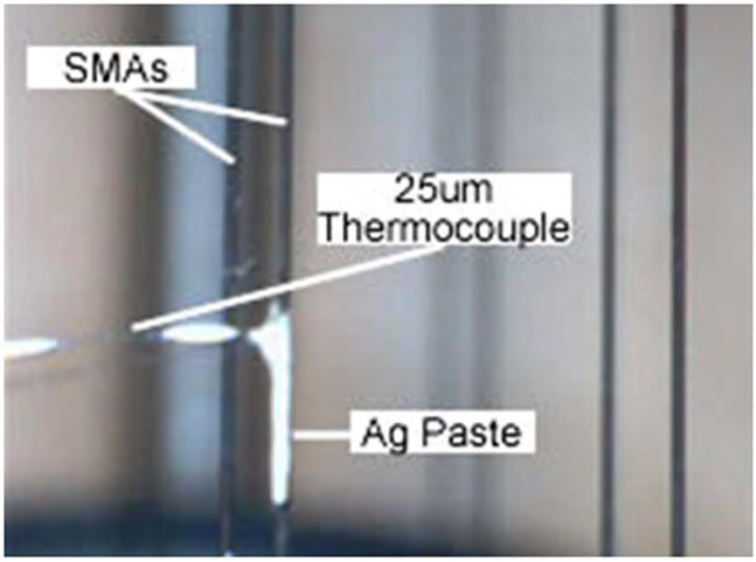

Figure 4-3. SMA Thermocouple Attachment

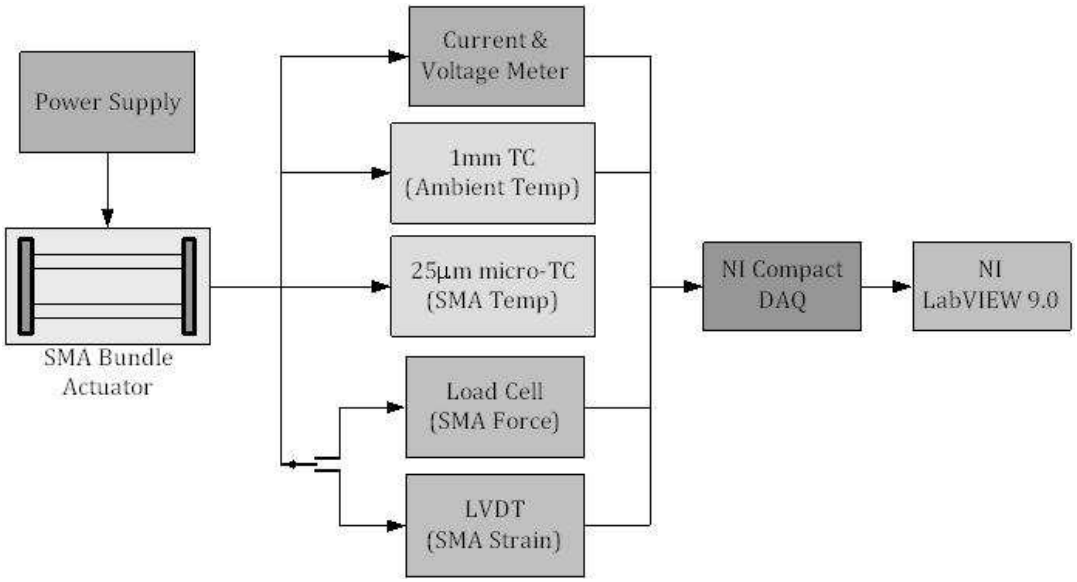

Figure 4-4. Schematic Diagram of Experimental Characterisation Test Bed

SMA bundles in the test bed are heated via joule heating, a result of passing an electrical current through the wires. As the SMA bundles undergo phase change, their electrical resistivity changes. This can lead to fluctuating currents,

resulting in inaccurate results. In order to overcome this problem and maintain constant current, a current regulation circuit was designed and implemented. The circuit diagram is detailed in Figure 4-5.

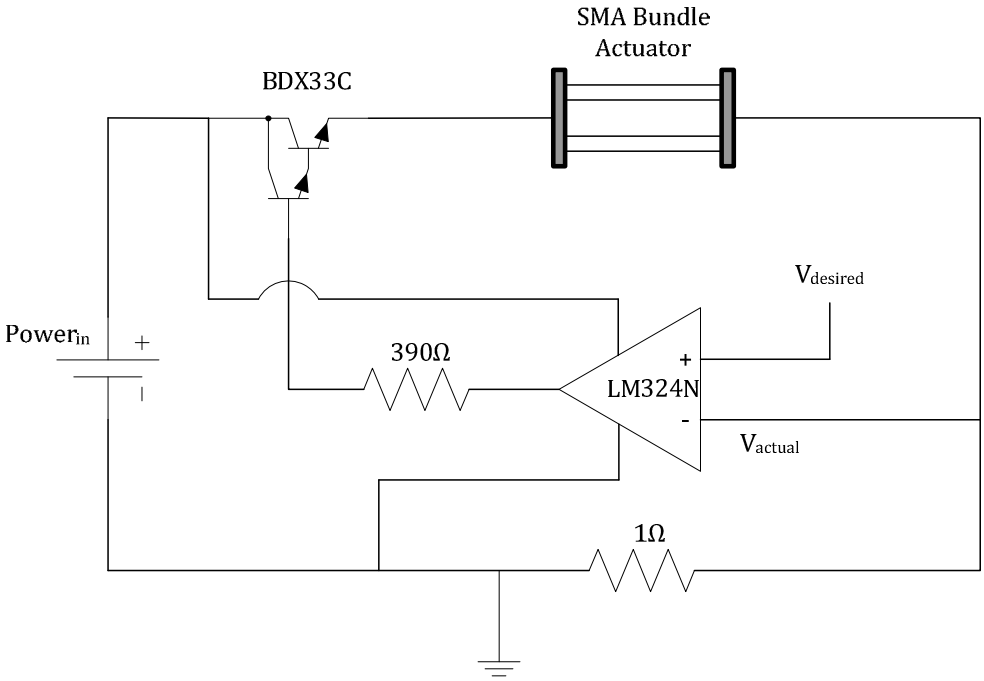

Figure 4-5. Implemented Current Regulation Circuit

The current regulation circuit utilises a LM324N operational amplifier to compare '$V_{desired}$' and 'V_{actual} across the SMA bundle actuator'. As the resistance in the SMA wires changes due to the effect of phase transformation, V_{actual} decreases. The difference between $V_{desired}$ and V_{actual} is amplified by the LM324N operational amplifier. The output is connected to the base of a BDX33C power transistor. Manipulation of the base current facilitates a decrease in current flowing through the SMA bundle actuator. The circuit uses a range of components rated for high power throughput and a suitable heat sink to prevent overheating and further inaccuracies in the testing procedure.

4.5 SMA Bundle Actuator Configuration

Identification of the optimum SMA bundle configuration in terms of wire length & diameter, wire quantity and bundle layout is required for the prosthesis design. This is in keeping with the specified actuator design methodology detailed in Section 1.7.

4.5.1 Experimental Setup

Steady state and transient SMA strain & force, and SMA wire temperature are required from testing owing to their influence on actuator make-up and selection (Table 4-4).

Table 4-4. SMA Characterisation Experimentation Summary

Test Ref.	SMA Diameter	Number of Wires	Input Current	Variable	Focus of Testing
MC1	150 μm	3,6,9, 12,15	400 mA	Force	Steady State
MC2	300 μm	3,6,9, 12,15	1750 mA	Force	Steady State
MC3	150 μm	3,6,9, 12,15	400 mA	Strain	Steady State
MC4	300 μm	3,6,9, 12,15	1750 mA	Strain	Steady State
MC5	150 μm	8	0-400 mA	Force	Steady State & Transient
MC6	150 μm	8	0-400 mA	Strain	Steady State & Transient
MC7	150 μm	8	0-400 mA	SMA Temp	Steady State

Flexinol SMA bundles consisting of various quantities of 150μm and 300μm wires were tested. The wire bundles are connected electrically in series, and mechanically in parallel to maximize force generation. The maximum safe currents for the selected SMA wire diameters recommended by the manufacturers of 400mA for the 150μm wires and 1.75A for the 300μm wires were strictly adhered to [42].

4.5.2 Experimental Procedure

Steady state characterisation of the force and strain capabilities of different SMA bundle actuators is carried out initially. The SMA bundle length of 66mm was chosen as it is the maximum length of actuator that can be inserted into the palmar region of an artificial hand (See Section 7.4). For tests MC1-MC4, the maximum safe input current is applied to the wires only. This facilitates the generation of the maximum force and strain potential of each SMA bundle actuator arrangement. Following the design of an artificial finger solution, this data will allow for the specification of appropriate SMA wire quantities for each joint within the finger. Experiments MC5-MC7 focused on the dynamic force capacity, dynamic strain capacity, and thermal characteristics of the SMA bundle actuators under investigation. The experimentation procedure follows a heat-cool cycle to facilitate a full investigation of the transient characteristics. The experiment features a 30 second heating period, allowing the system to come to steady state, prior to initiating the cooling period, by removing the input current. For the 150μm wires, consistent drops in applied input current from the maximum to minimum value specified for each test was used. This was done to ensure consistency in the experimental procedure. The ambient temperature

inside the test chamber remained steady at 21°C throughout the testing phase and was monitored continuously to ensure consistency in testing.

4.5.3 Results & Discussion

The results can be assimilated in terms of the steady state and transient capacity of the SMA bundle actuators. A successful SMA bundle actuator solution for prosthetic finger design must exhibit the optimum combination of steady state and transient performance, whilst having the lowest input power requirements.

4.5.3.1 Steady State Capacity of SMAs

Steady state force generation capability of SMA bundle actuators is vital in producing adequate mechanical work at the joints of an artificial finger. This allows for the artificial finger to perform rotational and prehensile movements. From Section 3.4.1.1, it can be seen that the maximum phalanx tip force generated in the index finger occurs in the distal phalanx where up to 28.8N of force is observed.

SMA bundles featuring 8×150μm diameter SMA wires have shown to generate approximately 32N of contractile force under maximum input current levels (approximately 4N per SMA wire). Bundles of 8 SMA wires, each 300μm in diameter, have been shown to generate approximately 128N in contractile force (approximately 16N per SMA wire). The forces decrease with decreasing input current values (Figure 4-6).

As expected, the wires with the larger diameters produce greater force. However, the input power required to heat the wires to the appropriate

temperatures to produce adequate forces increases by the square of the ratio of the diameter of the large SMA wire to the smaller SMA wire. Therefore, the power required to adequately heat the 300μm SMA wires is four times that required to heat the 150μm SMA wires. Thus, the force generated by the SMAs per unit input power is approximately equal across the range of wire diameters. As a result, the vital element to consider in the selection of appropriate SMA wire quantities is the transient response to applied input current.

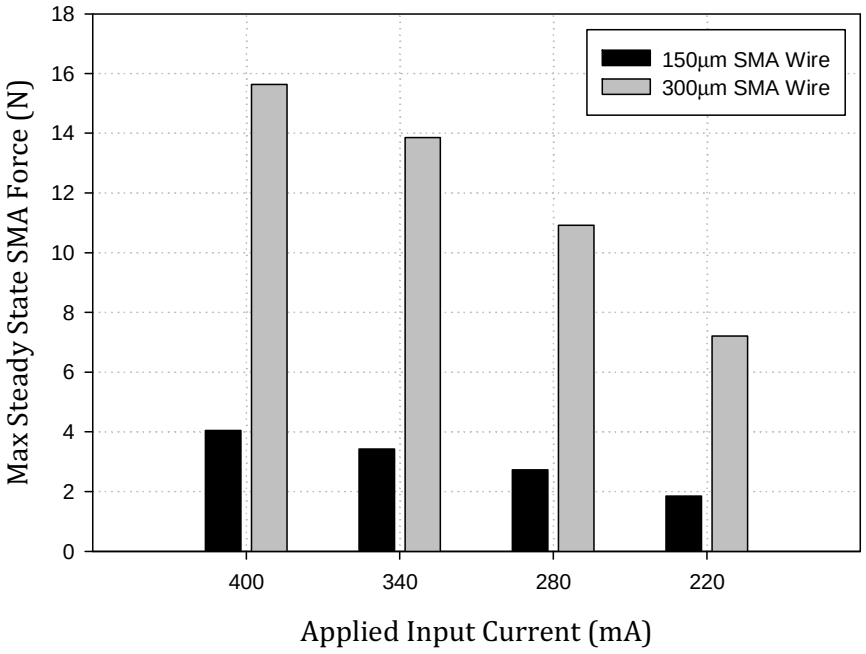

Figure 4-6. 150μm and 300μm SMAs – Steady State Force Generation per Wire

Maximum strain is independent of wire diameter. This variable is directly linked to SMA bundle length. Under maximum current input, the maximum contractile strain observed in the SMA bundles is approximately 3.6%, and is independent of SMA wire quantity within the bundle. It can be concluded that, during actuator design for a prosthetic solution, it is preferable to implement SMA

bundle actuators of maximum possible length in order to allow the highest possible levels of strain to occur.

4.5.3.2 Dynamic Capacity of SMAs – Maximum Input Current

The dynamic strain response of SMAs is directly related to the applied rate of heating or rate of cooling. Experiments to determine the optimum SMA bundle arrangement based on the dynamic capacity of the SMAs were conducted. 150μm and 300μm SMA bundles were evaluated using input currents up to the maximum safe recommended currents of 400mA and 1.75A respectively [42].

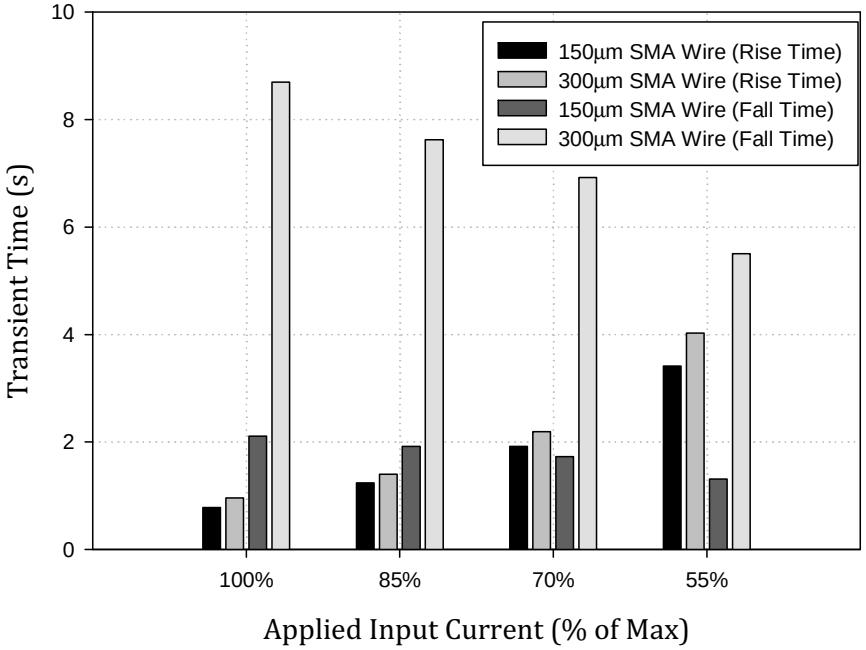

Figure 4-7. Transient capacity of 150μm and 300μm SMA Bundle Actuators

Results show that SMA bundle actuators comprising of multiple 300μm diameter SMA wires exhibit similar performance in terms of strain response during heating activity when compared with the 150μm diameter wires. However, the 300μm diameter wires exhibit severely diminished performance

during natural cooling activity with significant relaxation times evident (Figure 4-7). It is evident that as the applied input current increases, the cooling time also increases. Larger applied input currents result in higher steady state temperatures being achieved in the SMA wires. Consequently, the time taken to cool is increased. It can be seen also that the difference between heating and cooling times is less extreme when smaller SMA wire diameters are used. This is a result of the decreased surface area to volume ratio of larger diameter SMA wires which affects the cooling response. This will be explored further in Chapter 5. By comparing the performance of both SMA wire sizes, it can be seen that the 150μm diameter wires provide the better option in terms of delivering a responsiveness that is comparable to that of the human finger.

The required quantity of SMA wires per bundle is dependent upon the work required from the actuator during motion or gripping tasks involving the prosthetic finger design (See Section 3.6).

4.5.3.3 Dynamic Capabilities of SMAs – Varied Parameters

The dynamic performance of SMA bundle actuators is a function of the thermal response of the SMA wires. It is necessary to investigate the effects of this on the dynamic performance of the SMA bundle actuator as the thermo-mechanical relationship has been shown to be highly nonlinear and complex (See Section 2.7). Experiments are required to determine the effect of varying both SMA wire quantity per bundle and applied input current. The results gathered will allow for the basis of the nonlinear relationship between applied input current and resultant SMA bundle strain, and SMA bundle force generation to be established. Experiments were carried out on 150μm SMA bundles owing to their suitability

for prosthetic finger applications. The testing procedure consisted of applying various input currents to SMA bundle actuators of different wire quantities until steady state was established. Subsequently, the heated SMA wires were allowed to cool via natural cooling.

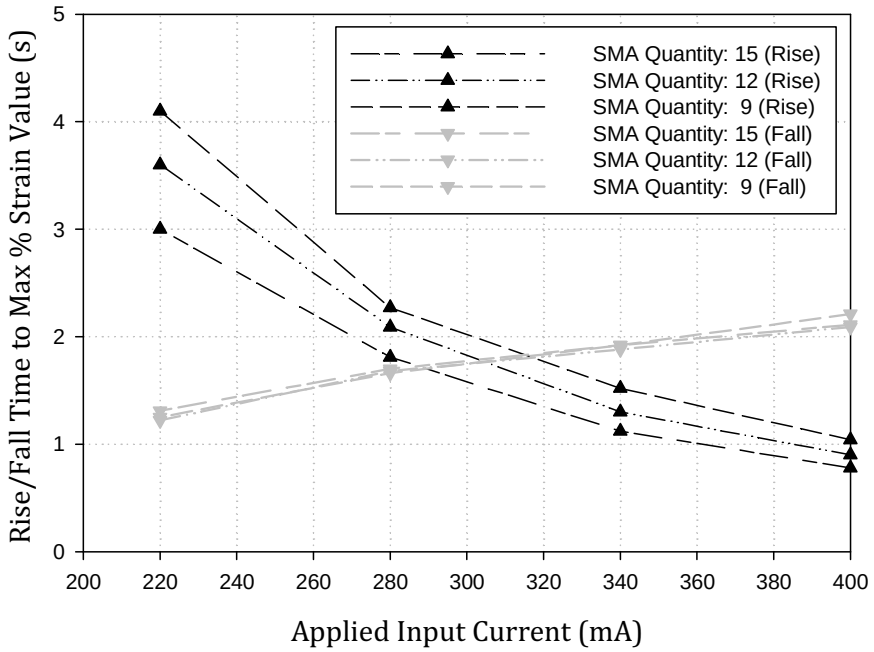

Figure 4-8. 150µm SMA Wire Experimentation - Various Numbers of SMAs

Results show that SMA bundle actuators featuring higher quantities of SMA wires responded faster during the heating phase than those featuring relatively few wires under equal loading conditions (Figure 4-8). The faster response can be attributed to the larger quantity of wires within the bundle producing a larger force and hence overcoming the force applied by the relaxation spring with greater ease. It is important to note that for consistent results, the current remains constant while power increases proportionally with the increase in SMA wires per bundle. Constant current supply to the SMA wires was achieved by implementing the Joule heating circuit as outlined in Figure 4-5.

Results indicate that SMA wire bundles of fifteen 150μm wires can exhibit a rise time of approximately 0.7 seconds under maximum applied input current of 400mA. This is within the specifications of a 'fast' gripping pace associated with the human index finger which has been established to be <1 seconds (Table 4-2). As the number of wires within the SMA bundle is decreased, an increase in rise time for the maximum input power, $\dot{Q}_{max}$, is evidenced. The increase follows an almost linear increase of approximately 0.05 seconds in rise time for every additional wire taken from the SMA bundle actuator. It can be seen that decreasing the applied input current to a fixed SMA bundle actuator size results in a highly nonlinear output in both the transient and steady state regions of the open loop strain response profile during the heating (Figure 4-9) and cooling (Figure 4-10) periods.

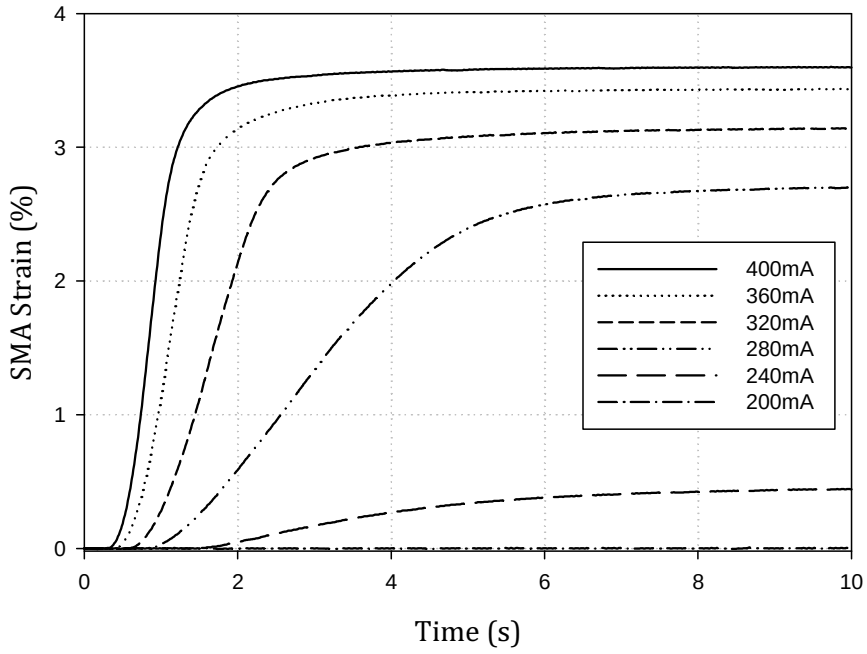

Figure 4-9. Open Loop Strain Response of 8-wire SMA Bundle Actuator during Heating

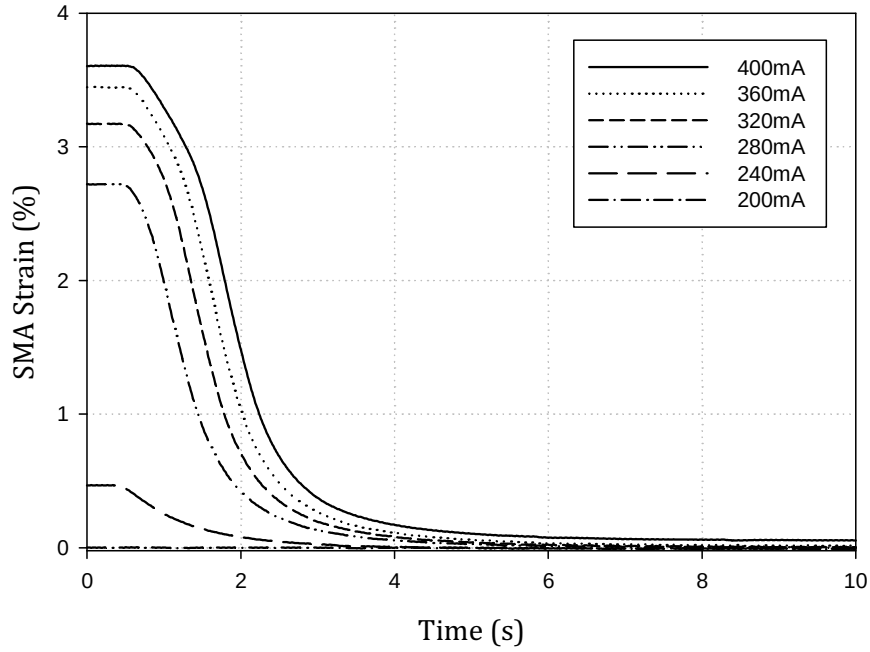

Figure 4-10. Open Loop Strain Response of 8-wire SMA Bundle Actuator during Cooling

It is noted that as applied input current is reduced, the time delay prior to SMA strain activity increases, the rise time increases and the steady state strain value decreases in a nonlinear fashion (Figure 4-9 & Figure 4-10). During cooling activity, the relaxation of the SMA bundle actuators occurs at approximately the same rate as each SMA wire is cooled to ambient temperature. This response observed during both the heating and cooling phase can be linked directly to the thermal characteristics of the SMA bundle actuators (See Section 2.7).

4.6 Heating-Cooling Hysteresis Identification

It can be noted from Section 4.5.3 that the steady state strain capabilities of SMA bundle actuators subjected to various applied input currents are highly nonlinear. A severe hysteresis is present as a result of the differences in phase transformation temperatures for the martensite-to-austenite transformation,

and the austenite-to-martensite transformation (See Chapter 5). The hysteresis can be identified using applied current as the input and SMA strain as the measured output. Hysteresis introduces nonlinearity into the system and is considered highly undesirable in terms of linear control system design as it can lead to severe inaccuracies [91]. It is therefore crucial to account for the hysteresis effects during the design of a suitable control strategy.

The Preisach model of hysteresis can be used to successfully eliminate the effects of hysteresis out of a system when applied in its inverse form [90, 99, 137]. The Preisach model is a numerically derived model which relies on accurate identification of the hysteresis in order to successfully eliminate hysteresis. As such, great care must be taken to avoid inaccurate characterisation.

4.6.1 Experimental Procedure

The typical empirical data collection methodology for hysteresis identification is employed [94]. The input profile outlined in Figure 4-11 is selected as it ensures that all combinations of step inputs are utilised during Preisach plane data population. A trade-off between hysteresis accuracy and data collection time is required, with numerical interpolation techniques available to estimate the undefined points. The inputs to the hysteresis can be defined as the ON-current, α, and the OFF-current, β (See Section 2.8). The steady state strain values are the outputs of the system. It is important to ensure that the experimental procedure permits enough time for the system to reach steady state for each applied input current for maximum accuracy.

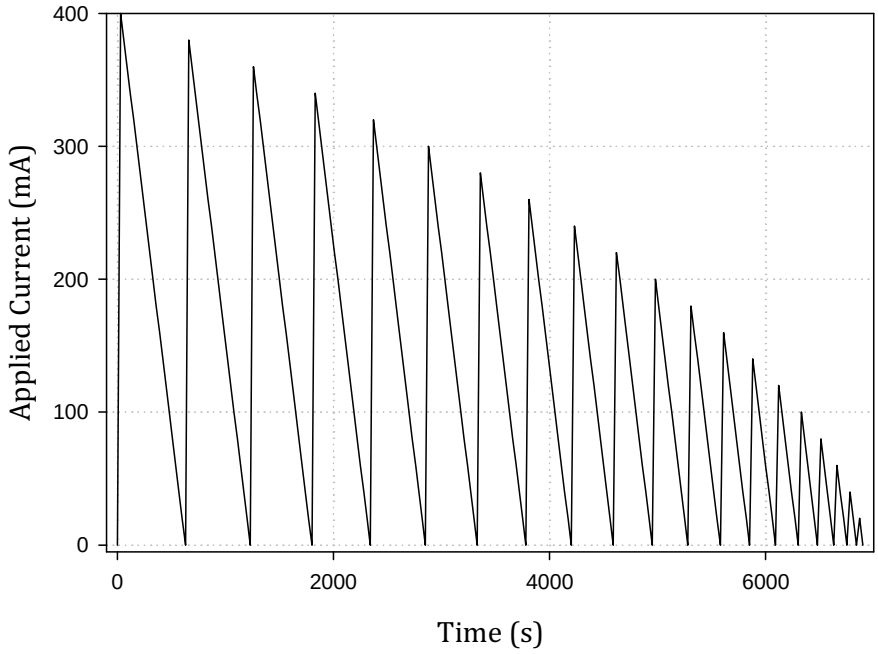

Figure 4-11. Experimental Procedure to Identify SMA Bundle Actuator Hysteresis

4.6.2 Results & Discussion

Data collected from the empirical data experimentation stage is compiled to illustrate the nature of the hysteresis for SMA strain per wire of the 150μm SMA bundle actuators (See Figure 4-12 and Figure 4-13). The α and β values are located on the x and y axes respectively, whilst the variable under measurement is displayed on the z axis to demonstrate the profile of the hysteresis. Furthermore, a two dimensional reference is outlined for each variable which shows the major and minor hysteresis loops associated with using different α and β values (Eq.(2-8)). The results illustrate the severity of the hysteresis associated with the heating and cooling cycles. The data values collected can be used to generate a model of the hysteresis, relating input current to SMA strain.

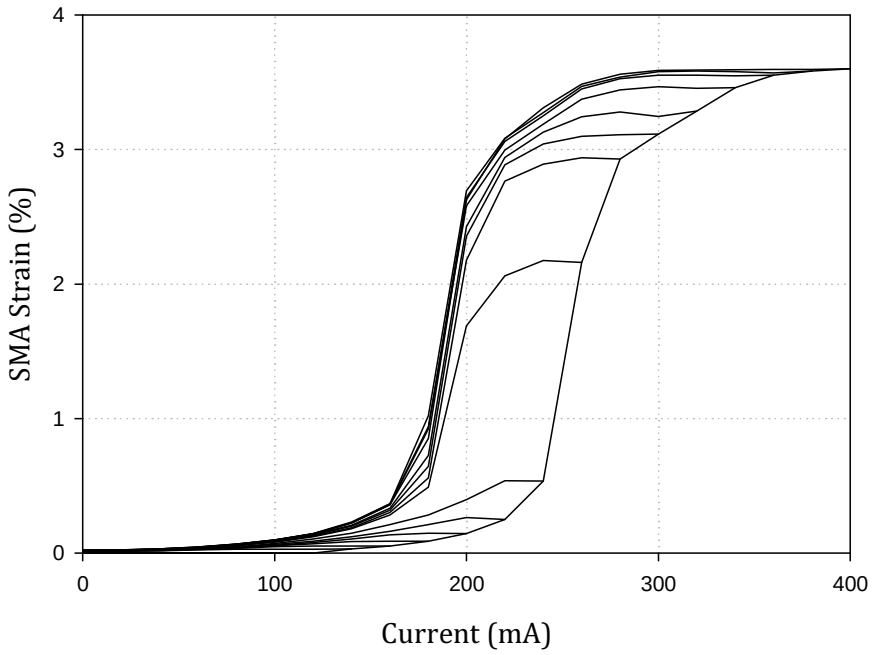

Figure 4-12. Major and Minor Loops of SMA Strain Hysteresis

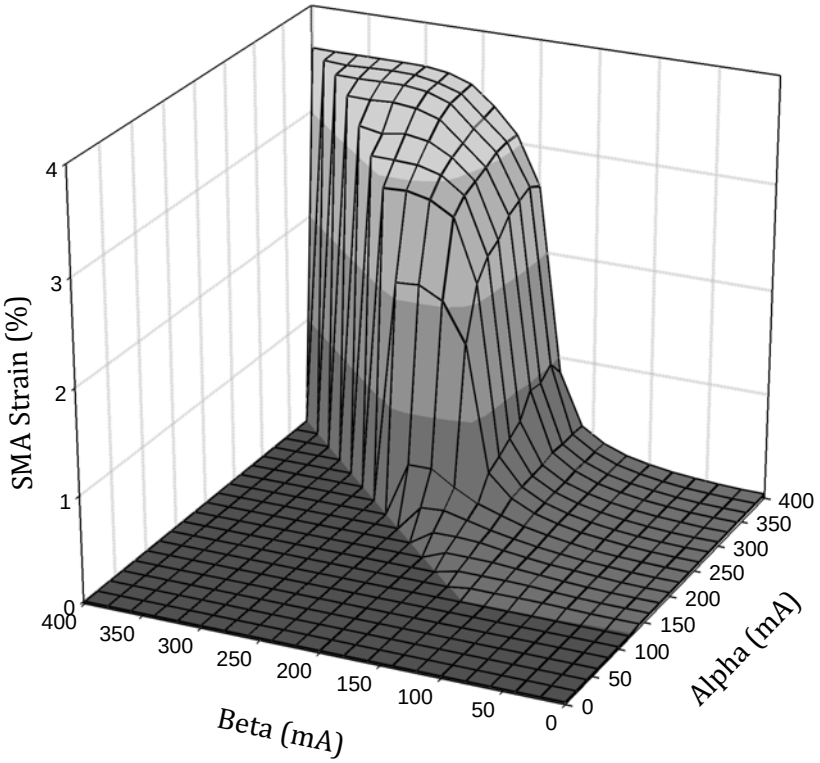

Figure 4-13. SMA Strain Hysteresis – 3D Representation

From the hysteresis outlined in Figure 4-12 & Figure 4-13, it is evident that the vast majority of the strain occurs over a narrow range of applied input current values, from approximately 160mA to 300mA. Furthermore, it can also be seen that minor changes to input current values within this narrow range leads to relatively large changes in SMA strain. It can be concluded that the sensitivity of the system is much greater in this range. A suitable control strategy is required to account for the sensitivity. This is considered further in Chapter 6. While the Preisach hysteresis model provides good detail on the relationship between input current and steady state output of the SMA bundle actuator, it does not provide any details on the nature of the dynamic response of the system. Therefore, it is evident that a model must be developed from which suitable controller gain values can be derived to facilitate optimum performance of the SMA bundle actuator.

4.7 Dynamic Model of SMA Bundle Actuators

A transfer function model of SMA bundle actuators describing the dynamic relationship between input current and output contractile strain can be found directly from experiments carried out in Section 4.5.3. The SMA bundle actuator can be modelled by a transfer function, G(s) which satisfies [41]

$$\varepsilon(s) = I(s)G(s) \tag{4-1}$$

Previous groups have noted the response to exhibit first order characteristics [29, 41, 105]. The experimental results show good alignment with this hypothesis. However unlike strongly linear systems, the first order variables of the transfer function, G(s), such as the gain, K, and the time constant, τ, are not

consistent across the full range of applied input currents. Additionally it is evident that a time delay is present which decreases as the applied input current value is increased. A time delay can be defined as 'the time interval between a change in the input signal to a process control system and the response to the signal' [138]. It is highly undesirable in prosthetic finger design. Therefore, the most appropriate general expression chosen for the transfer function is a first order plus time delay (FOPTD) model

$$G(s) = \frac{K(i)}{s\tau(i) + 1} e^{-T_d(i)s} \tag{4-2}$$

The effective selection, design and tuning of an appropriate controller in model-based control applications is dependent on having an accurate model of the system [138]. The dynamic response of a nonlinear FOPTD system exhibits varying K, τ and T_d values. The selection of fixed values for the three variables can lead to model and control inaccuracies. Each of the transfer function variables can be found by investigating the open loop mechanical and open loop thermal responses of the system. The work carried out in developing the Preisach model of hysteresis will serve as a basis for establishing the gain, K. The time constant, τ, and time delay, T_d, are strongly linked to the thermal response of the system and hence will be investigated further in Chapter 5. The complete model will be presented and compared with the system response in Chapter 6.

4.7.1 Dynamic Model - Gain

The gain, K, can be established by developing a computationally fast inversion of the Preisach hysteresis model. Importantly, this takes into account any

historical effects owing to the hysteresis which is essential if accurate SMA strain performance is desired.

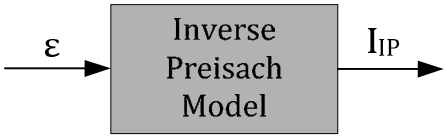

Figure 4-14. Inverse Preisach Block Diagram Representation

In the case of a descending input value, where the new desired input is smaller than the previous desired value, the input can be determined from

$$F(M_n, u(t)) = \sum_{k=1}^{n(t)-1} \left[F(M_{k,} m_{k-1}) - F(M_{k,} m_k)\right] + F(M_{n,} m_{n-1}) - y_d(t) \tag{4-3}$$

where $y_d(t)$ is the desired output value. Therefore, solving for u(t) as β gives

$$u(t) = \beta = G^{-1}\left[M_n\,, \left[F(M_{k,} m_{k-1}) - F(M_{k,} m_k) + F(M_{n,} m_{n-1})\right] - y_d(t)\right] \tag{4-4}$$

where G^{-1} is the inverse Preisach function. In the case of an increasing input value, the input can be determined from

$$F(u(t), m_{n-1}) = y_d(t) - \sum_{k=1}^{n(t)-1} \left[F(M_{k,} m_{k-1}) - F(M_{k,} m_k)\right] \tag{4-5}$$

Therefore solving for u(t) as α

$$u(t) = \alpha = G^{-1}\left[M_{n-1}\,, y_d(t) - \left[F(M_{k,} m_{k-1}) - F(M_{k,} m_k)\right]\right] \tag{4-6}$$

In a similar fashion to the forward case, the inverse can be chosen depending on whether the desired output is increasing (α) or decreasing (β).

On the Preisach plane representation, in the case of $y_d(t)$ *decreasing, it* can be seen that the required β value at instant *k*, β(k), can be calculated along line *s* (Figure 4-15).

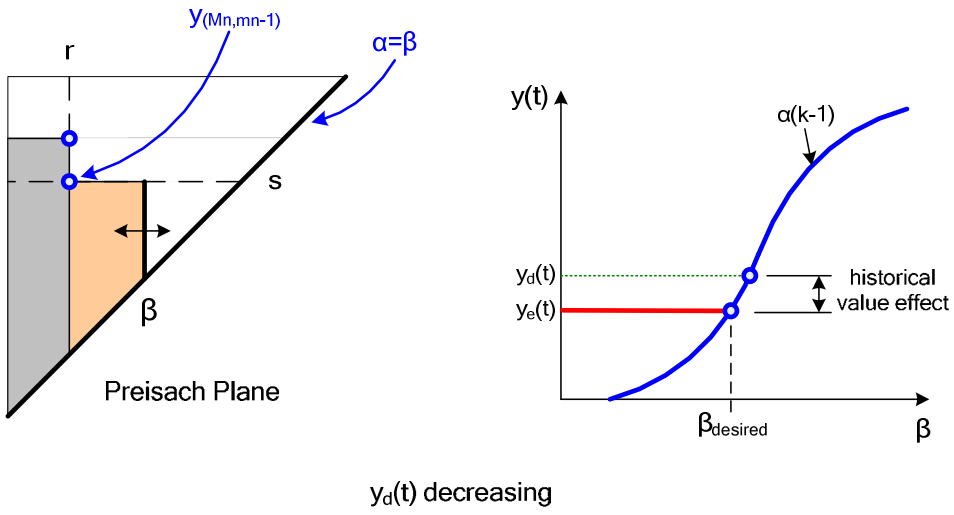

Figure 4-15. Representation of inverse Preisach model for decreasing input

Line *s* represents the previous α value, α(k-1), that occurred prior to β(k). The computation must take account of the total output required, $y_d(t)$, the calculated Preisach output history, $y_h(t)$, and $y_{(Mn,mn-1)}(t)$. This allows for a suitable input to be found which will result in the effective desired output value, $y_e(t)$. The variable $y_e(t)$ can be considered to be the 'new' desired value of the output after the various nonlinear effects such as the historical values have been compensated for.

$$y_e(t) = y_d(t) - y_h(t) + y_{(M_n, m_{n-1})}(t) \tag{4-7}$$

The $Y_e(t)$ line is compared with the array of the previous α value, $\alpha_{(k-1)}$. This is indicated by line *s* on the Preisach plane. The point of intersection between both

lines is the desired β value to give a system output of $y_d(t)$. If the new β value decreases to a value less than *r*, partial wiping out of y_h occurs. If β returns to 0, complete wiping out of historical values occurs.

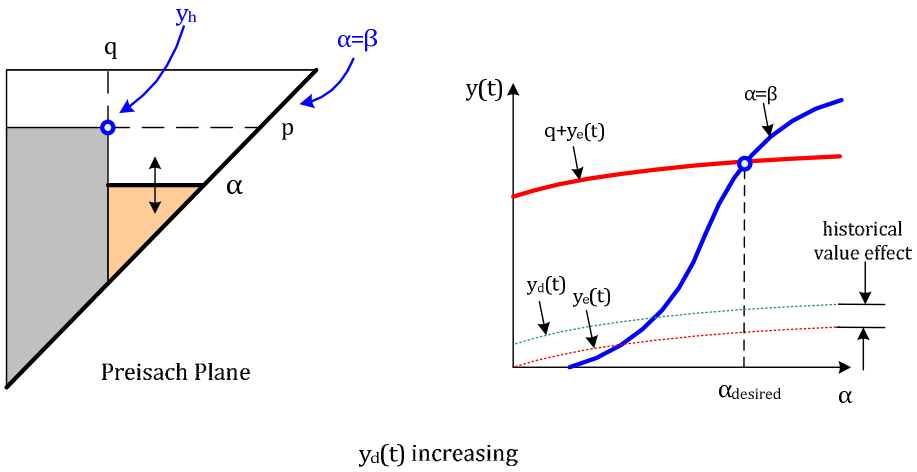

Figure 4-16. Representation of inverse Preisach model for increasing input

Wiping out can be thought of as the reversal of any truncation that occurs in the calculated output value during a series of desired inputs to the Inverse Preisach model. In the case of *increasing* $y_d(t)$, a comparable approach is required to eliminate the nonlinear effects before calculating the desired α value. The α value moves vertically along line *q* in response to change in the desired output value in Figure 4-16. The effective desired output value, $y_e(t)$, for increasing input values is found using

$$y_e(t) = y_d(t) - y_h(t) \tag{4-8}$$

The effective desired output is added to the *q* line. This new line, $q+y_e(t)$, is subsequently compared with the diagonal line α=β. The point of intersection between the two identifies the required α value for the desired output, $y_{d(}t)$. If

the new α value is greater than any other previous α value in the sequence, then partial wiping out occurs. If the new α value is greater than all previous α values in the sequence, then full wiping out occurs. This can be seen on the Preisach representation where the new α value goes above line *p*.

Thus, in order to establish K, the predicted output found using the Inverse Preisach (IP) procedure is related to the applied input current.

$$K = \frac{\text{IP Output}}{\text{IP Input}} = \frac{I_{ip}}{\varepsilon} \tag{4-9}$$

4.7.2 Validating Inverse Preisach Model Data

During data collection experimentation for the Preisach model (See Section 4.6.1), a balance was struck between the number of data points required for the Preisach plane and the time taken to collect the data. Interpolation was used to estimate data points outside of those collected.

The procedure was rationalized to facilitate fast computational times (Figure 4-17) and implemented into the LabVIEW environment using state-machine architecture (See Appendix III). State-machine architecture is chosen specifically due to the ease of implementation and modular layout. Validation of the success of the rationalized IP model can be carried out using the open-loop setup outlined in Figure 4-18. The IP model is utilised to determine the current for application to the SMA bundle actuator that will produce the desired SMA strain.

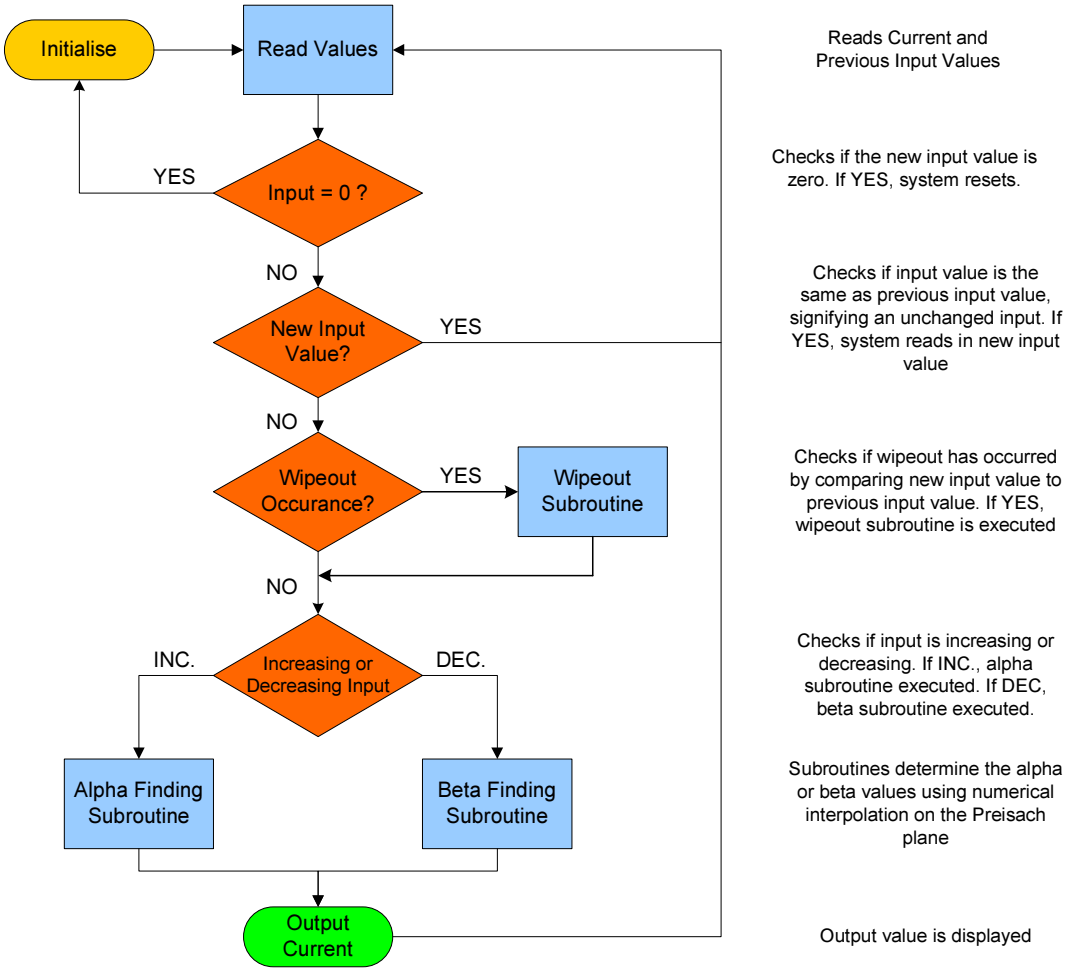

Figure 4-17. Rationalized Inverse Preisach Procedure for Computationally Fast Calculation of Input Current Value

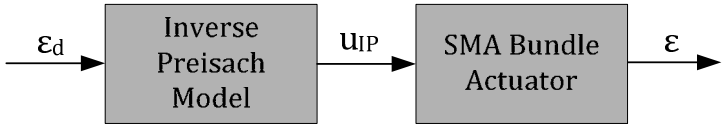

Figure 4-18. Open Loop Inverse Preisach Model Validation

A series of desired steady state strain values are selected. The IP model must determine and apply the correct input values to the SMA bundle actuator in order to reach the desired strain (Figure 4-19). It can be seen that the IP model accurately applies the correct input currents across the range of desired values.

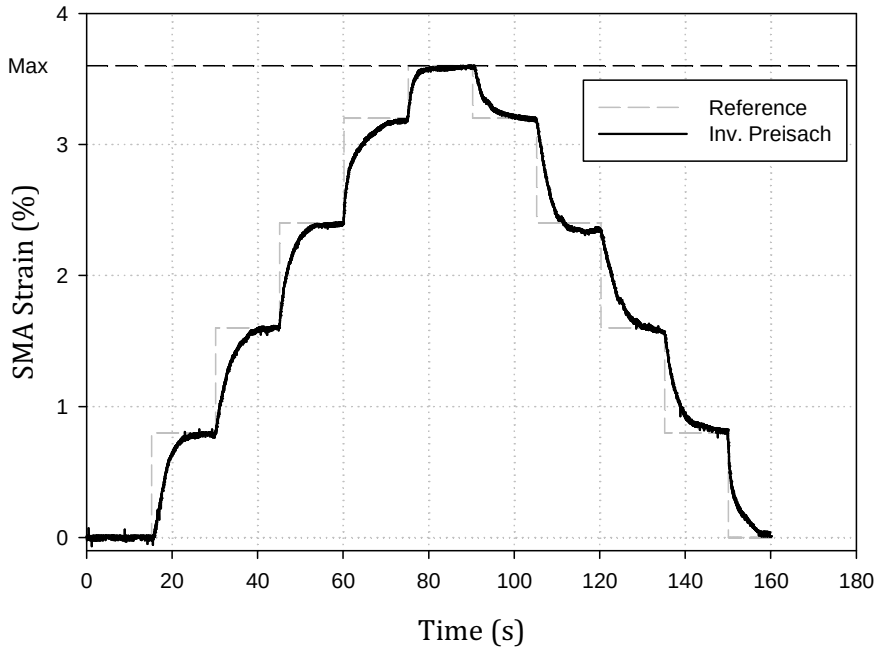

Figure 4-19. Validation of Inverse Preisach Data Point Collection

However, it can also be noted that the dynamic response varies depending on the applied current values and if the system is being heated or cooled. The dynamic response shown in Figure 4-19 is considerably slower than would be expected from an actuator tasked with controlling the movement of a joint in a prosthetic finger solution. It can take from 5 to 10 seconds to reach steady state depending on the sensitivity of the system to input current. This is highlighted in Figure 4-20 and Figure 4-21 which show magnified portions of the response outlined in Figure 4-19. The source of steady state error can be attributed to interpolation errors arising from the size of the discrete steps utilised in the development of the Preisach model. Furthermore, the responsiveness of the SMA wire is slow with a fall time of approximately 8-10 seconds per step being evdient. A suitable closed loop control scheme is therefore required to improve the responsiveness of the system while correcting any errors in the calculated current values as a result of limited data points available.

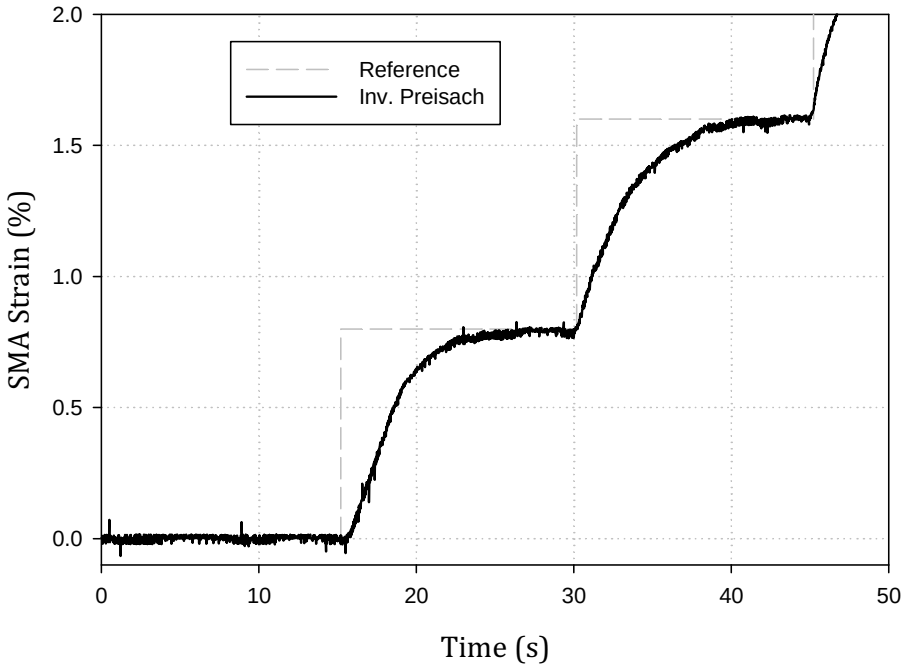

Figure 4-20. Close-up of SMA strain response to IP model output - heating

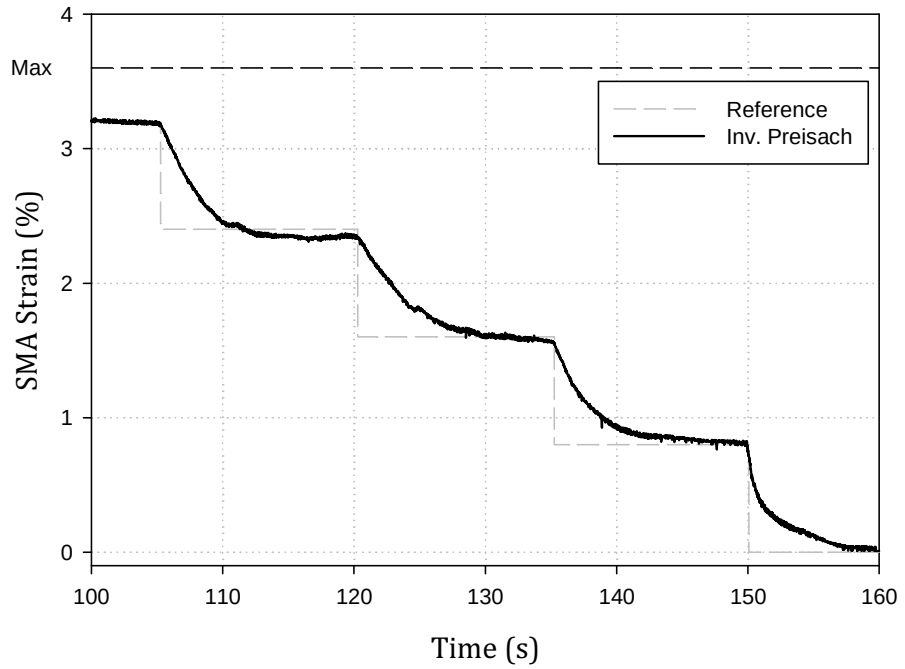

Figure 4-21. Close-up of SMA strain response to IP model output - cooling

4.8 Chapter Conclusions

Mechanical characterisation of SMA bundle actuators has been carried out in order to investigate the dynamics of SMA bundle actuation via joule heating and natural cooling. SMA strain, force generation capacity and nonlinear hysteresis effects have been fully characterised within the scope of prosthetic finger actuator design. The chosen SMA bundle, designed to fit into a volume similar to that of the palmar region of a hand, is made up of 150μm wires. These SMAs offer the best available force capacity to wire quantity per bundle ratio. Furthermore, the chosen SMA bundle exhibits relatively fast heating and cooling rates. It is therefore considered to be a suitable candidate for utilization in prosthetic finger design applications which attempt to mimic human finger performance.

The work carried out in this chapter satisfies a portion of the characterisation phase as outlined in the adopted design methodology (Figure 1-4). Further characterisation is required in terms of the thermal response of the system. This will allow for the remaining unknown variables in the dynamic model of the system (time constant and time delay) to be established. This is the focus of the work carried out in Chapter 5. This is a prerequisite for the synthesis of a suitable control strategy.

5. THERMAL CHARACTERISATION OF SHAPE MEMORY ALLOY BUNDLE ACTUATORS

5.1 Introduction

SMA bundle actuated prosthetic devices, owing to their portable nature, rely exclusively on energy derived from batteries for operation. While a small amount of this energy is used to power sensors and electric components within the device, a greater proportion is employed in the production of mechanical work in the actuators. The mechanical work production of SMAs is linked to the thermal response of the SMAs, and as such, SMAs are exposed to difficulties arising from undesirable energy loss via escaping heat. Correctly establishing the thermal behavior of the SMA bundle actuators can assist in the development of optimised prosthesis designs. Key benefits that can be derived from correctly identifying the thermal behaviour include;

i. The reduction or removal of undesirable dead time in the actuator response upon heating and cooling – leading to improved controller performance,

ii. The determination of cyclic and bandwidth limits of the SMA actuators – facilitating an investigation into the most suitable enhanced cooling strategies and most practical SMA bundle actuator design,

iii. The determination of the effects of mechanical loading on the dynamic performance of the SMA actuators.

5.2 Existing SMA Heat Transfer Model

Modelling of the thermal behaviour of SMA wires has been carried out by a number of groups [60, 139, 140]. It has been found that energy loss to the environment takes place primarily through natural convection. Losses attributable to conduction and radiation are negligible within the phase transformation temperature range [141]. As such, these modes of heat transfer are omitted from the pre-existing model. The heat transfer model of an SMA wire, based on the work of *Shahin* [83] (See Section 2.7), attempts to attribute heat loss mathematically and can be rewritten in terms of power input

$$P_{in} = [hA](T)[T_{SMA} - T_{\infty}] + m\Delta H\dot{\xi} + mC_p\frac{dT_{SMA}}{dt} \quad (5\text{-}1)$$

Where P_{in} is power input, h is the convection coefficient of the SMA bundle actuator, A is the surface area of the SMA wires, T_{SMA} is the SMA wire temperature, T_{∞} is the ambient temperature of the surrounding environment, m is the mass of the wires, ΔH is the latent heat of transformation, $\dot{\xi}$ is the rate of change of the martensitic ratio, and C_p is the specific heat capacity of the SMA material.

Errors can arise if the change in variables as phase transformation occurs due to the different mechanical properties of martensite and austenite is not accounted for. During the phase transformation from martensite to austenite, SMA wire resistance decreases from 9.603×10^{-4} Ωmm to 8.371×10^{-4} Ωmm. The thermal conductivity increases from 0.086 $W(cm.K)^{-1}$ to 0.18 $W(cm.K)^{-1}$. The specific heat capacity of martensite also differs from that of austenite with values of 4.506 $J(mm^3K)^{-1}$ and 5.92 $J(mm^3K)^{-1}$ respectively [142]. These result in an

increase in power required to heat the SMA wires when in the austenitic phase. The area of the SMA wires also reduces during phase transformation due to the contraction of the SMA wires. This decreases the heat losses to convection marginally. For example, for an SMA wire of length 66mm (which is utilised in the current work), the surface area decreases by $1.3\times10^{-6}m^3$ in the austenitic phase. At steady state, Eq.(5-1) reduces to Newton's Law of Cooling showing the rate of heat loss of a body is proportional to the difference in temperature between the body and its surroundings (Eq.(5-2)).

$$P_{in} = [hA](T)[T_{SMA} - T_{\infty}] \tag{5-2}$$

Eq.(5-1) & Eq.(5-2) can be used in the estimation of the power requirements (and hence the battery requirements) of the SMA wires within an SMA bundle actuator. As a result, the importance of establishing an accurate prediction for the heat transfer coefficient, h, becomes evident. Analytical methods are available within the literature to approximate the h value. Thin cylinders exhibit a similar geometry to SMA wires [67]. However, due to the highly nonlinear and complex nature of SMA wires during heating and cooling, the approximations established using alternative materials may not be sufficient [118].

5.2.1 Analytical Derivation of the Heat Transfer Coefficient

For the approximation of the heat transfer coefficient, h, using analytical methods, the thin SMA wire can be treated as a thin cylinder [67]. The heat transfer coefficient value can thus be established from

$$h = \frac{\overline{Nu}.L}{k} \tag{5-3}$$

where h is the heat transfer coefficient of the SMA wire, Nu is the Nusselt number, L is the SMA wire length, and k is the thermal conductivity. The most appropriate Nusselt number correlation for thin cylinders was previously established by *Elahinia* [143] as

$$\overline{Nu} = \frac{4}{3}\left[\frac{7.\mathrm{Ra.Pr}}{5(20 + 21.\mathrm{Pr})}\right]^{\frac{1}{4}} + \frac{4(272 + 315.\mathrm{Pr}).L}{35(64 + 63.\mathrm{Pr}).D} \tag{5-4}$$

where Ra is the Rayleigh number, Pr is the Prandtl number, L is the length of the SMA wire and D is the diameter of the SMA wire. Ra can be defined as

$$\mathrm{Ra} = \frac{g.\beta.\Delta T.L^3}{\alpha\upsilon} \tag{5-5}$$

where g is gravitational acceleration, β is the thermal expansion coefficient of the SMA wires, ΔT is the difference between the surface temperature and the ambient temperature of the environment, L is the length of the SMA wire, α is the thermal diffusivity and υ is the kinematic viscosity. Similarly, Pr can be defined as

$$\mathrm{Pr} = \frac{\upsilon}{k} \tag{5-6}$$

It is important to note that the analytical approximations do not specifically account for the phase transformation associated with SMA wires as they have been established using less complex materials. An investigation comparing these pre-established analytical methods to the experimentally derived values of h must be conducted. The outcome will determine whether it is prudent to

rely on the existing analytical approximations of h, or to alternatively use the experimentally derived values when estimating the heat transfer associated with SMA wire bundles.

5.2.2 Experimental Approximation of the Heat Transfer Coefficient

The general experimental approximation of the heat transfer coefficient can be established by solving Eq.(5-2) for h:

$$h(T) = \frac{P_{in}}{A(T_{SMA} - T_{\infty})} \tag{5-7}$$

Variations between the experimental values and the analytically derived values can be expected. The most likely causes of this are inaccuracy in the analytical model provided and the h-value being based on convection losses alone. As a result, the experimental values are expected to be higher than the analytical values for h.

5.2.2.1 Experimental Setup and Procedure

Precise experimental work is required to approximate the h value associated with SMA bundle actuators. This will be used to determine the effectiveness of the analytical method adopted while serving as a vehicle to gain insight into the complex thermal interactions specific to SMA bundle actuators. The enclosed experimental test rig detailed in Section 4.4.1 is utilised. 25μm thermocouples with a 0.1 second time constant are employed to accurately measure the changing SMA wire temperature. A highly conductive silver paste was used to attach the thermocouples to the SMA wires whilst providing maximum possible heat transfer to the thermocouple for most accurate results. The thermocouples

were fixed in position using a microscope to ensure integrity of contact. The fully enclosed and thermally stable environment ensures that the SMA wires are exposed to negligible external influences (Figure 4-1).

The SMA wire temperature is noted upon reaching steady state. The experiment is carried out for a range of input currents up to the maximum allowable value of 400mA. A summary of the testing procedure carried out is outlined in Table 5-1.

Table 5-1. SMA Wire Temperature Determination Experimental Summary

Test Ref.	SMA Diameter	No. of Wires	Applied Current	Measurement Variable	Experimental Focus
C1	150µm	1, 8	0-400mA	Wire Temp. & Strain	Steady State & Transient

5.2.2.2 Results & Discussion

The results gathered from experimental testing demonstrate h-values which compare reasonably well with the analytical results (Figure 5-1). At the lower end of the ΔT spectrum, between approximately 0-35K, the experimental results demonstrate a rapidly rising h as steady state temperature increases.

This is due to a changing Nusselt number, the ratio of convective heat transfer to conductive heat transfer (Eq.(5-8)).

$$\overline{Nu} = \frac{hL}{k} \tag{5-8}$$

At lower values, the Nusselt number is small due to the unmoving fluid (air) surrounding the SMA wires due to low buoyancy forces [67]. However, as the

temperature begins to rise, the heat given off by the wires leads to increased buoyancy forces and therefore enhanced natural convection.

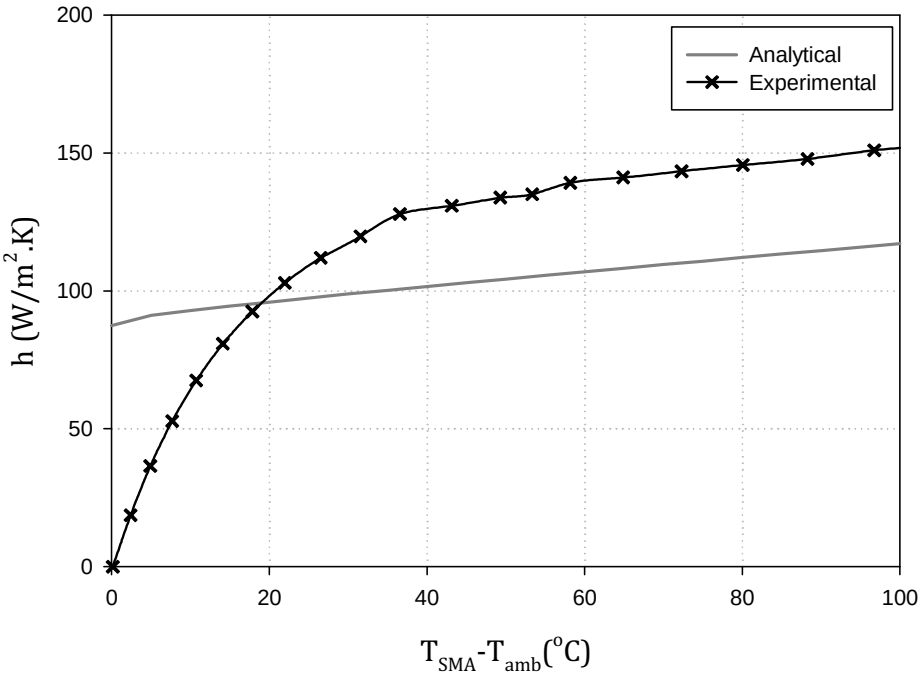

Figure 5-1. Convective Heat Transfer Coefficient, h - Experimental vs. Analytical

As a result the Nusselt number increases until it reaches a balance between buoyancy and friction [144]. The analytical method employs an average Nusselt number correlation and therefore does not account for the rise in h as demonstrated by the experimental values between ΔT values of 0-35^{o}C. The onset of phase transformation results in a drop in SMA resistance [142]. Accordingly, the power input drops to ensure a constant current supply to the wires. However, as the joule heating effect is a function of input current, the effect on the h-values observed as a result of the phase transformation is negligible.

The experimental results outlined in Figure 5-1 show a difference of approximately 30 W/m^2K between the h values predicted by the analytical model and those observed during experimental work. It can be noted that experimental differences can occur for a number of reasons such as

- *Minor Inaccuracies in SMA wire temperature measurement*. The minute diameter of the SMA wire results in significant difficulties in achieving accurate readings despite the steps taken to ensure high accuracy.

- *The miniscule volume of the SMA wires.* The SMA wires have a diameter of 150μm. As a result, minor fluctuations in environmental or experimental conditions can result in larger errors being witnessed.

- *The appropriateness of the analytical model.* The analytical derivation carried out used SMA wires aligned vertically. The experimental work carried out using SMA bundle actuators featured horizontally aligned SMA wires. Horizontally aligned wires can lead to slightly higher h-values than vertically aligned wires due to differences in buoyancy forces acting on the wires [67]. This is a result of a changing Reynolds number on the vertically aligned wires owing to increased buoyancy forces along the length of the wires. On horizontally aligned wires, the Reynolds number remains consistent across the length of the wires.

However, due to the selection and careful implementation of precision measurement equipment in the stable test bed environment, it is likely that the experimental inaccuracies are quite low. Therefore, the remaining possibilities

accounting for incompatibility between analytical results and experimental results are:

- *Discrepancy in analytical Nusselt number representation.* The Nusselt number correlation chosen is suitable for single thin cylinders. However, the presence of multiple SMA wires in close proximity to each other can lead to the discrepancies demonstrated.

- *Attributing all losses to convection.* Conduction and radiation can account for a small portion of the heat losses occurring. By omitting this from Eq.(5-7), a small increase in the h-value can be expected.

It is proposed that a new Nusselt number correlation specifically derived for SMA bundle actuators is required to improve accuracy. The new correlation would need to take into consideration the specific geometric layout for the selected SMA bundle actuator for maximum accuracy. However, this is beyond the scope of this work and is left as an invitation to further research. As a result of the demonstrated differences revealed between the analytical predictions and experimental observations of h, empirically derived approximations based on the experimental results will henceforth be used throughout this work.

5.3 Thermal Response of SMA Bundle Actuators

The thermal response of SMA actuators to applied input current and natural convection cooling is fundamental to gaining a complete understanding of the dynamics of SMA bundle actuators. The thermal behaviour is linked to the contractile strain and relaxation behaviour observed during operation. A series of experiments were carried out to determine the thermal response of SMA

bundle actuators when subjected to a range of applied input currents and natural convection cooling. A summary of the experiments is outlined in Table 5-2.

Table 5-2. Thermal Response Characterisation Experimental Summary

Test Ref.	SMA Dia.	No. of SMAs	Input Current	Variable	Action	Focus of Testing
TC1	150 μm	8	200mA-400mA (ΔI=40mA)	Temp.	Heating	Transient & S.S.
TC2	150 μm	8	0mA	Temp.	Cooling	Transient & S.S.

5.3.1 Experimental Results

The SMA wire temperature profiles observed during heating activity are outlined in Figure 5-2. The use of the micro-thermocouple has provided exceptionally clear and accurate temperature data in comparison with that available in existing literature on the subject. Temperatures A_s, A_f, M_s and M_f can clearly be seen in the temperature profiles outlined in Figure 5-2 and Figure 5-3, allowing for an accurate evaluation of the time taken to complete phase transformation. The transient portion of the SMA temperature profiles demonstrate a reduction in the temperature rise rate during heating as a result of phase transformation occurring. From Eq.(5-1), it can be observed that the slowing effect is a result of a significant fraction of the input power being used in the latent heat of transformation of the SMA as it transforms from martensite to austenite. During cooling, a similar process occurs where the phase

transformation reversal from austenite to martensite results in a decrease in the temperature fall rate (Figure 5-3).

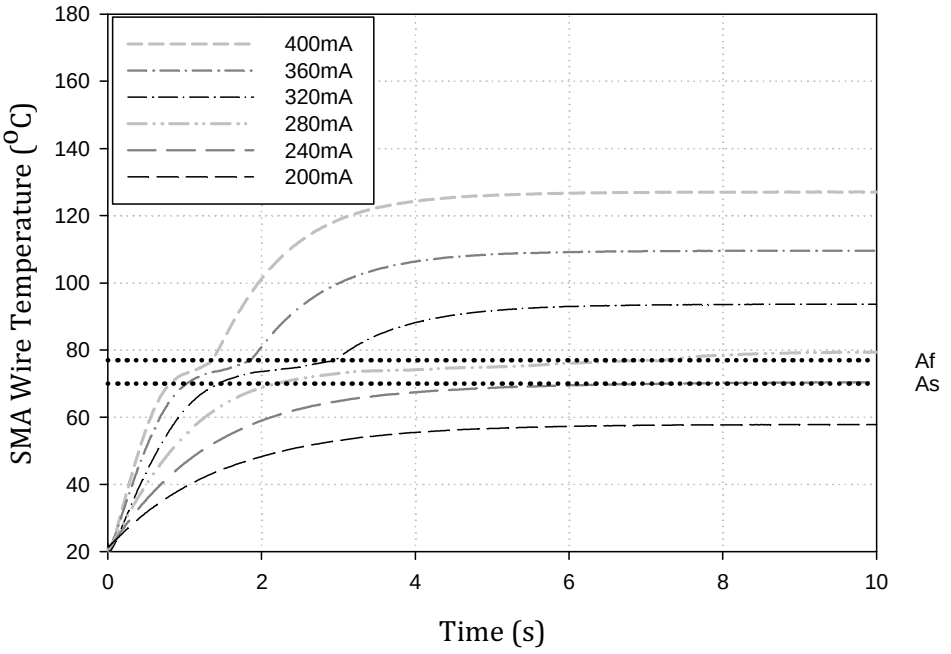

Figure 5-2. SMA Wire Temperature Heating Profiles

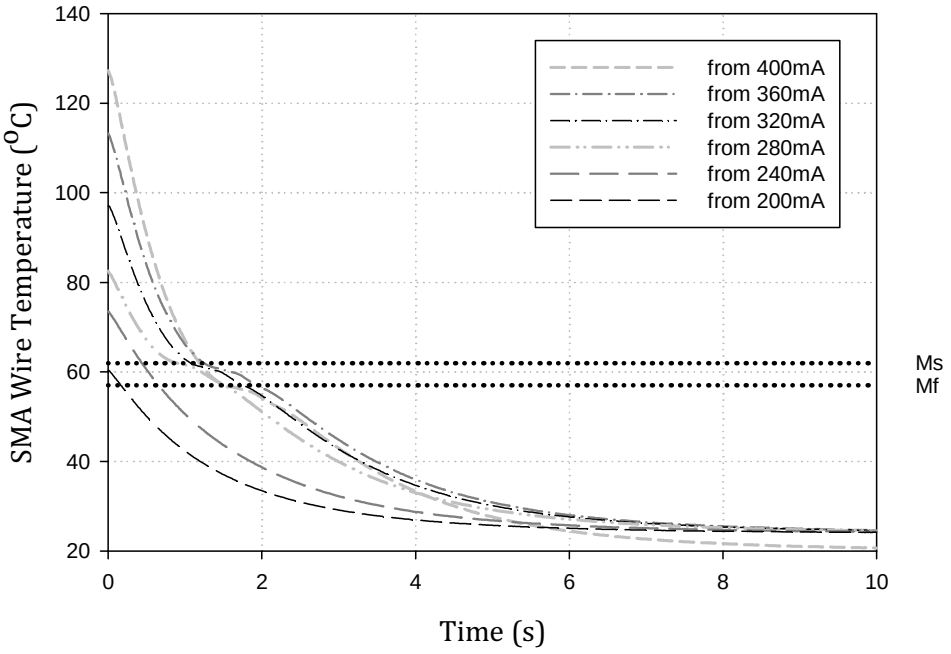

Figure 5-3. Dynamic SMA Wire Temperature Cooling Profiles

The results indicate that the heating and cooling response can be approximated as first order in nature outside of the bounds of the phase transformation region. Therefore, during heating

$$T_{SMA} = \begin{cases} T_{ss}\left(1 - exp^{-t/\tau}\right) & T_{SMA} > A_f \\ Mt + A_s & A_s < T_{SMA} < A_f \\ T_{ss}\left(1 - exp^{-t/\tau}\right) & T_{SMA} < A_s \end{cases} \quad (5\text{-}9)$$

Similarly during cooling

$$T_{SMA} = \begin{cases} T_{ss}\left(exp^{-t/\tau}\right) & T_{SMA} > M_s \\ M_s - Nt & M_s < T_{SMA} < M_f \\ T_{ss}\left(exp^{-t/\tau}\right) & T_{SMA} < M_f \end{cases} \quad (5\text{-}10)$$

where M and N are constants linked to the latent heat. The dynamic thermal data and SMA strain data can be directly compared (Figure 5-4). It can be seen that approximately 90% of the maximum possible SMA strain for any particular applied input current occurs prior to the A_f temperature being reached. This hold true for all input current values, although the absolute steady state SMA strain values are different for different input current values. This is a significant factor when investigating techniques to improve the overall efficiency of the system.

Greater system efficiency can be achieved by selecting SMA bundle actuators which are designed to operate over 90% of their total length. This can be done by increasing the length of the SMA bundle actuators, or increasing the gearing ratio where space limitations apply. Increased gearing ratios, however, will lead to an increase in the number of SMA wires required per bundle.

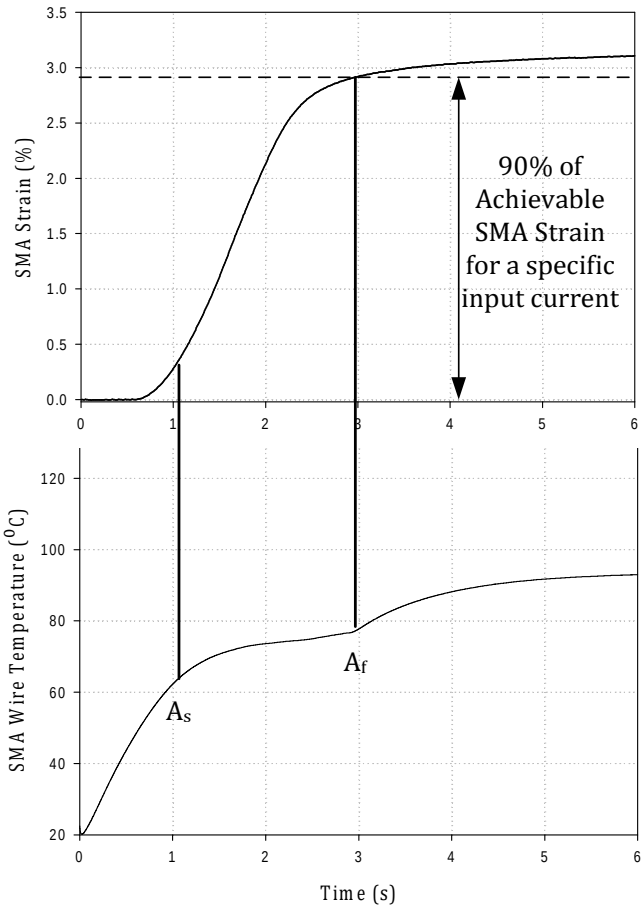

Figure 5-4. Comparison between SMA wire temp & SMA Strain – Illustrated with an input current of 320mA

5.4 Mathematical Basis of SMA Thermal-Strain Relationship

A relationship between the dynamic thermal response and the dynamic strain response is required to model the behaviour of SMA bundle actuators to applied input current. The dynamic thermal response of the SMA wires within the SMA bundle actuator is related to the applied input current which is a function of input power. From the experimental results demonstrated in Section 5.3, it can be shown that

$$\frac{d(\Delta T)}{dt} = f(P) \tag{5-11}$$

Since the SMA wires are thermally activated, the rate of strain is a function of the rate of heating or cooling and thus can be defined as

$$\frac{d\varepsilon_r}{dt} = f\left(\frac{d(\Delta T)}{dt}\right) \tag{5-12}$$

However, the SMA bundle actuators in situ in a prosthetic finger design must account for the dynamic forces associated with movement of each joint. As such, the work done by the actuator can be defined as

$$W = F \times \varepsilon_r \tag{5-13}$$

By substituting Eq.(5-13) into Eq.(5-12), it can be shown that the higher the rate of heat transfer delivered to, or lost from, the SMA bundle actuator, the higher the work rate.

$$\frac{dW}{dt} = f\left(F \times \frac{d(\Delta T)}{dt}\right) \tag{5-14}$$

This equation is significant in terms of controller design. It states that by controlling the rate of change of SMA wire temperature, the responsiveness of the SMA bundle actuator can be enhanced. This can be achieved by adjusting the applied input current accordingly during the transient period of activity.

5.5 System Efficiency

The portable nature of a prosthetic solution leads inevitably to reliance on the use of batteries as a source of power. Therefore, it is important for system

efficiency to be as high as possible in order to extend battery life, or facilitate the use of smaller battery packs. As battery technology advances, battery life and power available are being extended further, whilst size is ever reducing [145]. In spite of the advances and achievements to date, battery technology is still relatively bulky for demanding applications such as prosthesis actuation. It is therefore necessary to determine the optimum battery requirements for use, maintaining the key objective of adding minimum additional weight to the end user of the prosthetic device.

5.5.1 Identification of Inefficiencies during Heating

The empirically derived convective heat transfer coefficient, h (See Section 5.2.2), is vital in the estimation of the power requirements of an SMA bundle during dynamic response to applied input current. Comparisons between the SMA wire heating profiles and the SMA strain profiles (Figure 5-4) show that approximately 90% of the strain for any particular input current is completed by the time the SMA wire temperature reaches A_f. Therefore, excessive heating of the SMA wires beyond the A_f temperature causes a significant decrease in system efficiency. Figure 5-5 shows the heating profiles of two sample input currents, 400mA and 320mA, to illustrate the point. The utilization of a lower input current results in a reduction in speed of response of the SMA actuator. A controller solution can be designed to counteract this effect. It can be seen that the steady state temperature of the wire due to a 400mA applied current is significantly higher than the A_f line. Shaded region 1 shows the excessive increase in SMA wire temperature required to increase the SMA strain above 90% of the maximum possible level, leading to inefficiency.

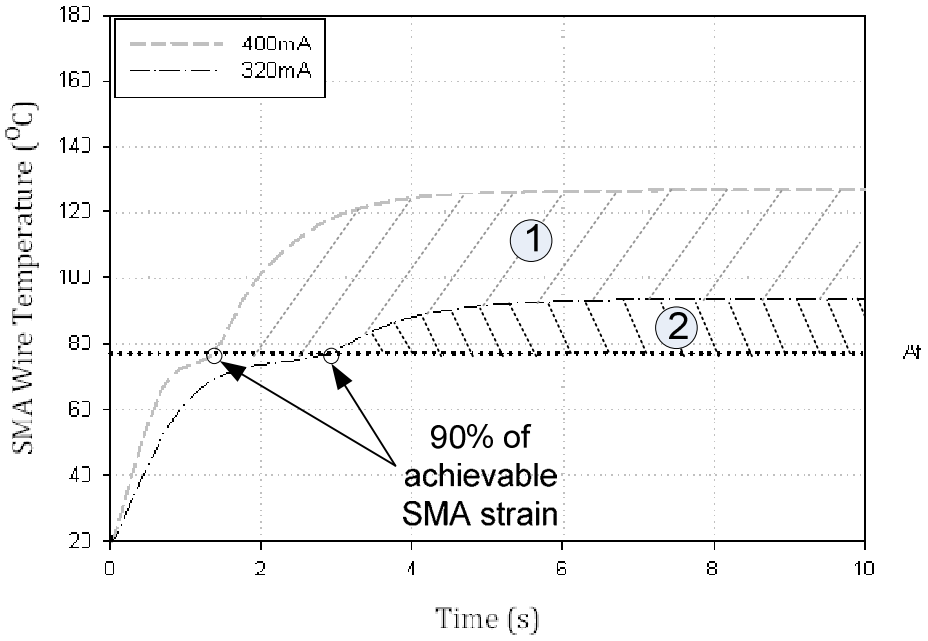

Figure 5-5. Identification of SMA Heating Inefficiencies

The inefficiency is not as significant when lower input current values are utilised. An estimate of the losses due to excessive heating can be found from

$$\dot{Q} = hA\Delta T + kA\Delta T + mC_p \frac{dT}{dt} \tag{5-15}$$

A typical 8-wire SMA bundle exhibiting a typical length of 66mm loses approximately 1.9 Watts due to excessive heating when an input current of 400mA is applied (*Shaded Region 1*). This equates to approximately 36.5% of the applied input power during steady state. The value associated with *Shaded Region 2* is lower at 0.66 Watts which accounts for 18.1% of the applied input power during steady state. Increased inefficiencies lead to the need for larger batteries, which can increase the cost and bulk of the overall system. Heating and maintaining SMA wire temperature far beyond the phase transformation region is highly undesirable for two reasons:

i. It is highly inefficient as any excess energy is lost through convection while delivering no significant increased benefits to the actuation cycle.

ii. It can lead to greater problems with SMA wire bundles in enclosed spaces. The excessive natural convection from the wires will raise the ambient temperature of the enclosed space resulting in a reduction in natural cooling capacity, and hence actuator performance and cyclic rate.

5.5.2 Designing for Improved System Efficiency

Excessive SMA wire heating has been shown to reduce the efficiency of SMA bundle actuators dramatically. Best possible efficiency can be achieved by heating the SMA wires to temperature A_f and maintaining them at this point. The rate of heating is a function of applied input current, which determines the maximum SMA strain possible. This can be illustrated by considering the following example: A 400mA input current results in a maximum SMA strain of 3.6%e, whereas a 320mA input current results in a maximum SMA strain of 3.1%e. Therefore, using 400mA to heat the wires to A_f will lead to a SMA strain of 3.24%e (90% of 3.6%e) whereas using 320mA to heat the wires to A_f will result in a SMA strain of 2.79%e (90% of 3.1%e). It can therefore be seen that although the final SMA wire temperature is the same, the SMA strain values differ.

Two variables can be identified and manipulated in order to improve the efficiency of the system:

i. Applied input current, and,

ii. SMA wire length.

Applied input current can be manipulated via the implementation of a suitable control strategy capable of adapting gain values accordingly. SMA wire length can be increased where possible. This produces a larger absolute SMA displacement as a result of SMA strain activity. The net result is a lower SMA wire temperature requirement, resulting in lower SMA strain, but providing the same absolute SMA displacement as shorter SMA bundles. Shorter SMA bundles must be heated to higher temperatures to increase the SMA strain required to achieve similar absolute SMA displacement. However, the constraints of the system in which the SMA bundle actuators are deployed may determine the size limitations, such as is the case in prosthesis design.

5.6 Dynamic Model - Time Constant

The general shape of the dynamic model of SMA bundle actuators is outlined in Section 4.7. The remaining variables yet to be established, τ and T_d, can be found directly from the open loop thermal response characteristics. The time constant in the time domain of a first order system response is a measure of how long the system takes to reach 63.2% of its steady state value [138]. As a result of the complex thermo-mechanical relationship associated with SMA bundle actuation, the resultant time constants can vary significantly across the range of system inputs. The key thermal factors which influence the time constant are the rate of heating (which is directly proportional to input power, and hence the applied input current) and the latent heat of transformation of the SMA material. It has been shown that the phase change region accounts for SMA strain from approximately 10% to 90% of the overall full SMA strain range for the SMA

bundle actuator for a particular applied input current. The remaining 20% of contraction occurs just outside of the phase change region boundaries. It is suspected that this is related to the initiation of molecular alignment of the SMA material prior to and just following phase transformation. Further investigation of this, however, is outside of the scope of this work. The time taken can be approximated by rearranging Eq.(5-1) and including any losses due to conduction

$$t_{10\%-90\%}(sec) = \frac{mH + mC_p\Delta T}{V(\xi)I - h(T)A(T_{SMA} - T_\infty) - kA(T_{SMA} - T_\infty)} \quad (5\text{-}16)$$

Radiation heat losses are on the order of three magnitudes smaller than conduction or convection and hence can be ignored [118]. The time taken to meet the latent heat energy requirements of the SMA wires during phase transformation can be used to establish the rate of SMA strain. This is linked to the time taken to transfer a quantity of energy into the SMA wires to meet the latent heat requirement during transformation while accounting for all other possible heat loss mechanisms. This time is determined to be the same as the time taken for the SMA to contract from 10% to 90% of the total strain for a particular applied input current (Figure 5-4). Based on Eq. (5-16), it can be determined that a large applied input current (and hence input power) results in a faster transfer of energy into the system. This allows for the phase transformation from martensite to austenite to be overcome in a shorter time period. For those input values which can only raise the temperature of the SMA wires to within the phase change region (A_s to A_f), a partial transformation will occur only, owing to insufficient availability of thermal energy. Resultantly, a significant decline in both SMA bundle contraction and rate of contraction is

evident. For the situation described, the rate of energy inputted to the system is not sufficient to replenish the energy lost during heat transfer to satisfy the requirements for full phase conversion.

The time constant can now be derived from the standard time domain representation of a first order system. Based on the mean observed change in output from 10% to 90% of its maximum value over the full range of the phase change region, the equation can be reduced to

$$\tau = \frac{t_{10\%-90\%}}{-\ln(0.2)} \tag{5-17}$$

5.7 Dynamic Model - Time Delay

Time delay plays an important role in the development of an accurate account of the system dynamics. It is possible to use known controller tuning methodologies to reduce the effect of time delay (See Chapter 6). Time delay is present during heating and cooling activity in SMA bundles as a result of the time required to heat or cool the SMA wires to the temperatures required for actuation, A_s and M_s, respectively. The stiffness of the bias spring also influences the time delay by increasing the stress on the SMA wires thus increasing the transformation temperatures. During the heating cycle, time delay can be estimated as the time taken for the SMA wire temperature to increase from its initial temperature to A_s where the initial SMA wire temperature is below A_s. This is demonstrated in Figure 5-4. Since the temperature response can be approximated as first order outside of the phase transformation region, the time delay due to heating can be approximated by

$$t_{dh} = -ln\left[1 - \frac{A_s(\sigma) - T_{SMA}}{T_{ss}(I)}\right] \qquad \text{where} \quad T_{SMA} < A_s \tag{5-18}$$

Similarly, during the cooling cycle, time delay can be estimated as the time taken for the wire temperature to fall from its maximum value to M_s. Again, taking into consideration the first order nature of the cooling response

$$t_{dc} = -ln\left[\frac{T_{SMA} - M_s(\sigma)}{T_{ss}(I) - T_\infty}\right] \qquad \text{where} \quad T_{SMA} > M_s \tag{5-19}$$

It can therefore be seen from Eq.(5-18) and Eq.(5-19), that maintaining the SMA wire temperature as close to the A_s and M_s temperatures as possible is beneficial in ensuring that the time delay is minimised. However, this may not always be prudent from an energy efficiency perspective. During the heating cycle, maintaining the SMA wire temperature as close to A_s as possible prior to actuation has detrimental effects on battery life. This is a result of the energy needed to heat the wires to just below A_s but which results in no mechanical work taking place. The implementation of a tuned controller based on the estimated time delay derived in Eq.(5-18) will serve to balance energy efficiency with desirable system responsiveness.

5.8 SMA Bundle Actuator Dynamic Response Model Validation

The required variables, gain (K), time constant (τ) and time delay (T_d) for the SMA bundle actuator dynamic response model have been established directly from the SMA open loop response (See Sections 4.7.1, 5.6 and 5.7). This can be validated against the actual open loop system response. The model can be used in the determination of accurate controller parameters. A typical SMA dynamic response model featuring a constant τ and T_d value for all current values is

shown in Figure 5-6. The improvement in accuracy brought about by using a nonlinear varying model based on the changing values from the governing heat transfer equations is demonstrated in Figure 5-7.

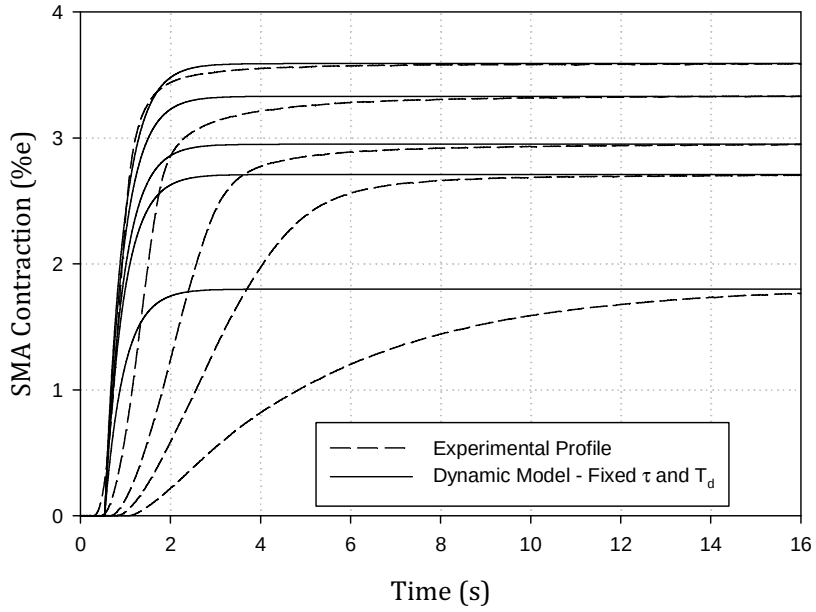

Figure 5-6. Actual SMA Strain vs. Dynamic Model - Fixed τ and T_d Values

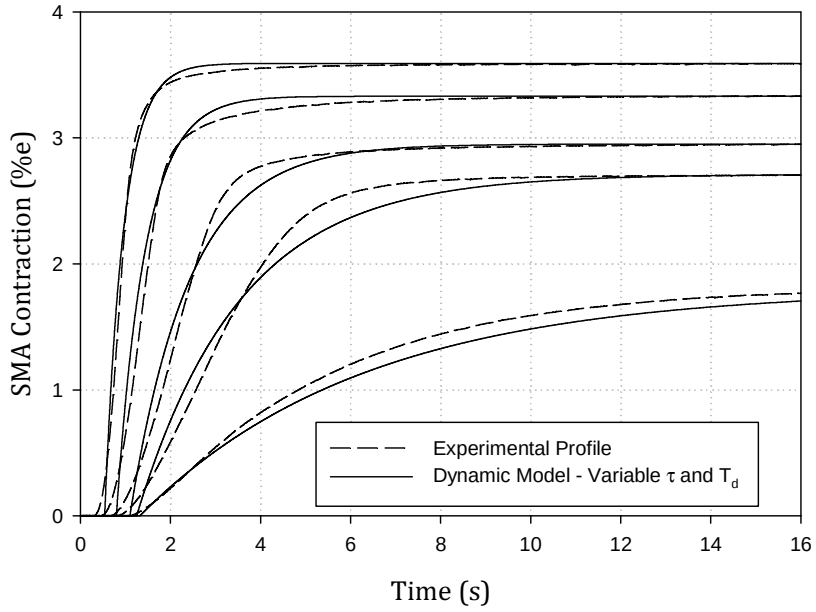

Figure 5-7. Actual SMA Strain vs. Dynamic Model - Variable τ and T_d values

The values were derived from the open loop response of the maximum input current of 400mA. Both models include hysteresis compensation using the IP model. It can be clearly seen in Figure 5-6 that an assumption of linearity in the dynamic response profile of the SMA bundle actuators to applied input current results in increasing inaccuracy as the input levels are decreased. However, by deriving the nonlinear parameters from the known thermal response of the system, a significant increase in model accuracy across many input currents can be achieved (Figure 5-7). A comparison of the errors arising using each modeling method is shown in Figure 5-8. It is evident that the inclusion of nonlinear parameters provides for a much closer match between the experimental data gathered and the modelling approach outlined. The success of the dynamic model outlined provides the basis for an adaptation law in response to the varying thermo-mechanical relationship of SMA wires during actuation. This will be discussed further in Chapter 6.

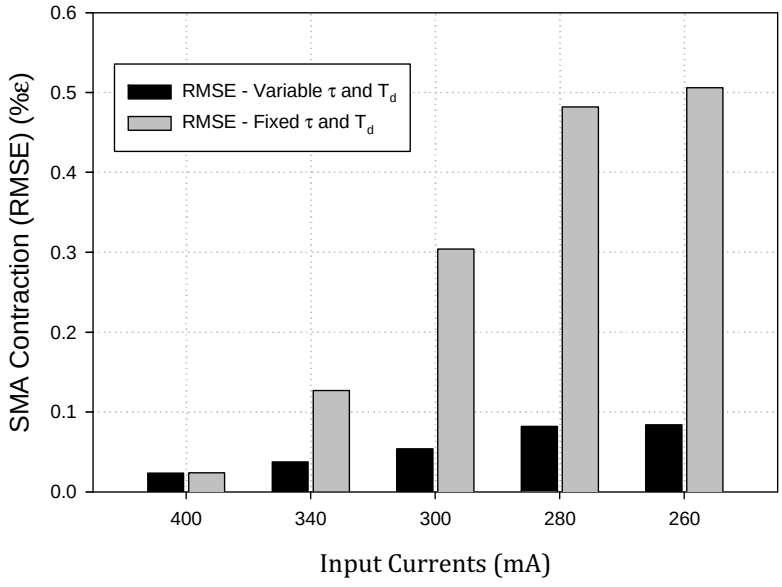

Figure 5-8. Error Comparison – Fixed vs. Variable τ and T_d Values

5.9 Enhanced Cooling of SMA Bundle Actuators

It has been shown that the mechanical work rate produced by SMA bundle actuators is directly related to the rate of heat transfer in and out of the SMA wires (Eq.(5-1)). Thus, it can be seen that during heating activity, the associated mechanical work of the actuators is easily controllable and has the potential to be fast acting. However, during cooling, due to the reliance of SMAs on slower natural cooling, the rate of phase reversal to the martensite phase can be limited. This suggests that the need for an investigation into methods aimed at improving the cooling time of the SMAs is warranted. Forced cooling can be implemented using a variety of techniques including conduction (heat sinks [71]), convection (forced air cooling & liquid cooling [72]) and radiation (Peltier cooling [74]). The nature of a prosthetic device dictates that many forced cooling techniques are rendered unsuitable for use. A successful cooling system for such a device must be cheap, portable, reusable, safe and offer a significant improvement in response time which outweighs the resultant increased complexity of the system. These criteria eliminate forced convection and peltier cooling strategies, leaving conductive cooling in the form of metallic heat sinks, applied at suitable timed intervals, as the only potentially suitable strategy. Experimental work is required to determine the precise benefits to be derived from implementation of a forced cooling solution.

5.9.1 Experimental Setup

For experimental purposes, heat sinks were manufactured from three materials, Aluminium (mc_p =18.3 J/K), Brass (mc_p =13 J/K) and Copper (mc_p =12.4 J/K). A

pneumatically controlled heat sink applicator has been designed as an attachment for use on the experimental test bed (Figure 5-9).

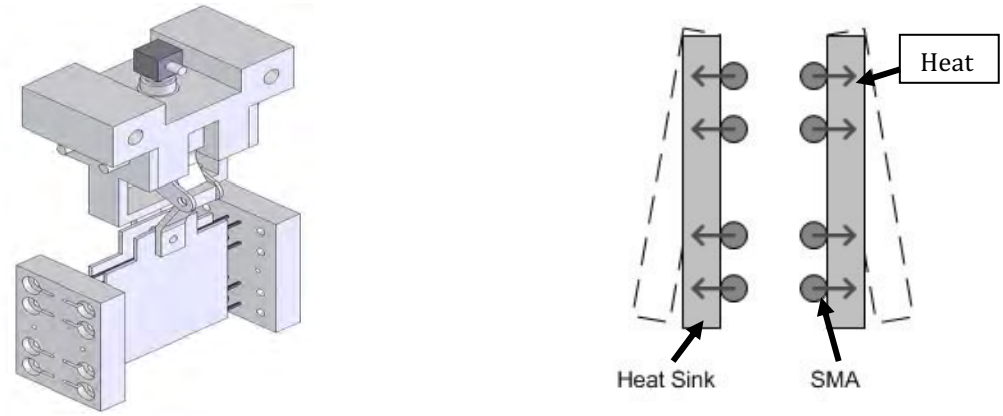

Figure 5-9. Forced Cooling via Conduction – Experimental Setup

The pneumatic applicator applies the heat sinks to the SMA wires within the SMA bundle actuator via a relay activated by a suitable on-off control algorithm implemented in LabVIEW 2009.

5.9.2 Experimental Procedure

Individual tests have been carried out using each heat sink material. Testing was carried out in a cyclic manner with the first half of the cycle designated as the heating period. Heat is delivered to the SMA via Joule heating until maximum contraction has occurred. Upon reaching this value, the current is switched off while a heat sink is simultaneously applied to the SMA wires to initiate the cooling phase. The heat sinks act to conduct heat away from the SMA wires in conjunction with heat lost through convection, thus improving the rate of cooling:

$$P_{out} = \frac{-k.A.\Delta T}{x_{conv}} - h.A.\Delta T \quad (5\text{-}20)$$

One experiment featuring no heat sinks (natural cooling) was also carried out as an experimental control for comparative purposes. A summary of the experiments is detailed in Table 5-3.

The heat sink exhibiting the fastest cooling time is examined further by heating the SMA bundles using a range of applied input currents. This allows for the determination of the cooling times from a range of various SMA steady state temperatures. Experimentation using forced air flow is used for comparative purposes.

Table 5-3. Enhanced SMA Cooling Experimental Summary

Test Ref No.	**SMA Wire Diameter**	**SMA Wire Quantity**	**Applied Input Current**	**Heat Sink (HS) Material**	**Cooling Application Time**
HS1	*150μm*	*8*	*400mA*	*Aluminium*	*10s*
HS2	*150μm*	*8*	*400mA*	*Brass*	*10s*
HS3	*150μm*	*8*	*400mA*	*Copper*	*10s*
HS4	*150 μm*	*8*	*400mA*	*Forced Air*	*10s*

Cooling of SMAs using the most suitable heat sink was compared to cooling via natural convection. The time to complete a full actuation cycle for the SMA bundle subjected to forced cooling was measured and compared to the complete cycle time of the SMA bundle undergoing natural cooling.

5.9.3 Results & Discussion

The results from experiments HS1-HS4 show that the cooling time is reduced significantly through the use of heat sinks (Figure 5-10) and forced air flow. All metallic heat sinks proved to be beneficial, reducing the cooling time (inclusive of time delay) to approximately 1.9 seconds, compared to 3.4 seconds for natural cooling. Furthermore, the presence of a significant time delay brought about by cooling the SMA wire temperature to M_s from its initial temperature reduced the responsiveness of the SMA bundle by up to 0.3 seconds.

Aluminium, brass and copper heat sinks resulted in comparatively similar improvements to SMA responsiveness. However the benefits of aluminium such as low weight and cost make it the most suitable candidate for prosthesis design applications. *Potapov and Da Silva* [139] stated that cooling time places limitations on the maximum possible frequency of actuation. In order to increase the frequency of actuation, cooling times must be decreased, time delay must be eliminated and a suitably tuned controller must be used.

The results of a cycle time analysis are illustrated in Figure 5-11. The results show that the frequency of actuation can be significantly improved using heat sinks during the cooling phase. The heating phase remains unaffected.

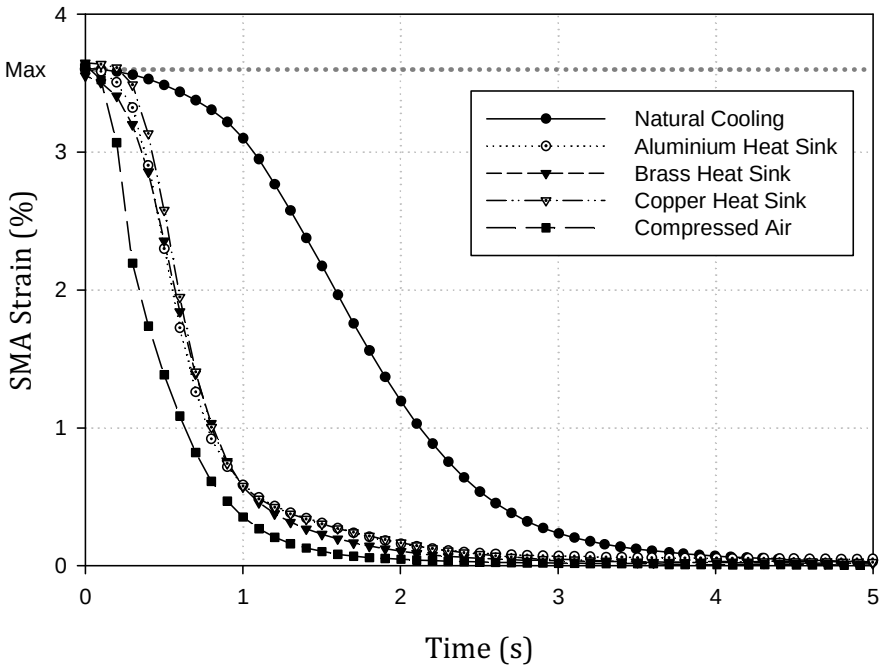

Figure 5-10. Enhanced Cooling Response of SMA wires via Heat Sinking

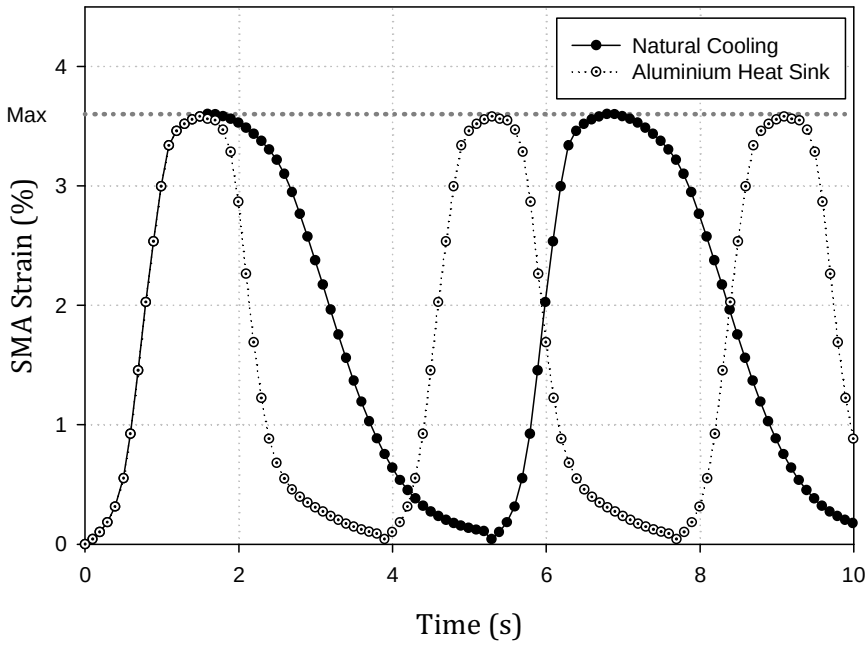

Figure 5-11. Enhanced Cooling Response of SMA wires via Heat Sinking

It is shown that the use of Aluminium heat sinks permits full open loop actuation cycles at 0.26Hz using the maximum recommended input current of

400mA. This compares favourably with natural cooling where full open loop actuation cycles are observed at a maximum rate of 0.18Hz.

5.9.4 Barriers to Implementation

In spite of the benefits seen in SMA actuator response owing to forced cooling via heat sinks, there are significant barriers to implementation when attempting to include heat sinks into a prosthetic solution. These can be identified as;

i. Significant increase in number of moving parts,

ii. Increase in required space to implement heat sinking action,

iii. Increase in controller complexity & energy requirement,

iv. Fin requirement to ensure heat sinks are kept in a cool state,

v. Performance dependence on differing climates and environments.

As a result of these barriers, enhanced cooling, while offering the possibility of increasing the cyclic rates of SMA bundle actuators, can only be justified in prosthesis design in extreme cases where performance can substantially benefit from their introduction.

The increase in the frequency of actuation by 0.08Hz is not sufficient to justify forced cooling implementation. Therefore, the only realistic option is to rely on optimising natural cooling capabilities as much as possible via a suitable well-tuned controller and maintaining a consistent ambient temperature in the surrounds of the wires. This can lead to an achievable frequency of actuation of

SMA bundle actuators that is acceptable for use in a prosthesis without the need for added mechanical complexity.

5.10 Conclusions

An investigation into the thermal response of the SMA bundle actuators has been carried out. The findings prepare the groundwork for the design and implementation of an optimised controller solution which takes advantage of the dynamic thermal properties of the SMA wires. The open loop thermal response was used to establish both the time constant and the time delay variables of a FOPTD transfer function. The dynamic model of SMA bundle actuator response was then implemented and validated, providing a good fit to the open loop characteristics of SMA bundle actuator response. Additionally, the importance of heating the SMAs to A_f or below, or increasing the length of the SMA bundle actuator are noted as the two best techniques available to maximize system efficiency.

The work outlined in Chapters 4 & 5 fulfills the characterisation phase and dynamic model of SMA strain phase of the adopted design methodology. The design and implementation of a suitable control strategy can now be carried out based on the findings. The focus of the control strategy will be to design a system capable of accurately tracking the response of SMA bundle actuators to desired setpoints and trajectories whilst maintaining a robust capacity to reject loading disturbances. A novel tuning methodology based on the dynamic model of SMA strain outlined will be implemented.

6. SHAPE MEMORY ALLOY BUNDLE ACTUATOR CONTROL STRATEGY SELECTION & OPTIMISATION

6.1 Introduction

Precise, robust control of SMA bundle actuators is the key to successfully developing a valid prosthetic finger design solution. The required high level of control is necessary to facilitate the reproduction of common prehensile postures in addition to the execution of delicate gripping activities. Accurate position and tracking control of the SMA bundle actuator is achieved by regulating the input current to the SMA wires within the bundle. A balance between set-point tracking and robustness to disturbance is preferable for actuators utilised in a prosthetic finger owing to the range of tasks required.

Difficulties in control arise due to the highly nonlinear behavior of the SMA material under thermal excitation, loading, and the changeable nature of the working environment (See Chapters 4 & 5). The successful controller must be able to compensate for all of these undesirable nonlinearities whilst maintaining a performance level within a set of specified criteria for SMA bundle actuated prosthetic devices.

This chapter focuses on the development of an adaptive control strategy and tuning methodology for a single 8-wire SMA bundle. The barriers to accurate control and the controller requirements are systematically identified and used to justify the parameters included in the chosen strategy. The control system architecture evolves from the fusion of the individual components. Validation of

the controller in terms of its capacity for position and tracking control is carried out under various typical working conditions. It must be taken into account that the input signal to the control system in a working prosthetic solution would most likely be a conditioned electromyographic (EMG) signal taken from the remaining limb of an end user. However, for the purpose of controller validation, a series of step and sinusoidal inputs will be utilised. The work outlined in this chapter covers the 'SMA Bundle Controller' phase of the controller subroutine in the adopted design methodology.

6.2 Identification of Barriers to Control

The complexity of the controller architecture is a result of the numerous barriers to successful control of SMAs that exist. Three main hindrances to accurate and repeatable SMA bundle actuation of prosthetic solutions are observed:

i. *Thermally Induced Hysteresis Effects*. These undesirable effects are due to differences in the rates of heating and cooling. Additionally, the slightly different temperature ranges for the martensite-to-austenite and the austenite-to-martensite phase transformations present difficulties.

ii. *Nonlinearities during Loading and Unloading*. This is a result of the effect of stress on the phase transformation temperatures combined with the differing mechanical properties associated with the martensite and austenite phases of the SMA material.

iii. *Ambient Temperature Fluctuations*. Fluctuations in ambient temperature influences SMA wire surface convection rates which can result in changes to SMA strain values.

6.2.1 Electromyographic Signals

An EMG signal is an electrical signal acquired from any organ that represents a physical variable of interest [146]. EMG signals play an important role in intelligent prosthesis design, being commonly used as control signals (Figure 6-1). It is important that the control system under development can utilise conditioned EMG signals in order to be seen as a viable prosthesis solution.

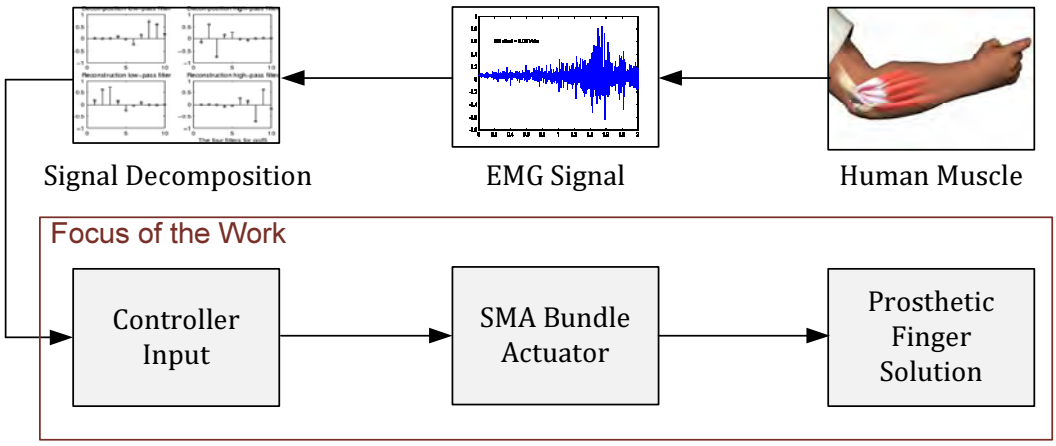

Figure 6-1. The Role of EMG Signals in Intelligent Prosthesis Control

Surface EMG (SEMG) signals are most commonly collected from the surface of the muscle tissue. Using this technique, it has been shown that the desired torque in a joint can be established [147]. Unsatisfactory EMG collection or subsequent decomposition can lead to problems with controller accuracy, and thus is seen as a potential barrier to control. Numerous researchers have developed satisfactory methodologies to collect and decompose EMG signals for

use in prosthesis design [10, 16, 146, 148]. The work described herein primarily focuses on the steps from 'controller input' to 'prosthetic finger solution' as outlined in Figure 6-1. It is assumed that the signal decomposition allows for a clean, usable signal as the controller input for utilisation in the work described herein. While it is important to recognize the parallel progress being made in this area, in-depth focus on these processes is considered to be outside of the scope of this work.

6.3 Identification of Control Strategy Performance Criteria

Several key performance criteria are essential in quantifying the degree to which the SMA actuators satisfy the actuator requirements specific to prosthetic finger solutions [58]. The criteria are described as follows:

i. *Set-point tracking response*. SMA bundle actuators must demonstrate the capacity to produce prosthetic finger joint movements which mimic those of the human finger. The benefits derived from this include user satisfaction and confidence in the prosthetic device, and the capacity of the device to operate consistently in the surrounding environment. Activities such as scrolling or finger-pointing rely on good set-point tracking capabilities.

ii. *Repeatable steady-state output*. Gripping/grasping ability is a central requirement of any prosthetic finger (and hand) solution. Actuation solutions must be able to guarantee repeatable steady state output which ensures consistency of operation in gripping/grasping tasks. This can ultimately inspire greater user confidence and satisfaction in the device.

iii. *Stability & overshoot*. Prosthetic finger (and hand) solutions are often tasked to perform delicate prehensile tasks (i.e. grasping an easily collapsible structure such as that of an egg). Good stability and minimum overshoot are essential in ensuring that these tasks are performed satisfactorily.

iv. *Robustness to external disturbances*. Prosthetic solutions, due to their very nature, are employed in changeable, unknown external environments. A successful prosthesis actuation control strategy must maintain the capacity to operate consistently in the presence of disturbances.

These criteria are intended as a reference for good practice in novel prosthetic actuator design and implementation. They will be used as a comparative guide for any experimental work carried out in this chapter.

6.4 Selection of Appropriate Controller Solution

Section 2.9 reviewed the variety of approaches used by researchers in an attempt to provide for best possible control of SMA actuators. A logical decision matrix can be employed to compare each of the approaches under a variety of appropriate headings. A five point scale is chosen to categorize the relative importance of each heading, while a rating between one and five is applied to each approach under each heading. The values are subjective and are chosen based on the experience of the author. However, since the aim of the exercise is to find one clear leading control approach, the spread of the matrix

demonstrates a certain amount of robustness to any errors that may arise as a result of subjective judgements.

The controller strategies reviewed in Section 2.9 are;

- Linear Control (LC)
- Adaptive Control (AC)
- VSC / Sliding Mode Control (VSC/SM)
- Combined inverse model-based feedforward & PID Feedback Control (IM-PID)

A series of comparative variables are selected that are considered appropriate to an application involving SMA bundle actuators working within a prosthetic finger framework. Equally, the ease of design of the controller and the development of relationships between the known thermo-mechanical behaviour of the SMA wires and the controller are considered important. The comparative variables that are selected as appropriate are identified as follows:

i. *Set-point & tracking response* – Can the SMA respond accurately to a series of desired input values? This is highly relevant in the context of a prosthetic finger design as it allows for positional movements to be carried out. Overshoot is considered undesirable due to the possible application of the prosthetic finger in delicate gripping tasks.

ii. *Hysteresis compensation* – Can the overall control system provide for adequate compensation of the hysteresis? Hysteresis is inherent in SMAs, and failure to account for this will result in both steady state and tracking control errors.

iii. *Apriori knowledge requirements* – Can the system be implemented and tuned without the need for expert knowledge on the SMA actuation cycle? The formulation of controller design parameters which can be derived directly from the known thermo-mechanical behaviour of the SMAs can lead to improved control schemes.

iv. *Implementation in real-time* – Can the controller solution be implemented as a real-time controller or do computational constraints result in limitations in terms of accuracy? Within a prosthetic solution, any control strategy must be compiled onto a suitable microchip to facilitate portability. The reduced availability of computational power can result in complex control routines being unsuitable in practice.

v. *Robust capacity* – Can the controller minimize the effects of external disturbances adequately? Furthermore, can the controller account for the changing sensitivity exhibited between applied input current and SMA strain across the actuation spectrum? The inability of a controller to demonstrate robustness to changes in sensitivity can lead to severe operational difficulties when applied to a prosthetic finger solution.

Each of these comparative variables has been assigned a weighting based on heuristic knowledge. The basis for the weighting assignments that are shown in Table 6-1 stems from a comprehensive review of relevant literature in the area. Key figures from the literature were extracted and directly compared in an attempt to identify the advantages and disadvantages of the multitude of approaches to SMA control available. The controller architecture with the highest resultant score is chosen as it is shown to demonstrate the best

potential for control of SMA bundle actuators within a prosthetic finger design. It is shown in Table 6-1 that IM-PID is the most suitable SMA bundle actuator control strategy. LC scored lowest in three of the five requirements, and hence scored lowest overall, due to the highly nonlinear hysteretic nature of the SMA phase transformations. AC and SMC/VSC tallied slightly higher scores, both exhibiting moderate potential to meet all requirements set out.

Table 6-1 Logical Decision Matrix for Controller Architecture Selection

	Weight	LC	AC	SMC / VSC	IM-PID
SP & Tracking Response	5	1	3	3	4
Hysteresis Accountability	5	1	2	2	4
Apriori Expert Knowledge	3	5	5	3	3
Implementation in Real-Time	5	5	2	4	4
Robust Capacity	4	1	2	4	4
	Total	54	58	65	85

6.4.1 Discussion of Applied Control Strategies

The results from the decision matrix can be used to form the basis for the derivation of an optimal control strategy for this application. Results indicate that an inverse model-based control strategy featuring an inverse mathematical model of the hysteresis nonlinearity in a feedforward loop combined with a PID (IM-PID) controller in feedback is suitable (Figure 6-2). The large score differential between IM-PID and other candidate strategies indicates that any errors occurring due to the subjective process of weight assignment are largely nullified. A closer result would require an increase in the quantity of key variables under consideration, or an increase in the weighting scale to

distinguish some key variables further. The inverse hysteresis model in feedforward seeks to compensate for the complex hysteresis effects observed during the heating and cooling cycles by selecting the appropriate open loop current to produce the desired SMA strain. However, since the open loop response is sluggish, a PID controller in the feedback loop (which is independent of the feedforward loop) can be utilised and tuned to reject disturbances while improving the speed of response. The control value, u, is a combination of the inverse hysteresis output and the appropriate output from the PID controller. The complex nonlinear thermo-mechanical relationship observed in SMA actuators cannot be sufficiently accounted for using linear control strategies. Nonlinear control strategies such as Adaptive Control and Variable Structure Control demonstrate reasonably good overall suitability. However, these approaches are not designed specifically to deal with the complexities associated with hysteresis. As a result, errors can occur.

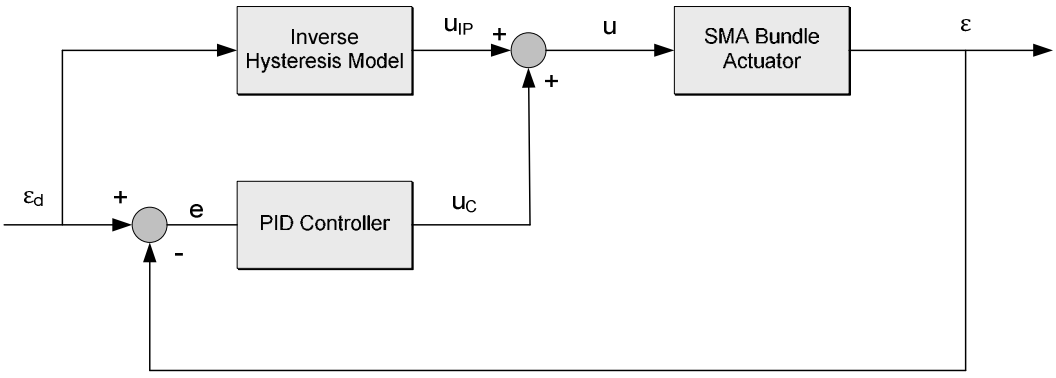

Figure 6-2. Inverse Model Based Feedforward with PID Feedback – "IM-PID"

Whilst the use of an IM-PID control strategy is seen to compare favourably with the other methods reviewed, there are considerable issues that must be resolved. Thus far, the work carried out by other groups in the area of IM-PID

control of SMA actuators has not demonstrated a valid controller design and tuning methodology that is derived from the thermo-mechanical characteristics of the SMA wires. Instead, these control strategies are derived using iterative numerical methods such as neural networks or fuzzy models based on the experience of the researcher. A phenomenological basis for the design and tuning of a controller solution can lead to more successful control as it potentially accounts for all the observed phenomena of SMA actuators.

The focus of much of the work in the available literature is based on proving the suitability of the inverse model derivation and does not make reference to the relevant tuning methodologies required in the feedback controller (See Section 2.9.3). It is important to specify an optimum tuning methodology which can strike a balance between set-point tracking and robust capacity of the controller.

Furthermore, within the literature, there is no reference to the variation in dynamic response of the SMA actuator over the range of applied input currents as noted in Sections 4.7, 5.6 & 5.7. The variation observed in the dynamic response suggests the need for an adaptable tuning methodology capable of adjusting to the different response profiles associated with each of the applied input current values. Tuning seeks to ensure that a balance between set-point tracking and robust capacity is maintained.

6.5 SMA Bundle Actuator Control Strategy

The SMA bundle actuator control strategy developed (Figure 6-3) attempts to take account for the full range of criteria described in Section 6.3. The controller

features an inverse Preisach model of SMA hysteresis in the feedforward loop and an adaptive PID controller in the feedback loop tasked with rejecting any external disturbances and improving the responsiveness of the system. The adaptive element of the controller focuses on selecting the appropriate gain values based on the nonlinear dynamic response of the SMA bundle actuators to applied input current.

The current value, U_{IP}, selected by the inverse Preisach model in response to the desired SMA strain is used in the determination of the correct controller gain values using the adaptation law. The applied current is directly related to the dynamic characteristics of the response (See Section 5.8).

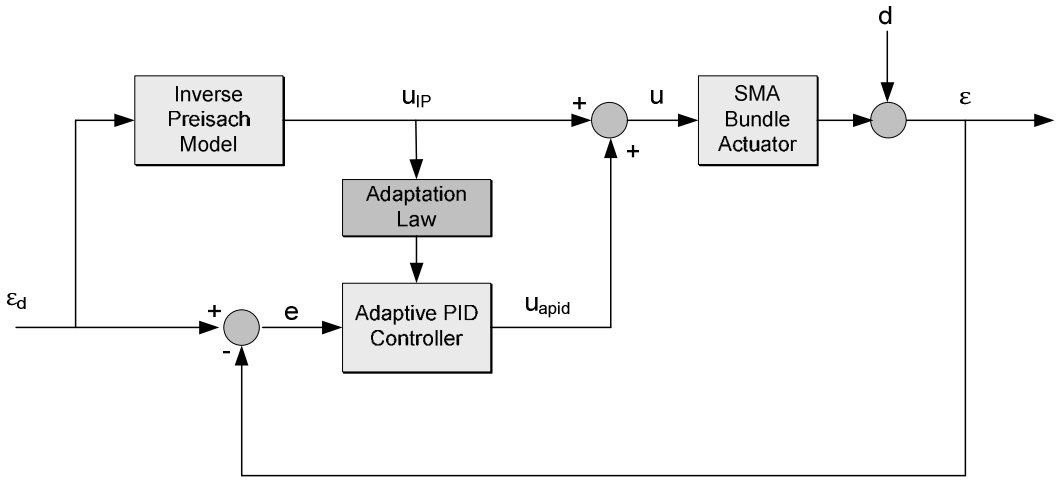

Figure 6-3. Selected SMA Bundle Actuator Control Strategy

Without the adaptation law, the controller gain values can only be optimally tuned for a narrow range of input currents. Once outside this range, tuning is suboptimal, leading to deterioration in performance of the SMA actuator.

6.5.1 Adaptive PID Controller Architecture

The law of adaptation for the a-PID controller is built on the assertion that the nonlinear dynamic response of the SMA bundle actuators to applied input current can be seen as a series of linear subsystems, each requiring appropriate tuning. The structure of each subcontroller for each subsystem in the Laplace domain is

$$C(s) = K_p\left(1 + \frac{1}{T_i s} + T_D s\right) \tag{6-1}$$

Tuning of the a-PID controller is simplified owing to the independence of the feedforward loop and feedback loop. As a result, an appropriate controller tuning methodology can be selected for the feedback a-PID controller. This approach utilises standard tuning laws already available in the literature [149]. As demonstrated in Section 5.8, the nonlinear SMA response can be considered to be a series of independent stacked linear subsystems. Each linear subsystem can be tuned using a suitable tuning methodology. This produces a profile of optimum values for the P, I and D components against applied input current chosen.

6.5.2 Tuning Methodology

There are numerous tuning methodologies available in the literature [149]. The challenge is to select the most appropriate based on the requirements of the SMA bundle actuators in prosthetic finger design. It has been shown previously that deviations owing to any model data inaccuracies can be treated as external

disturbances [150]. As a result, tuning is carried out using the Integral of Time-weighted Absolute Error (ITAE) method for disturbance rejection

$$ITAE = \int_0^\infty t|e(t)|\,dt \tag{6-2}$$

ITAE serves to penalize a slow settling time more when compared with other tuning methods such as Integral Square Error (ISE) and Integral Absolute Error (IAE) [149]. It has been shown that ITAE tuning demonstrates a good balance between set-point tracking and disturbance rejection as it exhibits medium integral gains and medium robustness measures [151]. Furthermore, ITAE offers inherent advantages over Zeigler-Nichols (Z-N) and Cohen-Coon (C-C) tuning methodologies which are considered unsuitable for large delays (if present) or are considered too aggressive.

The ITAE tuning method, by its very nature, is also considered to be relatively conservative. As a result, overshoot, which is highly undesirable in prosthesis design, will be minimized. A reduced settling time combined with an increased speed of response from the SMA bundle actuator will facilitate the generation of stable gripping postures in as short a time as possible. Tm and τc can be found using the process reaction curve method (Figure 6-4).

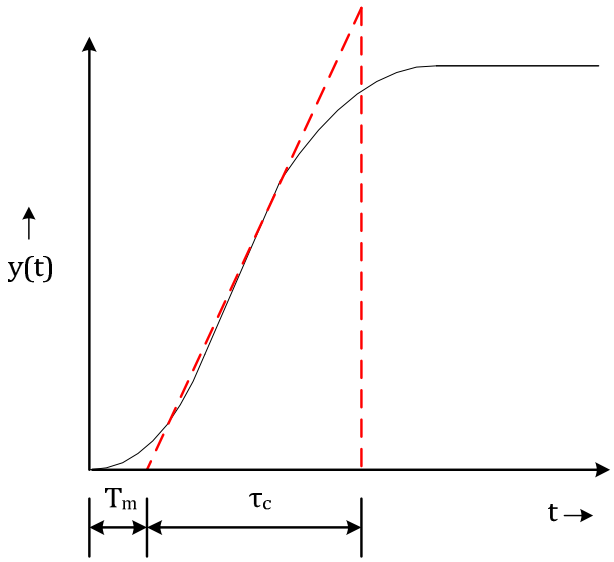

Figure 6-4. Process Reaction Curve

Table 6-2 Optimum ITAE Tuning Parameters [152]

Tuning Parameter	**Tuning Formula**
K_p	$\frac{1.034\tau_c^{\,0.8733}}{KT_m^{\,0.8823}}$
T_i	$1.6013\tau_c^{\,0.9011}T_m^{\,0.0884}$
T_D	$0.3088\tau_c^{\,0.1131}T_m^{\,0.9047}$

The ITAE tuning rules selected for implementation are suitable for a wide range of ratios of time delay to time constant for the observed system, from $0.02 \leq T_d/\tau \geq 4$ [152]. This is well suited to SMA bundle actuators owing to the nonlinear dynamic response characteristics across a wide range of applied input currents. The tuning rule for K_p indicates that systems with a large time constant and a small time delay will have a larger K_p value. However, for T_i and

T_D, if either the time constant and time delay are large, their values increase, thus reducing the integral and derivative gain values of the PID controller. The tuning rules are outlined in Table 6-2 and are suitable for SMA bundle actuators, independent of the number of SMA wires, featuring 150μm diameter wires.

6.5.3 Adaptation Law

An adaptation law can be implemented to vary the gain values of the PID controller in the feedback loop. It has been shown in Section 4.7, that the dynamic response of SMA bundle actuators to applied input current can be considered as a series of stacked independent linear systems. Therefore, a suitable adaptation law can be derived from the independent linear systems obtained across the spectrum of applied input currents. The minimum effective input current is approximately 200mA (See Section 5.3). Values below this do not sufficiently heat the SMA wires to the required transformation temperatures.

The adaptation law is therefore only active within the range of 200mA to 400mA of applied input current. The controller is designed to switch off for values below 200mA, thus saving battery power (See Appendix II – State 7 – pg.288). The adaptation laws for K_p, T_i and T_D over the range of usable input currents are shown in Figure 6-5, Figure 6-6 and Figure 6-7 respectively for SMAs at ambient temperature at time (t-1).

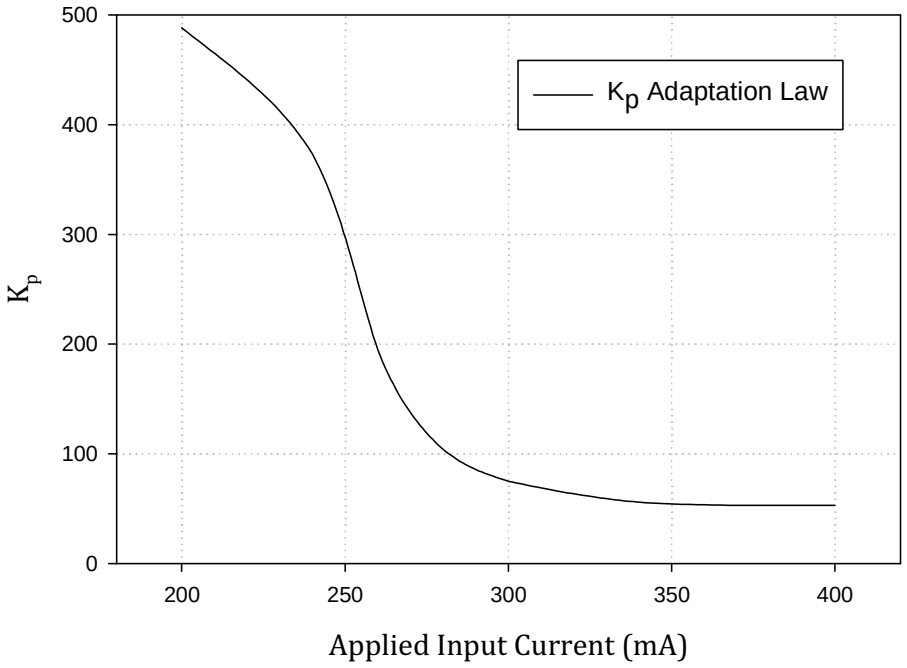

Figure 6-5. Adaptation law for K_p

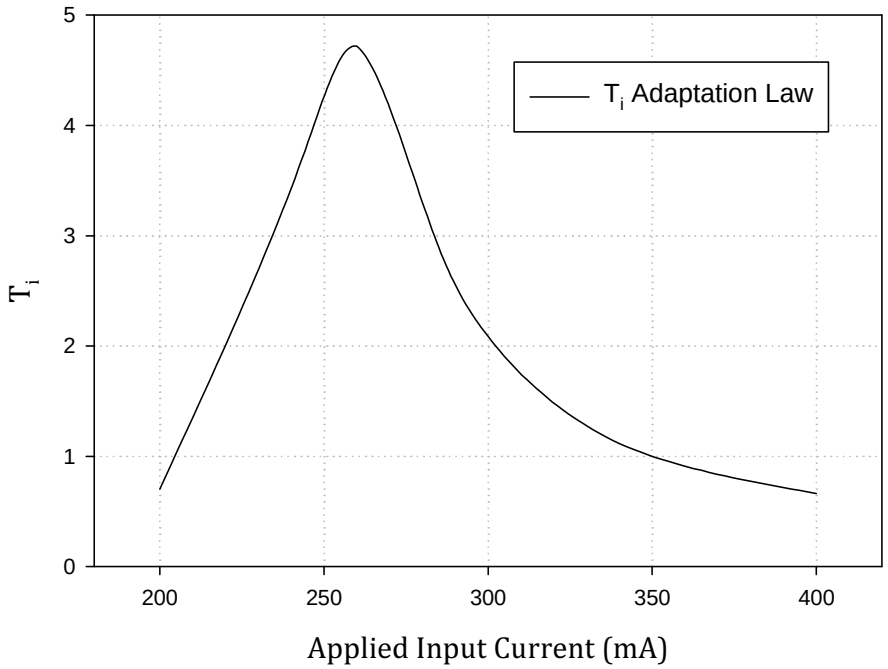

Figure 6-6. Adaptation law for T_i

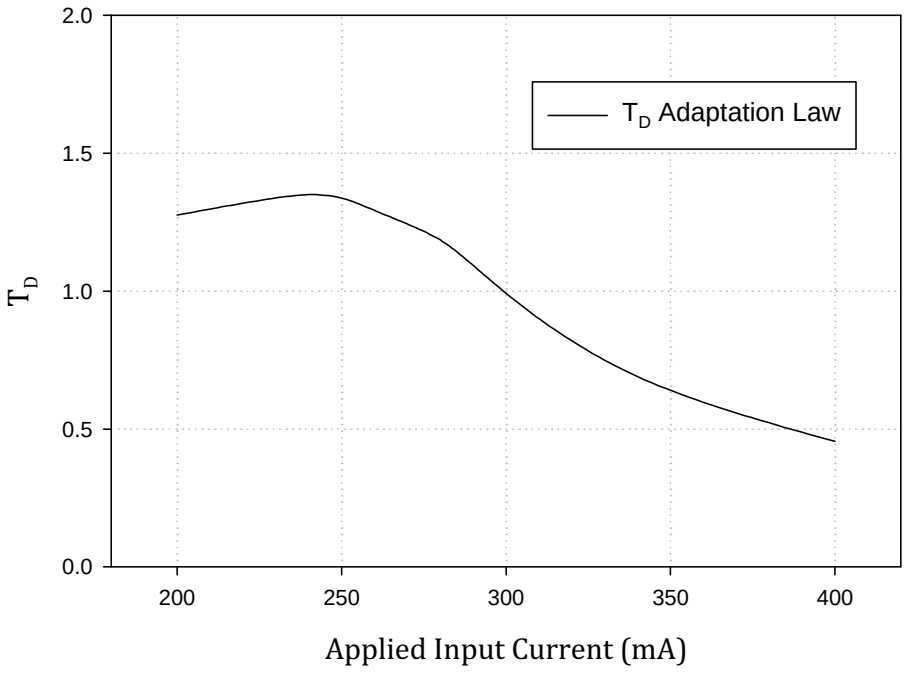

Figure 6-7. Adaptation law for T_D

The gain values change in accordance with the tuning formulae outlined in Table 6-2 for SMA temperatures at time (t-1) differing from ambient temperature. The required applied input current value can be found directly from the output of the inverse Preisach model. This value is used in the selection of the adaptive PID controller gains.

The K_p gain profile exhibits high gain values for low input current values, and low gain values for high input currents. Over the sensitive region of input currents, where small increases in input result in the largest increases in SMA strain, the gain values drop sharply. This is expected as large gain values in this region would lead to undesirable oscillation. The integral time, T_i, also increases rapidly over the sensitive region. This is inversely proportional to the integral gain and therefore results in a reduction in integral gain over the sensitive region. This is also expected as larger gain values in this region can lead to

unwanted oscillations occurring. Furthermore, the likelihood of steady state error occurring is greater at the limits of operation. T_i is low at these values, resulting in larger K_i gains to remove the steady state error. The derivative time profile, T_D, decreases as input current increases. This coincides with the increase in the rate of change of SMA strain owing to larger applied input currents. By decreasing the T_D value, further unwanted oscillations are prevented from occurring.

6.6 Control Strategy Experimentation

The controller solution is to be validated using the experimental test-bed previously described in Section 4.4.1. The proposed control strategy was implemented in LabVIEW 2009 using a state-machine programming approach (See Appendix II).

The experimental procedure consists of a series of position and tracking control tasks. Position control tasks consisting of a series of reference step inputs are designed to test the response of the SMA bundle actuators using the proposed adaptive control strategy. Tracking control tasks consisting of reference sinusoidal inputs at various frequencies are designed to facilitate analysis of the tracking performance of the SMA bundle actuators. A summary of the experiments performed is shown in Table 6-3.

Table 6-3. Adaptive PID Control Strategy Experimental Summary

Test Ref. No.	Control Task	Time (s)	Freq. (Hz)	Load per SMA (N)	Notes	Results Reference
CV1	Position	180	N/A	-	-	Figure 6-8 & 6-9
CV2	Robust Position	180	N/A	0.25→ 1.25	Loading	Figure 6-10
CV3	Robust Position	180	N/A	-	Air flow Cooling	Figure 6-11 & 6-12
CV4	Tracking	160	0.02→ 0.3	-	-	Figure 6-13 → 6-16
CV5	Robust Tracking	160	0.02, 0.15	0.25→ 1.25	Loading	Figure 6-17 & 6-18
CV6	Robust Tracking	160	0.02, 0.05	-	Air flow Cooling	Figure 6-19

Experimental data gathered from the sensors located on the experimental test bed are captured using a NI CompactDAQ system. The results were collected and compiled in NI LabVIEW 2009. External noise is filtered using a 4^{th}-order Butterworth filter. Current, voltage, temperature (SMA wire & Ambient), and displacement readings are recorded. Additionally, disturbances are inputted to examine the robustness of the proposed control strategy. The disturbances are introduced as

i. loading applied directly to the SMA bundle actuators, and

ii. airflow across the SMA bundle actuator resulting in undesired forced cooling

Prosthesis loading, and hence actuator loading resulting in stress being applied to the SMA wires, is highly relevant to prosthetic actuator solutions owing to the interactive nature of the device. Air cooling disturbance is used in experiments to examine the system response to an unexpected change in SMA wire h-value. Air flow across SMA wires results in an increased convective coefficient, and thus a corresponding reduction in strain is produced.

Each experiment is designed to demonstrate the capacity of the SMA bundle actuators to follow a desired series of step input values or sinusoidal input values covering the full actuation spectrum. This allows a complete analysis of the control strategy. Experiments CV2, CV3, CV5 and CV6 are compared with the results of experimentation using a similar control strategy tuned with fixed PID gains. Experimental data captured using fixed PID gains and a feedforward inverse Preisach model will be designated as 'PID', whereas experimental data captured using the adaptive gains combined with a feedforward inverse Preisach model will be designated as 'a-PID'.

6.7 Key Results & Discussions

The selected key results from the experimental procedure are divided into the response to a series of step inputs (CV1-CV3), and the response to sinusoidal inputs (CV4-CV6). Comparisons in terms of set-point tracking ability between the various control strategies are carried out by examination of the root mean square error (RMSE) of the steady state and transient portions of the response to the desired step inputs. This allows for the full error to be determined. Tracking control ability was compared in terms of the phase lag and RMSE

exhibited between the desired response and the actual response of the SMA bundle actuators.

6.7.1 Position Control – Step Response - No Loading, No Air-flow

A series of desired input step values spanning the full range of SMA bundle actuator strains were selected. The step inputs chosen represent the full spectrum of possible SMA strains, from 0 to 3.6%. The desired step values feature a range of strain values across the full spectrum of achievable SMA strain to demonstrate the consistent accuracy of the controller. Furthermore, the step inputs chosen allow for the examination of the response during heating tasks (increasing inputs) and cooling tasks (decreasing inputs).

The a-PID controller demonstrates excellent capacity to maintain accurate steady state response while improving the dynamic response considerably. This can be shown by a comparison with the Inverse Preisach (IP) model generated open loop response of the SMA bundle actuator (Figure 6-8). It can be observed that the transient response during cooling is marginally slower than that of the heating phase. This is a result of the limitations of natural cooling. Furthermore, the transient response at the max strain limit during heating is slower due to the heating limitations of the SMA wires being reached. The average rise time for each step is approximately 0.3 seconds using a-PID closed loop feedback, compared to between 3-4 seconds in open loop (Figure 6-9).

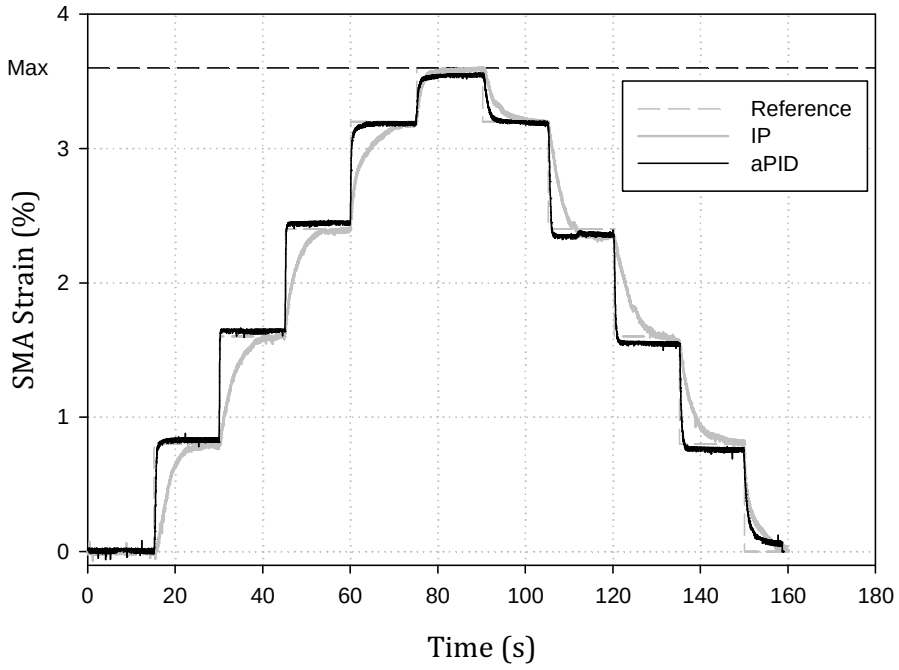

Figure 6-8. Step Response – No External Disturbances

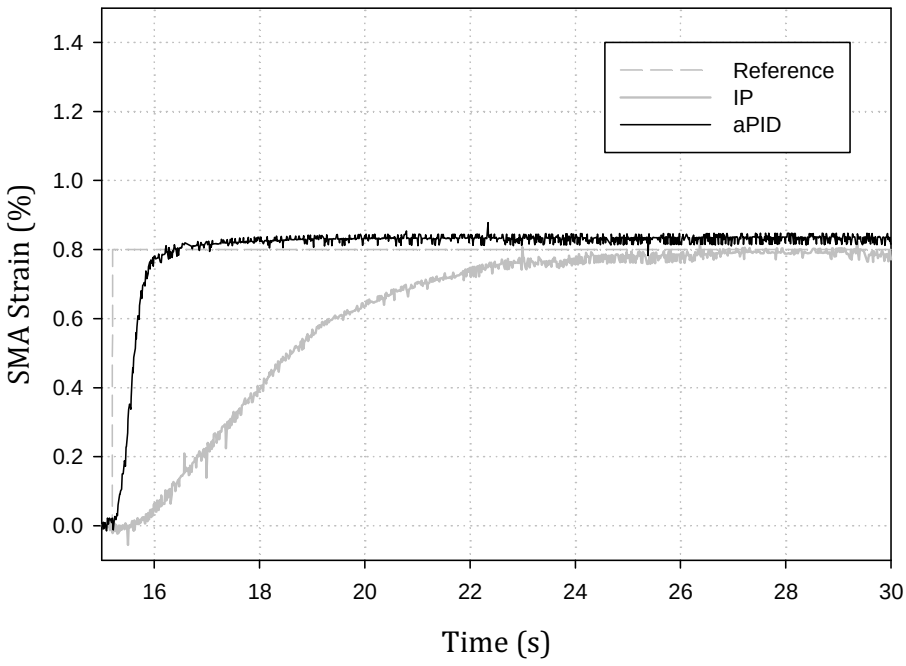

Figure 6-9. Step Response – No External Disturbances – Magnification of Step

Importantly, overshoot is minimized, leading to the possibility of successfully performing delicate tasks when utilised in a suitable prosthetic finger

framework. The maximum steady state error occurs at the actuation limits of the actuator. This is a result of limitations in allowable input currents. The RMSE demonstrated using the a-PID control strategy is approximately 0.07%ε during the steady state phase. If necessary, improvements can be made by taking more data points on the Preisach plane, thus ensuring that the inverse hysteresis model accuracy is enhanced further, leading to enhanced steady state performance. Measurement noise is attributable to mechanical vibrations from equipment within the laboratory. However, this noise does not noticably impact on the outcome of the results.

6.7.2 Position Control – Step Response – Loading

The robustness of the control strategy adopted can be examined initially by applying loads to the SMA bundle actuators (Figure 6-10). A range of loads from 0.25-1.25N per SMA wire (equating to approximately 15-75MN/m^2) are applied when the SMA material is in the austenite phase. The load is maintained through one full cycle and released upon returning to the following austenite phase.

It can be seen in Figure 6-10 that both the PID and a-PID control strategies work to compensate the error caused by loading. The a-PID strategy exhibits much higher robustness than the PID strategy in demonstrating the capacity to maintain the desired position.

The a-PID strategy immediately counteracts the effect of loading when applied, resulting in a maximum steady state error of 0.04%ε. This can be compared with the PID strategy which exhibits a maximum steady state error of 0.18%ε. The RMSE of the a-PID strategy during the full loading cycle is 0.2%ε compared

to 0.42%ε for the PID strategy. It can be seen that the effect of loading results in undershoot during the cooling cycle. The a-PID strategy works more effectively to counteract this effect in comparison with the PID strategy.

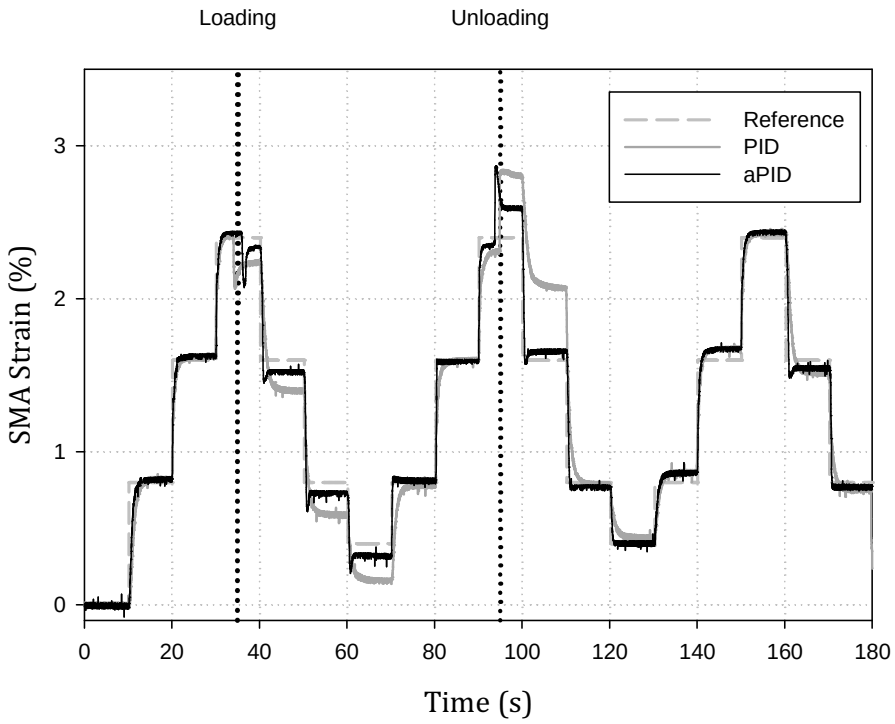

Figure 6-10. Step Response – Loading (0.5N per SMA)

Upon unloading, the SMA bundle actuator recoils significantly. The a-PID strategy attempts to rectify this immediately, whereas the PID strategy is unable to correct the SMA bundle actuator output for a significant time period. It can be noted that although the a-PID controller attempts to counteract the recoil effect immediately upon unloading, it is not completely successful. This is due to the highly nonlinear stress-strain dynamics of SMA bundle actuators. In order to allow for even greater compensatory effects in the face of loading, the inclusion of a nonlinear SMA bundle actuator stress-strain model would be required. This, however, is highly complex and cannot be achieved with the limited

computational power available for realizable real-time control. The transient response of the SMA bundle actuator is only marginally affected by the applied loading. Further experimentation has shown that typical loads up to and including 1.25N per SMA wire (75MN/m^2) are acceptable with only a small linear decrease in transient response observed. This is linked to the thermal behaviour of the SMA wires. With increased loading, the transformation temperatures of the SMA material rise in an approximately linear fashion (See Section 5.3). The transient response depends on time required to undergo phase transformation. Therefore, the transient response is a function of the input power into the SMA wires. Increased input power results in increased energy input in an attempt to overcome the latent heat of transformation in a faster time. If the applied input power is sufficient to allow the SMA to reach and exceed the latent heat of transformation, full actuation will occur and the transient response time will improve with the heating rate. However, if the input power is insufficient to overcome the latent heat, the transient response will degrade severely in a nonlinear fashion, whilst the steady state capacity will also be adversely affected (See Section 4.5.3.3). The fast transient response of the a-PID strategy is maintained under loading of 0.5N per SMA wire with an average rise time value of 0.32 seconds. This compares favourably with the PID controller which exhibits values of >1 second. This is due to the capacity of the a-PID controller to apply more suitable gain values for varying input currents.

6.7.3 Position Control – Step Response – Air-Flow

Air-flow was passed across the SMA bundle actuators with a flow rate of 0.3m/s for one step cycle. The experimental testing cycle begins in the highly sensitive

region of the SMA strain spectrum at 2.5%ε, then goes to a region of lower sensitivity of 0.5%ε and returns to the starting position via a series of steps. This allows for analysis of the performance of the controller across the spectrum of different SMA sensitivities to applied input currents (Figure 6-11). The air-flow resulted in an increased rate of convection from the SMA wires, resulting in a change in response to input current. The control strategy is thus required to input greater levels of input current to maintain accurate steady state response. The maximum strain capacity of the SMA wires is therefore decreased owing to the restrictions of the maximum permissible current values (400mA for 150μm wires) being applied. It can be seen from Figure 6-11 that the a-PID strategy compensates the undesirable effects of the air-flow across the SMA wires to a much greater extent than a PID strategy.

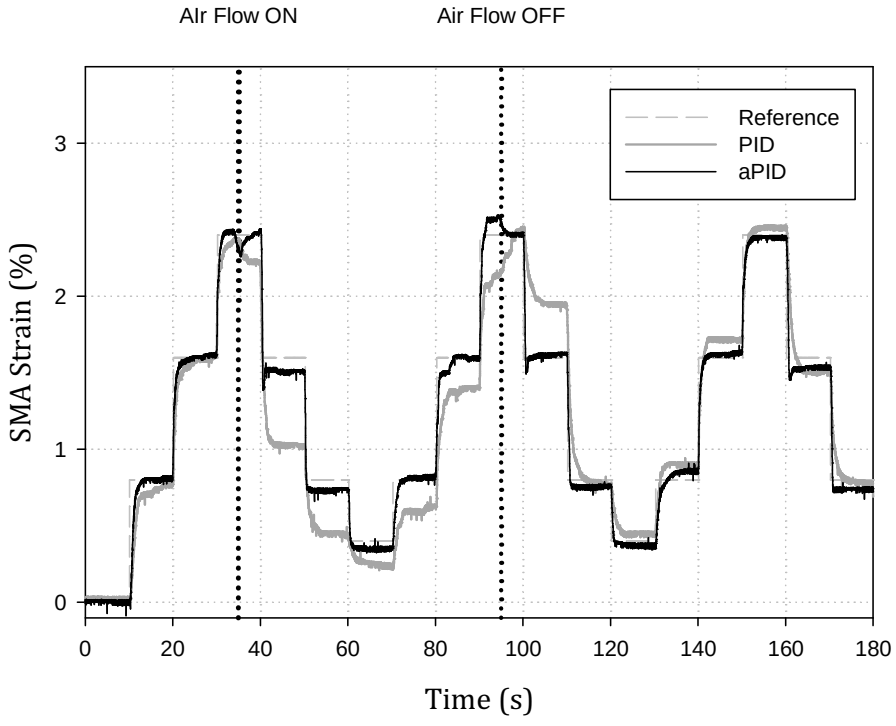

Figure 6-11. Step Response –Air-Flow (0.3m/s)

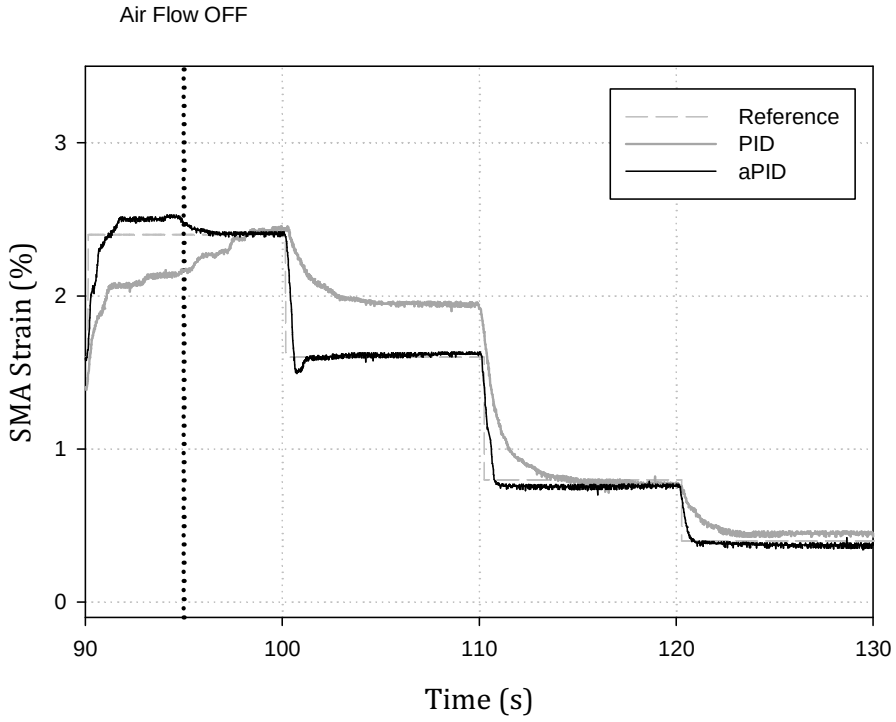

Figure 6-12. Step Response–Air-Flow (0.3m/s) – Magnification of Unloading Phase

As the air-flow is switched on, the a-PID strategy compensates by increasing the applied input current to compensate for the drop in SMA wire temperature. Results are shown to be excellent in terms of maintaining the steady state performance of the SMA bundle actuator during air-flow initiation, and in quickly adapting to the air-flow being switched off. The response from the PID strategy fails to compensate sufficiently.

The RMSE of the a-PID controlled SMA bundle actuator is approximately 0.185%ε which is a considerable improvement on the PID strategy which exhibits a RMSE of 0.41%. Furthermore, the steady state error in the presence of the undesirable air-flow is significantly larger using the PID strategy in comparison with the a-PID strategy.

6.7.4 Tracking Control – No Loading, No Air-flow

The capacity for sinusoidal set-point tracking is an important requirement as it allows for the evaluation of the bandwidth limitations of the SMA bundle actuators. Tracking facilitates common prosthesis actions such as scrolling and pointing. The frequencies selected range from a minimum value of 0.02Hz, to a maximum of 0.3Hz. This allows for the examination of the set-point tracking capacity over the full range of sinusoidal inputs. At 0.3Hz, tracking bandwidth decreases significantly and phase lag increases beyond reasonable limits. By taking this approach to testing, the gradual decline in performance can be noted and the limits of functionality ascertained.

Tracking performance using the a-PID strategy has been shown to exhibit good response under unloaded conditions. RMSE values of 0.1%ε and 0.14%ε at the low end frequencies of 0.02Hz & 0.08Hz respectively are recorded (Figure 6-13 and Figure 6-14).

Tracking is shown to exhibit little or no phase lag for frequencies up to 0.18Hz. However, SMA tracking bandwidth decreases above 0.18Hz (Figure 6-15). Breakdown in performance is reached at approximately 0.3Hz where the limitations of the SMA bundle actuators are evident (Figure 6-16). This is due to the natural limitations of SMA wires subjected to natural cooling. It has been shown in Section 5.9 that forced cooling via aluminium heat sinks can be used to improve this further. However, this is not a viable option for a portable prosthetic solution as it brings an added layer of mechanical and control strategy complexity.

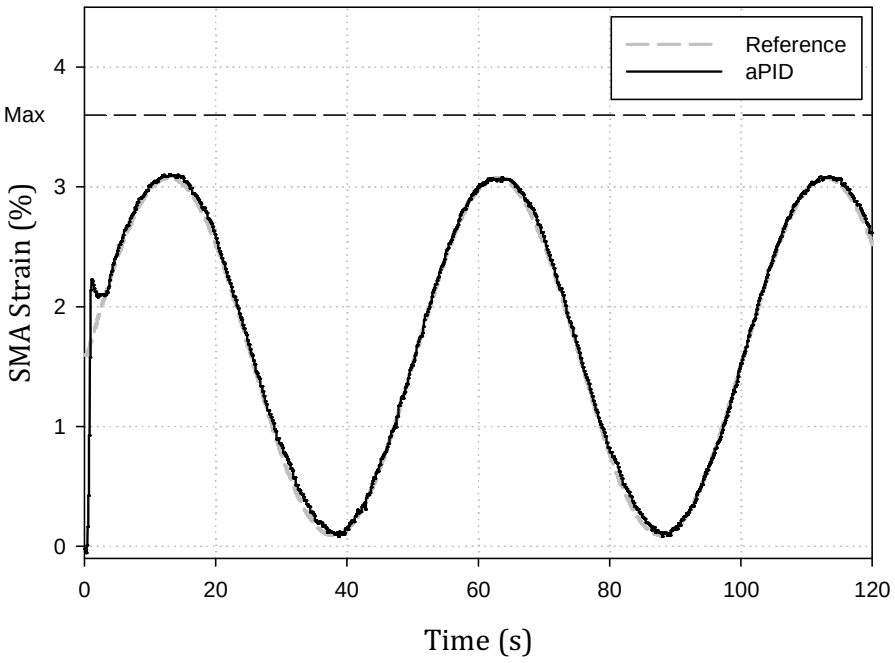

Figure 6-13. Sinusoidal Tracking Response – 0.02Hz

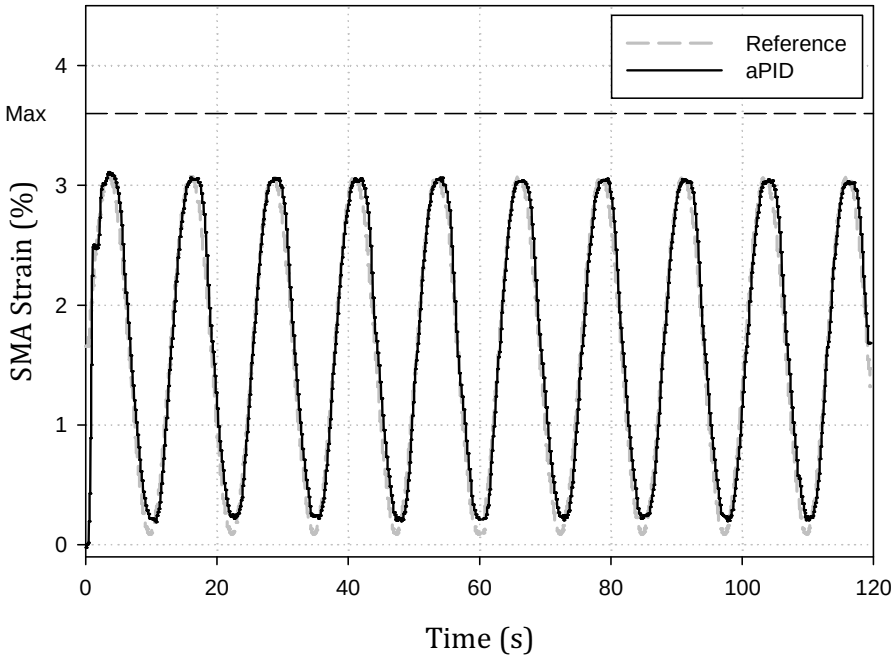

Figure 6-14. Sinusoidal Tracking Response – 0.08Hz

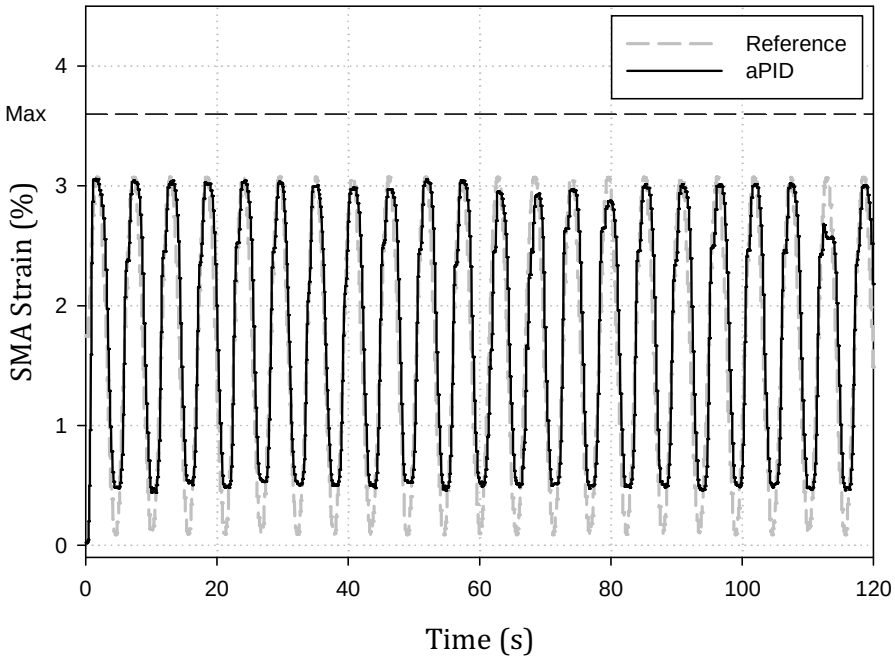

Figure 6-15. Sinusoidal Tracking Response – 0.18Hz

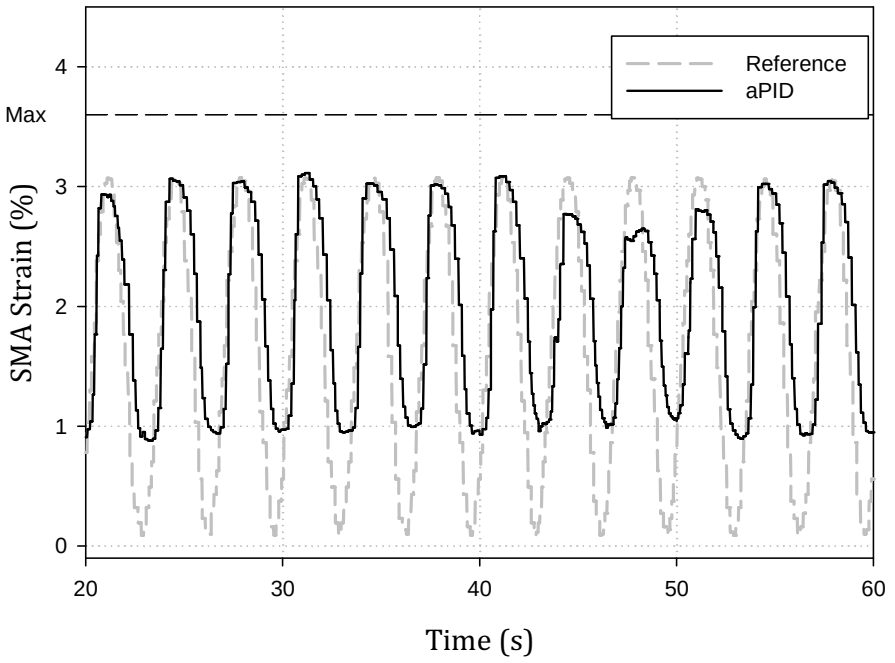

Figure 6-16. Sinusoidal Tracking Response – 0.3Hz

It can be seen in Figure 6-16 that during the heating cycle, tracking is possible using the a-PID control strategy. However, the reduction in bandwidth due to

natural cooling limitations results in tracking capacity being reduced over the lower half of the sinusoidal waveform.

6.7.5 Tracking Control – Loading

Robustness is examined by applying loads ranging from 0.25-1.25N per SMA (5-75MN/m^2) to the SMA bundle actuator for two full cycles. Results demonstrate that the a-PID strategy works to maintain a high degree of tracking accuracy (Figure 6-17). There are minor decaying oscillations observed on the rising portion due to the requirement for large gain values brought on by an increase in error as a result of loading. It is also evident that the a-PID strategy works more effectively to reduce the effect of loading in the martensite phase. The average RMSE of the a-PID strategy is 0.14%ε under the loading range shown in Table 6-3. This is good in comparison with the PID strategy exhibiting an average RMSE of 0.32%ε under an identical loading range. SMA bundle actuator limitations result in a minor tracking error at the peak of the sinusoidal cycle when loading is applied. The system also shows good recovery response following unloading, where the RMSE immediately returns to its unloaded value of 0.1%ε. Furthermore, it can be seen that an increase in frequency to 0.2Hz does not impact on the robustness of the controller (Figure 6-18). It is shown that the effect of the loading favourably influences the cooling cycle by increasing the M_s temperature of the SMAs and allowing relaxation to initiate at an earlier stage. This leads to an increase in bandwidth when compared to the unloaded SMA bundle actuator.

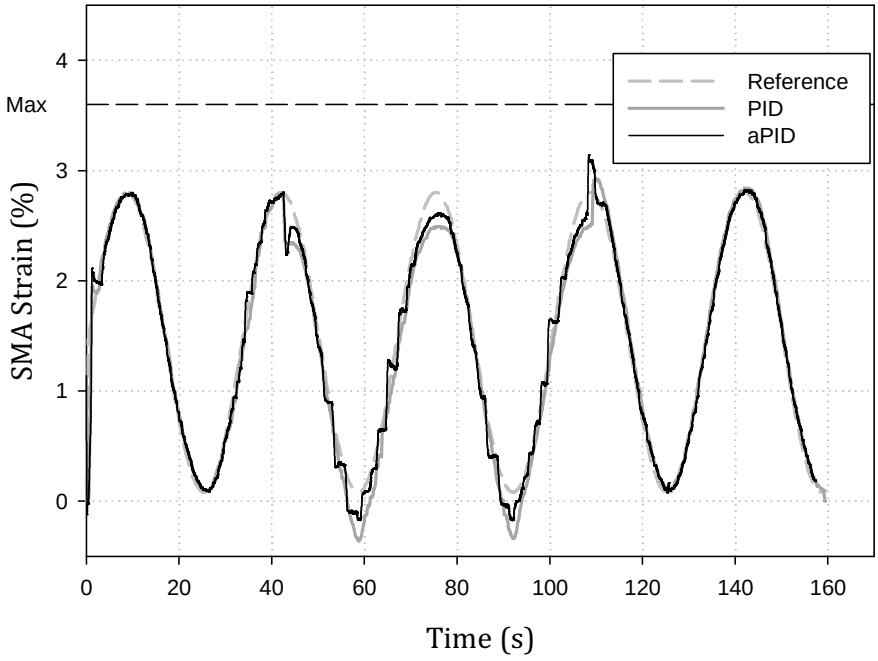

Figure 6-17. Sinusoidal Tracking Response (0.02Hz) – Loading (0.5N per SMA)

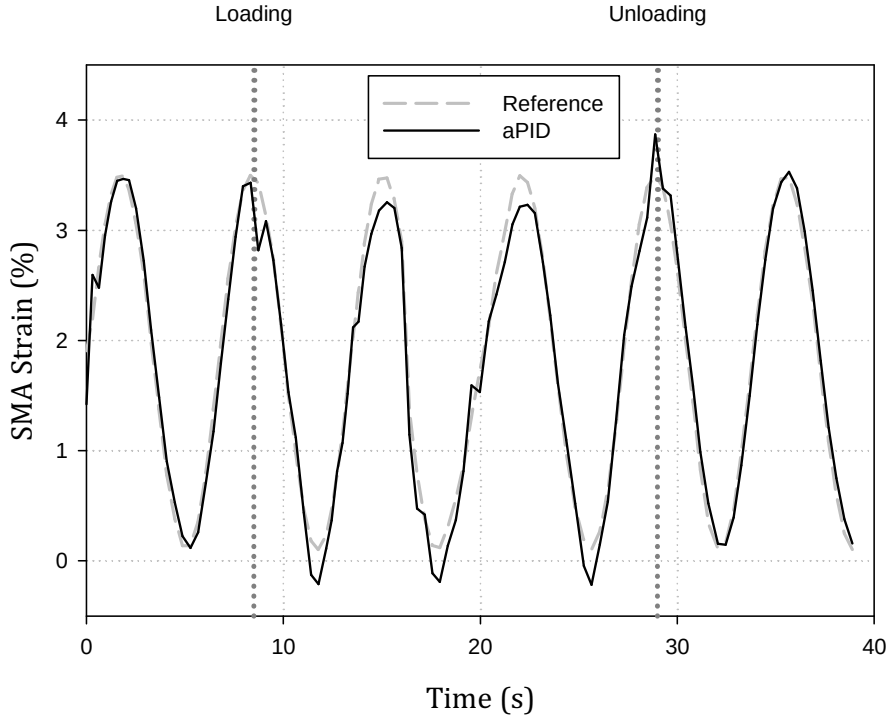

Figure 6-18. Sinusoidal Tracking Response (0.2Hz) – Loading (0.5N per SMA)

6.7.6 Tracking Control – Air-flow

Air-flow across the SMA bundle actuators has been shown to impact negatively on the thermal response, and hence the strain response (See Section 6.7.3). For set-point tracking tasks, the a-PID strategy demonstrates favourable results in compensating the effect of air-flow across the SMA wires. The average RMSE exhibited is 0.126%ε in comparison to the average RMSE exhibited by the PID strategy of 0.48%ε (Figure 6-19). Additionally it can be seen that the a-PID control strategy restores the full desired bandwidth of the SMA bundle actuators.

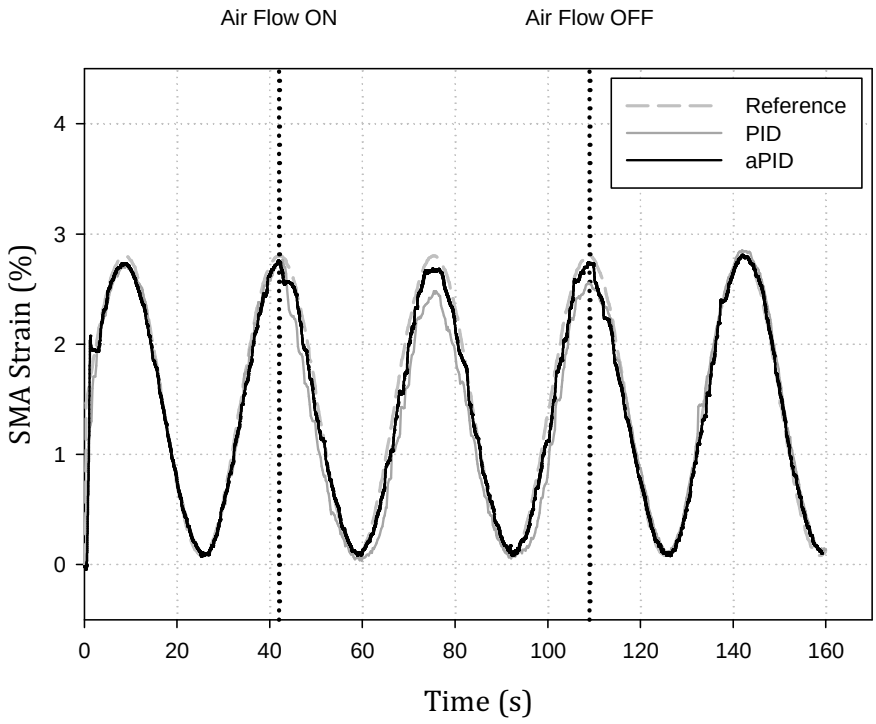

Figure 6-19. Sinusoidal Tracking Response – Air Disturbance (0.3m/s)

6.8 Conclusions

A comparison between the control strategies applied to SMA actuators in the literature has been carried out. A decision matrix was adopted to enable the selection of the best strategy based on a number of key parameters required for utilization in prosthetic finger actuation tasks. The chosen adaptive control strategy features an adaptively-tuned PID controller in a feedback loop in conjunction with an inverse Preisach model of hysteresis in a feedforward loop. The controller was tuned based on the phenomenological behaviour of the SMA wires. It has been shown conclusively in Section 6.7 that the a-PID control strategy offers increased benefits over the previous control strategies applied to SMA actuators (See Section 2.9). The dynamic model of SMA response utilised in the control strategy presents a more representative model of SMA behaviour than previous controllers. This therefore accounts for the improvements shown via experimental work. Furthermore, the strategy can be adopted and tuned directly from the phenomenological behaviour of the SMAs. The a-PID control strategy developed can be utilised in SMA bundles charged with rotating mechanical finger joints in a prosthetic finger framework. This is examined further in Chapters 7 & 8. The experimentation carried out in Section 6.7 indicates that the SMAs are naturally limited to slower movements even when subjected to enhanced cooling strategies. Therefore, a balance between the unavoidable disadvantages such as reduced rates of actuation and the advantages such as increased mechanical simplicity when compared to miniature DC motors is recommended prior to adoption in future prosthetic devices. The a-PID gains are independent of the number of wires in the SMA

bundle provided cross-talk is prevented. This allows for the implementation of SMA bundles of various sizes using the approach adopted in this chapter of the work.

7. MECHANICAL DESIGN OF A SMA BUNDLE ACTUATED PROSTHETIC FINGER SOLUTION

7.1 Introduction

The design of a prosthetic index finger that permits the implementation of SMA bundle actuators without compromising on biomimetic properties is necessary. The design requirements state that the prosthetic finger must exhibit properties comparable with that of the human finger in terms of geometry, aesthetics, mass and volume, and capacity to perform common prehensile postures. Suitable materials must be selected to facilitate the design of a prosthetic finger to match these requirements. The SMA bundle actuators are limited in size by specifying their inclusion within a volume similar to that of the palmar region of a human hand. A kinematic assessment and dynamic model of the completed design is necessary to assess the range of movement of a proposed finger and the effect of different joint rotation rates. This will allow for an appraisal of the prosthetic finger actuation solution. Furthermore, an investigation into the possibility of utilising miniature gearing systems to permit the SMA bundle actuators to produce the full range of desired rotation is required.

7.2 Key novel aspect of the artificial index finger design

Approaches to SMA actuated prosthetic finger designs vary greatly with the majority of designs divisible into two categories (See Section 1.4):

i. Designs featuring single wire & multiple wire SMA actuators located within the forearm region

ii. Designs featuring single wire actuators acting directly within the finger

Category (i) designs offer the key advantage of large SMA strain capacity due to longer SMA wires within the forearm, whereas, category (ii) offers the possibility of designing an independent hand structure unreliant on an additional forearm structure. However, there are major disadvantages associated with both approaches. Category (i) solutions result in prosthetic solutions where the hand structure cannot act independently without the accompanying large forearm structure. This eliminates the possibility of using these prosthetic solutions on patients with remaining forearms, ruling out use on 59% of patients suffering partial upper extremity limb loss [6]. Category (ii) solutions suffer from low finger tip force generation resulting in unstable and weak prehensile capacity. Furthermore, where groups have implemented larger SMA wires in an attempt to compensate for the loss in finger tip forces, the dynamic capability in terms of SMA strain and relaxation rates decreases significantly.

A novel approach to overcoming the disadvantages associated with previous designs whilst maintaining the advantages of each is to implement SMA bundle actuators within a workspace equal in volume to the palmar region of the human hand. This leads to the opportunity for an independent SMA hand which is capable of producing significant finger tip forces. Suitable gearing ratios can be used to enhance the rotational capacity of the implemented SMA bundle actuators while torque can be enhanced owing to increases in the number of SMA wires in the bundle.

7.3 Mechanical design aspects for consideration during design

There are a range of key mechanical design aspects to be adhered to during the design process. These can be subdivided into the two interrelated categories, (i) biomimetic criteria (Section 7.3.1) and (ii) SMA actuator implementation criteria (Section 7.3.2).

7.3.1 Prosthetic Solution Biomimetic Criteria

i. *Functionality* - The dynamic capacity of a prosthetic finger under the actuation of SMA bundle actuators must mimic that of the human hand.

ii. *Aesthetics & Feel* - The geometry of the prosthetic finger must be closely related to the geometry of the human index finger. The materials chosen for the design must be lightweight but durable in order to give the end-user a sense of familiarity with the device.

iii. *Realistic Actuation* - The SMA bundle actuators must deliver a level of actuation performance similar to the muscles in the human hand.

iv. *Safety* - The relatively high electrical currents and temperatures associated with SMA bundle actuators must be restricted from end user interference.

v. *Maintenance* - Ease of assembly and disassembly is critical to ensure quick and easy replacement of any failed components or fatigued SMA wires.

vi. *Manufacture* - Adherence to design-for-manufacture is crucial in maintaining an optimal cost basis for production of the device.

7.3.2 SMA Bundle Actuator Implementation Criteria

i. *Wire Quantity* - The number of SMA wires required within an actuator bundle is a function of the max joint torque required at joint.

ii. *Force/Torque Transfer* - The force generated by the contraction of the SMA actuator must be transferred from the SMA modules to the fingers of the prosthesis as efficiently as possible.

iii. *Actuator Housing & Connectivity* - SMA wires must be connected in series electrically and contact between adjacent wires/modules should be prevented.

iv. *Layout* - A counter-force to return the SMAs to their original shape upon cooling must be provided by bias-spring or antagonistic SMA wires.

v. *Heating Methodology* – A suitable heating methodology that is simple to implement and operate is required.

7.4 Partial Mechanical Hand Framework

A functioning partial mechanical hand framework is realized in Figure 7-1 in order to demonstrate that all necessary components can be inserted into the available volumetric area. The design is only intended to provide the reader with a reference design to allow for clarity in the descriptive details found in this chapter and is not seen as the optimum solution. The design is based on the

dimensions of a typical adult human hand. However, the design outlined does not take into consideration any aesthetic qualities.

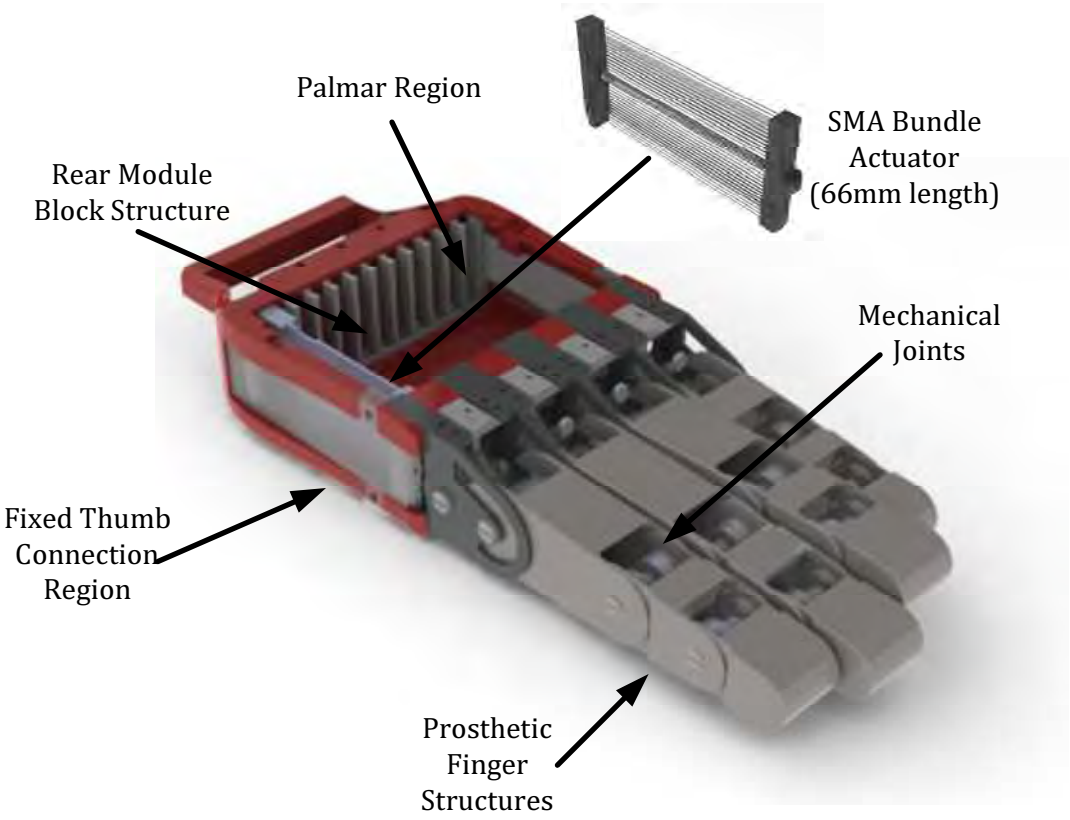

Figure 7-1. Design of SMA bundle actuated partial prosthetic hand

It can be seen in Figure 7-1 that the novel element of the design is that SMA bundle actuators are designed to fit into the palmar region of the hand. As a result, each SMA bundle must be thermally isolated from neighbouring bundles to allow for maximum frequency of operation and limited thermal disturbance. The maximum length of the SMA bundle actuators within the palmar region is 66mm. This will be taken as the maximum allowable SMA bundle actuator length during experimentation in Chapter 8 of this work.

7.4.1 The SMA Bundle Actuator Modules

The novel actuation system consists of two module-block structures located within the palmar area of the design (Figure 7-2). Each block is designed to house twelve individual SMA bundle actuator modules to which the SMA wires are attached. An SMA bundle actuator is designated to each joint in the prosthetic finger. Each module is separated by a distance of 56mm from face to face, and is 5mm in depth (66mm total length). Gearing is located between the SMA bundle actuator and prosthetic finger framework.

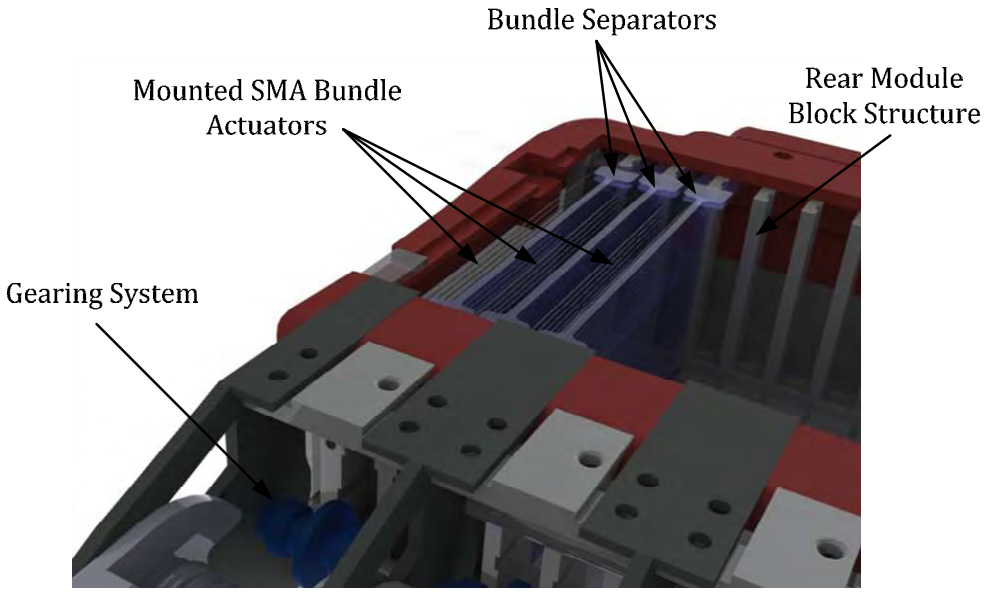

Figure 7-2. SMA Bundle Actuators Mounted in Palmar Region of Hand

The module-block holder located at the wrist end of the palm is designed to hold the SMA modules in a fixed position. The module-block holder located at the finger end of the design allows the SMA modules to slide back and forth under the forces generated during SMA strain and relaxation. Linear sliding motion is ensured through the provision of a series of shallow inlets within the module-block holder. The material selected for both the module-block holder and the

SMA modules is PTFE (PolyTetraFlouroEthylene) owing to its low coefficient of friction, high strength, high heat resistance, good electrical resistance and ease of moulding. Polycarbonate bundle separators are utilised to reduce the possibility of thermal cross-talk between the different SMA bundles.

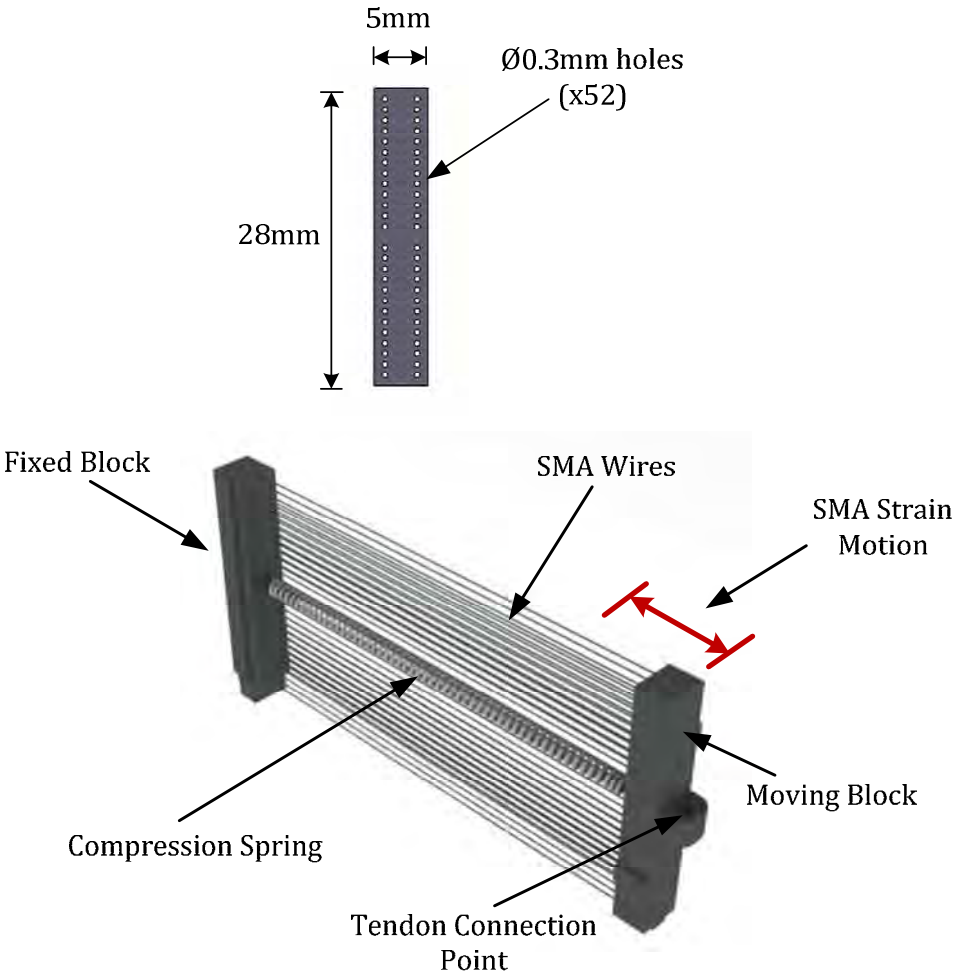

Figure 7-3. SMA Module Design– Maximum Wire Quantity of 52

Each SMA module features an array of holes to accommodate the mechanically parallel SMA wires. The number of holes can be increased for modules requiring larger quantities of SMA wires in parallel. However, due to size constraints, a maximum of 52 holes of diameter 0.3mm can fit onto any one SMA module. Each wire must be externally facing to facilitate heat sinking if required. Thus, the

SMA wires are limited to two vertical columns (Figure 7-3). One single elongated SMA wire can be threaded though all holes in the module and securely anchored. This ensures a maximum of only two wire anchoring points are required on any module whilst maintaining the parallel requirements of the SMA bundle. The centre distance between each hole must exhibit a minimum of 1mm to prevent crossover of the thermal boundary layer of each SMA wire during heating, and to ensure that the structure of the module does not collapse under the force generated by SMA strain. Furthermore, a central gap must be maintained to facilitate the inclusion of compression springs to provide the relaxation force necessary during cooling. The mechanical finger joints are connected to the SMA wires using an artificial tendon network. Furthermore, miniature tension or rotary springs can be mounted between each prosthetic phalanx to assist in returning the finger joints to their original position when required.

7.4.2 The Thumb

The thumb has been omitted from the current design as it is outside of the scope of this work. The work within is focused solely as an investigation of an SMA actuated prosthetic finger. However, it must be noted that within a full prosthetic hand design, the thumb plays an important role in grip stability. It works to counteract the forces applied by the finger joints during gripping tasks. Since the thumb must counteract the forces applied by all the fingers in the hand on occasion, many SMA wires would be required for a fully functioning thumb. The volumetric limitations do not permit this when all SMA bundle actuators are mounted within the palmar region. It is therefore recommended to utilise a

fixed thumb. If a fully functioning thumb is required, it may be necessary to mount SMA bundle actuators within the forearm region, thus reducing the universality of the design. Further investigation of the inclusion of a thumb is recommended as part of future work.

7.5 Outline of the Proposed Prosthetic Finger Design

The proposed prosthetic finger design consists of individual proximal, intermediate and distal phalanges which are linked together mechanically via titanium pins rotating in miniature ball bearings to minimise rotational friction (Figure 7-4). The length of each individual phalanx is consistent with that of an average adult human index finger at 42mm, 26mm and 19mm for the proximal, intermediate and distal phalanges respectively. Each phalanx has a depth of 20mm over the entire length enabling a series of similarly constructed fingers to fit within the constraints imposed by the size of a typical human hand.

The mass of each finger will be approximately 30g based on the adoption of lightweight, high strength materials such as aluminium and PTFE during manufacture. This will ensure that the moment of inertia of the finger joints is maintained as low as possible without compromising structural integrity. A low moment of inertia requires less torque to accelerate during dynamic motion (See Section 7.9.1) and hence the energy requirements are lower. The width of each finger is tapered slightly from the metacarpophalangeal (MP) joint to the tip of the finger in line with the human finger. A lightweight, high-friction 'skin' can be applied to the skeletal structure at a later stage to adapt the aesthetics of the design to that of a human finger.

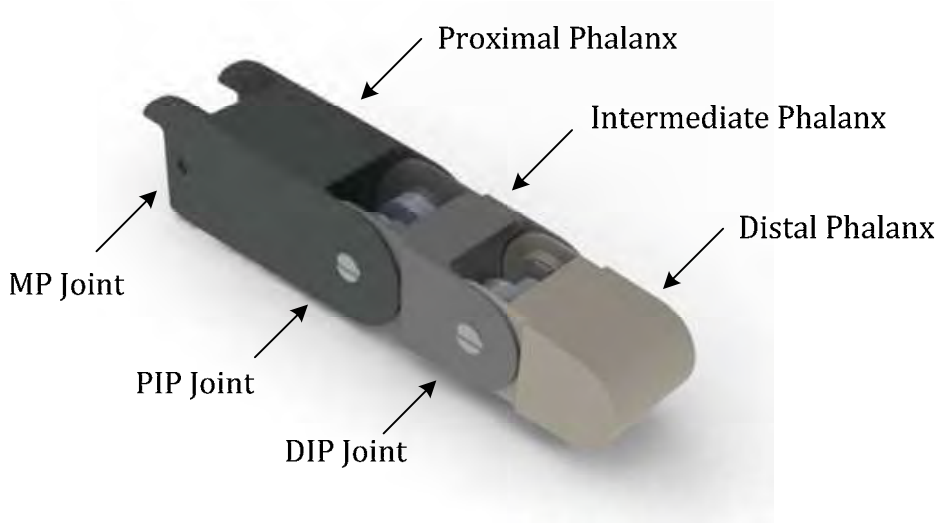

Figure 7-4. Mechanical design of a SMA actuated artificial index finger

The MP, PIP and DIP joints are each constructed in a slightly different manner to account for their active and passive requirements (Figure 7-5). An active element can be defined as a direct connection between an artificial tendon and a rotational component which results in direct rotation of the associated joint. A passive element can be defined as one which permits the passing over of an artificial tendon to the next joint along the artificial finger. The MP joint consists of one active element to induce rotation of the proximal joint, and two passive elements allowing for the passing over of the artificial tendons destined for the PIP and DIP joints. The PIP joint consists of one active and one passive element, while the DIP joint consists of one active element only. Artificial braided Teflon tendons are used to transmit the force and displacement of the SMA bundle actuator to the finger joints. Braided Teflon is chosen to minimise friction, whilst providing a high tensile strength to resist breakage under the actuation forces applied [153].

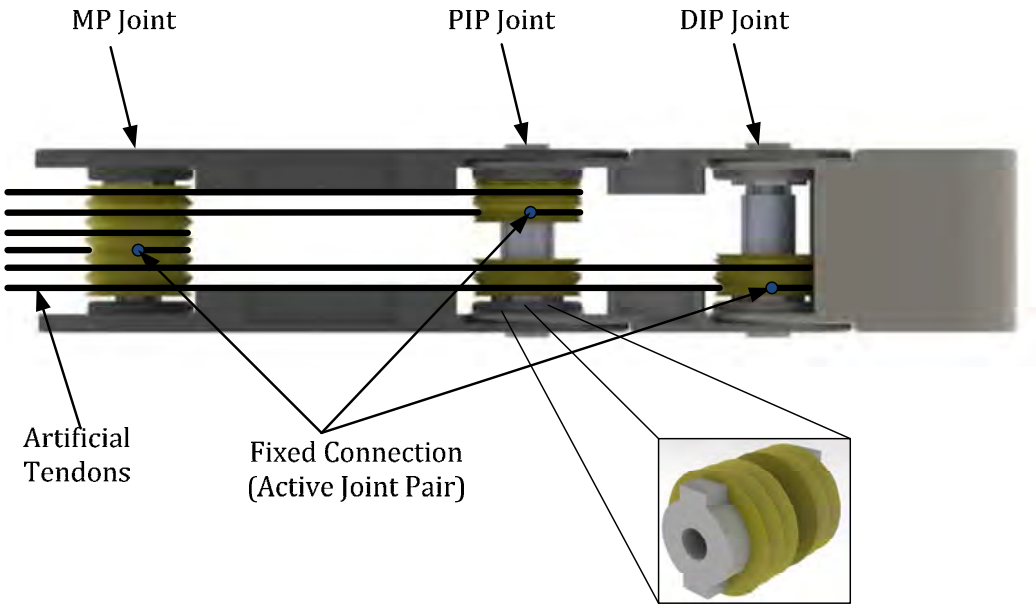

Figure 7-5. Active/Passive Joint & Artificial Tendon Layout

One SMA bundle is permitted to provide actuation to each individual joint within the finger to maximise the possibility of human-like motion. Since the allowable size of each SMA bundle actuator is limited by space restrictions, it is crucial to maximise length as far as possible within the space available. The maximum available length is calculated to be 66mm based on the volume of the human hand palmar volume (See Section 7.4). Based on the 3.6% maximum strain capacity, the SMA length constraints allow for a maximum actuator displacement under the maximum allowable current to be 2.37mm per SMA bundle. A suitable miniature gearing system can be employed to increase the actual displacement to a larger value where required. Gearing however diminishes the applied force of the bundle, so a larger number of SMA wires, and larger input power is required. Therefore, an efficient balance between actuator displacement and SMA wire quantity must be found.

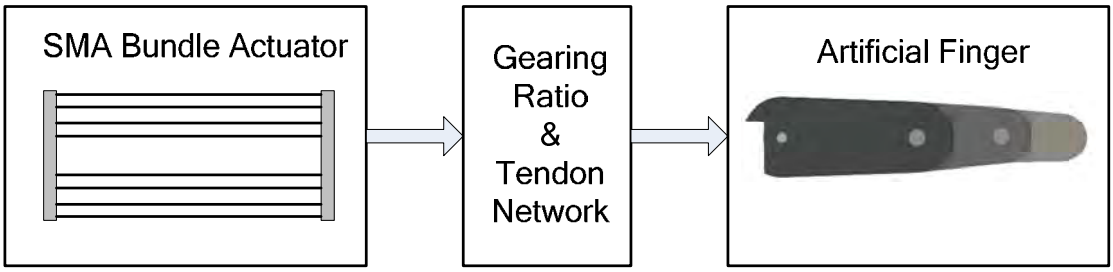

Figure 7-6. SMA Bundle Actuator Layout

Returning the finger to its original position can be achieved using bias-springs or using a non-equal antagonistic actuator layout (See Section 2.5). Bias-springs are advantageous owing to their simple implementation and the reduction in controller complexity. However, bias springs are susceptible to

i. restricting the motion of the prosthetic finger when extended to a large degree

ii. being unable to produce sufficient torque within the finger to return to starting position

Antagonistic wiring arrangements require additional power and volumetric space which comes at a premium in a portable prosthetic solution. It is therefore recommended to attempt to utilise a bias-spring to return SMA bundle actuators to their original position in so far as possible.

7.6 Finger Joint Position vs. SMA Bundle Actuator Strain

The achievable motion paths of the prosthetic finger can be described using a suitable model of the forward kinematics. Forward kinematics can be defined as a methodology which permits the determination of the position and orientation

of the end effector given the values for the joint variables for the links [154]. This can be used to determine if the proposed prosthetic finger design is capable of forming common shapes associated with the typical prehensile activities outlined in Section 3.3.

Forward kinematic models contain a series of homogeneous transformations which are multiplied together to calculate the position and orientation of each coordinate frame with respect to the previous frame (Figure 7-7).

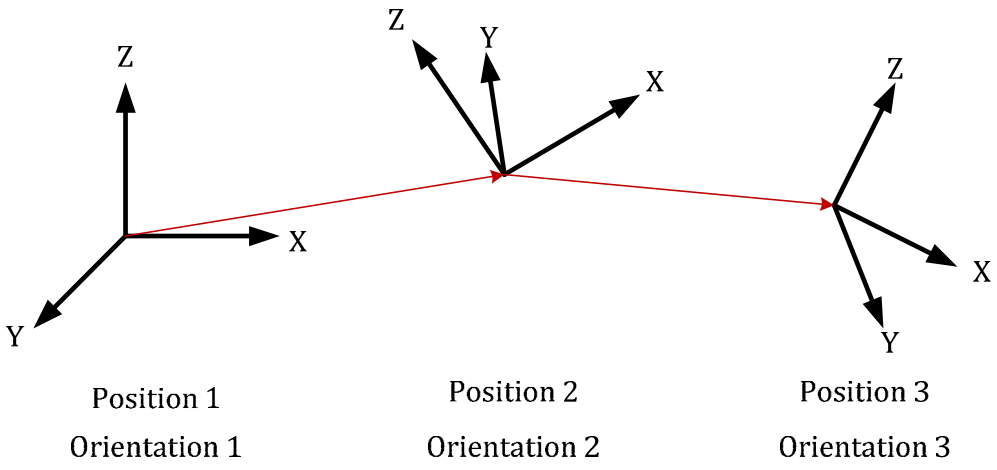

Figure 7-7. Three dimensional coordinate transformation

However, as each transformation matrix describes rotation about, and translation along, the X, Y and Z coordinate frame, it can become a complex procedure. As a result, conventions to simplify and streamline the procedure have been developed. One of the most common is the Denavit-Hartenberg representation of a joint [154] (Figure 7-8).

In the Denavit-Hartenberg (D-H) convention, each homogeneous transformation (A_i) is represented as a product of four basic transformations

$$A_i = Rot_{z,\theta_i} Trans_{z,d_i} Trans_{x,a_i} Rot_{x,\alpha_i} \tag{7-1}$$

The product of A_i is thus

$$A_i = \begin{bmatrix} c_{\theta_i} & -s_{\theta_i} s_{\alpha_i} & s_{\theta_i} s_{\alpha_i} & a_i c_{\theta_i} \\ s_{\theta_i} & c_{\theta_i} s_{\alpha_i} & -c_{\theta_i} s_{\alpha_i} & a_i s_{\theta_i} \\ 0 & s_{\alpha_i} & c_{\alpha_i} & d_i \\ 0 & 0 & 0 & 1 \end{bmatrix} \tag{7-2}$$

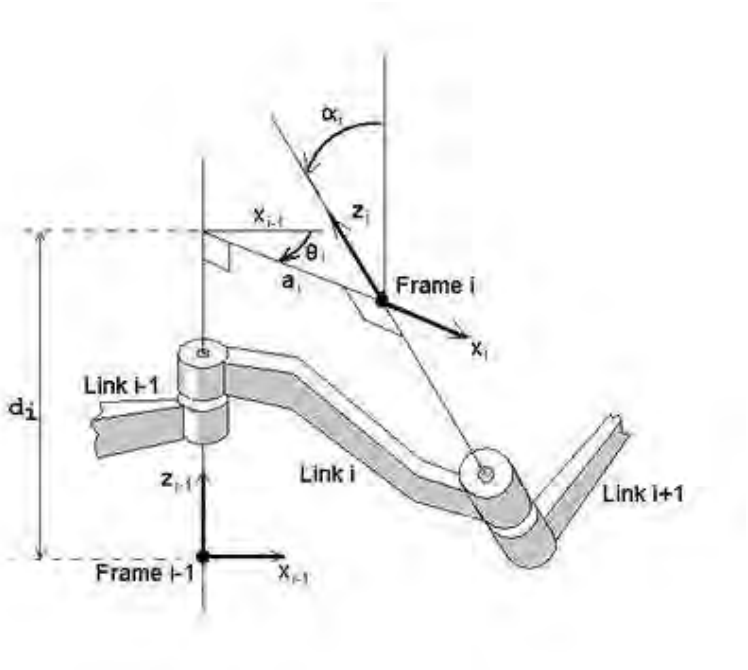

Figure 7-8. D-H Parameter Graphical Representation [155]

The parameters in Eq.(7-2) are link length (a_i), link twist (α_i), link offset (d_i) and joint angle (θ_i). This methodology significantly simplifies the calculations of the forward kinematics. The D-H parameters are usually listed in tabular form. Table 7-1 outlines the D-H parameters for the artificial index finger designed.

Table 7-1. D-H Parameters for Prosthetic Index Finger Design

i	**a_i**	**α_i**	**d_i**	**θ_i**
1	*42*	*0*	*0*	θ_1
2	*26*	*0*	*0*	θ_2
3	*19*	*0*	*0*	θ_3

As the prosthetic finger is designed to rotate in flexion and extension only, there is no link twist or link offset present. The prosthetic finger can thus be defined as a 3R (three revolute joints) arrangement. The joint angles are a function of the prehensile posture adapted.

7.6.1 Underactuation

The tendon network layout results in minor induced movements in joints which are not under direct actuation. This is a direct result of the geometric layout adopted. The phenomenon is referred to as 'underactuation'. Underactuation occurs naturally in the human finger as a result of tendon layout (See Section 3.2). The following must be accounted for when determining the ability of the prosthetic finger to recreate human finger prehensile postures accurately:

i. The underactuation effect of each joint on the neighbouring joints within the prosthetic finger.

ii. The absolute angular displacement achievable by the actuator and gearing system.

The kinematic underactuation calculation does not take into account the torque required to accelerate the finger joint. This will be dealt with in detail in Section 7.9 of this work.

7.6.1.1 Selection of Active Element Radius

In order to model and calculate the effect of underactuation on the joint movements of the prosthetic finger, it is necessary to first determine the radius for the active joint element. The active joint element is coupled directly to the joint and results in joint rotation. The passive joint element serves to transfer artificial tendons with minimal friction throughout the prosthetic finger. The joint radius must satisfy two key criteria:

i. *Size* – the element must fit within the dimensions of the prosthetic finger housing.

ii. *Rotational and torque capacity* – the element size must provide a balance between sufficient rotation and torque across all joints in the prosthetic finger. As the requirements of each joint are different, miniature gearboxes can be implemented to enhance their rotational capabilities at the expense of torque. This can be tempered by increasing the number of SMA wires in the bundle if required.

A suitable radius can be determined mathematically using Eq.*(7-3)* & *(7-4)* based on the known strain capacity of SMA bundle actuators (See Section 4.5.3), and the desired angles of rotation for biomimetic prosthetic finger design (See Section 3.4.1.2).

$$r = \frac{180.\varepsilon_{sma}.}{\pi.\theta_{desired}} \tag{7-3}$$

$$\tau_{joint} = F_{SMA} \times r \tag{7-4}$$

A compromise between rotation per unit strain of the SMA bundle, and the torque generated from the force supplied by the SMA bundle actuator as it undergoes phase transformation is necessary. A radius of 2.3mm is determined as a suitable candidate which satisfies (i) and (ii).

7.6.1.2 Computing Underactuation

A trigonometric model is used to determine the knock-on effect of rotation in one joint on the subsequent joints. Underactuation occurs due to the eccentric positioning of the tendon as it passes over the passive element (Figure 7-9).

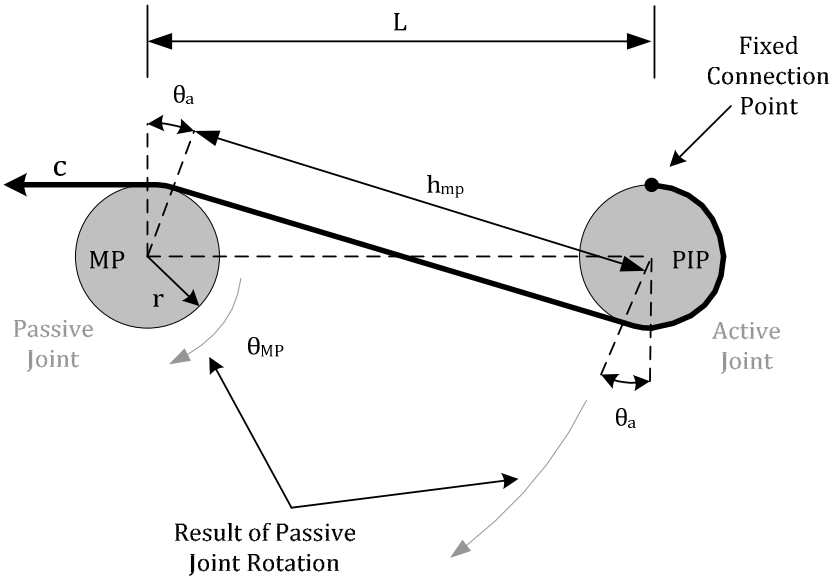

Figure 7-9. MP *& PIP Joint Artificial Tendon Layout and Connection*

Direct actuation of the MP active element results in underactuation at the PIP active element, which is compounded further at the DIP active element. Direct

actuation of the PIP active element results in underactuation of the DIP active element only, while direct actuation of the DIP active element does not result in any further underactuation at any other joints. The passive element of the MP joint features the artificial tendon passing over it which is wrapped around the active element of the PIP joint from the underside and fixed to the topside.

Upon actuation by the active element of the MP joint, a rotation of the PIP joint about the centre of the MP joint occurs. This has the effect of increasing the contact area between the artificial tendon connected to the active element of the PIP joint and the passive element of the MP joint as it partially wraps around it. However, as the hypotenuse, *h*, cannot be lengthened to compensate for this due to its rigid connection to the PIP SMA bundle actuator, the increase of θ_{MP} results in an induced rotation of the PIP active element. This is considered to be the underactuated effect.

The effect is compounded for the DIP joint as a result of MP joint rotation as the DIP artificial tendon passes over both the MP and PIP passive joints. Underactuation increases with larger diameters (Figure 7-10).

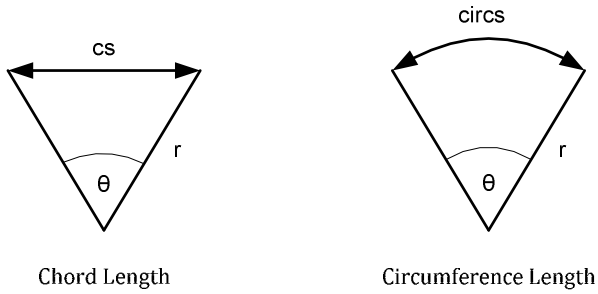

Figure 7-10. Rotational Effect on Artificial Tendon Length

The rotation due to underactuation can be determined by calculating the difference in artificial tendon length as the tendon wraps around the passive element during rotation. As the MP joint is rotated through θ_{MP}, the contact area between the artificial tendon and the passive MP joint increases by

$$\Delta L_{contact}(MP) = circs - cs \tag{7-5}$$

where

$$cs = \frac{\pi r \theta}{180} \tag{7-6}$$

and

$$circs = \frac{(sin\theta)(r)}{sin\frac{(180-\theta)}{2}} \tag{7-7}$$

Due to the fixed length, L, and the fixed contact between SMA bundle actuator and the artificial tendon at c, the difference in length induced by the increased contact area of the artificial tendon is balanced by the underactuated rotation of the active pulley element in the PIP joint calculated by

$$\theta_{ua\_pip}(MP) = \frac{\Delta l_{contact}(MP)}{2\pi r} \times 360 \tag{7-8}$$

The resultant effect of the underactuated rotation of the PIP joint is induced rotation of the DIP joint. Subsequent direct rotation of the PIP joint via the SMA bundle actuator will result in a further underactuated effect in the DIP joint. Simultaneous actuation of both the MP and PIP joints will compound the underactuation effect at the DIP joint resulting in greater joint rotation according to

$$\theta_{ua\_dip} = \theta_{ua\_dip}(MP) + \theta_{ua_{dip}}(PIP) \quad (7\text{-}9)$$

where θ_{ua_dip}(MP) and θ_{ua_dip}(PIP) are the resultant underactuation effects in the DIP joint brought on by direct actuation of the MP and PIP joints respectively.

The equations described can be used in the determination of optimum SMA wire quantity and length in each bundle. Due to the small size of the rotary elements in the specified design, underactuation effects will be minor. However, increased element size leads to greater underactuation.

7.7 Miniature gearing requirements

The human index finger has maximum angular displacement values of 27.3^o, 90^o and 75.6^o for the MP, PIP and DIP joints respectively during prehensile activity (See Section 3.4.1). The strain required from the SMA bundle actuators to provide sufficient rotation in the joints of the prosthetic finger design must be found. If insufficient angular displacement is produced at the maximum SMA strain, gearing can be implemented to provide additional rotation at a cost of reduced torque in the joint.

Whilst miniature gearboxes result in additional mechanical complexity in the system, their inclusion permits scaling of the outputs to provide for biomimetic joint rotational capacity and is thus deemed necessary. Table 7-2 outlines the gearbox requirements. The inclusion of gearing in the prosthetic hand framework is outlined in Figure 7-2. Gearing is located between the SMA bundle actuator and the prosthetic finger.

Table 7-2. Sizing miniature gearing requirements

Joint	SMA Strain	Active Element Diameter	Angular Disp.	Human Finger Angular Disp.	Gearing Required	Gearing Ratio
MP	*3.6%*	*4.6mm*	*59.04°*	*27.3°*	*N*	-
PIP	*3.6%*	*4.6mm*	*59.04°*	*90°*	*Y*	*1.6:1*
DIP	*3.6%*	*4.6mm*	*59.04°*	*75.6°*	*Y*	*1.3:1*

Where gearing ratios are necessary, it is preferable to maintain small gearing ratios to ensure that the force capacity of the SMA bundle actuator is maximized. This requires an increase in the number of SMA wires in the bundle which in turn results in higher power requirements and reduction in battery life. The importance of selecting an appropriate bundle size is clearly evident.

7.7.1 Computing SMA Bundle Actuator Strain Requirements

The strain criteria for each of the SMA bundle actuators within the prosthetic finger must include the underactuation effect to maintain high levels of accuracy. In the case where three target angles are specified, θ_i, θ_j and θ_k, for the MP, PIP and DIP joints respectively, the procedure is identified as follows:

i. Determine the underactuation effect at the PIP and DIP joints using Eq's *(7-7)* & *(7-8)*.

ii. Determine the remaining rotation required at the PIP and DIP joints by subtracting the total underactuated values calculated from the desired PIP and DIP angles, θ_j and θ_k.

iii. Use the values at the MP, PIP and DIP joints when determining the strain requirement of the SMA bundle actuators

The values of strain calculated from (iii) are absolute values and must be calculated relative to the initial starting position of the SMA bundle actuator (Figure 7-11).

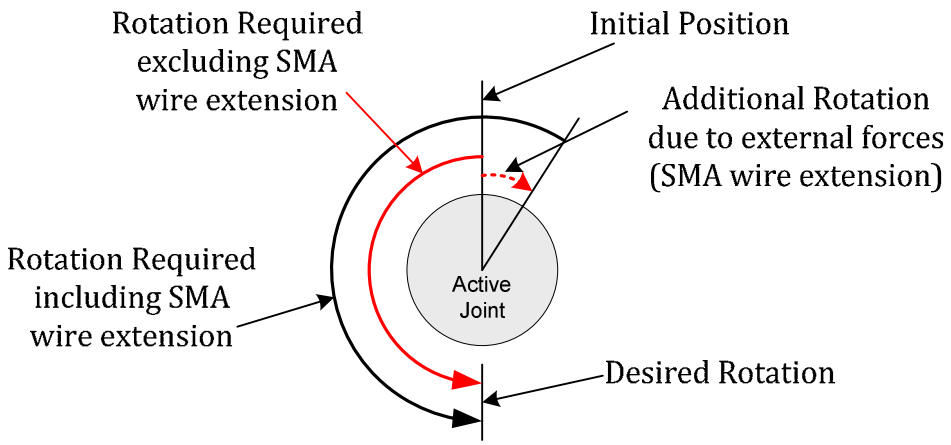

Figure 7-11. Concept of Absolute Rotation of Joints

This is important to note as external forces, such as gravity, acting on the prosthetic finger and hence on the SMA bundle actuator can result in SMA wire extension if the stress values are high. This extension must also be overcome to achieve the desired joint angular rotation.

7.8 Prehensile positional capacity of the proposed design

Four different prehensile index finger postures which are sufficiently different in terms of angular displacement have been identified. These prehensile shapes are

i. Cylindrical

ii. Tip/Palmar

iii. Lateral

iv. Fully Closed

Other prehensile postures such as the palmar and hook postures are very similar to the tip and cylindrical postures respectively in terms of their associated angular displacements. The SMA bundle actuator strain required to reproduce the chosen prehensile postures must be found to demonstrate the functionality of the mechanical design. Based on the maximum strain values available from the SMA bundle actuators, gearing is required to facilitate full rotation.

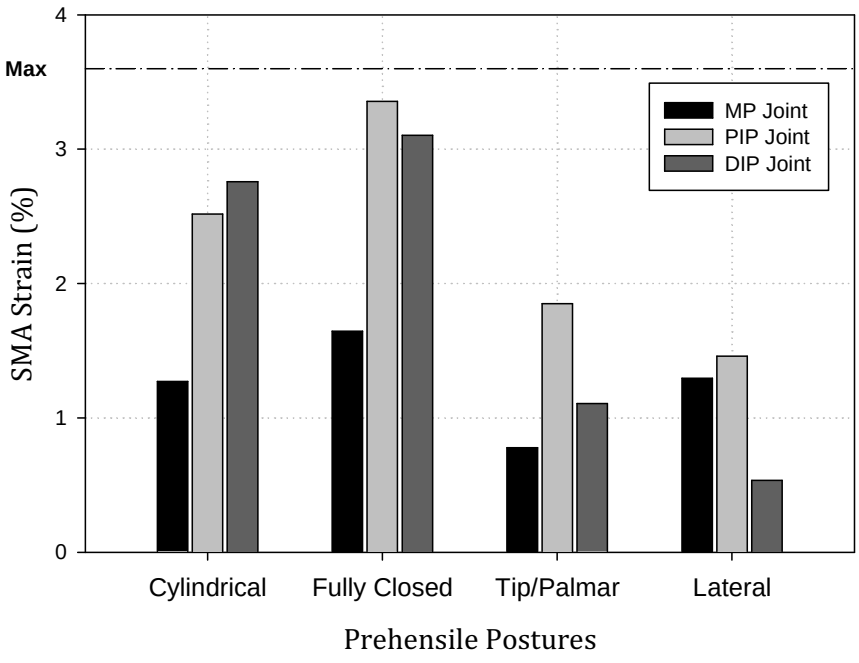

Figure 7-12. Maximum SMA Bundle Actuator Strain Required during Prehensile Activity

The gearing ratios are 1:1, 1:1.6 and 1:1.3 for the MP, PIP and DIP joints respectively. It is critical that the strain requirement from the SMA bundle actuator be less than the maximum achievable strain of 3.6% in order to allow full posture formation. The required strain values, taking the gearing into account, are outlined in Figure 7-12.

Furthermore, it can be noted that the larger the difference between the required strain and the maximum strain, the greater the residual capacity of the SMA bundle actuator to exert a force, or overcome the negative effects associated with external disturbances. This is important in prosthesis design as it allows for the production of a strong grip.

7.9 Dynamic Model of Prosthetic Finger

The kinematic modelling of the prosthetic finger carried out has shown that SMA bundle actuators are capable of producing the angular displacements required to reproduce the common grip postures of the human finger. However, it is equally as important to ensure that the SMA bundle actuators demonstrate the capacity to rotate the prosthetic finger at a rate comparable to the human finger in order to be considered as a feasible actuation solution. This can be achieved by calculating the torque required at each joint in the finger during dynamic rotation. This is implemented using suitably sized SMA bundle actuators for each joint within the prosthetic finger.

The Euler-Lagrange (E-L) dynamics equation (Eq.(7-11)) can be used to calculate the torque required at each joint to rotate the 3-R prosthetic finger arrangement outlined in Figure 7-13 through a predetermined trajectory [154].

The trajectories of each joint are taken from the human finger joint trajectories previously outlined in Section 3.6. It is imperative that a rate of rotation is chosen to ensure that the trajectory is completed in a time frame comparable to that of human finger joint rotation. The E-L equation accounts for all external forces acting on the prosthetic finger during rotation such as friction, inertia, centripetal force, coriolis force and gravity. Furthermore, additional loading associated with some prehensile gripping and pinching activities can also be accounted for. The E-L equation is

$$\tau_{joint} = D(q)\ddot{q} + C(q,\dot{q})\dot{q} + g(q) + J^T(q)F \qquad 7\text{-}10)$$

where τ_{joint} is the joint torque, D is the inertia matrix, C is the Christoffel symbol matrix, g is gravitational matrix, J^T is the transpose of the Jacobian matrix, F is force vector, q is angular displacement, $\dot{q}$ is angular velocity, and $\ddot{q}$ is angular acceleration. From Eq.(7-10), it can be found that the torque required to reproduce the movements of the human finger in the prosthetic finger can be calculated for each individual joint using

$$\tau_{joint\_k} = \sum_{j=1}^{n} d_{kj}(q)\ddot{q}_j + \sum_{i=1}^{n}\sum_{j=1}^{n} c_{ijk}(\dot{q}) + \mu\dot{q} + g_k(q) + J^T{}_k(q)F_k \qquad (7\text{-}11)$$

A typical 3-R link arrangement is outlined in Figure 7-13 where l is the length of the joint, l_c is the length to the centre of the joint, q is the angular displacement, m is the mass of the joint, and g is gravitational acceleration.

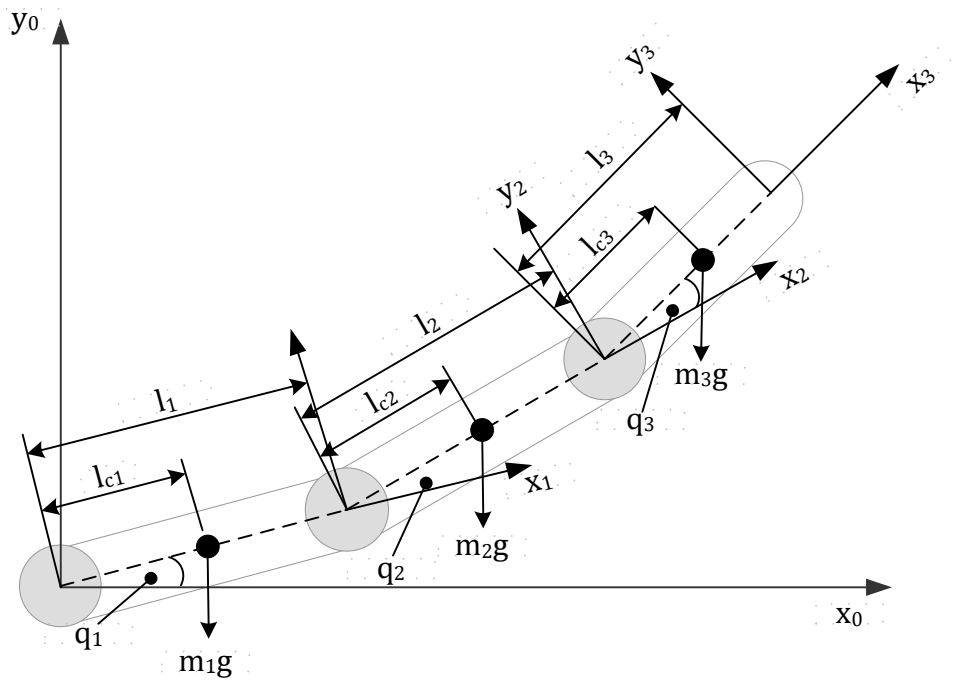

Figure 7-13. 3-R Prosthetic Finger Arrangement

The physical parameters of the prosthetic finger design outlined in Table 7-3 are exploited to calculate the specific torque required at each step in time to adhere to a desired trajectory. The desired trajectories have been derived from experimentation on the human index finger (Section 3.6.1).

Table 7-3. Prosthetic Index Finger Phalangeal Parameters

Phalanx	**Length (mm)**	**Mass (kg)**	**Moment of Inertia ($kg.m^2$)**
Proximal	*42*	*0.00779*	*$4.91x10^{-6}$*
Intermediate	*26*	*0.0035*	*$9.5x10^{-7}$*
Distal	*19*	*0.00342*	*$1.41x10^{-6}$*

7.9.1 Computing Torque for Prehensile Postures and Rotation Rates

The E-L dynamics equation is implemented in LabVIEW to facilitate calculation of torque at each joint for each prehensile posture and rotation rate using the trajectories derived from human finger rotation (Figure 7-14). The dynamics computation algorithm allows for the specific parameters of the prosthetic finger design to be utilised in the calculation.

Underactuation effects are accounted for in order to maintain a high level of accuracy in the calculation of the torque requirements. The algorithm outputs the instantaneous torque required during each time period to rotate each joint of the finger through a desired trajectory.

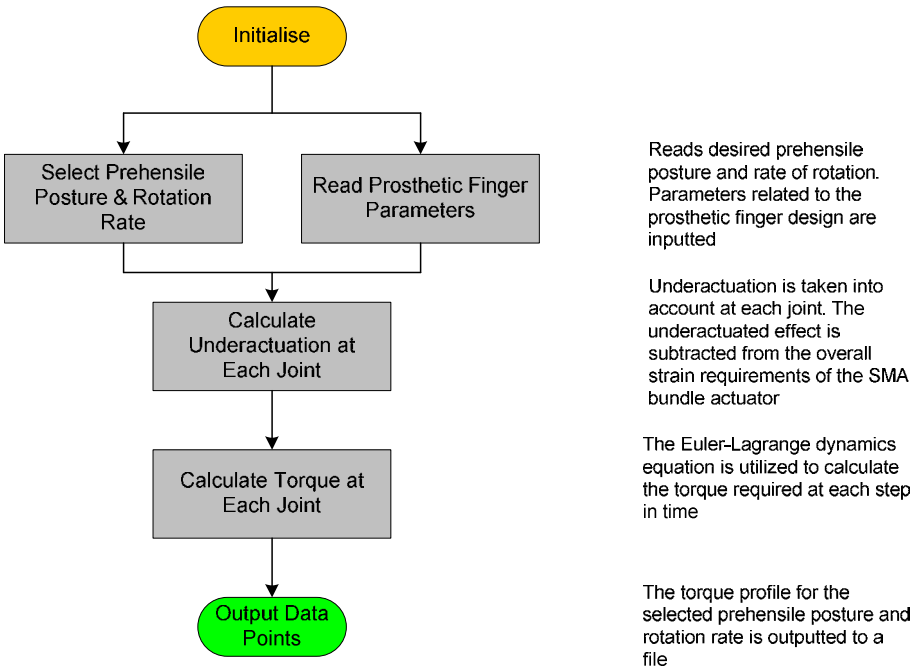

Figure 7-14. LabVIEW State-Machine Architecture for Dynamics Computation

7.9.2 Results & Discussion

Torque calculated varied across the range of the rotation induced. As the rotational rate increases, the torque required also increases due to the larger velocity and acceleration values associated with faster angular rotation rates. The variation in torque against time for each joint in the prosthetic finger can be clearly seen in Figure 7-15. The orientation of the prosthetic finger is set to rotate the joint against gravitational forces thus maximizing the required torque during calculation. Torque values for all other orientations will be smaller owing to the positive influence of gravity. It can be seen from Figure 7-15 that the maximum torque values can be estimated from the torque curves. The process was repeated for all common prehensile postures and rotation rates under examination. The maximum torque requirements are summarized in Figure 7-16.

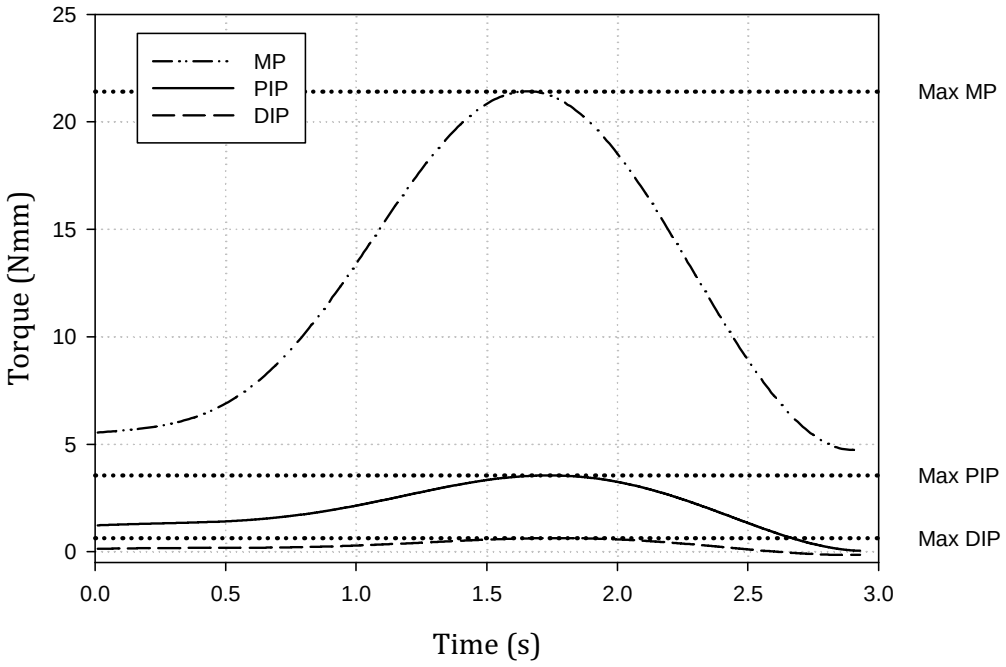

Figure 7-15. Example of torque requirements calculated for each joint in the

prosthetic finger for cylindrical prehensile motion at a 'slow' pace.

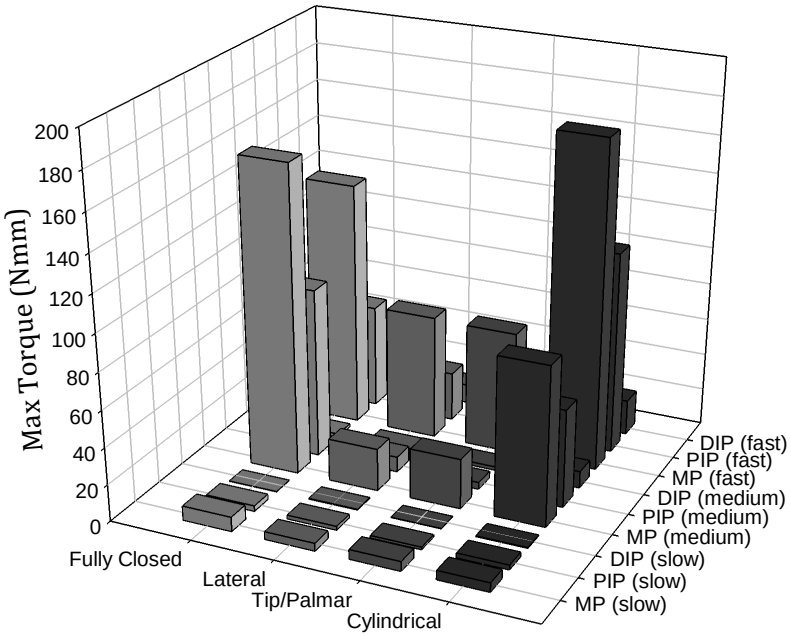

Figure 7-16. Maximum torque values for common prehensile postures and rotation rates

The torque values for the MP joint are the largest for each prehensile posture and rotation rate. This is as expected owing to the greater inertial requirements. Furthermore, as the rotation rate increases, the torque requirements increase. The maximum torque values outlined will be utilised in the selection of appropriate SMA bundle wire quantities (See Section 8.5).

7.10 Conclusions

A three degree of freedom prosthetic index finger has been designed. The prosthetic finger is designed to fit into a conceptual prosthetic hand framework. The finger is designed using biomimetic criteria. A kinematic analysis of the design has been carried out which demonstrates the capacity of the prosthetic

finger in reproducing the prehensile postures of the human index finger. Three individual SMA bundle actuators are recommended to produce flexion, one specified for each joint to allow maximum flexibility. Extension is accounted for using a bias-spring arrangement. Gearing is suggested in order to increase the angular rotation capacity of each joint, thus ensuring each required prehensile posture is satisfied. The importance of producing a dynamic model of the proposed finger design has been shown. The E-L dynamics equation has been utilised to facilitate dynamic modeling of the prosthetic finger during rotation. It has been shown that the torque values are largest in the MP joint of the finger due to the higher inertial demands. The maximum torque requirements for each prehensile posture and rotation rate have been identified. The work described in this chapter completes the prosthetic finger design, kinematic analysis, and dynamics analysis stages of the SMA bundle actuated prosthetic finger design methodology. It is now possible to size and fully assess SMA bundle actuators as a viable actuation solution for prosthetic finger design. The optimum SMA bundle solution must be capable of satisfying the kinematic, dynamic and control requirements of the prosthetic finger simultaneously to be deemed a suitable actuation solution. This will form the basis of Chapter 8 of this work.

8. ASSESSMENT OF SMA BUNDLE ACTUATORS IN PROSTHETIC FINGER APPLICATIONS

8.1 Introduction

SMA bundle actuators have demonstrated the capacity to meet the kinematic requirements of the proposed prosthetic finger design using suitable gearing (See Chapter 7). However, the capacity of each bundle to produce adequate torque to overcome the external forces acting on the joints of the prosthetic finger requires further investigation. This must be done while meeting the desired angular velocities and accelerations required to mimic the movements of the human finger.

The torque produced in the prosthetic finger joints owing to SMA bundle actuation can be increased by adding additional SMA wires to the connected bundle. However, this must be tempered by considering the additional power requirements necessary to implement such an approach. There are also inherent limitations on angular velocities and accelerations of each joint due to the limitations in the responsiveness of the SMA wires to applied input current. The goal of this chapter is to complete the remaining stages of the proposed design methodology outlined in Section 1.7. The SMA bundles must be appropriately sized for each joint within the prosthetic finger thereby facilitating a broad range of typical finger movements and phalangeal tip forces. This can be carried out by implementing the findings from the dynamic model outlined in Section 7.9 and the SMA bundle characterisation in Chapter 4.

The best possible SMA bundle arrangement meeting all the needs of the prosthetic finger will be examined by:

i. assessing the capacity of the SMA bundle actuator in tracking a range of desired angular trajectories during a scaled experiment. The a-PID control strategy developed in Chapter 6 will be utilised.

ii. assessing the range of phalangeal tip forces achievable using suitably sized SMA bundle actuators.

Results will serve to establish the overall suitability of SMA bundle actuators as a viable actuation solution in prosthetic finger applications.

8.2 Determining SMA Bundle Actuation Trajectories

The actuation of each joint within the prosthetic finger can be directly related to the SMA strain produced during heating and cooling activity. The forces that are exerted during SMA strain activity have been outlined in Section 4.5.3. It was also shown that force produced can be amplified by increasing the quantity of SMA wires in each bundle (at the expense of increased energy requirements). Rotation of a prosthetic joint using SMA bundle actuators requires a combination of torque to overcome any external forces acting on the joint, and linear displacement (SMA strain) to produce adequate angular displacement in a connected rotary joint. The product of the torque and angular displacement can be referred to as mechanical work according to

$$W_{joint} = \tau_{joint} \times \theta_{\text{joint}} \tag{8-1}$$

where joint torque in a directly coupled rotary joint is given by

$$\tau_{joint} = F_{SMA} \times r_{joint} \tag{8-2}$$

An appropriate quantity of wires in each bundle can be selected based on the maximum mechanical work requirements of the bundle. Upon selection, the suitability of SMA bundle actuators can then be assessed by examining their capacity to actuate a joint tasked with tracking a desired angular trajectory and producing the required forces associated with each joint in the human finger during a range of prehensile motions (See Section 3.6).

8.3 Experimental Approach

The SMA strain required to induce adequate rotation at each joint in the prosthetic finger, ε_r, is related to the desired posture, and therefore angular trajectory. A trajectory of required SMA strain can be derived from the kinematic relationship between instantaneous joint rotation and instantaneous SMA strain for each point along a desired angular trajectory of a prosthetic finger joint (See Section 7.6). The required SMA strain can be calculated in a straight forward manner using

$$\varepsilon_r = \left(\frac{\frac{\pi . r_{joint}}{180} \times \theta_{req}}{l} \right) \times 100\% \tag{8-3}$$

However, while the kinematic criterion can be easily satisfied by suitable SMA length and associated gearing, the dynamic criterion is more complex. If the dynamic forces acting on the finger during rotation are too large, a SMA bundle actuator designed using an insufficient quantity of SMA wires will not exhibit

the capacity to induce the desired rotation. Hence, the importance of the dynamic model is evident when attempting to design appropriately sized SMA bundle actuators.

Using the E-L dynamics equation, it has been possible to determine the instantaneous torque requirement for each point along a desired angular trajectory (See Section 7.9.2). This takes into account the rate of rotation and the orientation of the prosthetic finger. An experimental procedure has been designed that allows for the assessment of the performance of an appropriately sized SMA bundle actuator in meeting the kinematic, dynamic and control requirements. The experimental procedure is designed to allow simulated performance assessment without the need to manufacture a prosthetic finger for the following reasons:

i. *Time to completion.* The manufacture of any prosthetic finger solution can be time-consuming owing to the complexity of the manufacturing processes required. During the design and testing process of a prospective actuation solution, it may be necessary to carry out multiple design modifications and prototype developments. This adds to the developmental time of the prosthetic solution. An offline procedure to evaluate actuator performance would significantly decrease the overall design time.

ii. *Precision & expense*. The production of multiple prototypes results in increased project costs in addition to extensive developmental time. Prototype solutions require a high level of precision, thus requiring specialized manufacturing processes and operators for completion.

Flaws in the design or work cannot be tolerated as this can negatively influence the experimental results leading to substandard performance.

The experimental procedure is designed to utilise the experimental test-bed previously described in Section 4.4.1. The assessment of the SMA bundle is carried out by utilising the calculated torque values and kinematic analysis.

8.3.1 Modelling Friction

Experimentation to assess the suitability of SMA bundle actuators in prosthetic finger design is based on the prerequisite that the prosthetic finger can be manufactured to function as predicted in the 3D modelling environment. However, all physical systems experience friction and this must be included in the dynamic model. The most appropriate model for friction is a torque that is negatively proportional to the angular velocity [154].

$$\tau_{friction} = -\mu\dot{\theta} \tag{8-4}$$

The dynamic calculations carried out in Section 7.9.2 feature a minimal estimated friction coefficient of 0.1 symbolizing an optimally manufactured prosthetic finger. For systems exhibiting higher levels of friction, the friction coefficient can be increased. The net effect of this will be an increase in the force required to overcome the effects of friction during rotation. The capacity to produce phalangeal tip force will not be affected as friction is a function of angular velocity. The dynamic response will be affected however, as increased

torque result in increased stress acting on the SMA wires, thus increasing the phase transformation temperatures.

8.3.2 Justification of Experimental Approach

The SMA strain (ε_r) trajectories which satisfy the angular displacement required in each joint of the prosthetic finger for each prehensile posture under examination (See Section 3.6) can be derived from Eq.(8-3). The torque trajectories for same can be derived from the E-L equation, Eq.(7-11).

The SMA characterisation test-bed outlined in Section 4.4.1, featuring a minor modification to allow for loading of the SMA bundle actuator, can be utilised to facilitate experimentation. This is done by equating the mechanical work requirements due to rotation of the prosthetic finger with the capacity of the SMA bundle to move a known force through a vertical distance (Figure 8-1).

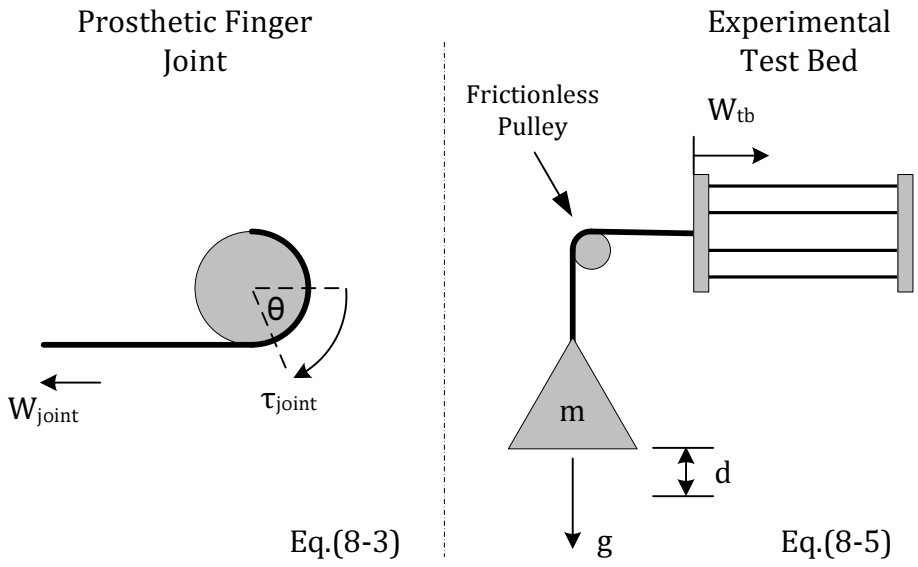

Figure 8-1. Equating SMA bundle actuator work required in the prosthetic finger joint and the experimental test bed

The mechanical work of the prosthetic joint can be found from Eq.(8-1) for each point along a desired angular trajectory. The mechanical work of the SMA bundle actuator on the experimental test bed is the product of a known force (mg) and the distance travelled as a result of SMA strain activity according to

$$W_{t\mathrm{b}} = (mg) \times d \tag{8-5}$$

where distance is a function of SMA strain activity. Therefore, since $W_{tb} = W_{joint}$, rearranging Eq.(8-5) can allow for the mass requirement at each point on the desired SMA strain trajectory, ε_r, to be found according to the equivalence of testing by

$$m = \frac{\mathrm{W}_{\mathrm{joint}}}{g.\varepsilon_r} \tag{8-6}$$

The maximum mass value found using Eq.(8-6) along the ε_r trajectory is selected for use during experimentation. Therefore, if the SMA bundle actuator demonstrates the capacity to track the associated ε_r trajectory derived from Eq.(8-3), whilst subjected to the load applied by mass m, it is considered to be a suitably sized SMA bundle for the task of joint rotation. However, the role of the SMA bundle actuator in prosthesis is not limited to joint rotation only. The SMA bundle must also demonstrate the capacity to exert appropriate phalangeal tip forces to be considered as a suitable candidate for prosthesis design. This can be achieved by examining the force capacity of SMA bundle actuators and the geometry of the prosthetic finger.

8.4 Phalangeal Tip Force Calculation

Phalangeal tip forces are necessary to produce functioning grips using the prosthetic finger. In stable grip postures, the grip force exerted by the prosthetic finger is counteracted by an opposable structure such as a thumb. The maximum phalangeal tip forces that can be exerted by a phalanx actuated by SMA bundle actuators is a function of SMA wire quantity in the bundle and the physical arrangement of the finger (Figure 8-2).

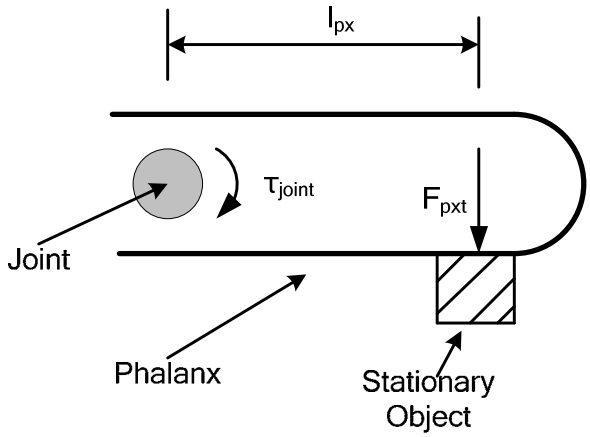

Figure 8-2. Determination of Phalangeal Tip Force

The phalangeal tip force can be calculated using

$$F_{pxt} = \frac{\tau_{\text{joint}}}{l_{\text{px}}} \qquad (8\text{-}7)$$

Torque at the joint is limited by the quantity of SMA wires within the bundle. During a stable grip, the Euler-Lagrange equation reduces to

$$\tau_{joint} = g(q) + J^T(q)F \qquad (8\text{-}8)$$

as joint acceleration and velocity are reduced to zero. Therefore, any torque used to produce rotation of the joint prior to forming a stable grip becomes available for utilization during phalangeal tip force generation.

8.5 Sizing of SMA Bundle Actuators

The careful selection of SMA bundle actuator wire quantity is required. The optimal bundle quantities must balance three key criteria in order to be deemed adequate for the task.

i. *Production of joint torque to satisfy rotation requirements*. The E-L equation, (Eq.(7-11)), and the mechanical work equation, (Eq.*(8-1)*), show that an increase in desired angular velocity and acceleration requires an increase in SMA bundle force to overcome the resulting increase in dynamic forces.

ii. *Production of joint torque to satisfy phalangeal tip force requirements*. It has been shown in Section 4.5.3 that larger quantities of SMA wires per bundle allow for larger force production. This can be utilised to produce stronger grip forces.

iii. *Energy efficiency.* There are limitations on the number of SMA wires that can be utilised in each bundle due to the availability of battery power to facilitate heating and the limitations in space available in order to avoid thermal cross-talk. Applied input current is utilised to heat the SMA wires via Joule heating. Hence, the power required to heat a SMA wire of fixed diameter is a function of the SMA length, SMA wire quantity per bundle, and the levels of heating necessary

(See Section 4.5.3). The maximum power requirement per wire can therefore be calculated using Eq.(5-1) to be 0.5W based on the limitations in SMA wire length (66mm) set out by the prosthetic hand framework. This is achieved using the maximum allowable input current (400mA) for the 150μm diameter SMA wire chosen. This can be used to estimate the bundle power requirements.

The portable nature of a prosthetic device results in a reliance on available battery power. While (i) and (ii) above advocate using larger bundles to provide greater phalangeal tip forces and increase joint work capacity, this is restricted by the current technological limitations of battery power. Furthermore, the advocation of large bundles in (i) and (ii) requires a prosthetic hand framework which can successfully dissipate the excess heat generated via convection during the heating phase.

8.5.1 SMA Bundle Sizing to Satisfy Rotation Requirements

The maximum SMA torque requirement occurs during a 'fast' cylindrical prehensile motion based on the results outlined in Section 7.9.2. Eq.*(8-2)* is utilised to convert the maximum torque requirement at each joint into the maximum SMA bundle force requirement at each joint. This can now be used to determine the quantity of SMA wires needed to satisfy typical phalangeal tip force requirements (Table 8-1). The SMA quantity outlined takes into account the effect of gearing as outlined in Section 7.7. The gearing ratios are 1:1, 1.6:1, and 1.3:1 for the MP, PIP and DIP joints respectively. The SMA wire quantities are estimated based on the average maximum steady state force produced by a single 150μm SMA wire (See Section 4.5.3).

Table 8-1. SMA Wire Quantity – Reproduction of Human Phalangeal Rotation

Joint	SMA Force Required	Associated Grip	SMA Quantity	Estimated Max Power
MP	76.83N	Cylindrical	20	10W
PIP	47.68N	Cylindrical	20	10W
DIP	8.26N	Cylindrical	4	2W

It can be seen that in order to produce the forces necessary to induce rotation in the prosthetic finger joints, a maximum of 22W of power per finger is required.

8.5.2 SMA Bundle Sizing for Phalangeal Tip Force Requirements

It has been shown previously that previous designs of SMA actuated prosthetic finger designs suffer from poor phalangeal tip force production, thus rendering them unsuitable for most gripping tasks (See Section 1.4.1). However, the implementation of SMA bundle actuators provides an opportunity to rectify this drawback by using appropriate quantity of wires to produce satisfactory phalangeal tip forces. Table 8-2 outlines the estimated quantity of wires required to satisfy the maximum tip forces summarized previously in Table 3-1. Eq.(8-2) can be utilised to determine the joint torque required to produce the required phalangeal tip forces, while Eq.(8-6) can then be utilised to determine the SMA force required to produce the joint torque. As in Table 8-1, the requirement for additional SMA wires to accommodate the effects of gearing is included.

Table 8-2. SMA Wire Quantity – Reproduction of Human Phalangeal Tip Forces

Joint	Max Tip Force	Associated Grip	SMA Quantity	Power
MP	12.9N	Cylindrical	43	21.5W
PIP	16.1N	Cylindrical	53	26.5W
DIP	28.8N	Cylindrical	133	66.5W

The results clearly show that the SMA bundle wire quantities necessary to satisfy the phalangeal tip force requirements are significantly larger than the quantities necessary to satisfy the rotation requirements of the prosthetic finger. However, it is not necessary to reproduce maximum phalangeal tip forces for all everyday activities. Furthermore, a high friction artificial 'skin' can be used to cover the mechanical framework of the prosthetic finger. The friction between the finger and an object during certain gripping and holding activities will result in a lower force requirement from the actuators as sliding is minimized.

8.5.3 SMA Bundle Sizing to Satisfy Energy Efficiency

An operational prosthetic index finger solution is required to imitate both the rotational capabilities and the phalangeal tip forces exerted by the human finger. To facilitate both requirements, the maximum bundle values from Table 8-1 and Table 8-2 must be chosen as the appropriate SMA bundle actuator wire quantities. This leads to bundle sizes of 43, 53 and 133 SMA wires for the MP, PIP and DIP joints respectively. The combined required power to achieve this,

neglecting any computational power requirements and cooling strategy requirements to remove the large quantities of excess heat accumulated, is approximately 114.5W. This is excessive.

To demonstrate the context for these power requirements, DC micromotors typically require 0.18-15W of power and can produce up to 67.1 Nmm of torque prior to gearing [27] leading to finger tip forces of up to 30N in the case of the DLR hand [13]. This leads to a maximum power requirement of up to 45W. Therefore, the SMA bundle actuated prosthetic finger requires almost three times the power of a similar DC motor actuated prosthetic finger. Furthermore, it has been shown in Section 7.4.1 that the maximum quantity of wires available to fit into a SMA bundle actuator sized for the palmar areas of the hand is 52.

It is deemed appropriate to use 45W as the typical maximum available power since suitable battery solutions are currently available for DC motor actuated prosthetic finger solutions. Current commercially available battery technology shows that typical 9-cell lithium-ion batteries can produce up to 85Wh of power. Based on these limitations, the quantity of SMA wires per bundle is restricted to one third of the maximum wire quantities at 15, 18 and 45 SMA wires for the MP, PIP and DIP joints respectively, resulting in reduced phalangeal tip forces.

8.5.4 Achievable Phalangeal Tip Forces

The maximum achievable phalangeal tip forces in the presented prosthetic finger design are outlined in Figure 8-3. The DIP tip force of 9.74N is 0.26N below the target force as outlined in Section 1.7.1. This is a good result, and is a

32% improvement on the previous best phalangeal tip force of 6.67N for a SMA actuated prosthetic finger design [46]. The presented design has the capacity to demonstrate further improvements by increasing the number of wires in each bundle. This is reliant, however, on significant advances in battery technology and forced cooling solutions.

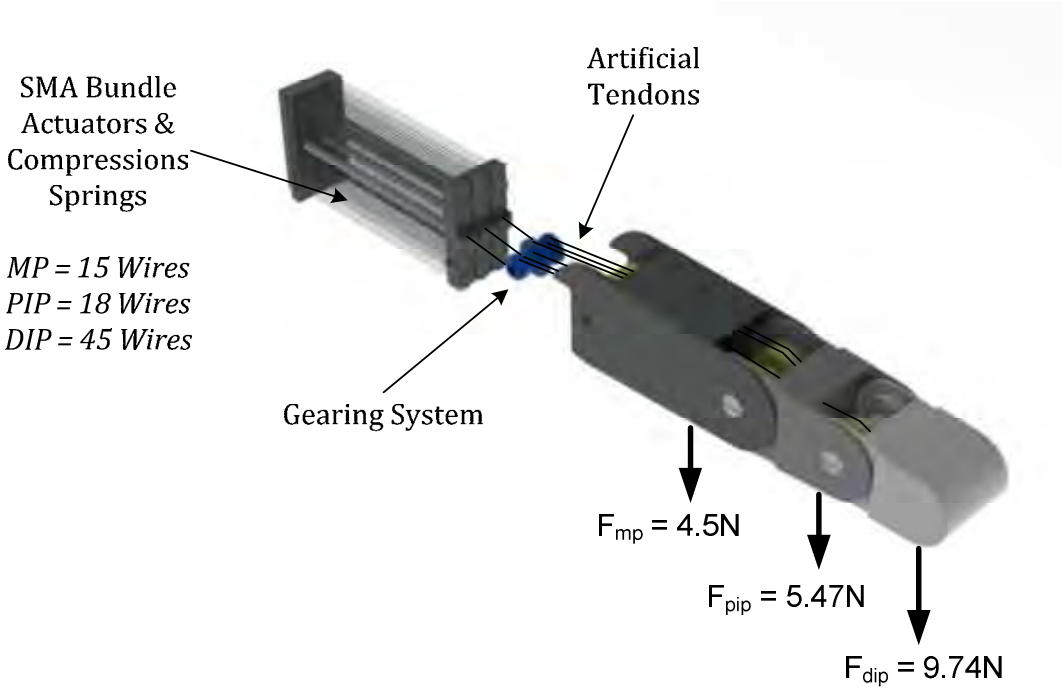

Figure 8-3. Phalangeal Tip Forces using Energy Efficient SMA Bundle Actuators

8.6 Assessing SMA Bundle Actuators for Prosthesis Design

The SMA bundle actuators have been sized to satisfy a balance between the rotational requirements, phalangeal tip force requirements and power requirements.

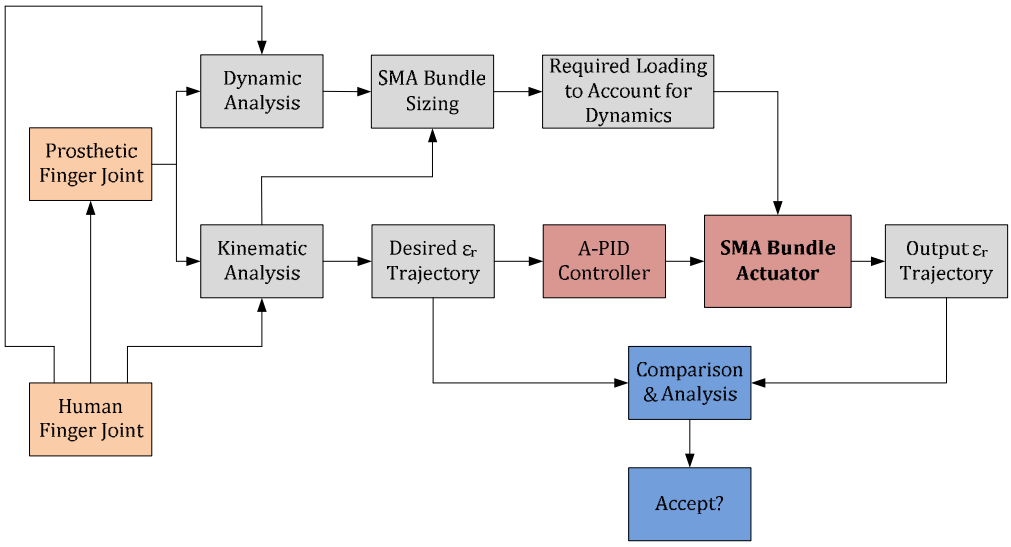

Figure 8-4. SMA Bundle Actuators Assessment Procedure

Experimentation is now necessary to investigate if appropriately sized and loaded SMA bundle actuators can be adequately controlled using the a-PID control solution to track the desired ε_r trajectories for each prehensile motion. This will allow for a conclusive determination of the suitability of SMA bundle actuators in prosthetic finger applications. The complete experimental procedure is summarized in Figure 8-4.

ε_r trajectories are calculated, based on the kinematic analysis of the prosthetic finger (See Section 7.6). This is done for joint rotation at *slow* pace, where the posture is formed within 2-4 seconds, *medium* pace, where the posture is formed within 1-2 seconds and *fast* pace, where the posture is formed in less than 1 second. Gearing has been shown as important in fulfilling the kinematic aspect of the prosthetic finger design owing to the limitations associated with mounting the SMA bundle actuators in the palmar region of a mechanical hand framework (See Section 7.7). This is accommodated on the experimental test-

bed which allows for the use of longer or shorter SMA wire lengths when required.

Appropriate loads are calculated and applied to the SMA bundle actuators based on the maximum mechanical work requirements of each SMA bundle (See Section 7.9.2), the estimated quantity of SMA wires required in the bundle under examination (See Section 8.5) and frictional effects (See Section 8.3.1). The loads are applied in addition to the bias spring which is necessary to induce the relaxation force during SMA cooling. The experimental test bed features an 8-wire SMA bundle to facilitate scaled experimentation. As the loads applied are calculated per SMA wire, the total load required for the 8-wire SMA bundle is straight forward to calculate. The calculated loads per 8-wire SMA bundle that were utilised during experimentation are outlined in Table 8-3.

Table 8-3. Equivalent loading per 8-wire SMA bundle (exclusive of applied bias spring force)

Posture	**Rate**	**Load (N)**			**Posture**	**Rate**	**Load (N)**		
		MP	**PIP**	**DIP**			**MP**	**PIP**	**DIP**
Cylindrical	Slow	0.05	0.05	0	*Lateral*	Slow	0.04	0.04	0
	Med	0.91	0.97	0.02		Med	0.24	0.15	0
	Fast	1.86	1.99	0.04		Fast	0.71	0.48	0
Tip/Palmar	Slow	0.06	0.02	0	*Fully Closed*	Slow	0.08	0.05	0
	Med	0.29	0.07	0		Med	1.75	1.67	0
	Fast	0.70	0.36	0		Fast	1.39	1.02	0

The highest loading values are reserved for the prehensile motions which require the highest torque demands from the actuator. These are fast cylindrical activity in the MP and PIP joints, and medium & fast fully closed activity in the MP and PIP joints. The DIP joints exhibit lower loading requirements across all motions due to much lower torque demands. Generally, the loading values are low across all joints and all prehensile postures. This is a result of the large ratio between the relatively low forces required to rotate the joints of the lightweight prosthetic finger, and the high forces required for high phalangeal tip forces.

8.6.1 Experimental Setup & Procedure

An experimental procedure has been designed to test the full cycle of grip formation, grip maintenance, and grip release. Each experiment is therefore broken into three stages which are executed in series (Figure 8-5). These stages are described as follows:

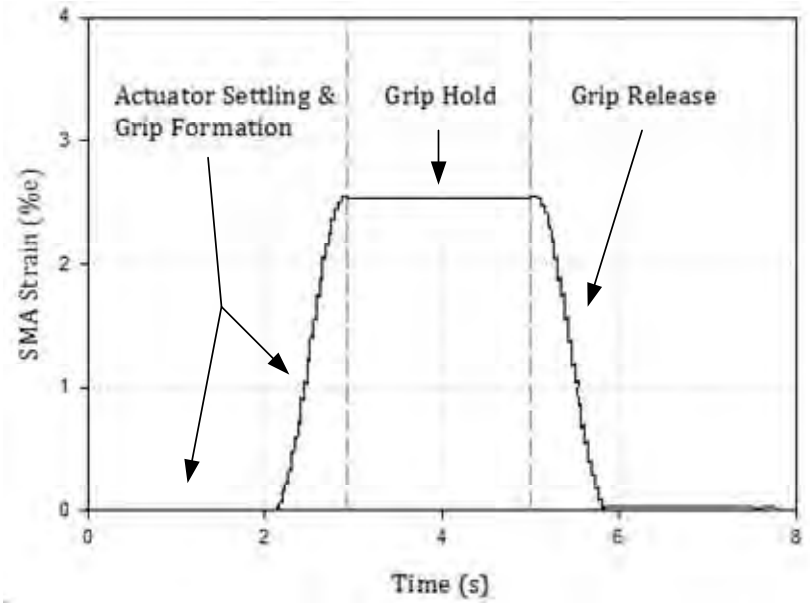

Figure 8-5. Grip Formation, Hold and Release Cycle

i. *Actuator settling & grip formation*. The SMA bundle actuator is allowed to settle for 2 seconds prior to testing to ensure consistency in testing. Following this, the loaded SMA bundle actuator attempts to track the desired joint rotation trajectory to form a prehensile grip. This experimental component aims to assess the SMA bundle actuators capacity to track a range of typical prehensile trajectories during the SMA heating cycle.

ii. *Grip hold*. The SMA bundle actuator is required to maintain a desired strain value for 2 seconds. Additional force can be applied if desired at this point to facilitate stable gripping. This experimental component aims to demonstrate the capacity of the SMA bundle actuator to maintain a stable position and grip.

iii. *Grip release*. The SMA bundle actuator is required to follow the inverse trajectory to that of grip formation. This experimental component checks the capacity of the actuator to track a range of typical prehensile trajectories during the SMA cooling cycle.

A complete experimental system has been developed in LabVIEW to facilitate the implementation of the outlined procedure. The flow of the experimental work is as outlined in Figure 8-6. The prosthetic joint trajectory algorithm, SMA strain conversion algorithm and a-PID controller algorithm are all implemented in the LabVIEW environment as separate blocks. Data analysis is also carried out in the LabVIEW environment following completion of testing.

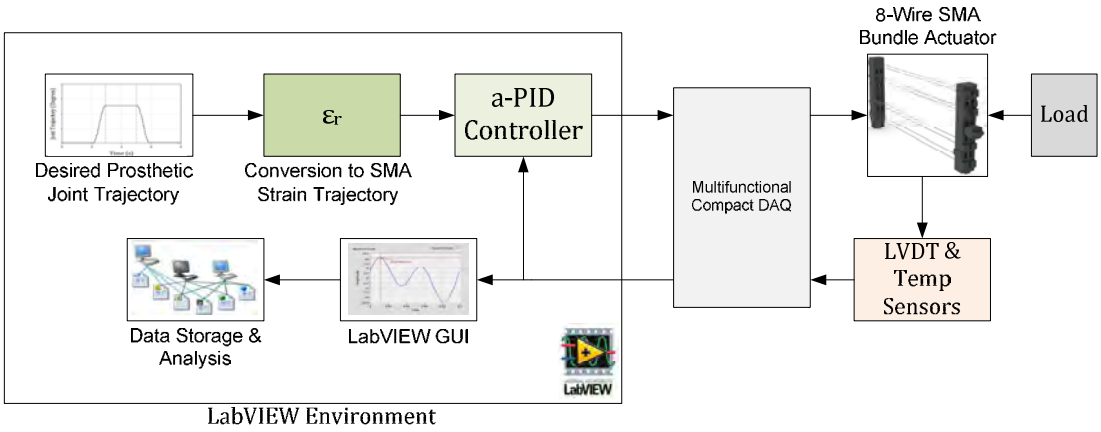

Figure 8-6. Implementation of SMA Bundle Actuator Assessment Procedure in the LabVIEW Environment - Experimental Setup

8.7 Results & Discussion

The results from experimental tests on the suitability of SMA bundle actuators as primary actuators in a prosthetic index finger design are outlined. The discussion of the results is subdivided into three categories based on the desired rotational pace of the prosthetic finger joint.

8.7.1 *Slow* Rotational Pace

The slow rotational pace results in lower torque and work demands owing to the lower velocity and acceleration values required when compared to medium and fast pace. The results outlined in Figure 8-7 and Figure 8-8 show the compliance of the SMA bundle actuators to the desired trajectories for the cylindrical and fully closed postures respectively.

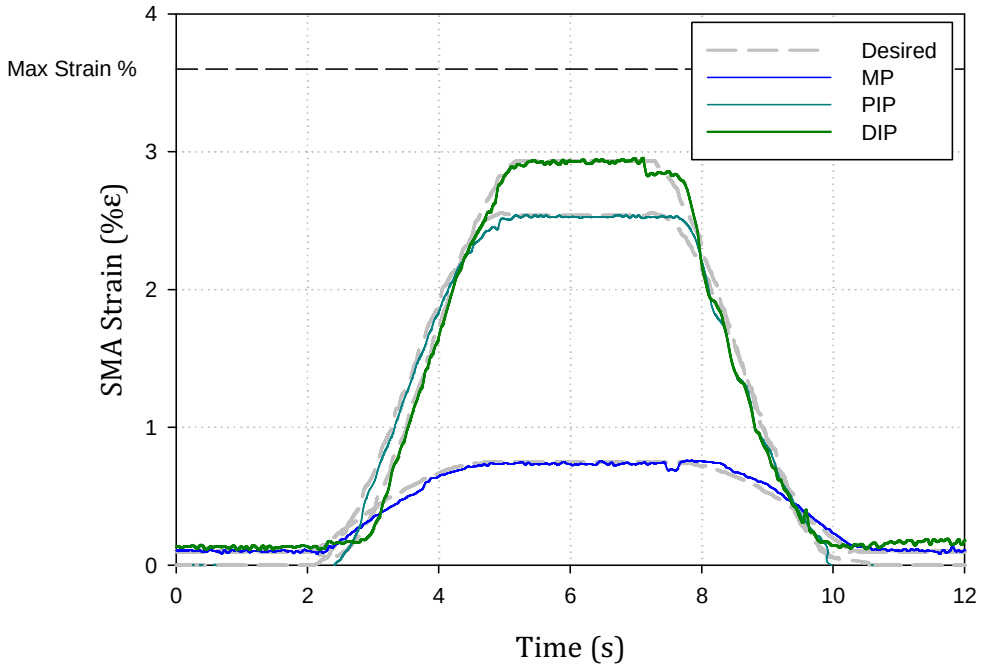

Figure 8-7. Cylindrical Posture – Slow Pace

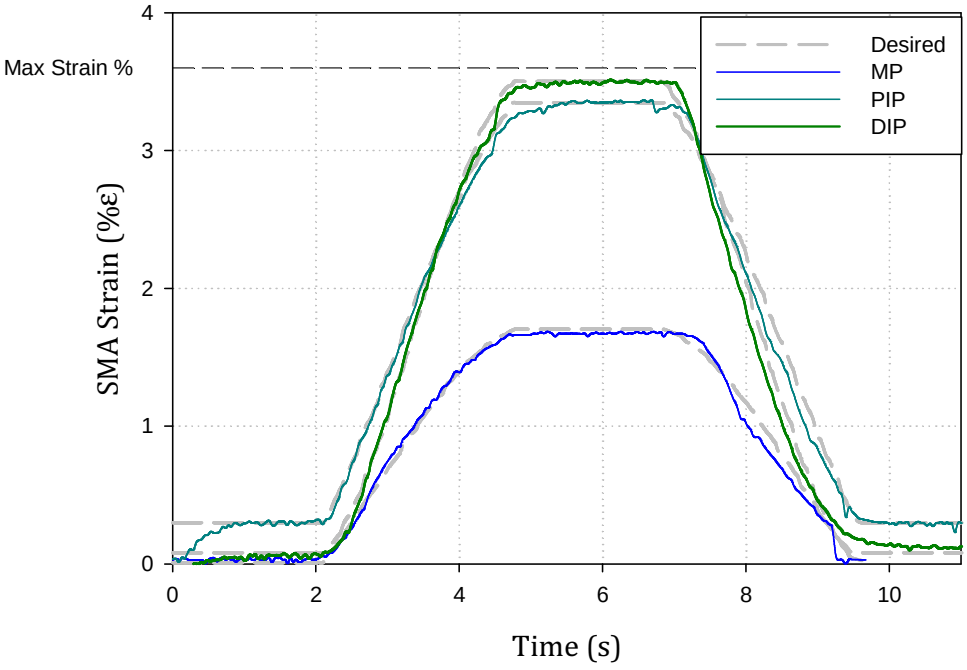

Figure 8-8. Fully Closed Posture – Slow Pace

These postures require significant joint rotation for successful execution in comparison with less demanding postures such as tip/palmar and lateral.

Hence, tip/palmar and lateral tracking are expected to be satisfactory for slow paced rotation. The results indicate that the tracking capability displayed by the SMA bundle actuators is highly satisfactory. Very minor tracking errors can be seen during the grip release phase of the trajectory.

The root mean square errors (RMSE) recorded were low primarily due to the low demands of the slow rotational pace employed. Similarly, tests were carried out for the tip/palmar and lateral prehensile postures. RMSE values were once again very small due to the slow rotational pace and undemanding trajectories. A comparison of recorded RMSE values is outlined in Figure 8-9.

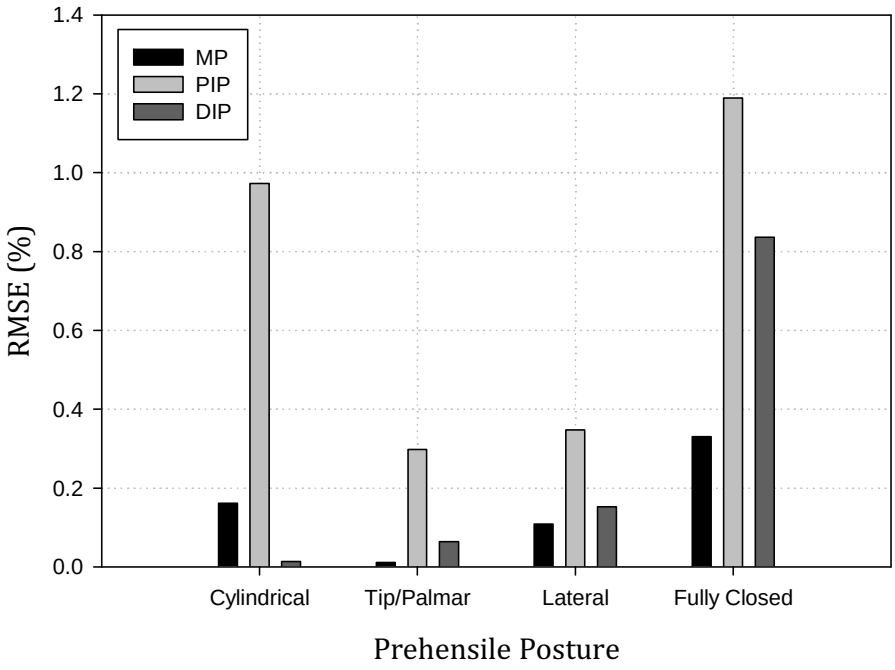

Figure 8-9. Slow Rotation Pace – RMSE Comparison

As can be expected, the larger RMSE values are found in the more demanding actuation cycles, such as those associated with the cylindrical and fully closed trajectories. The PIP joint displays the largest RMSE values of any joint for all prehensile postures examined. This is due to the greater rotation required at the

PIP joint for all postures. Furthermore, it can be seen that no overshoot is present during the grip holding cycle. This is especially important in delicate gripping tasks where accurate control of joint rotation is vital.

In spite of the satisfactory performance during rotation, typical prehensile postures during a 'slow' rate of rotation take between 3-4 seconds to form. This is considered highly impractical for a functioning prosthesis. Higher rotation rates are necessary to provide a response that mimics human response.

8.7.2 *Medium* Rotational Pace

Medium rotational pace increases the demand placed on the SMA bundle actuator due to the increase in dynamic forces, and hence loading, associated with faster rotation. Furthermore, adherence to the desired trajectory is more challenging. It is shown in Figure 8-10 and Figure 8-11, that the SMA bundle actuator performs adequately, however, larger errors in tracking performance can be detected. Tracking errors are noticeable on the fully closed trajectory, towards the maximum strain limits. In this region, the increase in SMA strain is minimal for larger increases in applied input current. As a result, the SMA bundle actuator takes longer to reach the desired strain level at the limits of operation. Conversely, it can be observed that the dynamic response is good throughout the remainder of the response profile, with the SMA bundle actuators showing the capacity to track the desired trajectory during both the grip formation and grip release phases of the cycle. It is evident that the SMA bundle actuator can track the desired trajectory of both the tip/palmar and lateral postures with ease due to the decrease in required strain levels.

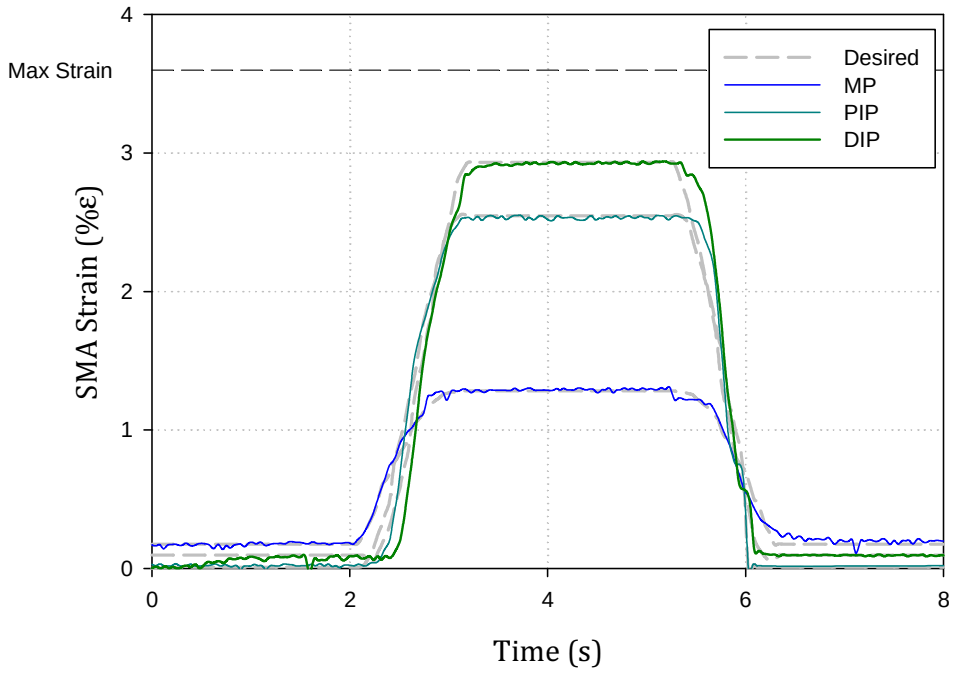

Figure 8-10. Cylindrical Posture – Medium Pace

The observed dynamic response is effective in tracking the desired trajectory. However, a minor tracking error can be identified during the grip release phase of the PIP joint trajectory. This is due to the natural cooling limitations of the SMA bundle actuators. A comparison of RMSE's are shown in Figure 8-14.

It can be seen that the magnitude of the RMSE is similar for medium paced rotation and slow paced rotation. This is as expected as SMA bundle actuators have previously been shown to operate effectively at the frequencies associated with a medium rotational pace. Furthermore, the relatively small size of the load required to account for the effects of dynamic forces acting on the joint during rotation have been overcome with ease by the selected quantity of SMA wires per bundle.

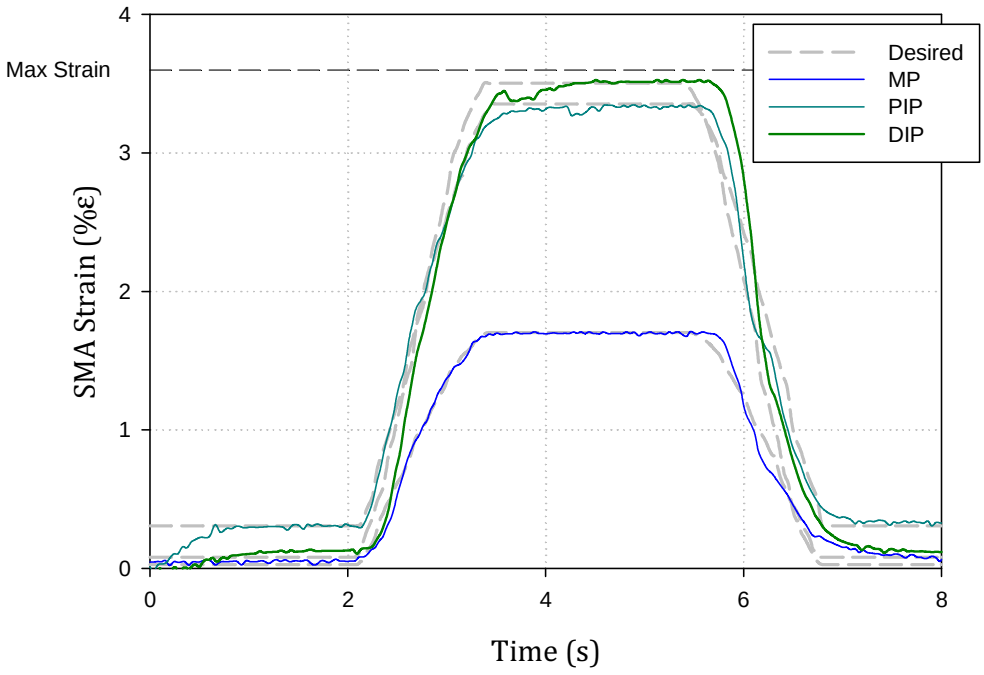

Figure 8-11. Fully Closed Posture – Medium Pace

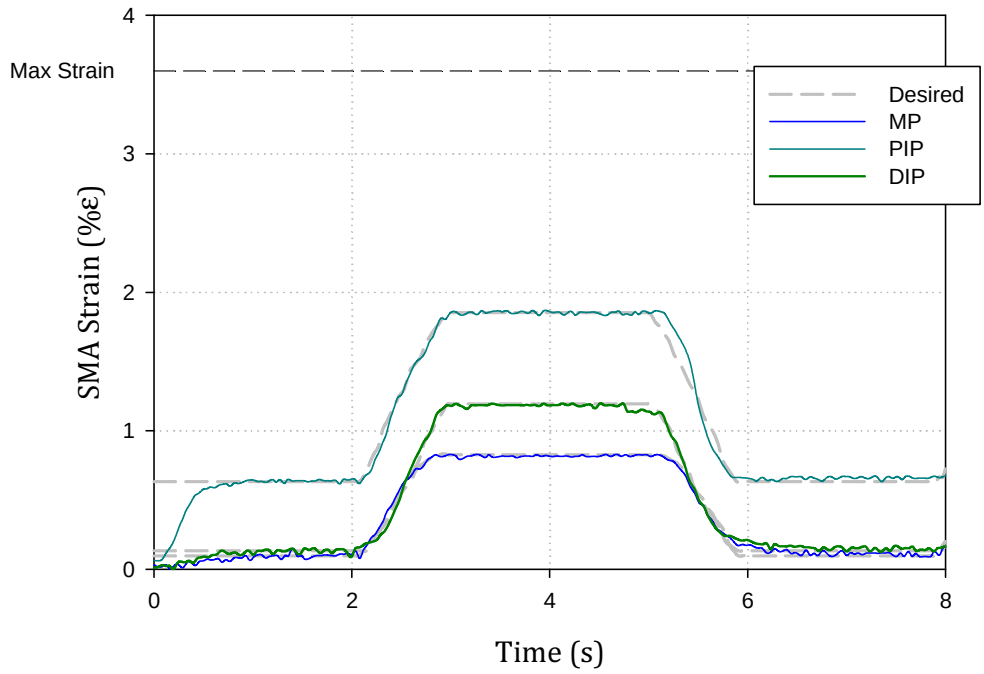

Figure 8-12. Tip/Palmar Posture – Medium Pace

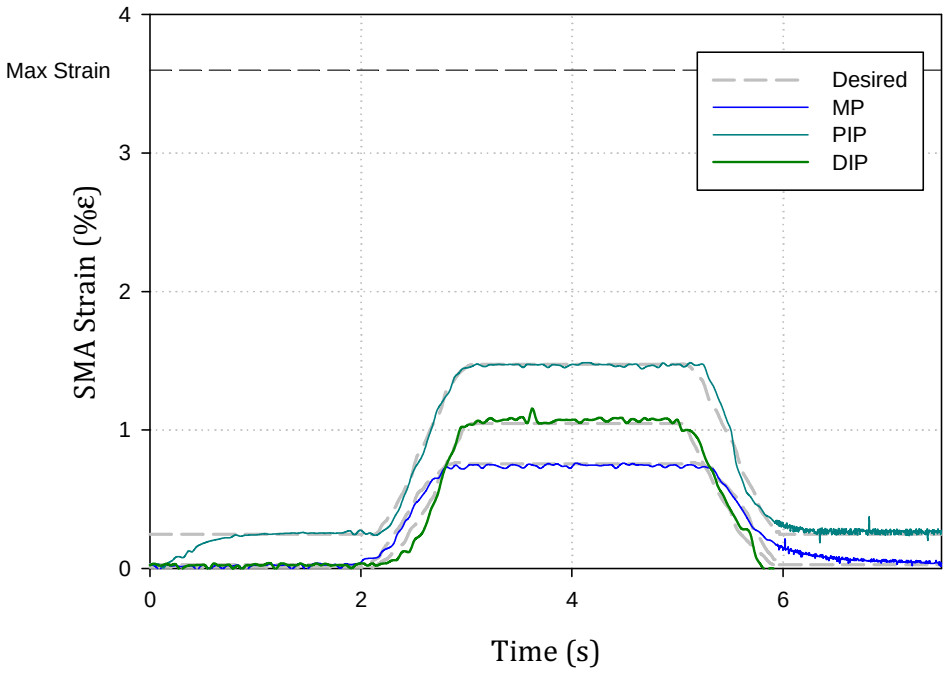

Figure 8-13. Lateral Posture – Medium Pace

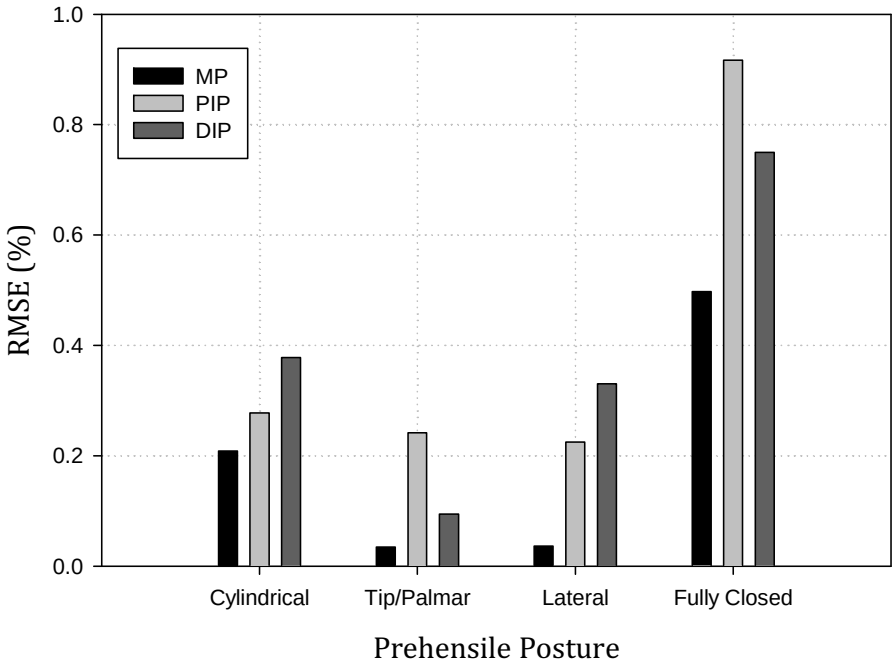

Figure 8-14. Medium Rotation Pace – RMSE Comparison

8.7.3 Fast Rotational Pace

A fast desired joint rotational pace places the greatest demand on the SMA bundle actuators. The increase in rotational velocity and acceleration result in larger torque and work requirements, in addition to an increase in the demand placed on the controller in terms of tracking response. It can be seen that the response deteriorates slightly across all prehensile postures.

Steady state errors are prevalent particularly in the MP and PIP joints. It is suspected these are the result of limitations placed on the quantity of SMA wires per bundle as a result of restricting the maximum power level to 45W per finger (See Section 8.5.3). Furthermore, the increase in friction as a result of faster rotation rates may also result in the deterioration in performance exhibited.

A tracking delay exists owing to the required fast rate of response of the SMA bundle actuator. The delay exists due to the time required to heat or cool the SMA wires to the phase transformation region and is within a range of 0.1-0.3 seconds in length.

However, although such delays are undesirable and unavoidable in a system where heating and cooling is limited, it evident that once the SMA bundle actuator begins to respond, it demonstrates the capacity to carry out grip formation and grip release at the desired pace.

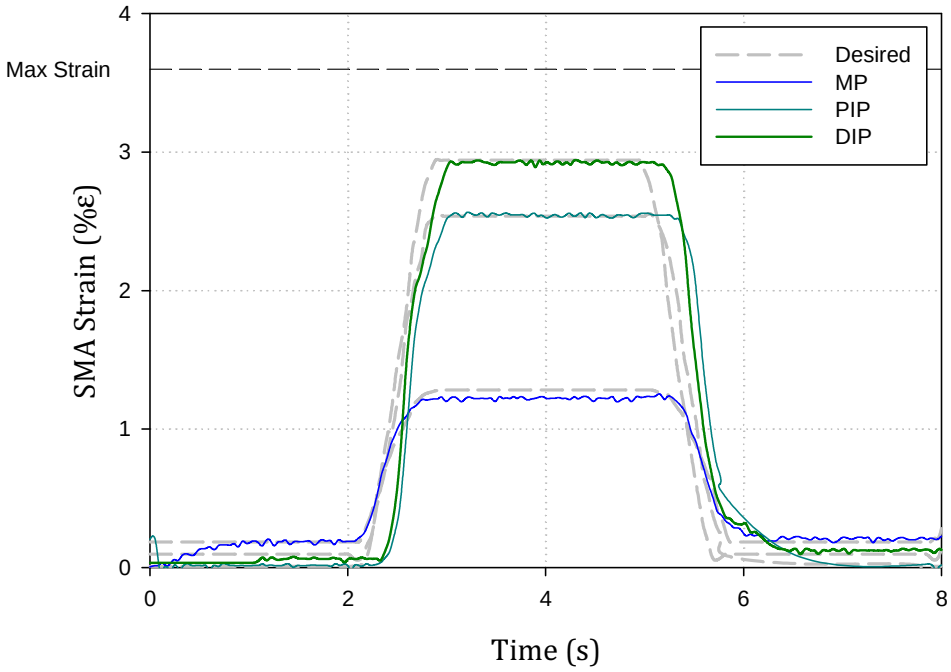

Figure 8-15. Cylindrical Posture – Fast Pace

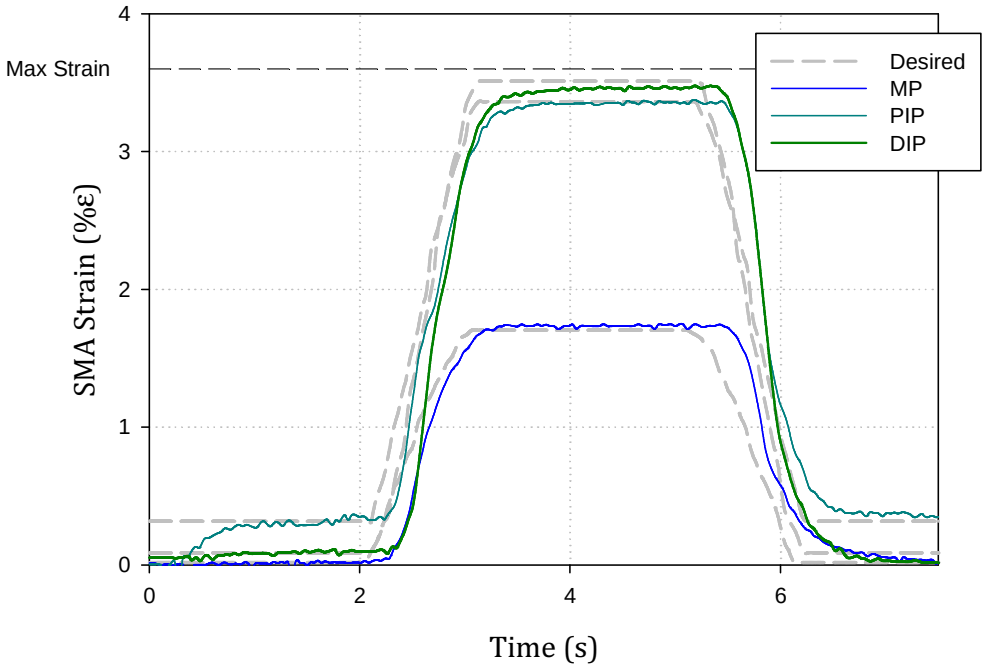

Figure 8-16. Fully Closed Posture – Fast Pace

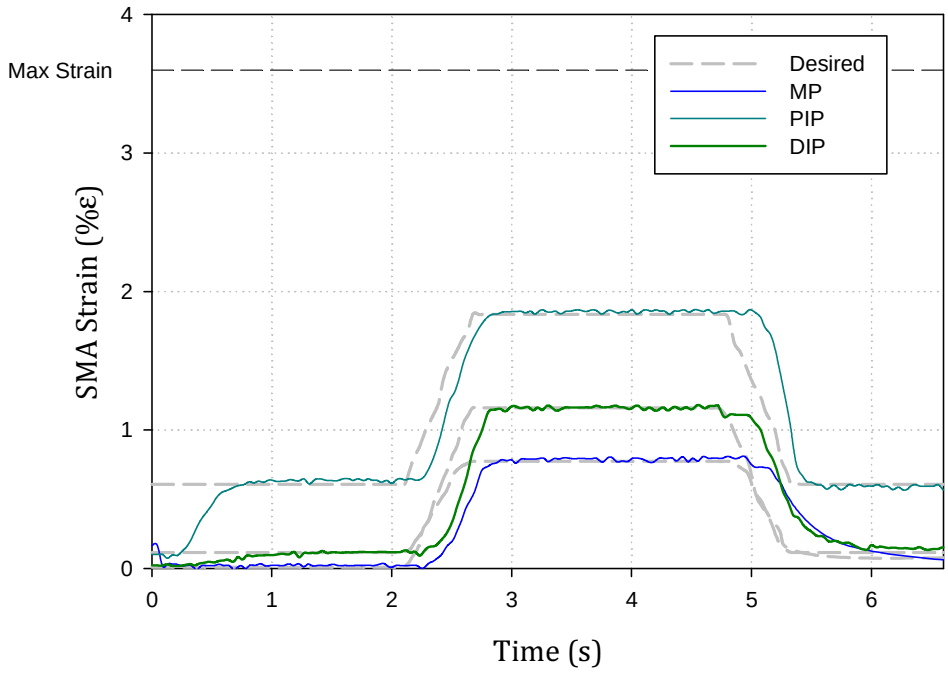

Figure 8-17. Tip/Palmar Posture – Fast Pace

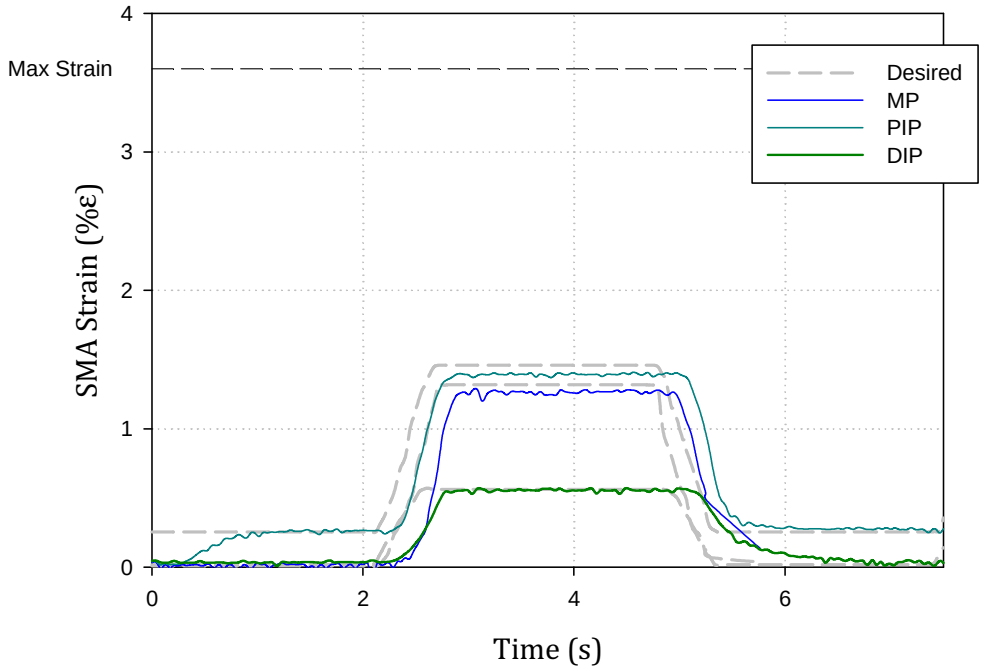

Figure 8-18. Lateral Posture – Fast Pace

It can also be seen that a minor steady state error is evident in a portion of the experimental results. This is noticeable at the limits of SMA operation and can

be linked to the fact that large increases in applied input current only result in very minor increases in SMA strain at these levels. However, in the lateral posture outlined in Figure 8-18, a steady state error is present at lower strain values. It is suspected that this is the result of lower quantities of SMA wires due to power limitations.

The observed RMSE values for all postures tested using a fast rotational pace are generally consistent with those of slow and medium pace, with cylindrical and fully closed postures exhibiting large values. It can be seen however that the lateral postures have recorded high RMSE values also. This is a result of the steady state error present which has been ascribed to insufficient SMA wires in the MP and PIP bundles due to compromises made on available power.

Overall, the response of the SMA bundle actuators to the desired trajectories is considered to be good across the range of prehensile postures. This is evident from the RMSE values recorded. While the RMSE values are more pronounced than with slow and medium rotational paces, the magnitude of the errors are similar for all rotational paces. The fast rotation pace allows for a prehensile posture to form in less than 1 second. This is sufficient for prosthesis performance. These results suggest that the SMA bundle actuators exhibit the capacity to perform adequately as actuators in prosthetic finger design albeit with a slightly delayed response. The speed of response is approaching the upper limit of SMA performance during fast rotational pace. Although the human finger can respond faster than the 'fast' pace applied during this experimentation, the majority of prosthetic applications involving finger motion can be satisfied without the need to achieve this.

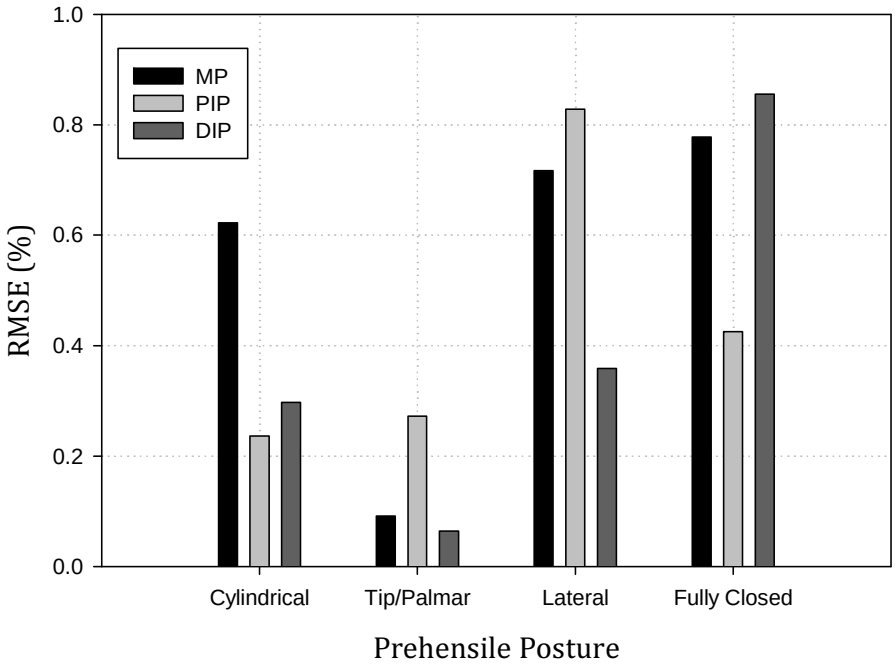

Figure 8-19. Fast Rotation Pace – RMSE Comparison

It is not possible to enhance the rate of rotation of an SMA bundle actuated joint any further without using current values beyond those recommended by the manufacturer, or by using segmented binary control. However, these options are undesirable and are considered to be highly impractical for a prosthetic solution. It is possible, however, to improve the steady state performance of the MP and PIP joints during fast rotational pace by increasing the available power, and thus facilitating an increase in quantity of SMA wires per bundle. This is heavily reliant on the availability of improved battery technology and space limitations to become feasible.

8.8 Conclusions

An investigation into the suitability of SMA bundle actuators in prosthesis design has been carried out. The performance of the SMA bundle actuators was

compared to the performance of the human index finger. Appropriately sized SMA bundle actuators based on the required rotational performance and necessary phalangeal tip forces for exerting an adequate gripping force were calculated for each joint within the prosthetic finger. The SMA bundle actuator wire quantities were sized to overcome the dynamic forces present during rotation and to provide adequate phalangeal tip forces similar to that of the human finger. Wire quantities were limited by available battery power and bundles were sized accordingly. Experimental results carried out on an 8-wire SMA bundle featuring scaled load quantities indicate that the SMA bundle actuators perform well at slow and medium rotational paces with good tracking response with only minor steady state errors present. At a fast rotational pace, a time delay due to the heating and cooling limitations of the SMA wires is present. However, the time delay is minimal at 0.1-0.3 seconds, and the SMA bundle actuators exhibit the capacity to operate at the pace required once the delay has been overcome.

9. CONCLUSIONS & FUTURE WORK

A detailed investigation into the application of SMA bundle actuators in prosthetic finger design has been carried out. A novel design methodology was adopted in the course of this work which facilitated the flow of the work from the identification of the requirements of the finger prosthesis featuring SMA bundle actuators to the realization of the best possible solution. This has resulted in the successful identification of an appropriate SMA bundle actuator for prosthesis design taking into account the size, power and functional limitations of the finger framework whilst optimising the performance of the SMA actuators.

Following comprehensive experimental work, it was found that 150μm SMA wires offer the best balance between dynamic response and steady state force capacity when utilised in a bundle layout. Larger diameter wires offer more force production, however, cooling time is significantly slower. It was also determined that the response to applied input current varies significantly. A novel dynamic model of the nonlinear SMA bundle actuator response was developed from the existing phenomenological heat transfer and hysteresis models. It was found that the nonlinear dynamic system can be viewed as a stack of linear subsystems. This is significant as the dynamic response of an SMA actuator was previously modelled as a single FOPTD model. The resultant errors in the response associated with the implementation of single FOPTD models have been reduced significantly by the nonlinear dynamic model. The dynamic model developed presents a truer reflection of the behaviour of the

SMA bundle actuator when subjected to the manufacturer-specified range of possible input current values.

The dynamic model was utilised in the development of a suitable SMA bundle actuator control strategy. A detailed review of existing strategies was carried out presenting the advantages and disadvantages of each. A decision matrix was employed to help select the best control strategy to meet a series of criteria identified as important in prosthetic actuation tasks. From this, the best approach to SMA bundle actuator control was established. This consisted of an inverse model of hysteresis in feedforward to compensate for the effects of hysteresis, while simultaneously using a suitably tuned adaptive PID (a-PID) controller in feedback to reject any disturbances and to speed up the response of the actuator. The a-PID controller was developed and tuned appropriately using the dynamic model. Significantly, the dynamic model permits the utilization of existing robust tuning techniques across the range of linear subsystems, therefore ensuring optimum performance levels are achieved. Prior to this development, tuning of PID controllers in control strategies featuring inverse hysteresis models in the feedforward loop and a PID controller in the feedback loop was carried out by trial and error. The inclusion of a formal tuning methodology based on the thermo-mechanical response is therefore noteworthy, allowing for the possibility of optimized controller response and ease of replication by other researchers.

The a-PID controller adapts well to step and sinusoidal input values. The solution works well over the full range of SMA strain. However, when tracking sinusoidal waveforms, there is a breakdown in performance at approximately

0.3Hz when using joule heating and natural cooling. This is due to the SMA bundle actuators reaching their maximum frequency of operation. This limitation is identified as a key area requiring further study. It has been shown in this work that enhanced cooling using heat sinks can improve the performance, but the frequency of operation falls short of the >1Hz level of operation of the human finger. Noticeably the a-PID control strategy showed excellent robustness to external air-flow and loading, with only a minor deterioration in performance recorded within the operative range.

Shortcomings identified with the use of SMA actuators in prosthetic finger design led to work being carried out to determine the most appropriate arrangement of SMA wires per bundle for prosthetic finger joint actuation. The prosthetic finger was designed with due reference of the geometric and dynamic characteristics of the human index finger. A kinematic and dynamic analysis was completed and the requirements of the SMA bundle actuators were clearly identified. Experimental work, carried out to compare the performance of the prosthetic finger to the human finger over a range of common prehensile postures and rotational paces indicates that SMA bundle actuators show good potential to be utilised in prosthesis design and can be recommended as a viable actuation alternative to DC motors.

The kinematic and dynamic analyses were used to determine the quantity of SMA wires per bundle required to overcome the dynamic forces associated with rotation, and to provide adequate phalangeal tip forces to emulate the human finger. Tracking performance was shown to be consistent and accurate at slow and medium rotational paces. At fast rotational pace, tracking was adequate

despite the formation of minor tracking and steady state errors as the SMA bundle actuators reached their performance limits. As the desired rate of rotation increased, a notable increase in time delay is evident due to the heating and cooling limitations of the SMA wires.

In spite of the promising performance of the SMA bundle actuators, significant actuator design issues must still be overcome. Power limitations restrict the maximum quantity of SMA wires per bundle. Improvements in this are reliant on the development of new high power density battery solutions. Additionally, the utilization of larger quantities of SMA wires per bundle leads to increased difficulties in removing excess heat. The implementation of a cooling solution that is both effective and usable in a prosthetic framework is a significant factor opposing implementation at present. It is foreseen that a mechanically-based forced cooling solution will be required to achieve this.

Furthermore, excess heat build-up coupled with the safety concerns surrounding the relatively high temperatures required to actuate the SMA wires will be problematic and require a practical solution prior to their deployment in prosthesis applications. The solutions to these issues may depend on the discovery of a new alloy exhibiting lower transition temperatures but featuring the high power density associated with Ni-Ti alloys.

The design outlined in this work is based on SMA bundle actuators mounted in the palmar region of the hand. This places severe limitations on SMA length and therefore requires a gearing system to enhance the achievable displacement. However, this impacts negatively on the force generation capacity of the SMA bundle actuators. In more general applications in which SMA bundle actuators

can be applied, and where space is not limited, larger forces can be achieved with smaller SMA bundle sizes if the application dictates no gearing requirements. The minimum length of actuator required to fully achieve this has been found to be 106mm. This is particular to the joint designs utilised in this work. By utilising longer SMA wires and thus removing the need for gearing, smaller quantities of SMA wires per bundle can be satisfactory for operation. This leads to a decrease in required power.

Throughout this work, SMA bundle actuators have been shown to exhibit many favourable characteristics allowing them to be considered as a viable actuation technology for a range of applications beyond prosthesis applications. The methodology carved out throughout this work is not limited to applications involving SMA actuators, but rather can be applied to a wide range of actuators that display similar hysteresis effects. This has huge implications for a vast range of applications and industries that rely on miniature, lightweight and cheap actuation technology, from space technologies, to consumer products, to rehabilitation robotics.

9.1 Future Work Direction

Cooling has been identified as a key area in which improvements in SMA response can be found. An investigation into the possibilities of using novel cooling systems such as solid-state and carbon-nanotubes solutions is a primary candidate for future work. Benefits can be gained from implementing more advanced biomimetic designs in conjunction with SMA bundle actuators. Future designs of prosthetic hand solutions featuring SMA bundle actuators should focus on maximizing the length of the actuator within the hand for mounting of

the actuator. This approach can also be taken in designs featuring SMA bundle actuators mounted in the forearm region in larger prosthetic solutions. Additionally, as the SMA bundle actuators are intended for utilization in a portable prosthesis solution, it is appropriate to utilise electromyographic (EMG) signals (or similar signals that may be picked up from the human body) as a way to set the desired inputs of the SMA bundle actuator controller. The interaction between EMG signals and the control strategy outlined in this work will serve to play a major part in the development of a successful SMA bundle actuated prosthesis design.

9.2 Guidelines for Future Work Applications

The appeal of SMA bundle actuators is not limited to deployment in a prosthetic finger actuation solution. As such, the approach taken in this work can be adapted in more generic terms. The potential benefits of using suitably designed and controlled SMA bundle actuators can potentially outweigh rival actuation technologies in other areas. For example, the accurate control combined with high forces exhibited by SMA bundle actuators in this work allows them to be considered for a number of different roles, particularly in environments where weight and size are a major concern. Some opportunities for SMA bundle actuator utilisation lie in the fields of aerospace applications, such as miniature grippers for space applications, where size and weight are critical. Other areas of application may be robotics for use in environments dangerous to humans, and more common linear actuation applications where actuators are required for the hoisting of loads accurately and quickly, or the opening and closing of shutters.

All future work involving the use of SMA bundle actuators would benefit from an approach to their design, sizing and implementation that encompasses all of the important considerations required when dealing with SMAs. It is therefore considered beneficial to present guidelines for fellow researchers who wish to become involved in the field. While the work thus far has outlined a detailed methodology designed to specify the ideal SMA bundle actuators for prosthesis design, the approach outlined below is more generic in nature. Thus, as a secondary benefit, this generic approach can also be utilised with actuation technologies similar to SMAs such as piezoelectric and electroactive polymer actuators which also exhibit common nonlinearities such as hysteresis. It is hoped that this approach will assist in the development of more advanced actuation systems using alternative actuation solutions.

The approach is outlined as follows:

i. *Definition of application*. This allows for the determination of the role of the actuator in the application. From this, key actuator characteristics, targets and requirements can be determined. The range of motions and speeds required must be established. Key targets in terms of accuracy, repeatability and stability must be defined. In the case of SMA bundle actuators in prosthesis design, it is important to determine the functions, motions and limitations of the human finger to allow for the derivation of targets for the prosthetic device.

ii. *Scientific principles of actuator operation.* The underlying scientific principles of operation of the actuator play a vital role in the development of a suitable mathematical model and control system.

Characterisation of the actuators is required to establish their functionality and identify operational limits. Furthermore, any nonlinearities present can be established and utilised in a suitable controller design later in the process. The thermo-mechanical relationship between SMA strain and wire temperature governs the dynamic behaviour of SMA wires.

iii. *Sizing of the actuators*. Based on the actuator characteristics and requirements, the geometry of the actuator can be determined. Single or multiple actuators may be required depending on the role of the actuator in the application. Sizing, both physically and electrically must be determined, in conjunction with the determination of any potential issues arising from actuator tendencies. SMA wires of different sizes and lengths respond differently to applied input current. Larger diameter wires offer greater force production capacity, while smaller diameter wires offer faster heating and cooling cycle times. Dynamic response is considered to be of primary importance as force requirements can be achieved by bundling suitable SMA wires in parallel.

iv. *Actuator response and modelling*. Nonlinearities present, such as hysteresis, must be fully modeled to facilitate their inclusion in a suitable control strategy. A suitable hysteresis identification methodology and modelling technique must be selected. The effect of nonlinearities on the steady state and dynamic response of the actuator must also be investigated. With SMA bundle actuator design, the Preisach model demonstrates suitable qualities that can account for

major and minor loops of the associated hysteresis, relating applied input current to SMA strain. Data point population of the Preisach plane can be carried out using a suitable data acquisition system if appropriate. An accurate SMA wire temperature profile can be used to determine the time delay and time constant of the SMA strain response for any applied input current, thus allowing for a dynamic model of the response to be acquired.

v. *Determine inverse hysteresis model*. An inverse hysteresis model allows for a suitable input to the actuator to be calculated which takes into account the effects of hysteresis to produce a desired output response from the actuator. With SMA actuated prosthesis design, the inverse Preisach model can be used to calculate a suitable input current that will give a desired SMA strain value.

vi. *Software platform identification.* A suitable software platform and programming approach is required which can be used to implement the inverse hysteresis model in real-time. Furthermore, the software platform must facilitate interaction with a data acquisition and control system to allow for the development and testing of a suitable controller solution. Other issues such as the learning curve associated with the chosen software and the ease-of-use of any software toolboxes that facilitate data acquisition and control must be considered. Throughout the course of this work, LabVIEW was chosen as a suitable software platform owing to its in-built data acquisition and programming capabilities. Furthermore, the graphical programming environment

allows for fast adoption of the software. A state-machine approach to programming was adopted as it facilitates real-time calculation of the inverse model and is flexible in structure.

vii. *Controller development*. The controller should be designed based on the relationship between the control inputs and the response of the actuator. Its basis lies in the scientific principles of operation previously identified. In systems with hysteresis, the response is typically nonlinear. It is therefore prudent to explore a range of nonlinear control strategies. In SMA bundle actuators, the underlying scientific principle of operation is the relationship between wire temperature and SMA strain. The wire temperature can be modified as desired by manipulating the value of an applied input current to the SMAs. This results in a change in SMA strain. An adaptive controller was developed which facilitated a change in controller gain values for different applied input currents based on the changing thermo-mechanical relationship observed.

viii. *Controller Tuning*. Techniques to tune any identified controller must be utilised to ensure optimum response from the actuator. It is not sufficient to rely on trial-and-error tuning. Determination of what is necessitated from the tuning methodology, such as set-point tracking or a robust control effort, play a key role in selecting appropriate tuning formulae. The dynamic model of SMA bundle actuators provided the basis for tuning the a-PID controller developed in this work. Robust ITAE tuning rules from the literature were utilised for each linear sub-model making up the full dynamic model. A spline approximation was

then implemented to estimate the optimum gains for each applied input current.

ix. *Verification of the actuator in the application*. To further examine the suitability of the actuator in the required application, it is necessary to carry out a series of experimental tests. These tests can be used to validate the approach taken to actuator design, control and implementation. SMA strain and force production were examined in the context of rotating a prosthetic finger joint for the work described herein. The outcomes have led to the identification of some key areas requiring further work.

REFERENCES

[1] P. A. Padula and L. W. Friedmann, "Acquired Amputation and Prostheses Before the Sixteenth Century," *Angiology,* vol. 38, pp. 133-141, 1987.

[2] A. J. Thurston, "Pare and Prosthetics: The Early History of Artificial Limbs," *ANZ Journal of Surgery,* vol. 77, pp. 1114-1119, 2007.

[3] I. Dudkiewicz*, et al.*, "Evaluation of prosthetic usage in upper limb amputees," *Disability & Rehabilitation,* vol. 26, pp. 60-63, 2004.

[4] W. J. Gaine*, et al.*, "Upper limb traumatic amputees: Review of prosthetic use," *The Journal of Hand Surgery: Journal of the British Society for Surgery of the Hand,* vol. 22, pp. 73-76, 1997.

[5] D. M. Desmond, "Coping, affective distress, and psychosocial adjustment among people with traumatic upper limb amputations," *Journal of Psychosomatic Research,* vol. 62, pp. 15-21, 2007.

[6] L. Walters. *Statistics on Hand and Arm Loss*. Available: http://www.aboutonehandtyping.com/statistics.html (Accessed 7th August, 2009)

[7] E. M. Schaffalitzky, "Optimising the prescription and use of lower limb prosthetic technology: A mixed methods approach.," PhD Thesis, Dublin City University, 2010.

[8] D. G. Smith*, et al.*, *Atlas of Amputations and Limb Deficiencies*. American Academy of Orthopaedic Surgeons, Rosemount, IL, 2004.

[9] A. Muzumdar, *Powered Upper Limb Prostheses*. Springer, New York, NY, 2004.

[10] M. Zecca*, et al.*, "Control of Multifunctional Prosthetic Hands by Processing the EMG Signal," *Critical Reviews in Biomedical Engineering,* vol. 30, pp. 459-485, 2002.

[11] L.-R. Lin and H.-P. Huang, "NTU hand: A new design of dexterous hands," *Journal of Mechanical Design, Transactions of the ASME,* vol. 120, pp. 282-292, 1998.

[12] S. C. Jacobsen*, et al.*, "Design of the Utah/MIT dexterous hand," in *IEEE Int. Conf. on Robotics and Automation*, 1986, pp. 1520-1532.

[13] J. Butterfass*, et al.*, "DLR-Hand II: Next generation of a dextrous robot hand," in *IEEE International Conference on Robotics and Automation (ICRA), May 21 - May 26*, Seoul, Korea, Republic of, 2001, pp. 109-114.

[14] J. Butterfass*, et al.*, "DLR's multisensory articulated hand.," in *IEEE International Conference on Robotics and Automation*, Leuven, Belgium, 1998, pp. 2081-2086

[15] C. S. Lovchik and M. A. Diftler, "The Robonaut hand: a dexterous robot hand for space," in *IEEE International Conference on Robotics and Automation*, 1999, pp. 907-912.

[16] T. Iberall*, et al.*, "On the development of EMG control for a prosthesis using a robotic hand," in *Proceedings of the 1994 IEEE International Conference on Robotics and Automation, May 8 - May 13*, San Diego, CA, USA, 1994, pp. 1753-1758.

[17] P. J. Kyberd and P. H. Chappell, "The Southampton Hand - An Intelligent Myoelectric Prosthesis," *Journal of Rehabilitation Research and Development,* vol. 31, pp. 326-334, 1994.

[18] *Shadow Robot Arm*. Available: http://www.shadowrobot.com/ (Accessed 23rd March, 2008)

[19] M. Folgheraiter and G. Gina, "Blackfingers: an artificial hand that copies human hand in structure," in *1st IEEE-RAS International Conference on Humanoid Robots (Humanoids 2000), Sept 7th - Sept 8th*, MIT, Cambridge, Mass., USA, 2000.

[20] S. Mackay. *RoMeLa develops low cost dexterous robotic hand*. Available: http://www.eng.vt.edu/news/virginia-techs-romela-develops-low-cost-dexterous-robotic-hand-operated-compressed-air (Accessed October 21st, 2009)

[21] R. Bogue, "Exoskeletons and robotic prosthetics: a review of recent developments," *Industrial Robot,* vol. 36, pp. 421-427, 2009.

[22] P. Kyberd, "Historical Review of Multifunction Hands," in *13th ISPO World Congress*, Leipzig, Germany, 2010.

[23] *Fluidhand - each finger can be moved separately*. Available: http://www.physorg.com/news128082539.html (Accessed 10th January, 2009)

[24] F. Sebelius and M. Bonazzi. *The Smart Bio-adaptive Hand Prosthesis*. Available: http://www.elmat.lth.se/~smarthand/ (Accessed 12th January, 2010)

[25] B. Massa*, et al.*, "Design and development of an underactuated prosthetic hand," in *Proceedings - IEEE International Conference on Robotics and Automation, May 11 - May 15*, Washington, DC, United States, 2002, pp. 3374-3379.

[26] M. C. Carrozza*, et al.*, "A Cosmetic Prosthetic Hand with Tendon Driven Under-Actuated Mechanism and Compliant Joints: Ongoing Research and Preliminary Results," in *Proceedings of the IEEE International Conference on Robotics and Automation (ICRA 2005)*, 2005, pp. 2661-2666.

[27] F. Farzan and P. Pietruszczak. Artificial Muscle Actuators for Upper Limb Prosthesis (PDF Edition). *lecture notes online, website:*

http://www.ece.mcmaster.ca/~ibruce/courses/EE3BA3_2004/EE3BA3_presentation4.pdf.

[28] V. Bundhoo and E. J. Park, "Design of an artificial muscle actuated finger towards biomimetic prosthetic hands," in *International Conference on Advanced Robotics, ICAR '05*, Seattle, WA, United States, 2005, pp. 368-375.

[29] K. Kuribayashi*, et al.*, "An upper extremity prosthesis using SMA actuator," in *IEEE International Workshop of Robot and Human Communication*, 1992, pp. 52-57.

[30] A. Ölander, "An electrochemical investigation of solid cadmium-gold alloys," *Journal of the American Chemical Society,* vol. 54, pp. 3819-3833, 1932.

[31] A. B. Greninger and V. G. Mooradian, "Strain transformation in metastable beta copper-zinc and beta copper-tin alloys," *American Institute of Mining and Metallurgical Engineers -- Transactions,* vol. 128, pp. 337-355, 1938.

[32] G. V. Kurdjumov and L. G. Khandros, *Dokl. Akad. Nauk. SSSR 66,* pp. 211-213, 1949.

[33] L. C. Chang and T. A. Read, "Plastic deformation and diffusionless phase changes in metals -- Gold-cadmium beta phase," *American Institute of Mining and Metallurgical Engineers -- Journal of Metals,* vol. 191, pp. 47-52, 1951.

[34] M. Kohl, *Shape Memory Microactuators*: Springer, 2004.

[35] W. J. Buehler and F. E. Wang, "A summary of recent research on the nitinol alloys and their potential application in ocean engineering," *Ocean Engineering,* vol. 1, pp. 105-108, 1968.

[36] G. B. Kauffman and I. Mayo, "The Story of Nitinol: The Serendipitous Discovery of the Memory Metal and Its Applications," *The Chemical Educator,* vol. 2, pp. 1-21, 1997.

[37] L. Schetky. (1979) Shape memory alloys. *Scientific American*. 74-82.

[38] C. A. Heisterkamp*, et al.*, "Nitinol. A New Biomaterial," *Proceedings of the 8th International Conference on Medical & Biological Engineering, July 20 - July 25,* 1969.

[39] F. J. Gil and J. A. Planell, "Shape memory alloys for medical applications," *Proceedings of the Institution of Mechanical Engineers, Part H: Journal of Engineering in Medicine,* vol. 212, pp. 473-488, 1998.

[40] R. Bogue, "Shape-memory materials: A review of technology and applications," *Assembly Automation,* vol. 29, pp. 214-219, 2009.

[41] Y. H. Teh, "Fast, Accurate Force and Position Control of Shape Memory Alloy Actuators," Ph.D. Thesis, The Australian National University, 2008.

[42] *Dynalloy - Flexinol Technical Data*. Available: http://www.dynalloy.com/TechData_Metric.html (Accessed 20 February, 2007)

[43] J. Van Humbeeck, "Non-medical applications of shape memory alloys," *Materials Science and Engineering A,* vol. 273, pp. 134-148, 1999.

[44] P. Pappas*, et al.*, "Transformation fatigue and stress relaxation of shape memory alloy wires," *Smart Materials and Structures,* vol. 16, pp. 2560-2570, 2007.

[45] Y. Nakano*, et al.*, "Hitachi's Robot Hand," *Robotics Age,* vol. 6, pp. 18-20, 1984.

[46] K. J. De Laurentis and M. Constantinos, "Mechanical design of a shape memory alloy actuated prosthetic hand," *Technol. Health Care,* vol. 10, pp. 91-106, 2002.

[47] M. J. Mosley and C. Mavroidis, "Experimental non-linear dynamics of a shape memory alloy wire bundle actuator," *American Society of Mechanical Engineers, Dynamic Systems and Control Division (Publication) DSC,* vol. 67, pp. 709-717, 1999.

[48] K. Yang and C. Gu, "A novel robot hand with embedded shape memory alloy actuators," *Proceedings of the Institution of Mechanical Engineers, Part C: Journal of Mechanical Engineering Science,* vol. 216, pp. 737-745, 2002.

[49] G. Roznowski and M. Drzewiecki, "The design of the prosthetic index finger actuated by shape memory alloy wires," in *Proceedings of the IASTED International Conference on Biomedical Engineering, Febrary 16 - Febrary 18*, Innsbruck, Austria, 2004, pp. 27-30.

[50] C. S. Loh*, et al.*, "New shape memory alloy actuator: Design and application in the prosthetic hand," in *Annual International Conference of the IEEE Engineering in Medicine and Biology - Proceedings*, Shanghai, China, 2005, pp. 6900-6903.

[51] Y. Mazoguchi*, et al.*, "Integration of a Multi-D.O.F. Individual Adaptable with Tactile Feedback for an EMG Prosthetic System," in *2nd International Workshop on Man-Machine Symbiotic Systems*, 2004, pp. 421-427.

[52] V. Bundhoo*, et al.*, "A shape memory alloy-based tendon-driven actuation system for biomimetic artificial fingers, part I: Design and evaluation," *Robotica,* vol. 27, pp. 131-146, 2009.

[53] T. Maeno and T. Hino, "Miniature five-fingered robot hand driven by shape memory alloy actuators," in *12th IASTED International Conference on Robotics and Applications, RA 2006, August 14 - August 16*, Honolulu, HI, United states, 2006, pp. 174-179.

[54] K.-J. Cho*, et al.*, "SBC hand: A lightweight robotic hand with an SMA actuator array implementing C-segmentation," in *IEEE International*

Conference on Robotics and Automation (ICRA'07), April 10 - April 14, Rome, Italy, 2007, pp. 921-926.

[55] C. Cocaud*, et al.*, "Position control of an experimental robotic arm driven by artificial muscles based on shape memory alloys," *International Journal of Mechanics and Materials in Design,* vol. 3, pp. 223-236, 2006.

[56] A. D. Price*, et al.*, "Design and control of a shape memory alloy based dexterous robot hand," *Smart Materials and Structures,* vol. 16, pp. 1401-1414, 2007.

[57] K. Andrianesis and A. Tzes, "Design of an Anthropomorphic Prosthetic Hand Driven by Shape Memory Alloy Actuators," in *Proc. of the 2nd Biennial IEEE/RAS-EMBS Int. Conference on Biomedical Robotics and Biomechatronics*, Scottsdale, AZ, USA, 2008.

[58] J. E. P. Puig*, et al.*, "A methodology for the design of robotic hands with multiple fingers," *International Journal of Advanced Robotic Systems,* vol. 5, pp. 177-184, 2008.

[59] T. W. Duerig*, et al.*, *Engineering Aspects of Shape Memory Alloys*: Butterworth-Heinemann, 1990.

[60] D. Lagoudas, *Shape Memory Alloys - Modeling and Engineering Applications*: Springer, 2008.

[61] K. Tanaka*, et al.*, "Thermomechanics of transformation pseudoelasticity and shape memory effect in alloys," *International Journal of Plasticity,* vol. 2, pp. 59-72, 1986.

[62] M. Kohl and K. D. Skrobanek, "Linear microactuators based on the shape memory effect," *Sensors and Actuators A: Physical,* vol. 70, pp. 104-111, 1998.

[63] S. Chikkamaranahalli*, et al.*, "Precision instrument for characterizing shape memory alloy wires in bias spring actuation," *Review of Scientific Instruments,* vol. 76, pp. 65 - 105, 2005.

[64] C. Liang and C. A. Rogers, "Design of shape memory alloy actuators," *Journal of Intelligent Material Systems and Structures,* vol. 8, pp. 303-313, 1997.

[65] M. Ho and J. P. Desai, "Characterisation of SMA actuator for applications in robotic neurosurgery," in *31st Annual International Conference of the IEEE Engineering in Medicine and Biology Society: Engineering the Future of Biomedicine, EMBC 2009, September 2 - September 6*, Minneapolis, MN, United states, 2009, pp. 6856-6859.

[66] M. Moallem and V. A. Tabrizi, "Tracking control of an antagonistic shape memory alloy actuator pair," *IEEE Transactions on Control Systems Technology,* vol. 17, pp. 184-190, 2009.

[67] F. Incropera and D. DeWitt, *Fundamentals of Heat and Mass Transfer*, 5th ed.: John Wiley & Sons, Inc., 2002.

[68] B. Selden*, et al.*, "Segmented binary control of shape memory alloy actuator systems using the peltier effect," in *Proceedings- 2004 IEEE International Conference on Robotics and Automation, April 26, 2004 - May 1, 2004*, New Orleans, LA, United states, 2004, pp. 4931-4936.

[69] N. Dechev*, et al.*, "Multiple finger, passive adaptive grasp prosthetic hand," *Mechanism and Machine Theory,* vol. 36, pp. 1157-1173, 2001.

[70] G. Song*, et al.*, "Application of shape memory alloy wire actuator for precision position control of a composite beam," *Journal of Materials Engineering and Performance,* vol. 9, pp. 330-333, 2000.

[71] R. A. Russell and R. B. Gorbet, "Improving the response of SMA actuators," in *IEEE International Conference on Robotics and Automation*, Nagoya, Jpn, 1995, pp. 2299-2304.

[72] S. A. Mascaro and H. H. Asada, "Wet shape memory alloy actuators for active vasculated robotic flesh," Taipei, Taiwan, 2003, pp. 282-287.

[73] D. Reynaerts and H. Van Brussel, "Design aspects of shape memory actuators," *Mechatronics,* vol. 8, pp. 635-656, 1998.

[74] J. Abadie*, et al.*, "An integrated shape memory alloy micro-actuator controlled by thermoelectric effect," *Sensors and Actuators A: Physical,* vol. 99, pp. 297-303, 2002.

[75] J. A. Ewing, "Experimental Research in Magnetism," *Philosophical Transactions of the Royal Society London,* vol. 176, 1895.

[76] I. D. Mayergoyz, "Mathematical Models of Hysteresis," *IEEE Transactions on Magnetics,* vol. MAG-22, 1986.

[77] A. Pai, "A Phenomenological model of Shape Memory Alloys Including Time-Varying Stress," Master of Applied Science, University of Waterloo, 2007.

[78] C. Liang and C. A. Rogers, "One-dimensional thermomechanical constitutive relations for shape memory materials," in *31st AIAA/ASME/ASCE/AHS/ASC Structures, Structural Dynamics and Materials Conference. Part 3 (of 4): Structural Dynamics I, April 2 - April 4*, Long Beach, CA, USA, 1990, pp. 16-28.

[79] L. C. Brinson, "One-dimensional constitutive behavior of shape memory alloys: Thermomechanical derivation with non-constant material functions and redefined martensite internal variable," *Journal of Intelligent Material Systems and Structures,* vol. 4, pp. 229-242, 1993.

[80] K. Ikuta*, et al.*, "Mathematical model and experimental verification of shape memory alloy for designing micro actuator," Nara, Jpn, 1991, pp. 103-108.

[81] D. R. Madill and D. Wang, "Modeling and L2-stability of a shape memory alloy position control system," *IEEE Transactions on Control Systems Technology,* vol. 6, pp. 473-481, 1998.

[82] M. H. Elahinia and M. Ahmadian, "An enhanced SMA phenomenological model: II. the experimental study," *Smart Materials and Structures,* vol. 14, pp. 1309-1319, 2005.

[83] A. R. Shahin*, et al.*, "Enhanced cooling of shape memory alloy wires using semiconductor `heat pump' modules," *Journal of Intelligent Material Systems and Structures,* vol. 5, pp. 95-104, 1994.

[84] M. H. Elahinia and M. Ahmadian, "An enhanced SMA phenomenological model: I. The shortcomings of the existing models," *Smart Materials and Structures,* vol. 14, pp. 1297-1308, 2005.

[85] M. A. Krasnosel'skii and A. V. Pokrovskii, *Systems with Hysteresis*: Springer-Verlag, 1989.

[86] L. Prandtl, "Ein gedanke modell zur kinetischen theorie der festen korper," *ZAMM,* vol. 8, pp. 85-106, 1928.

[87] A. Ishlinskii, "Some applications of statistical methods to describe deformations of bodies," *Isz. AN SSSR,* vol. 9, pp. 580-590, 1944.

[88] J. W. Macki*, et al.*, "Mathematical models for hysteresis," *SIAM Rev.,* vol. 35, pp. 94-123, 1993.

[89] F. Preisach, "Uber die magnetische nachwirkung," *Zeit. fir Physik,* vol. 94, pp. 227-302, 1935.

[90] S. Mittal and C.-H. Menq, "Hysteresis compensation in electromagnetic actuators through Preisach model inversion," *IEEE/ASME Transactions on Mechatronics,* vol. 5, pp. 394-409, 2000.

[91] D. C. Hughes and J. T. Wen, "Preisach modeling of piezoceramic and shape memory alloy hysteresis," in *Smart Structures and Materials: Mathematics and Control in Smart Structures, February 26-29*, San Diego, CA, USA, 1996, pp. 507-528.

[92] P. Ge and M. Jouaneh, "Generalized Preisach model for hysteresis nonlinearity of piezoceramic actuators," *Precision Engineering,* vol. 20, pp. 99-111, 1997.

[93] A. Stancu*, et al.*, "New Preisach model for structured particulate ferromagnetic media," *Journal of Magnetism and Magnetic Materials,* vol. 290-291, pp. 490-493, 2005.

[94] R. B. Gorbet*, et al.*, "Preisach model identification of a two-wire SMA actuator," in *Proceedings of the IEEE International Conference on Robotics and Automation. Part 3 (of 4), May 16 - 20*, Leuven, Belgium, 1998, pp. 2161-2167.

[95] B.-J. Choi and Y.-J. Lee, "Preisach model of SMA actuators using proportional relationship of major loop of hysteresis," in *2002 IEEE/RSJ International Conference on Intelligent Robots and Systems, September 30, 2002 - October 4, 2002*, Lausanne, Switzerland, 2002, pp. 1986-1991.

[96] B.-J. Choi*, et al.*, "Fast Preisach modeling method for shape memory alloy actuators using major hysteresis loops," *Smart Materials and Structures,* vol. 13, pp. 1069-1080, 2004.

[97] A. Ktena*, et al.*, "A Preisach model identification procedure and simulation of hysteresis in ferromagnets and shape-memory alloys," in *3th International Symposium on Hysteresis (HMM 2001), May 23*, Ashburn, VI, United states, 2001, pp. 84-90.

[98] S. Majima*, et al.*, "Modeling of shape memory alloy actuator and tracking control system with the model," *IEEE Transactions on Control Systems Technology,* vol. 9, pp. 54-59, 2001.

[99] K. K. Ahn and N. B. Kha, "Internal model control for shape memory alloy actuators using fuzzy based Preisach model," *Sensors and Actuators, A: Physical,* vol. 136, pp. 730-741, 2007.

[100] N. Troisfontaine*, et al.*, "Optimal design of micro-actuators based on SMA wires," *Smart Materials and Structures,* vol. 8, pp. 197-203, 1999.

[101] M. Hashimoto*, et al.*, "Application of Shape Memory Alloy to Robotic Actuators," *Journal of Robotic Systems,* vol. 2, pp. 3-25, 1985.

[102] K. Ikuta*, et al.*, "Shape Memory Alloy Servo Actuator System with Electric Resistance Feedback and application for Active Endoscope," in *Proceedings - IEEE International Conference on Robotics and Automation.*, Philadelphia, PA, USA, 1988, pp. 427-430.

[103] Y. Eren*, et al.*, "B-spline based adaptive control of shape memory alloy actuated robotic systems," in *ASME International Mechanical Engineering Congress and Exposition* New Orleans, LA, United States, 2002, pp. 471-478.

[104] Y. H. Teh and R. Featherstone, "Accurate force control and motion disturbance rejection for shape memory alloy actuators," Rome, Italy, 2007, pp. 4454-4459.

[105] D. Grant and V. Hayward, "Variable structure control of shape memory alloy actuators," *IEEE Control Systems Magazine,* vol. 17, pp. 80-88, 1997.

[106] G. Song and R. Mukherjee, "Comparative study of conventional nonsmooth time-invariant and smooth time-varying robust compensators," *IEEE Transactions on Control Systems Technology,* vol. 6, pp. 571-576, 1998.

[107] M. H. Elahinia and H. Ashrafiuon, "Nonlinear control of a single-link shape memory alloy actuated arm," Montreal, Que., Canada, 2002, pp. 1455-1464.

[108] H. Ashrafiuon*, et al.*, "Position Control of a Three-link Shape Memory Alloy Actuated Robot," *Journal of Intelligent Material Systems and Structures,* vol. 17, pp. 381-392, 2006.

[109] S.-B. Choi, "Position control of a single-link mechanism activated by shape memory alloy springs: Experimental results," *Smart Materials and Structures,* vol. 15, pp. 51-58, 2006.

[110] E. Shameli*, et al.*, "Stability analysis and nonlinear control of a miniature shape memory alloy actuator for precise applications," *Mechatronics,* vol. 15, pp. 471-486, 2005.

[111] M. Kumon*, et al.*, "Shape memory alloy actuator with simple adaptive control," in *Second International Conference on Innovative Computing, Information and Control, ICICIC*, Kumamoto, Japan, 2008.

[112] Z. Iwai and I. Mizumoto, "Robust and simple adaptive control systems," *International Journal of Control,* vol. 55, pp. 1453-1470, 1992.

[113] B. K. Nguyen and K. K. Ahn, "Feedforward control of shape memory alloy actuators using fuzzy-based inverse Preisach model," *IEEE Transactions on Control Systems Technology,* vol. 17, pp. 434-441, 2009.

[114] G. Song, *et al.*, "Active position control of a shape memory alloy wire actuated composite beam," *Smart Materials and Structures,* vol. 9, pp. 711-716, 2000.

[115] G. Song, *et al.*, "Precision tracking control of shape memory alloy actuators using neural networks and a sliding-mode based robust controller," *Smart Materials and Structures,* vol. 12, pp. 223-231, 2003.

[116] J. V. Tu, "Advantages and disadvantages of using artificial neural networks versus logistic regression for predicting medical outcomes," *Journal of Clinical Epidemiology,* vol. 49, pp. 1225-1231, 1996.

[117] J. P. Briggs and J. P. Ostrowski, "Experimental feedforward and feedback control of a one-dimensional SMA composite," *Smart Materials and Structures,* vol. 11, pp. 9-23, 2002.

[118] S. Szykowny and M. H. Elahinia, "Heat transfer analysis of shape memory alloy actuators," Chicago, IL, United States, 2006, p. 8.

[119] A. Kumagai, *et al.*, "Neuro-fuzzy model based feedback controller for Shape Memory Alloy actuators," *Proceedings of SPIE - The International Society for Optical Engineering,* vol. 3984, pp. 291-299, 2000.

[120] P. H. Thakur, *et al.*, "Multidigit Movement Synergies of the Human Hand in an Unconstrained Haptic Exploration Task," *J. Neurosci.,* vol. 28, pp. 1271-1281, 2008.

[121] C. L. Taylor and R. J. Schwarz, "The anatomy and mechanics of the human hand," *Artificial limbs,* vol. 2, pp. 35, 22-35, 22, 1955.

[122] D. J. Cunningham, *Cunningham's Textbook of Anatomy*, 12th ed., 1981.

[123] N. Brook*, et al.*, "A biomechanical model of index finger dynamics," *Medical Engineering and Physics,* vol. 17, pp. 54-63, 1995.

[124] A. Nimbarte*, et al.*, "Finger joint motion generated by individual extrinsic muscles: A cadaveric study," *Journal of Orthopaedic Surgery and Research,* vol. 3, pp. 27-27, 2008.

[125] J. A. Clavero*, et al.*, "Extensor Mechanism of the Fingers: MR Imaging-Anatomic Correlation," *RadioGraphics,* vol. 23, pp. 593-593, 2003.

[126] J. M. Landsmeer and C. Long, "The mechanism of finger control, based on electromyograms and location analysis," *Acta Anat (Basel),* vol. 60, pp. 330-347, 1965.

[127] H. P. von Schroeder and M. J. Botte, "Anatomy of the extensor tendons of the fingers: variations and multiplicity," *J Hand Surg [Am],* vol. 20, pp. 27-34, 1995.

[128] C. L. Mackenzie and T. Iberall, *The Grasping Hand*: Elsevier, 1994.

[129] J. R. Napier, "The prehensile movements of the human hand," *Journal of Bone and Joint Surgery - British Volume,* vol. 38-B, pp. 902-913, 1956.

[130] G. Schlesinger, "Der Mechanische Aufbau der kunstlischen Glieder," *Ersatzglieder und Arbeitshilfen fur Kriegsbeschadigte und Unfallverletzte,* vol. 21, 1919.

[131] Y.-K. Kong and B. D. Lowe, "Optimal cylindrical handle diameter for grip force tasks," *International Journal of Industrial Ergonomics,* vol. 35, pp. 495-507, 2005.

[132] J. W. Lee and K. Kim, "Measurement of finger joint angles and maximum finger forces during cylinder grip activity," *Journal of Biomedical Engineering,* vol. 13, pp. 152-162, 1991.

[133] H. Kinoshita*, et al.*, "Contributions and co-ordination of individual fingers in multiple finger prehension," *Ergonomics,* vol. 38, p. 1212, 1995.

[134] H. Kinoshita*, et al.*, "Grip posture and forces during holding cylindrical objects with circular grips," *Ergonomics,* vol. 39, pp. 1163-1176, 1996.

[135] K. J. De Laurentis*, et al.*, "Optimal design of shape memory alloy wire bundle actuators," in *IEEE International Conference on Robotics and Automation, ICRA '02.* , 2002, pp. 2363-2368.

[136] F. Daerden and D. Lefeber, *Pneumatic artificial muscles: Actuators for robotics and automation* vol. 47. Brussels, Belgium: Belgian Society of Mechanical and Environmental Engineering, 2002.

[137] G. Song, *et al.*, "Tracking control of a piezoceramic actuator with hysteresis compensation using inverse Preisach model," *IEEE/ASME Transactions on Mechatronics,* vol. 10, pp. 198-209, 2005.

[138] W. Bolton, *Control Engineering*, 2nd ed.: Harlow : Longman, 1998.

[139] P. L. Potapov and E. P. D. Silva, "Time Response of Shape Memory Alloy Actuators," *Journal of Intelligent Material Systems and Structures,* vol. 11, pp. 125-134, 2/1 2000.

[140] A. Bhattacharyya, *et al.*, "On the role of thermoelectric heat transfer in the design of SMA actuators: theoretical modeling and experiment," *Smart Materials and Structures,* vol. 4, pp. 252-263, 1995.

[141] F. Schiedeck and S. Mojrzisch, "Design of a robust control strategy for the heating power of shape memory alloy actuators at full contraction based on electric resistance feedback," *Smart Materials and Structures,* vol. 20, 2011.

[142] M. G. Faulkner, *et al.*, "Experimental determination of thermal and electrical properties of Ni-Ti shape memory wires," *Smart Materials and Structures,* vol. 9, pp. 632-639, 2000.

[143] M. Elahinia, "Effect of System Dynamics on Shape Memory Alloy Behaviour and Control," PhD Thesis, Virginia Tech, Blacksburg, VA, 2004.

[144] Y. A. Cengel, *Heat and Mass Transfer*, 3rd ed., 2006.

[145] B. Scrosati, "Recent advances in lithium ion battery materials," *Electrochimica Acta,* vol. 45, pp. 2461-2466, 2000.

[146] M. B. I. Raez*, et al.*, "Techniques of EMG signal analysis: detection, processing, classification and applications," *Biological Proceedings Online,* vol. 8, pp. 11-35, 2006.

[147] E. A. Clancy and N. Hogan, "Estimation of joint torque from the surface EMG," in *Proceedings of the 13th Annual International Conference of the IEEE Engineering in Medicine and Biology Society, October 31 - November 3*, Orlando, FL, USA, 1991, pp. 877-878.

[148] H. Wang*, et al.*, "EMG-based design of mechanical hand prosthesis," *Dongbei Daxue Xuebao/Journal of Northeastern University,* vol. 27, pp. 1018-1021, 2006.

[149] A. O'Dwyer, *Handbook of PI and PID Controller Tuning Rules (3rd Edition)*: Imperial College Press, 2009.

[150] A. Wallen, "Tools for Autonomous Process Control," PhD Thesis, Lund Institute of Technology, 2000.

[151] W. Tan*, et al.*, "Comparison of some well-known PID tuning formulas," *Computers and Chemical Engineering,* vol. 30, pp. 1416-1423, 2006.

[152] F.-B. Zhang, *et al.*, "Optimal ITAE tuning formulae for parameters of PID controller," *Dongbei Daxue Xuebao/Journal of Northeastern University,* vol. 26, pp. 755-758, 2005.

[153] C. Pfeiffer, *et al.*, "Shape memory alloy actuated robot prostheses: initial experiments," *Proceedings - IEEE International Conference on Robotics and Automation,* vol. 3, pp. 2385-2391, 1999.

[154] M. W. Spong, *et al.*, *Robot Modeling and Control*: Wiley, 2005.

[155] R. Manseur. *Denavit-Hartenberg Parameters*. Available: http://uwf.edu/ria/robotics/robotdraw/DH_parm.htm (Accessed 9th April, 2009)

APPENDIX I - Key Nitinol Technical Properties

Transformation Properties

Transformation Temperature	*-200 to 110°C*
Latent Heat of Transformation	*24.19 kJ/kg*
Transformation Strain (Max)	*8 %*

Physical Properties

Melting Point	*1300°C*
Density	*6450 kg/m^3*
Thermal Conductivity	
Austenite	*18 W/m.K*
Martensite	*8.6 W/m.K*
Coefficient of Thermal Expansion	
Austenite	*11*10^{-6}/°C*
Martensite	*6.6*10^{-6}/°C*
Heat Capacity	
Austenite	*1273 J/kg.K*
Martensite	*969 J/kg.K*

Electrical & Magnetic Properties

Resistivity	
Austenite	*≈100 μΩ.cm*
Martensite	*≈80 μΩ.cm*
Magnetic Permeability	*<1.002*

Nitinol Mechanical Properties

Young's Modulus	
Austenite	*≈83 GPa*
Martensite	*≈28-41 GPa*
Yield Strength	
Austenite	*195-690 MPa*
Martensite	*70-140 MPa*
Ultimate Tensile Strength	
Fully Annealed	*895 MPa*
Work Hardened	*1900 MPa*

*Key properties taken from Johnson Matthey Medical Online.

APPENDIX II - Adaptive Control Strategy Virtual Instrument

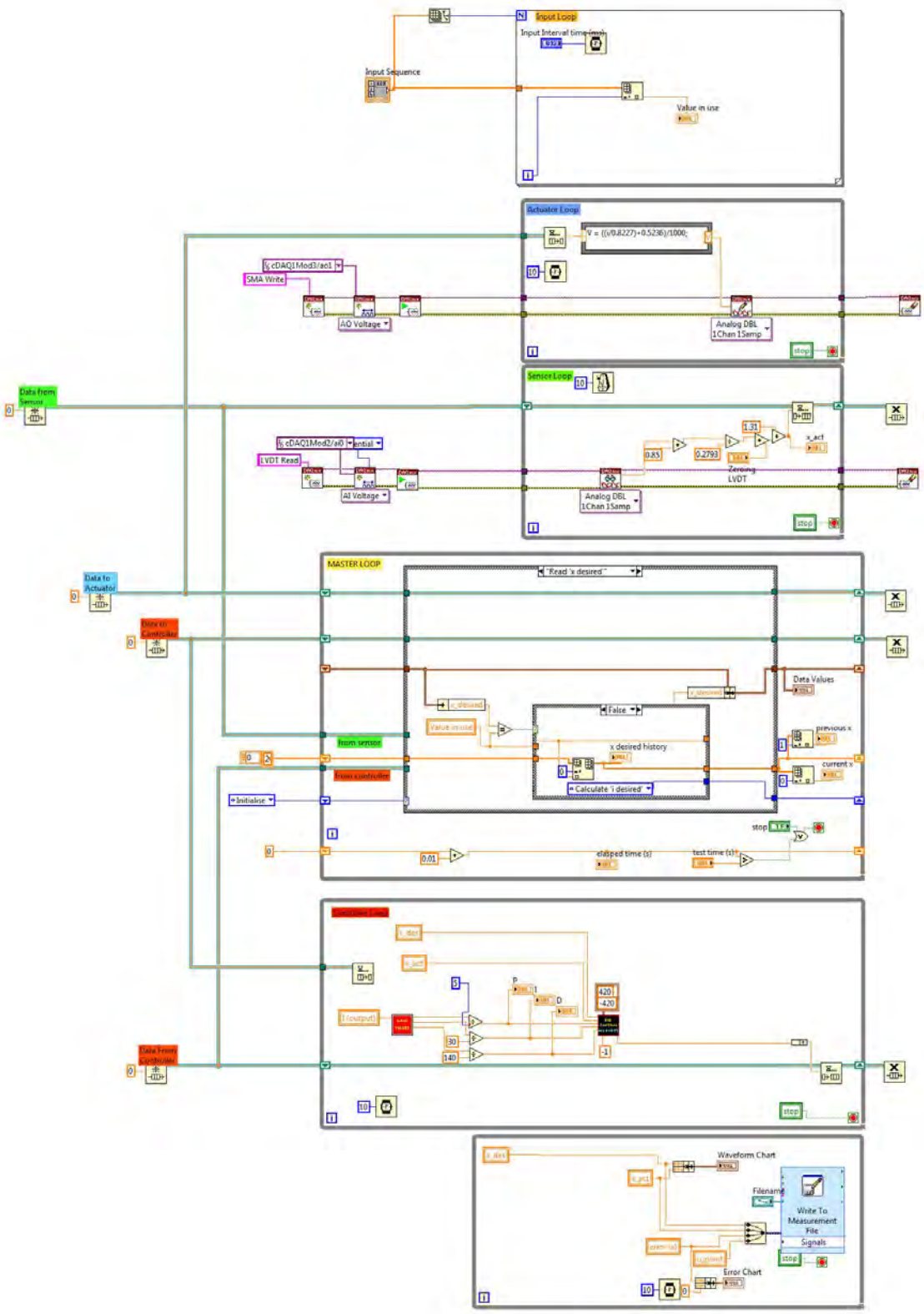

a-PID Controller State Machine Layout

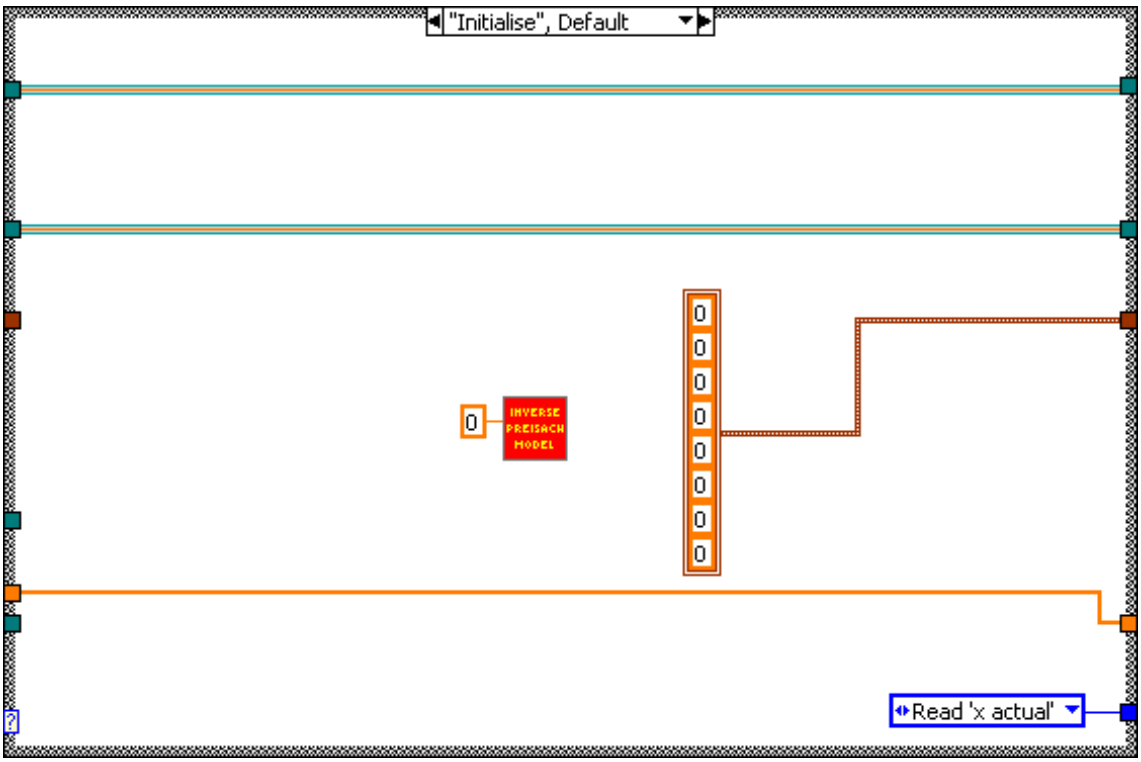

Master Loop - State 1 – Initialising Values

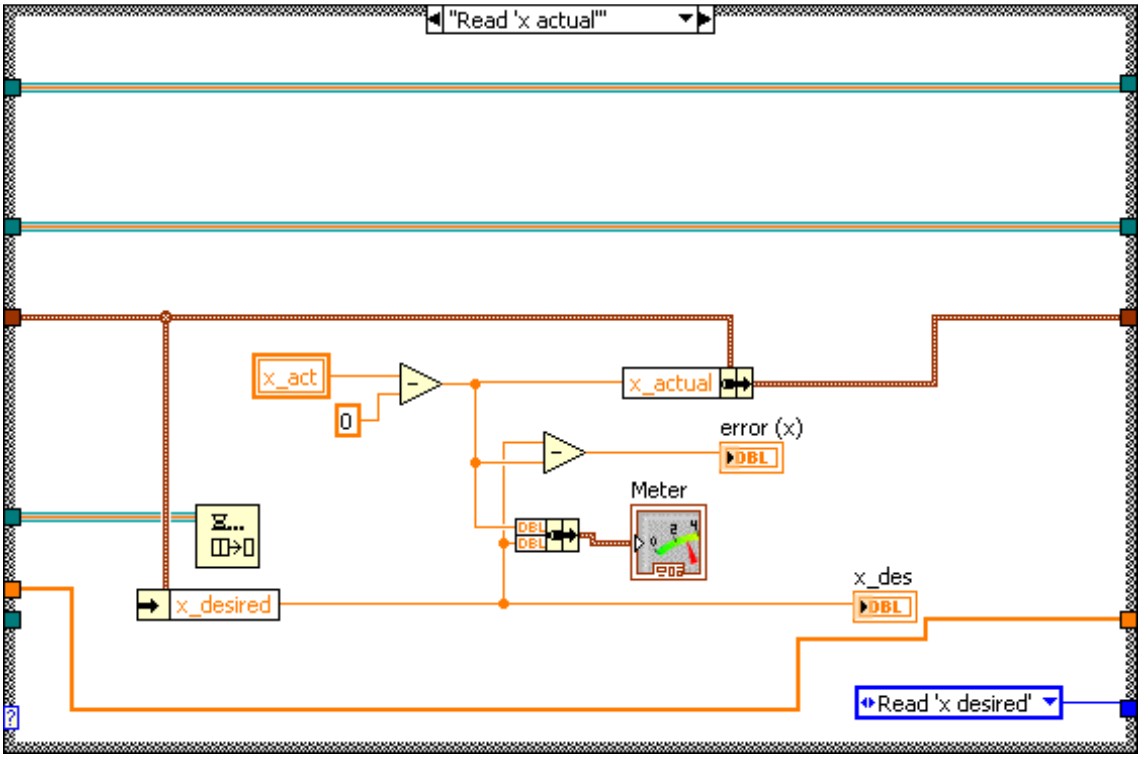

Master Loop State 2 – Reading 'Actual Value' from Feedback Sensors

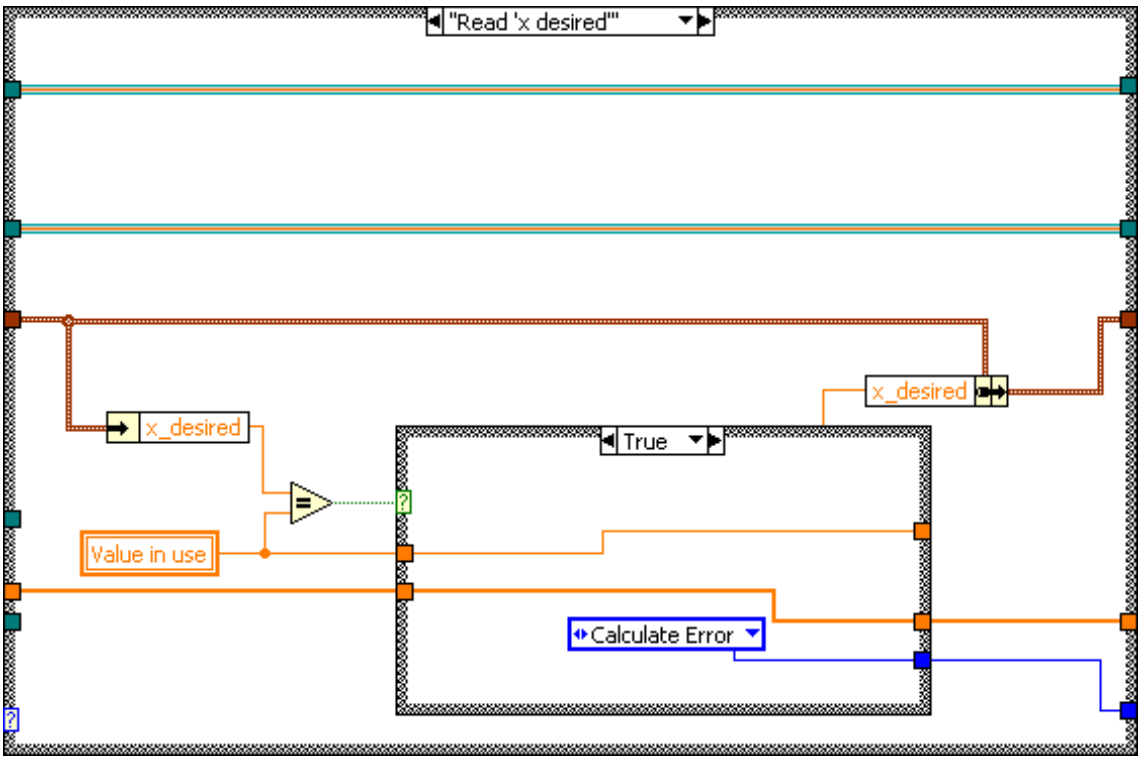

Master Loop - State 3 – Reading Desired Value from Profile Path Data

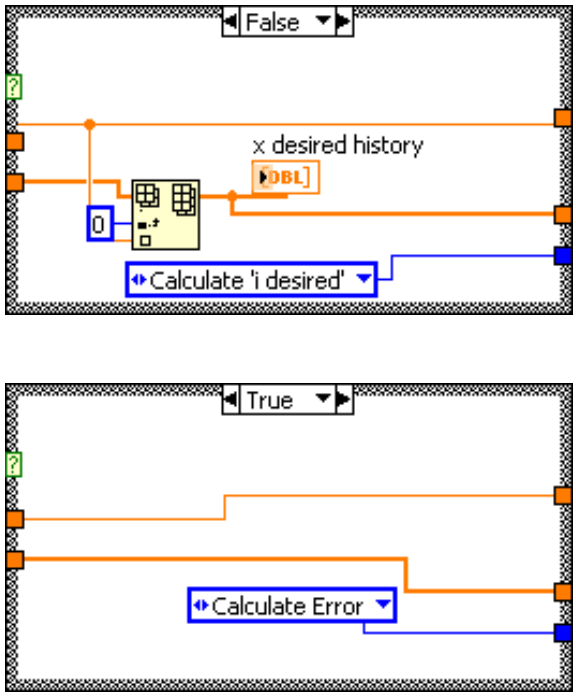

Master Loop - State 3 – Sub-Functions

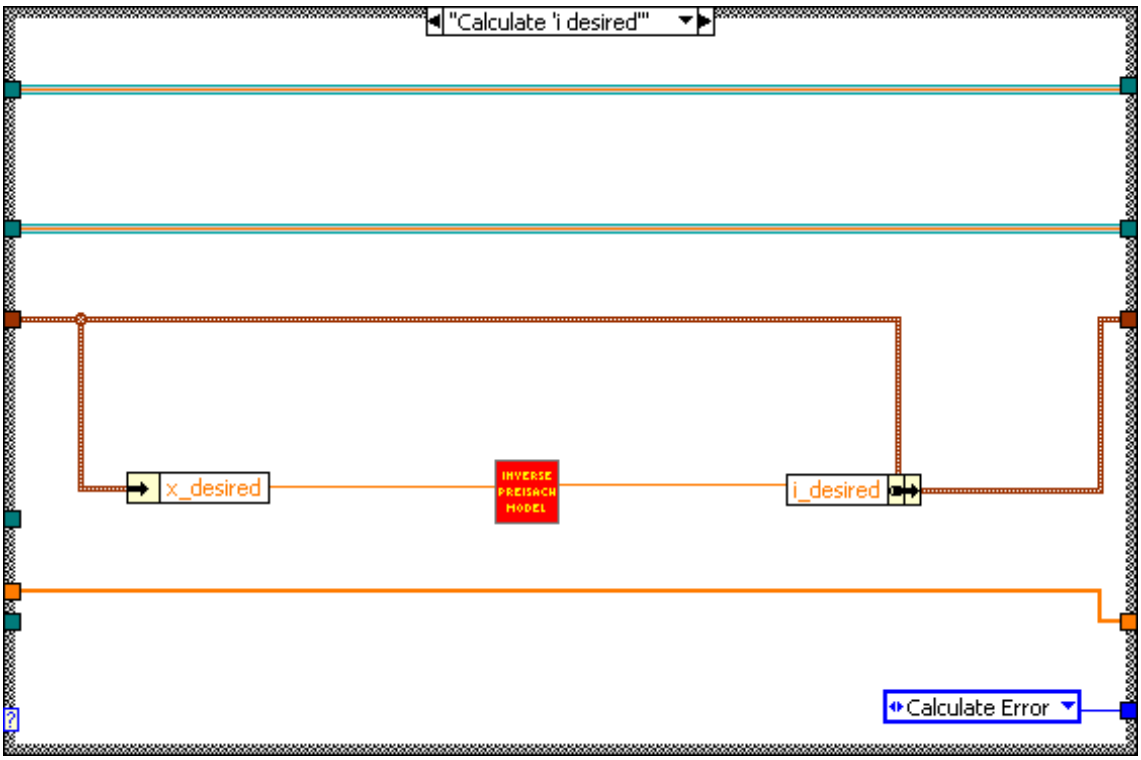

Master Loop - State 4 – Determining the input current from 'Inv. Preisach Model

,

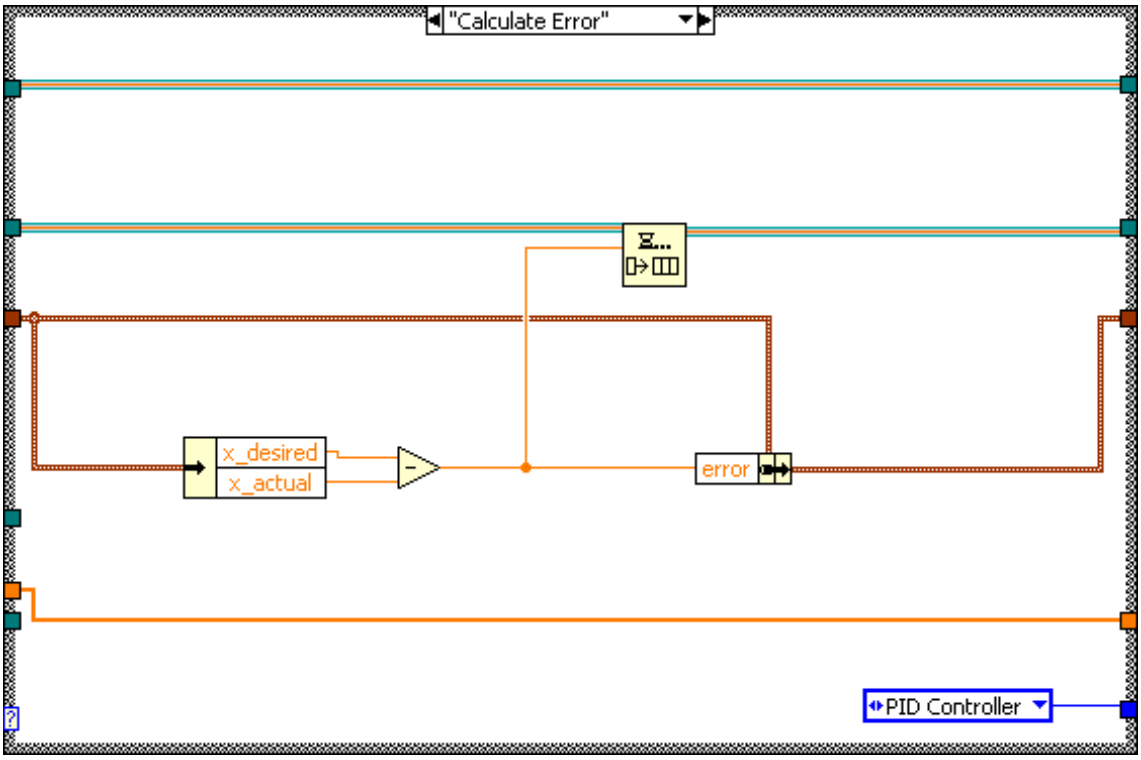

Master Loop - State 5 – Calculating Error between 'Desired' and 'Actual'

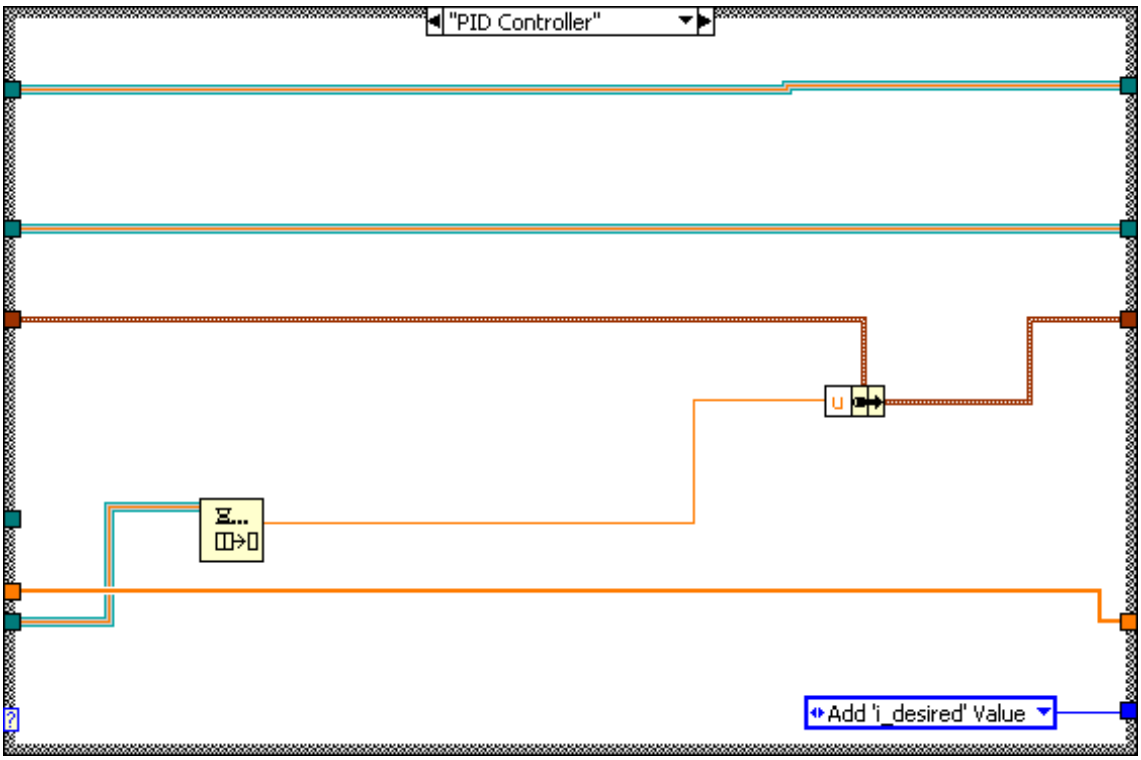

Master Loop - State 6 – Reading a-PID controller value from 'Controller Loop'

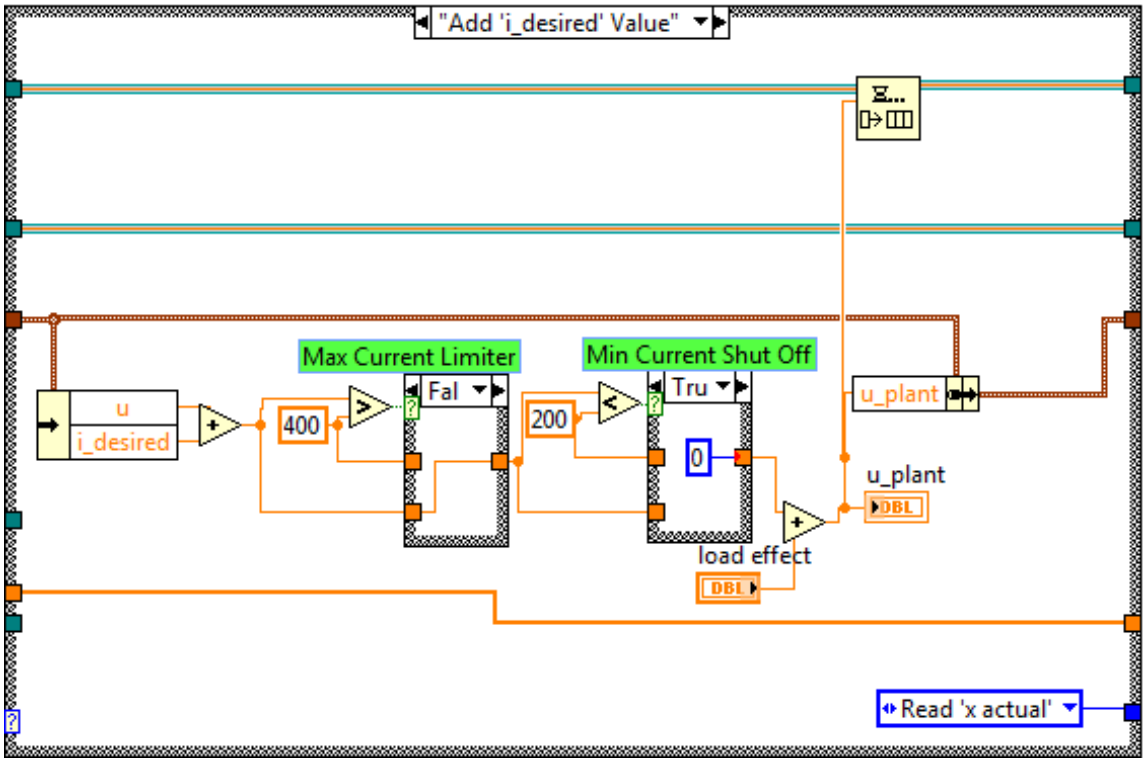

Master Loop - State 7 – Calculating current value output to SMA bundle actuator

APPENDIX III - Inverse Preisach Model Virtual Instrument

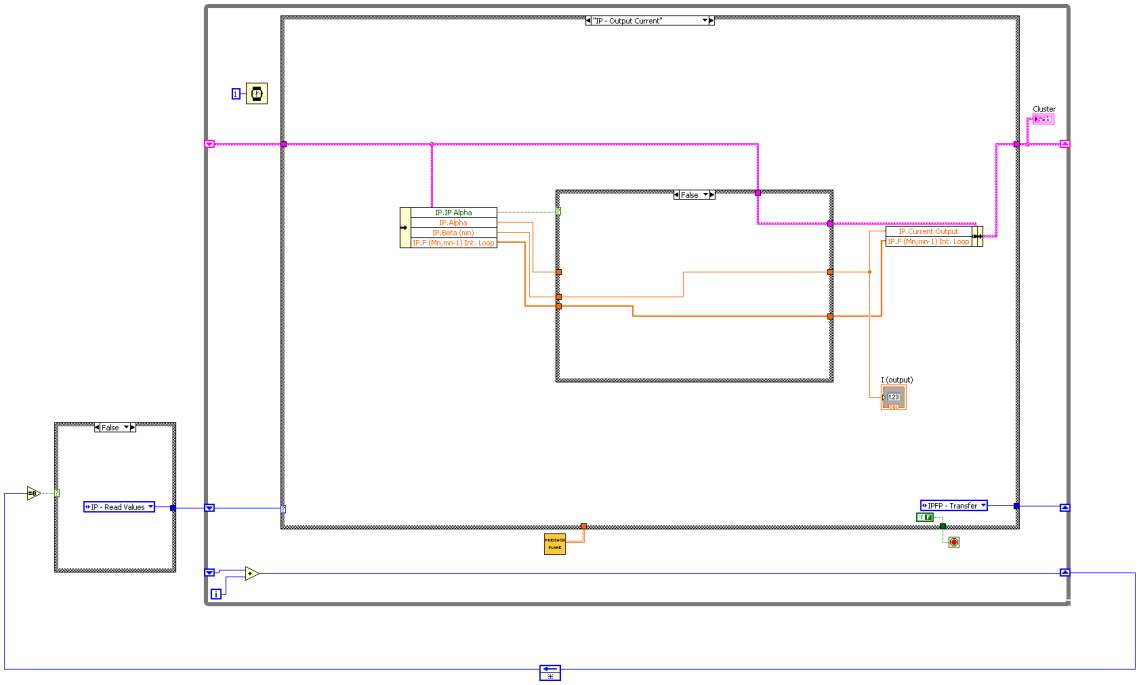

Inverse Preisach Model State Machine Layout

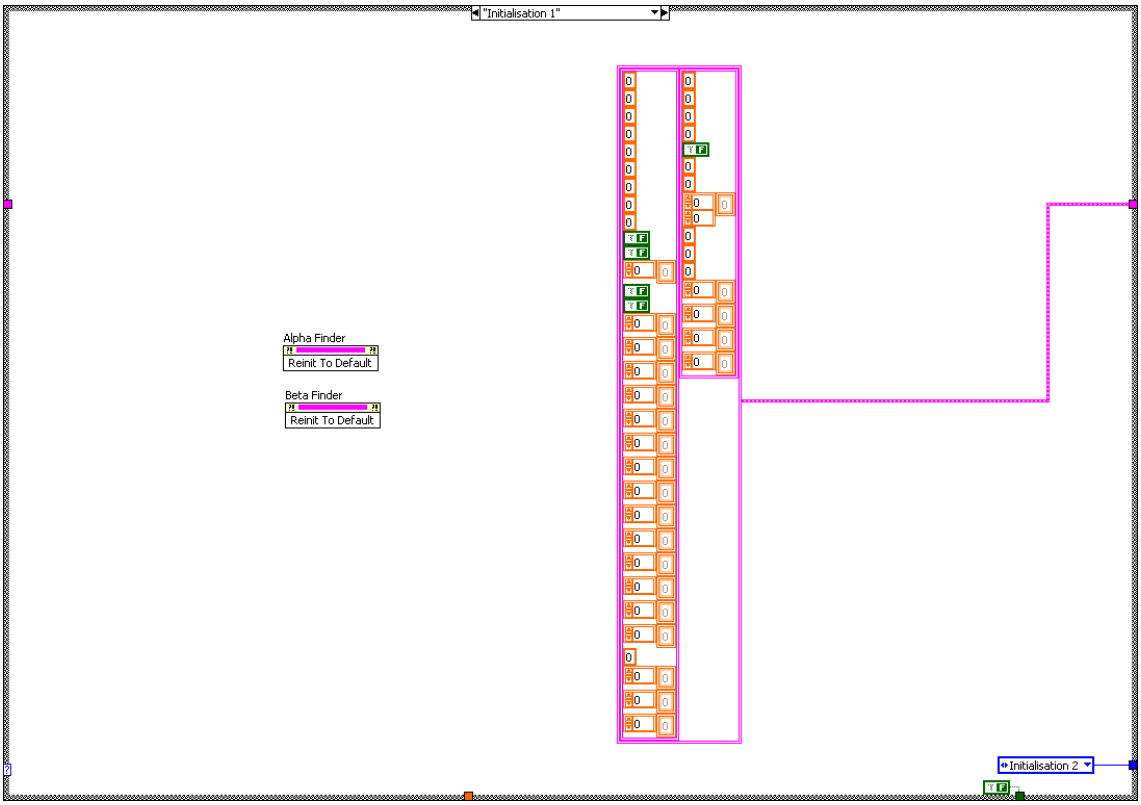

State 1 – Initialisation Part 1

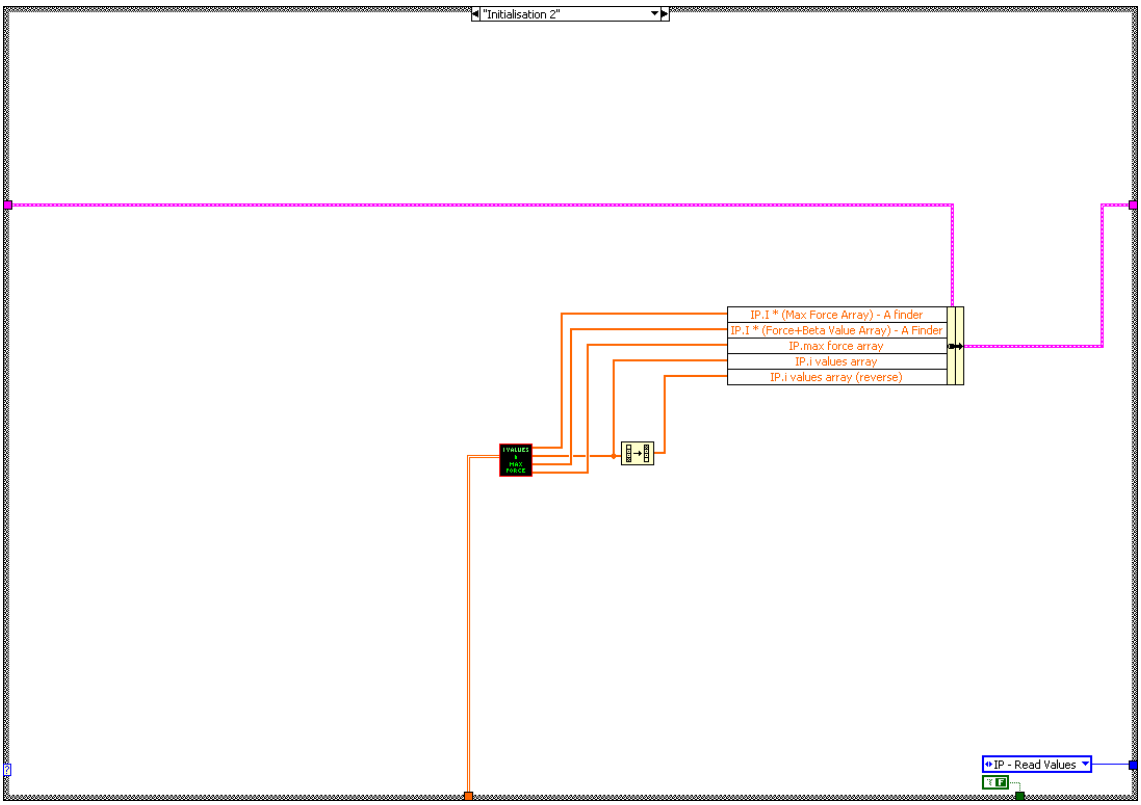

State 2 – Initialisation Part 2

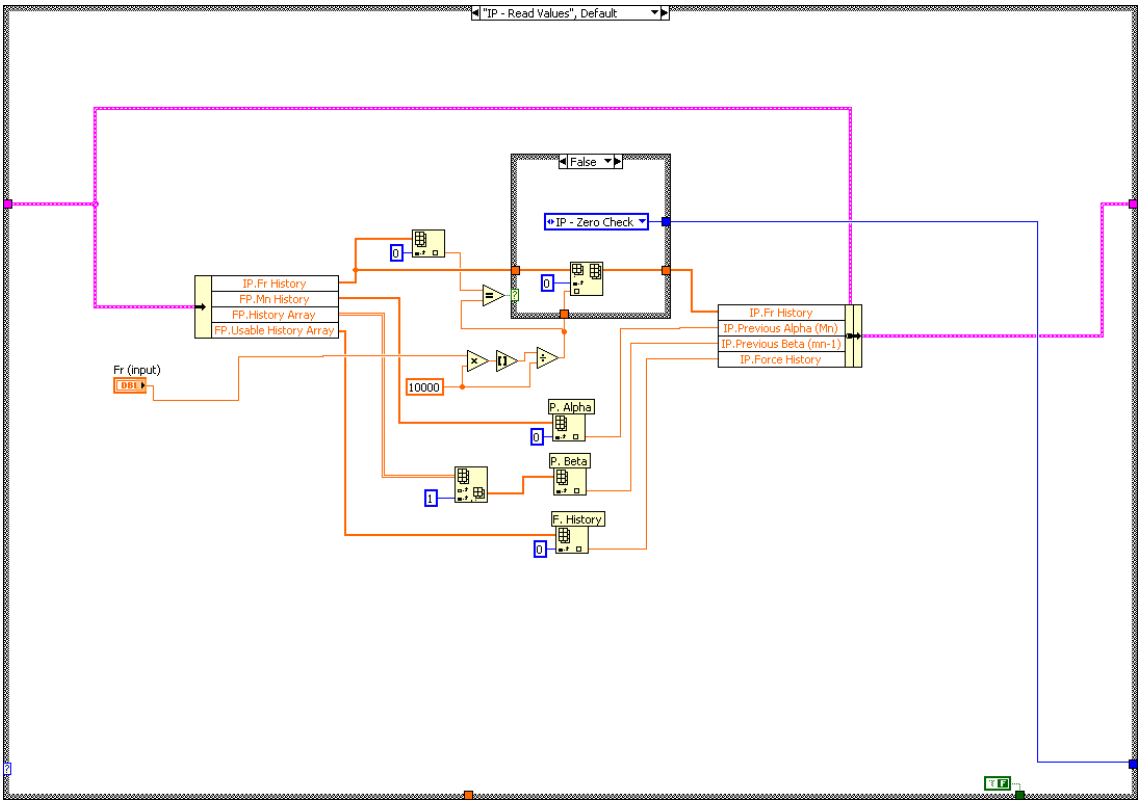

State 3 – Reading Physical Input Values and Feedback Values

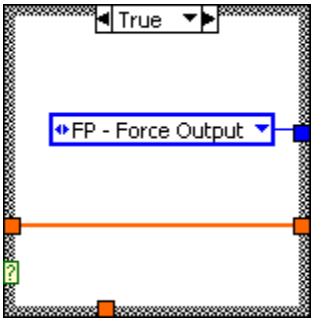

State 3 – Alternate State Sub-Routines

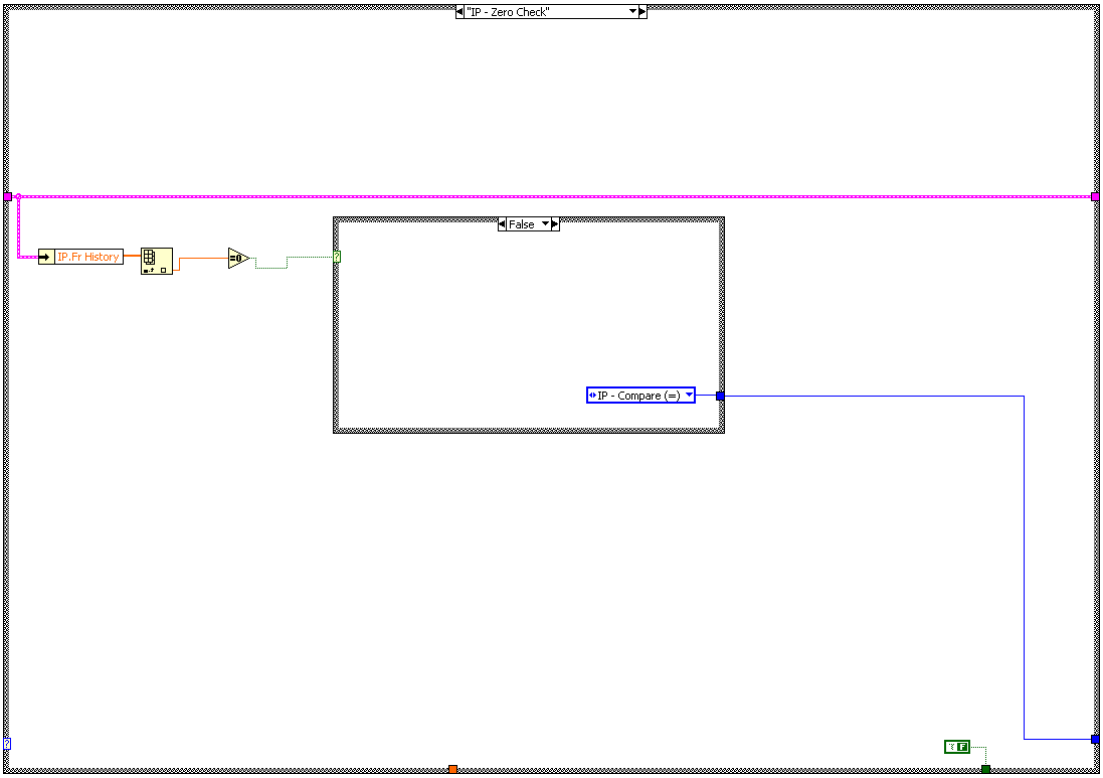

State 4 – Check if Input Value = 0

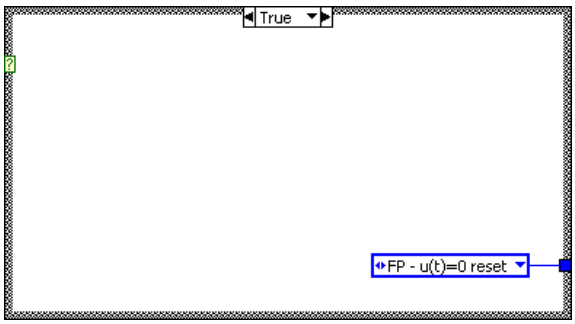

State 4 – Alternate State Sub-Routines

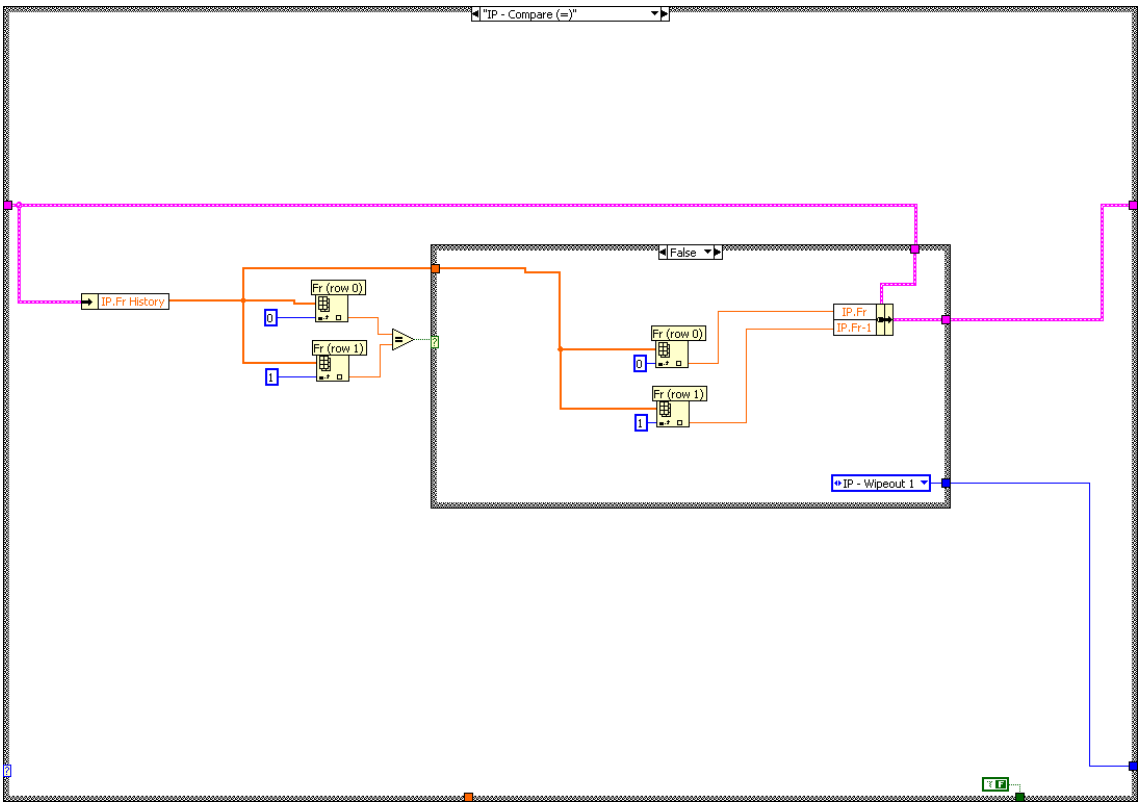

State 5 – Check if Input Value = Previous Input Value

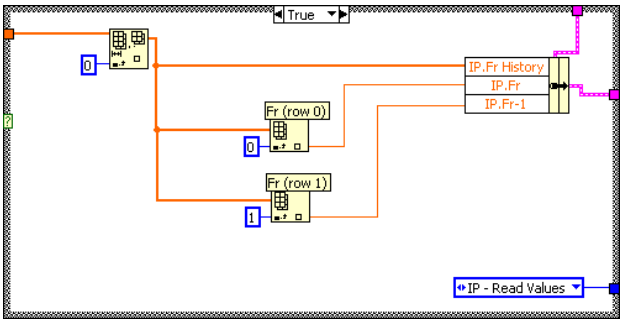

State 5 – Alternate State Sub-Routines

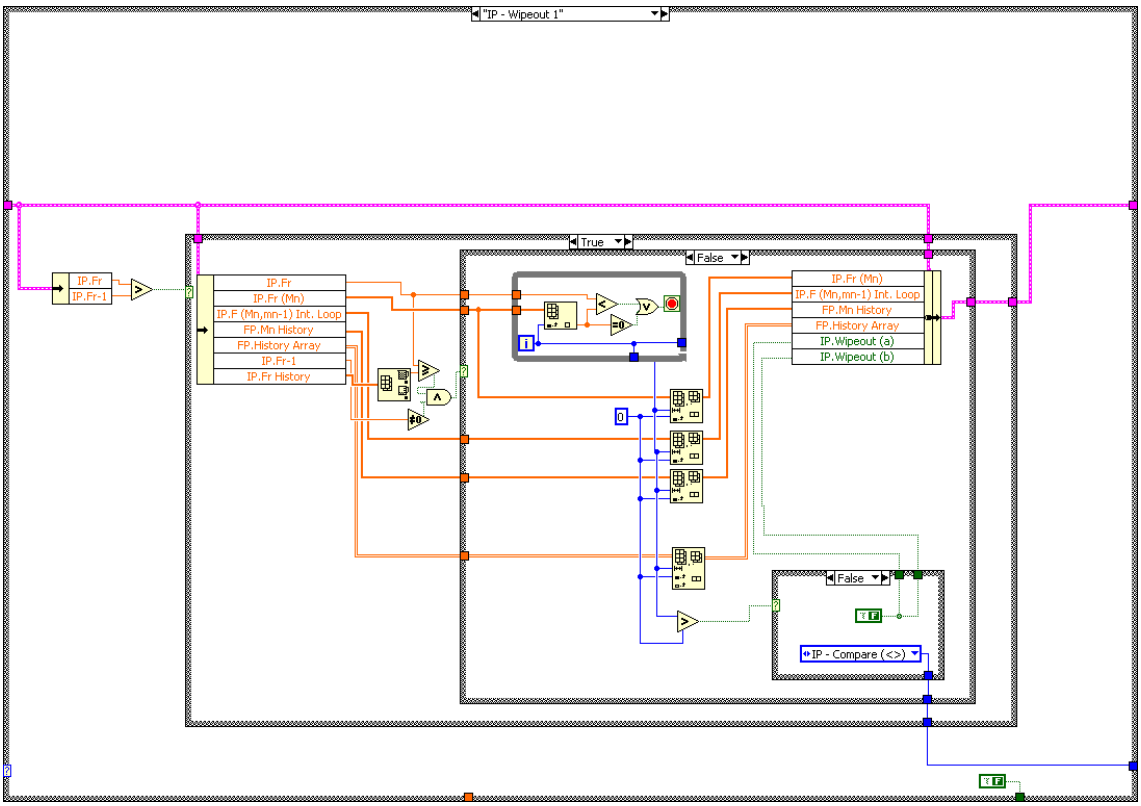

State 6 – Check for 'Wipeout' occurrence against previous alpha values

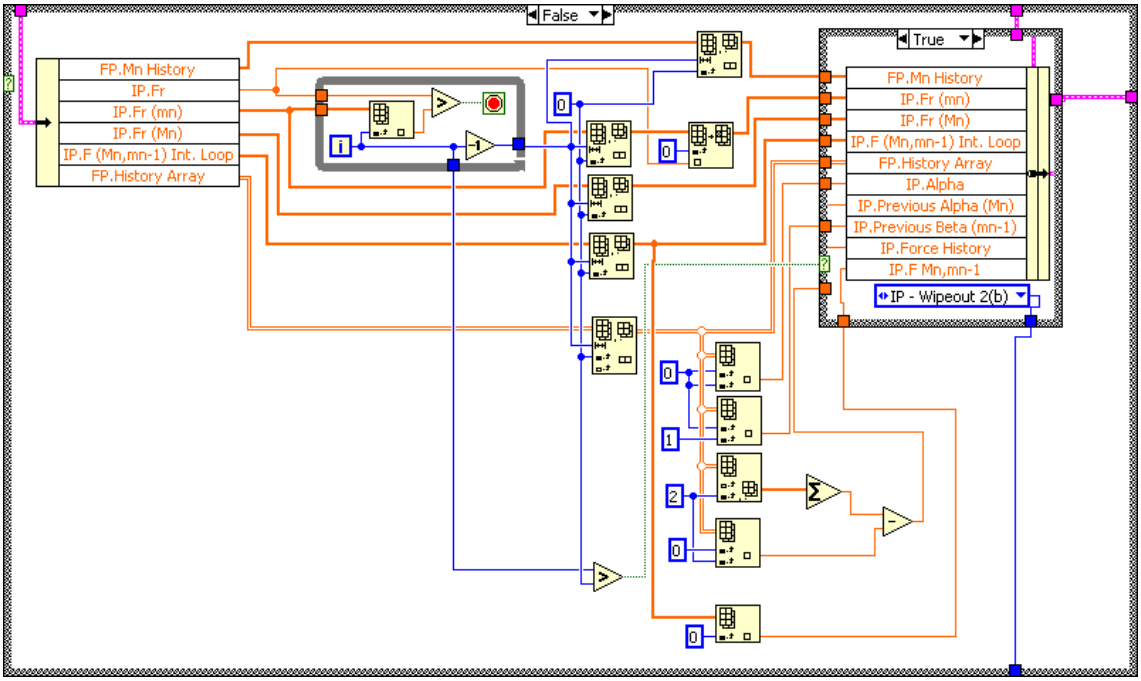

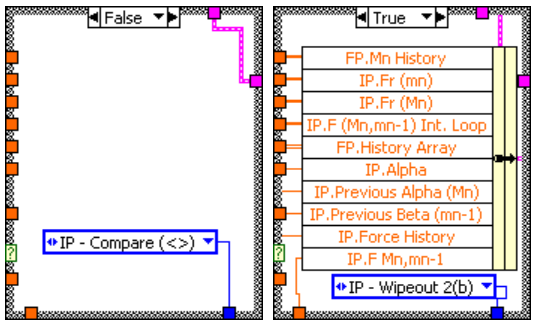
False
True
FP.Mn History
IP.Fr (mn)
IP.Fr (Mn)
IP.F (Mn,mn-1) Int. Loop
FP.History Array
IP.Alpha
IP.Previous Alpha (Mn)
IP.Previous Beta (mn-1)
IP.Force History
IP.F Mn,mn-1
IP - Compare (<>)
IP - Wipeout 2(b)

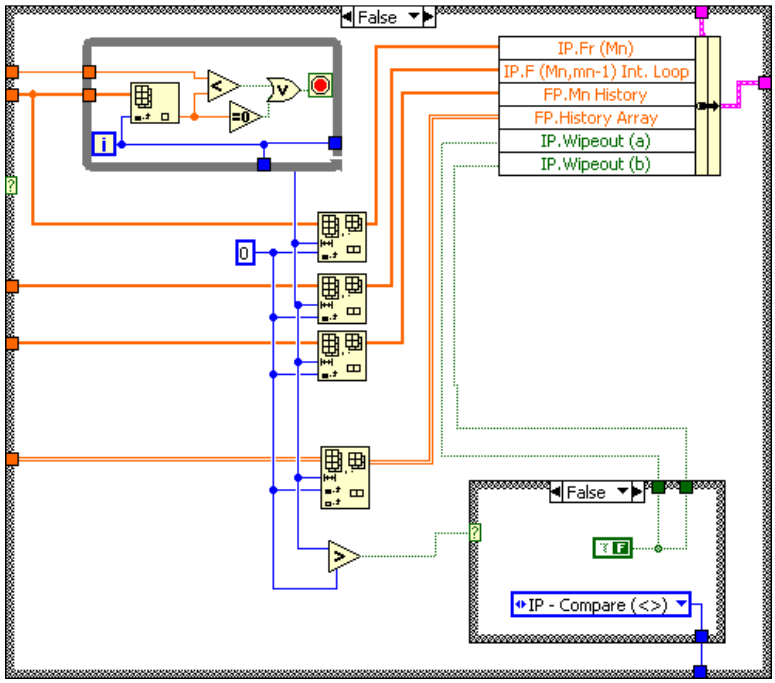
False
IP.Fr (Mn)
IP.F (Mn,mn-1) Int. Loop
FP.Mn History
FP.History Array
IP.Wipeout (a)
IP.Wipeout (b)
i
<
=0
0
>
False
IP - Compare (<>)

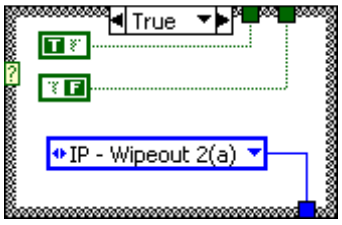
True
IP - Wipeout 2(a)

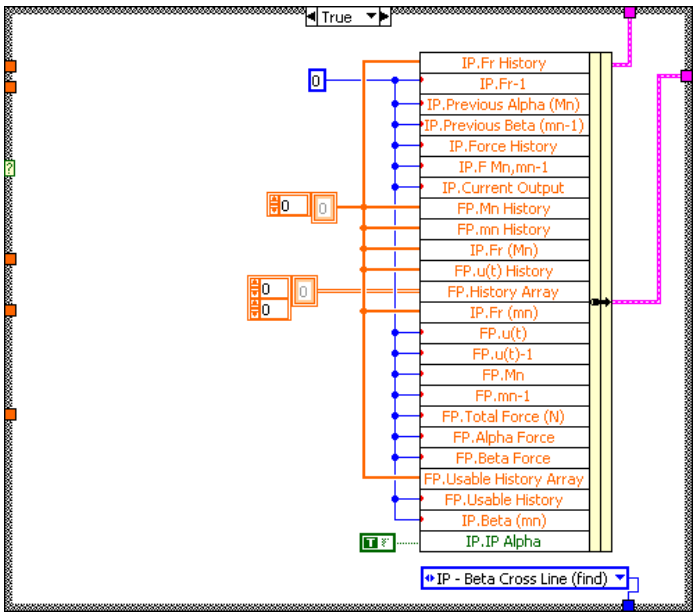

State 6 – Alternate State Sub-Routines

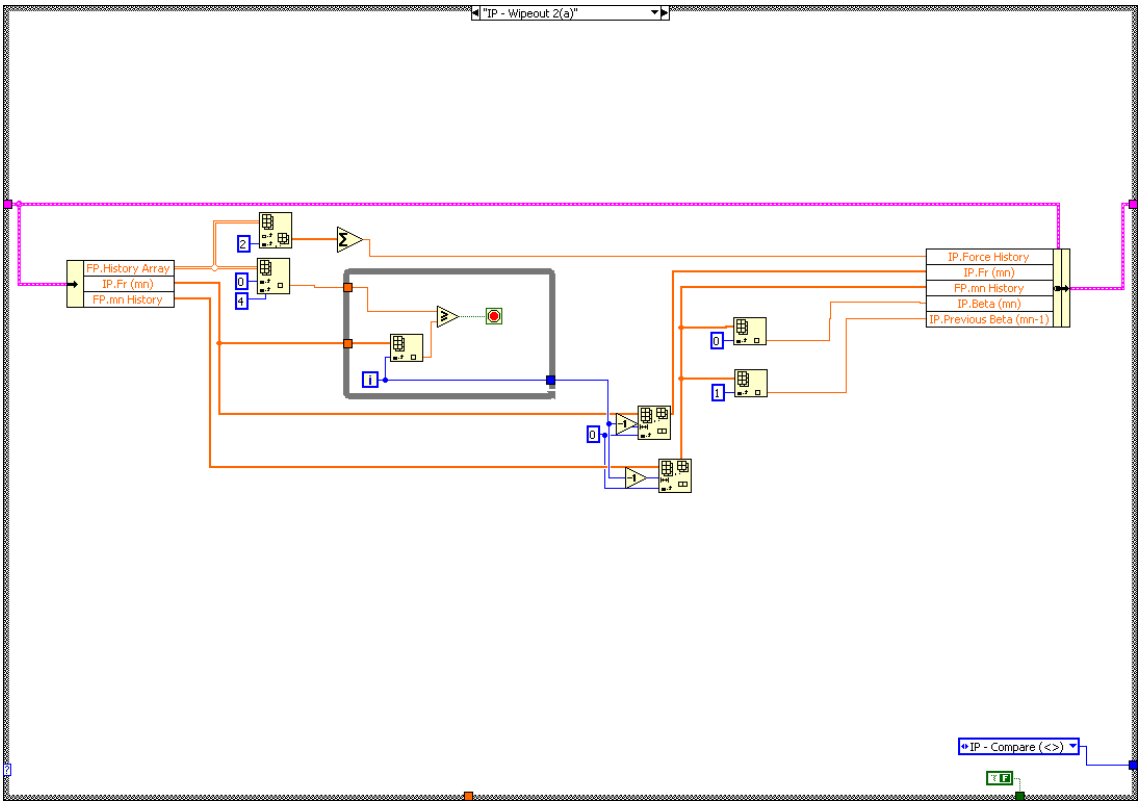

State 7 - Check for 'Wipeout' occurrence against previous beta values part 1

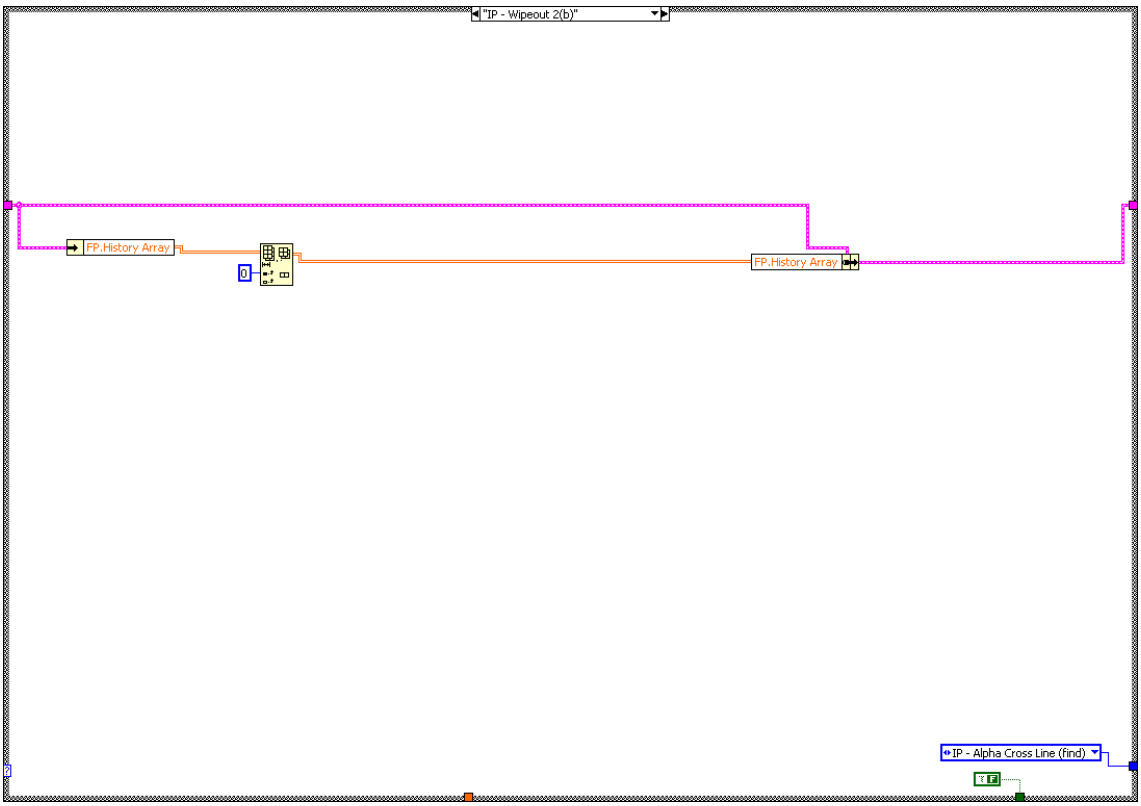

State 8 - Check for 'Wipeout' occurrence against previous beta values part 2

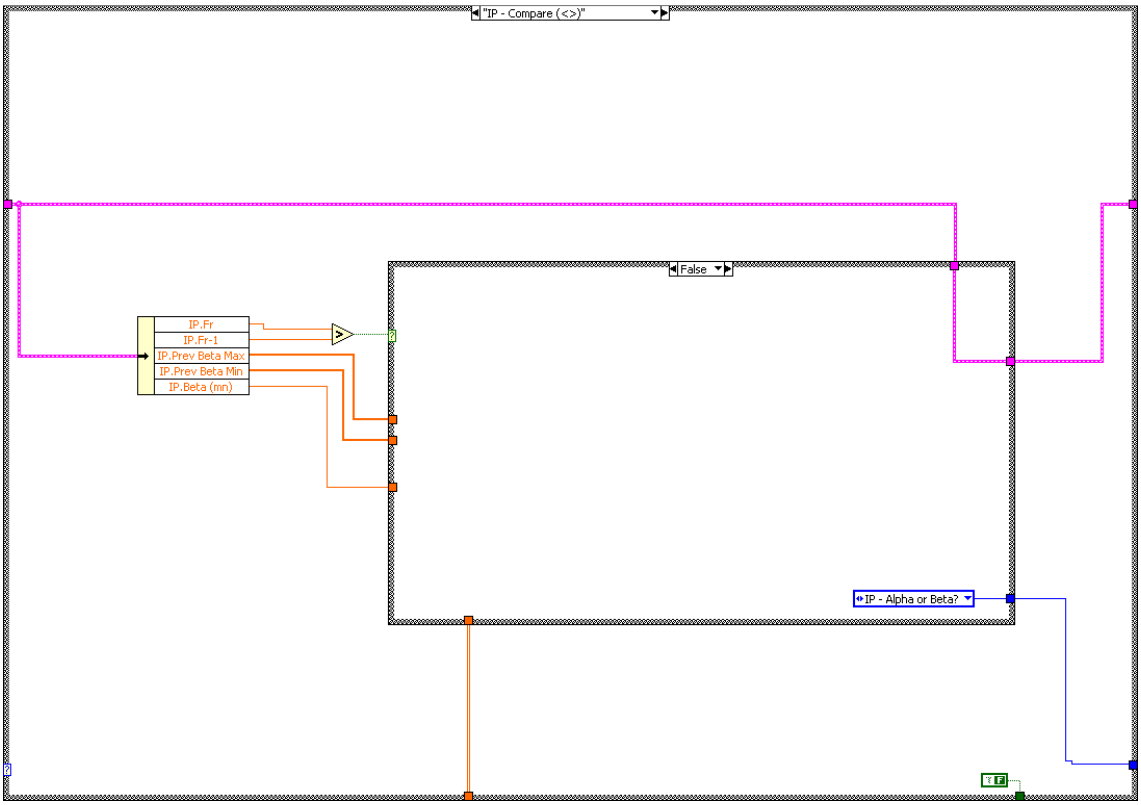

State 9 – Determining if Input is an Alpha or Beta Value

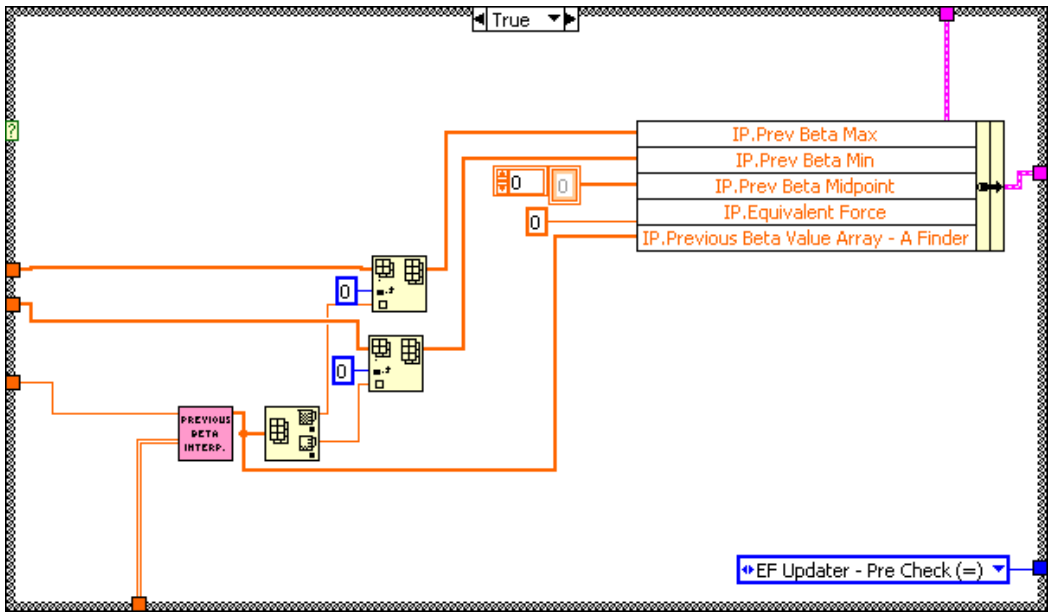

State 9 – Alternate State Sub-Routines

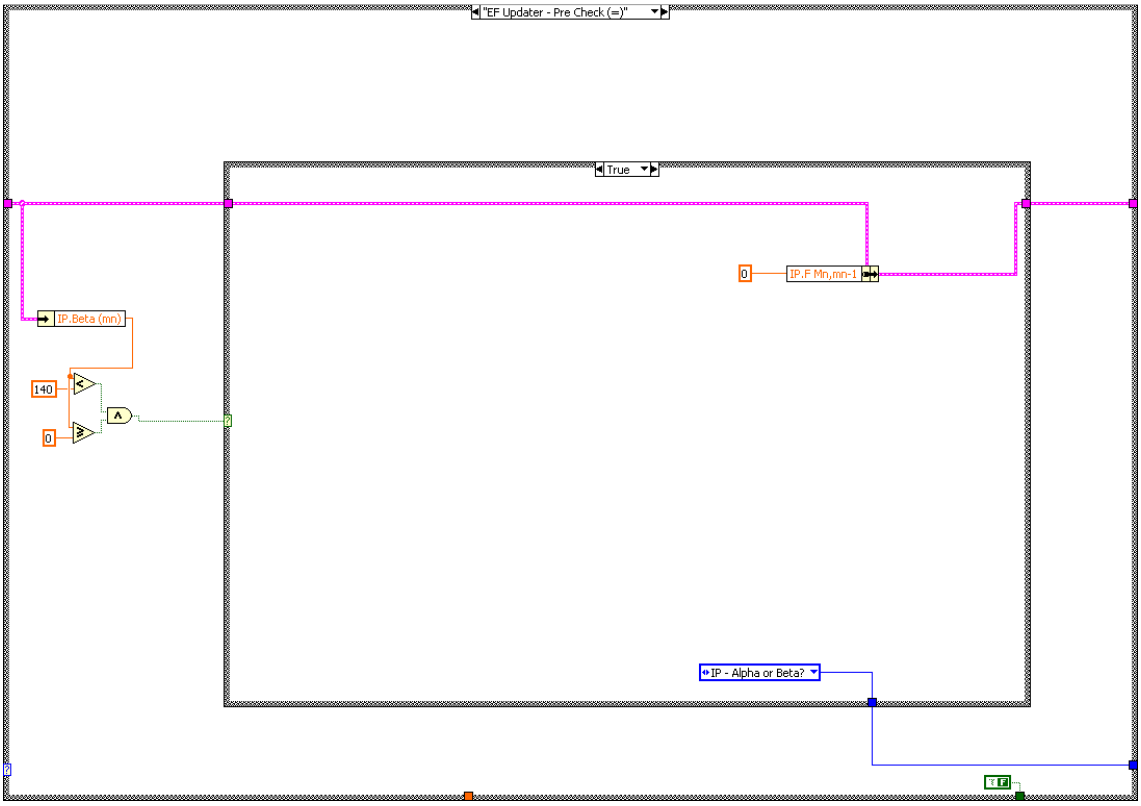

State 10 – Inverse Algorithm – Part 1

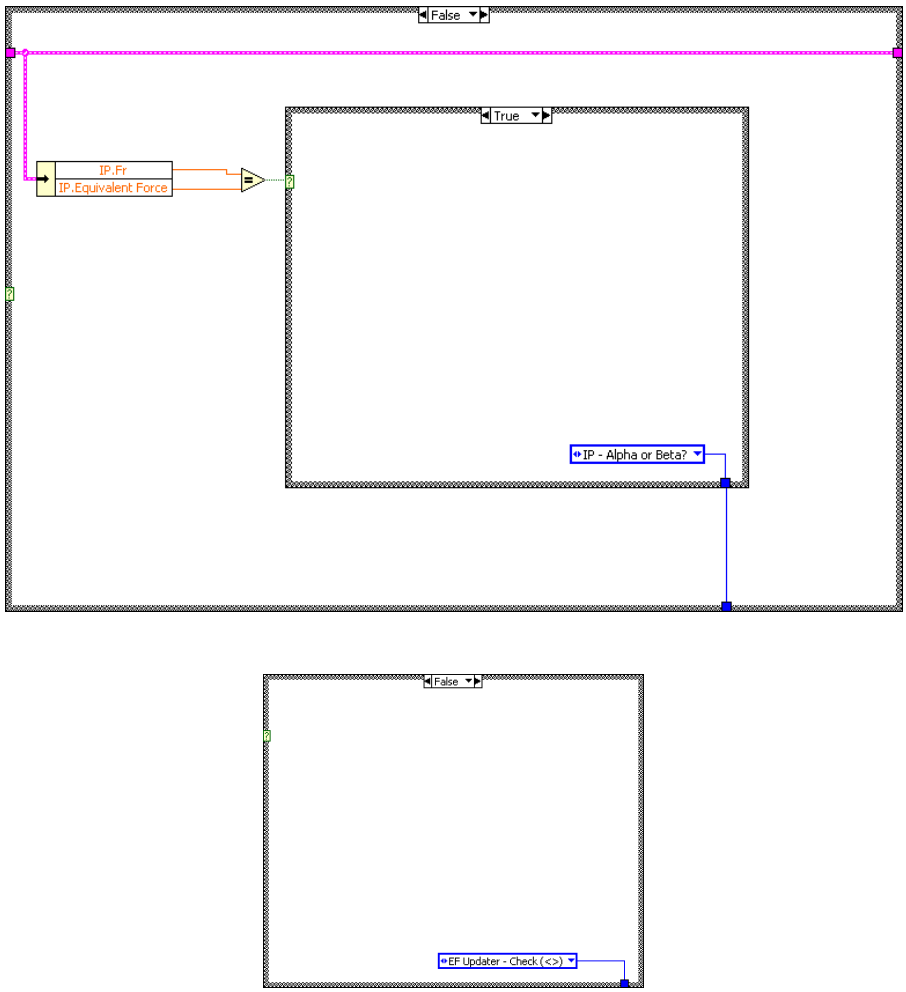

State 10 – Alternate State Sub-Routines

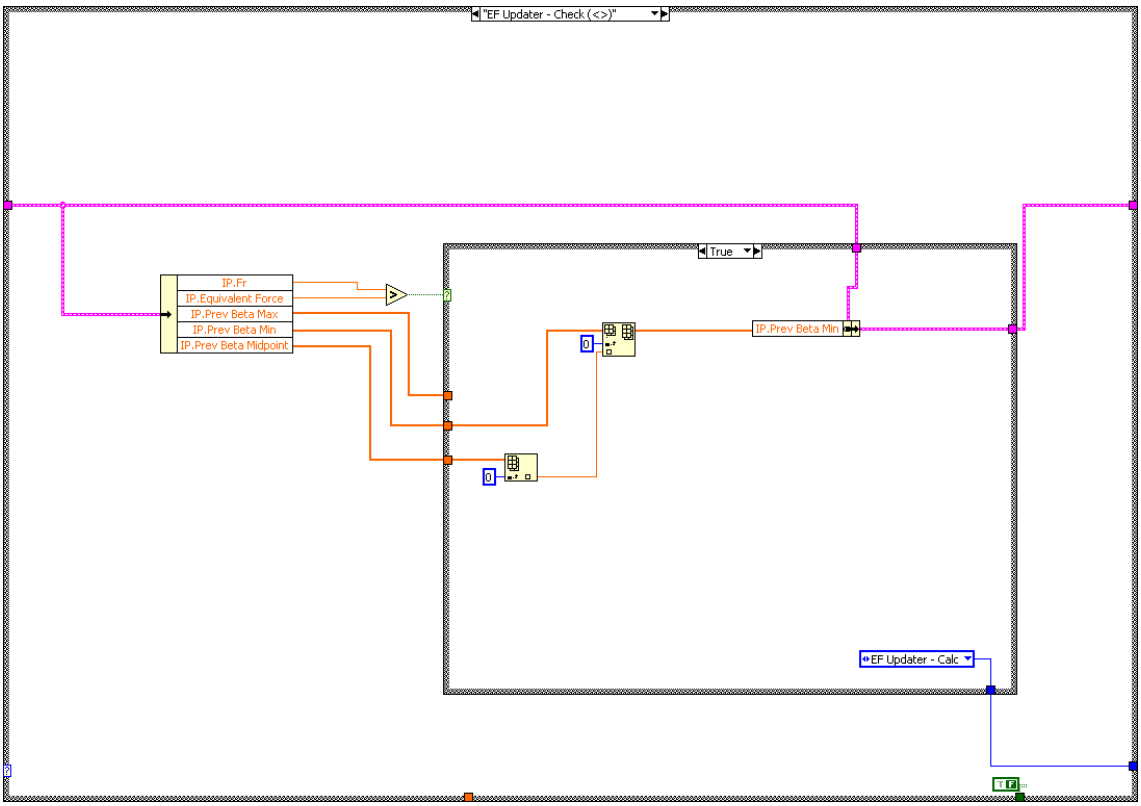

State 11 – Inverse Algorithm Part 2

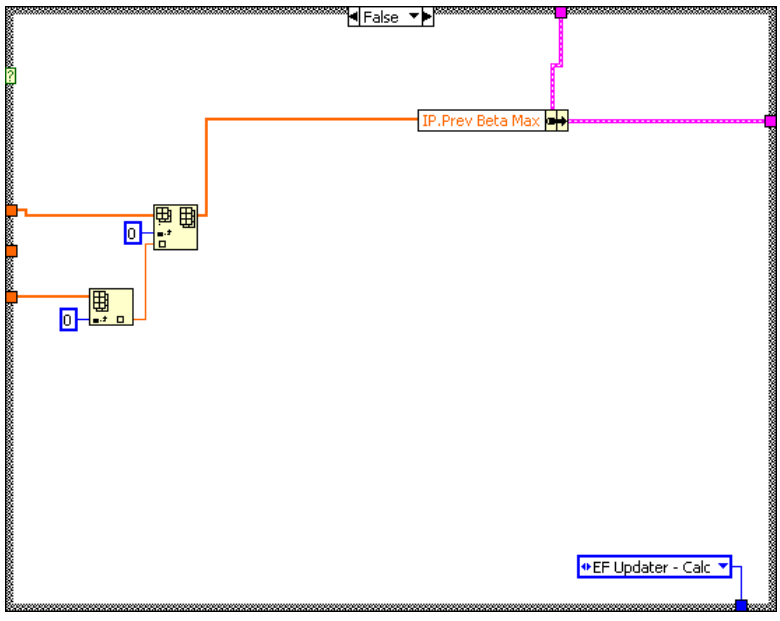

State 11 – Alternate State Sub-Routines

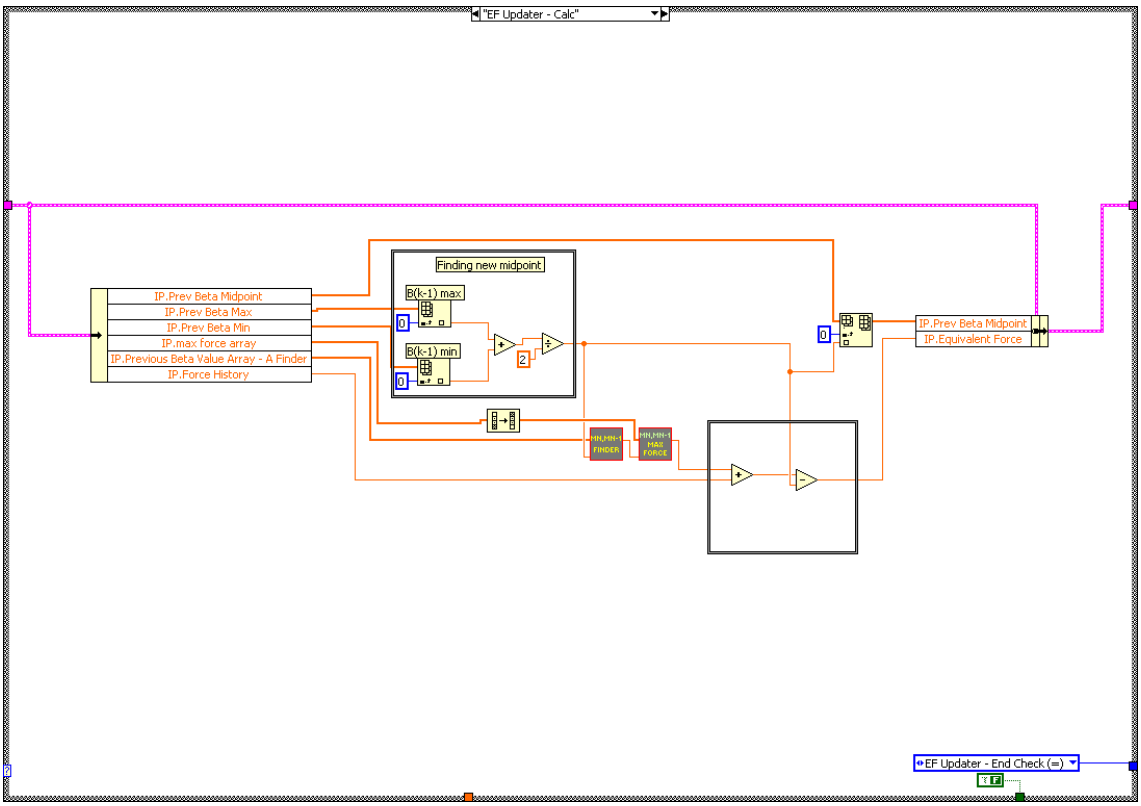

State 12 – Inverse Algorithm Part 3

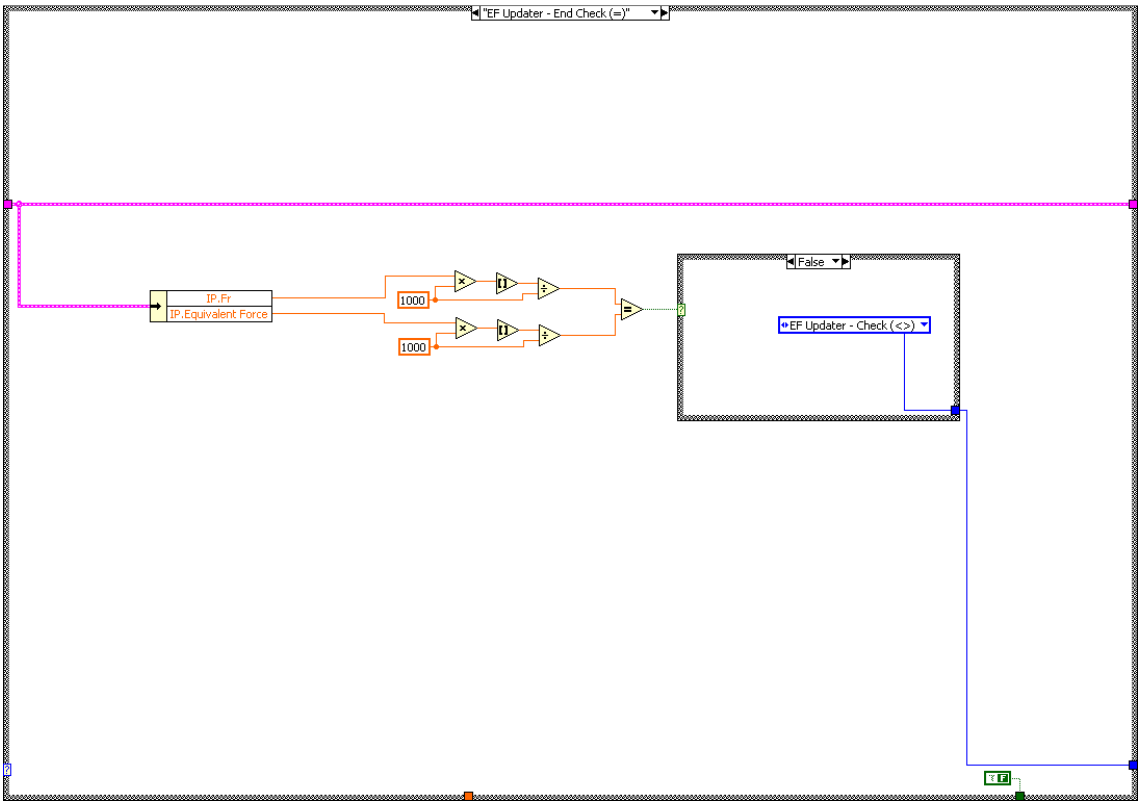

State 13 – Inverse Algorithm Part 4

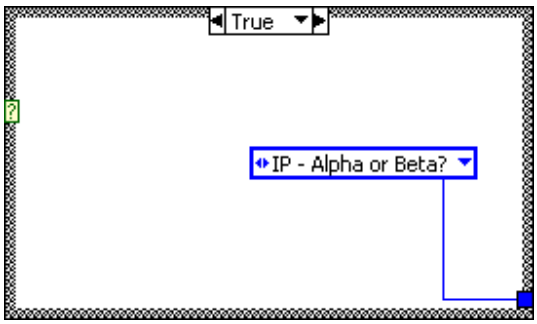

State 13 – Alternate State Sub-Routines

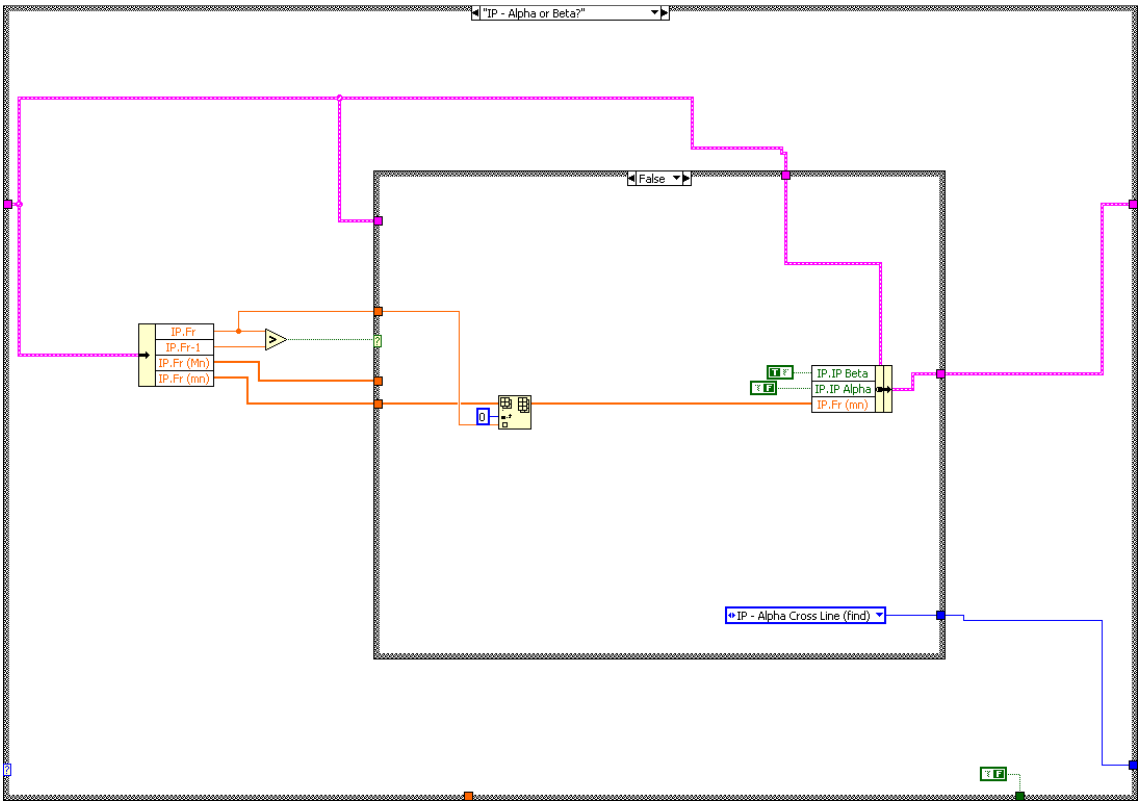

State 14 – Writing M_n and m_n values

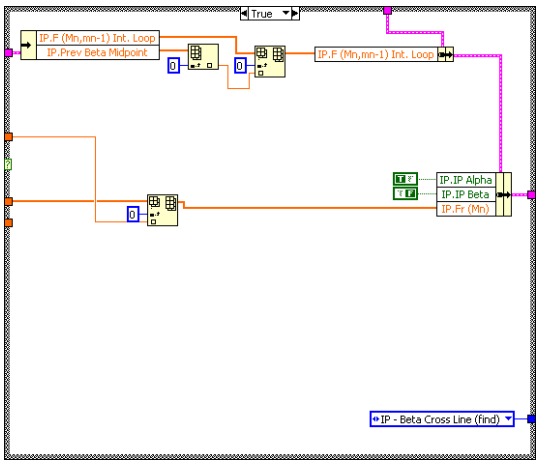

State 14 – Alternate State Sub-Routines

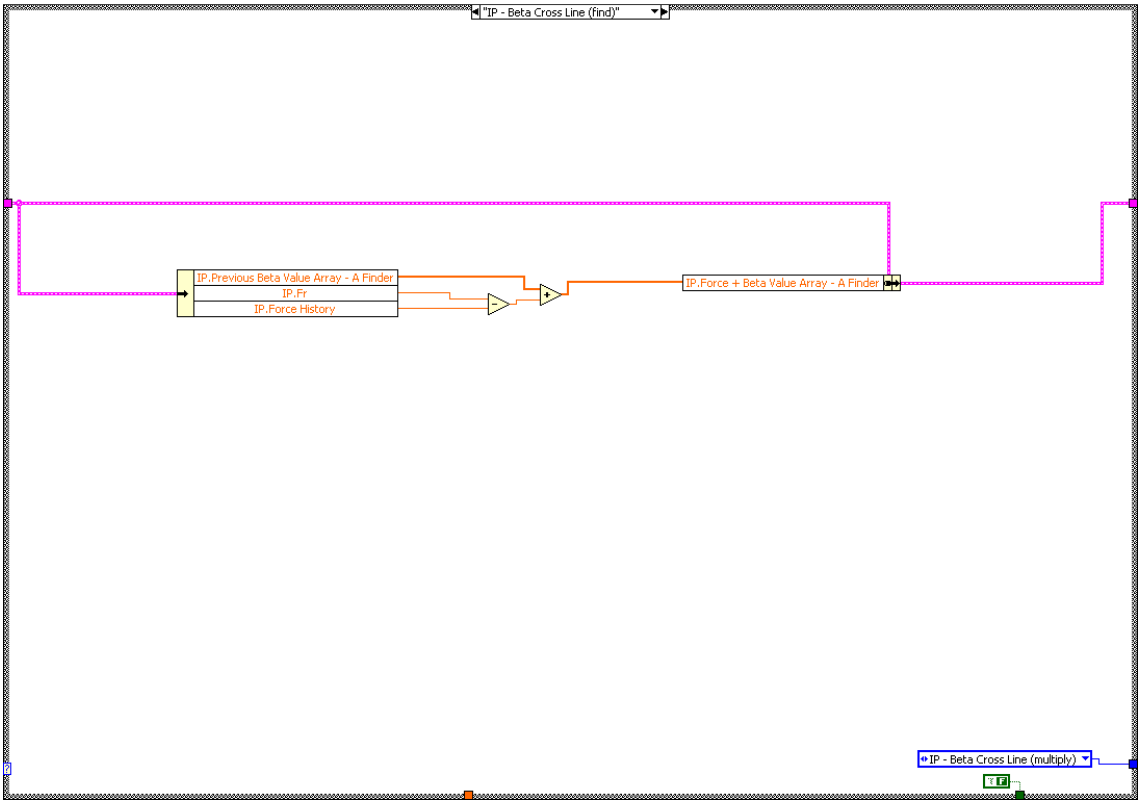

State 15 – Determining Output Alpha Part 1

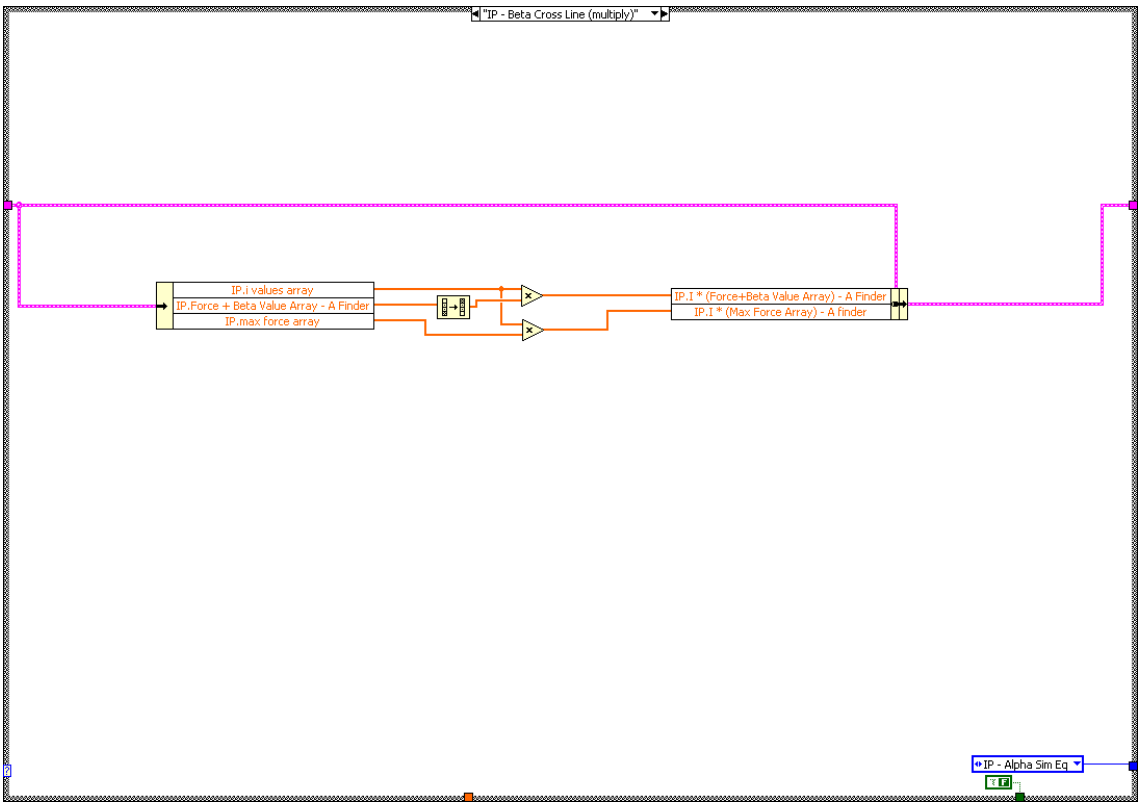

State 16 – Determining Output Alpha Part 2

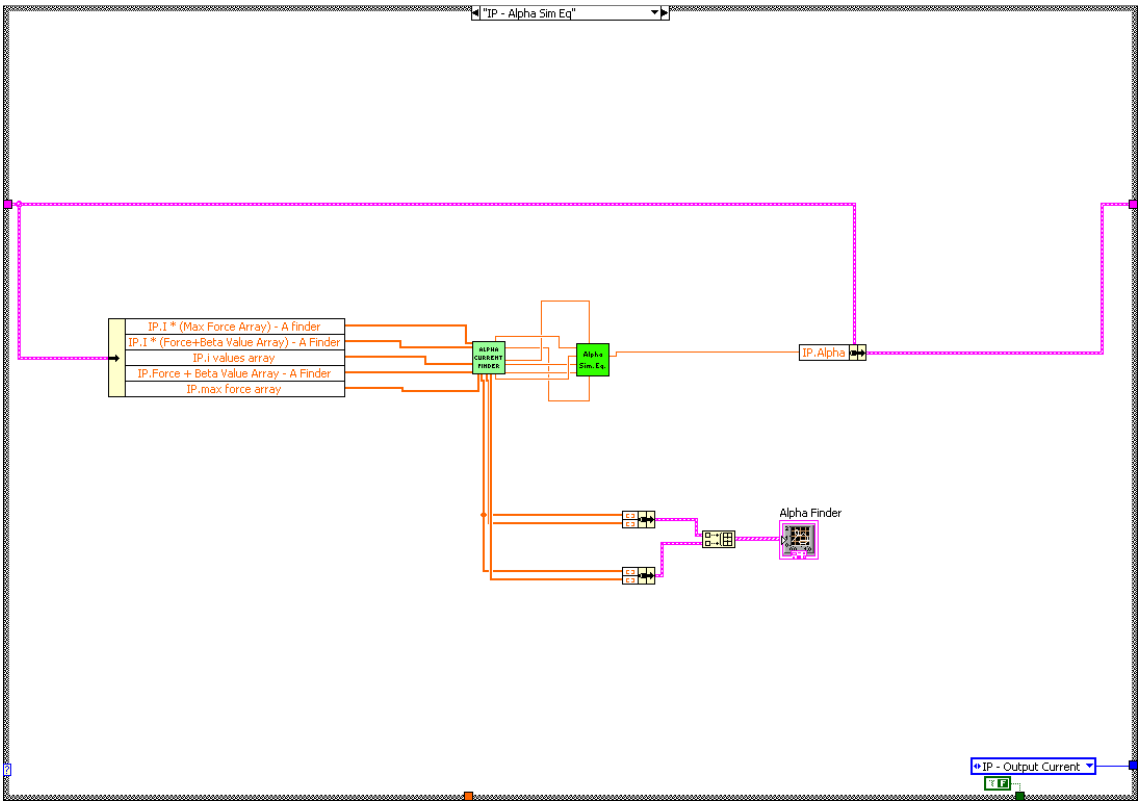

State 17 – Finalising Alpha Output

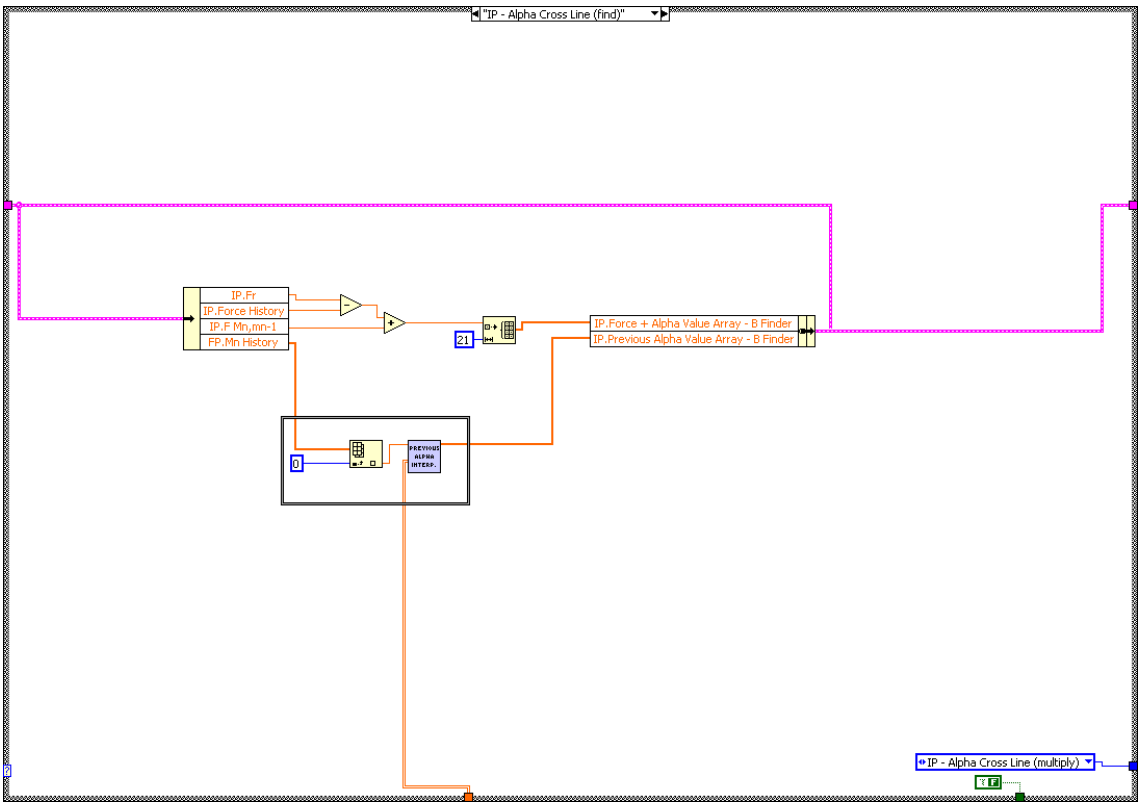

State 18 – Determining Output Beta Part 1

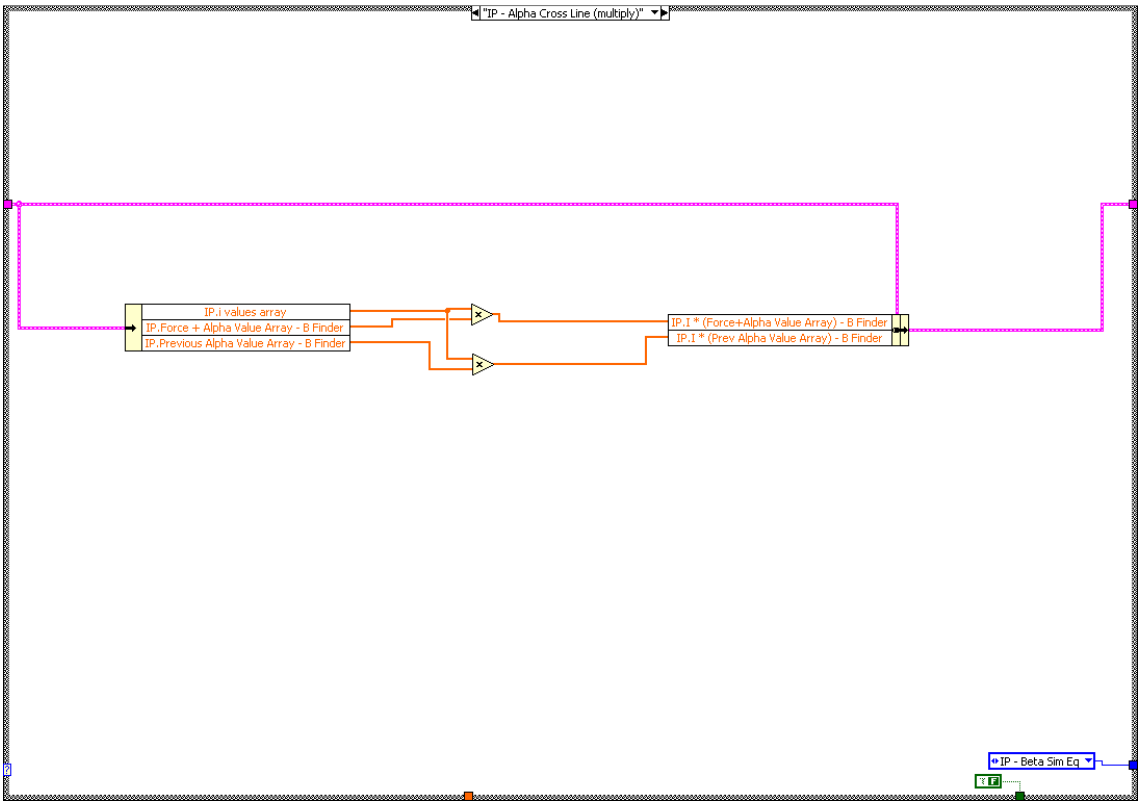

State 19 – Determining Output Beta Part 2

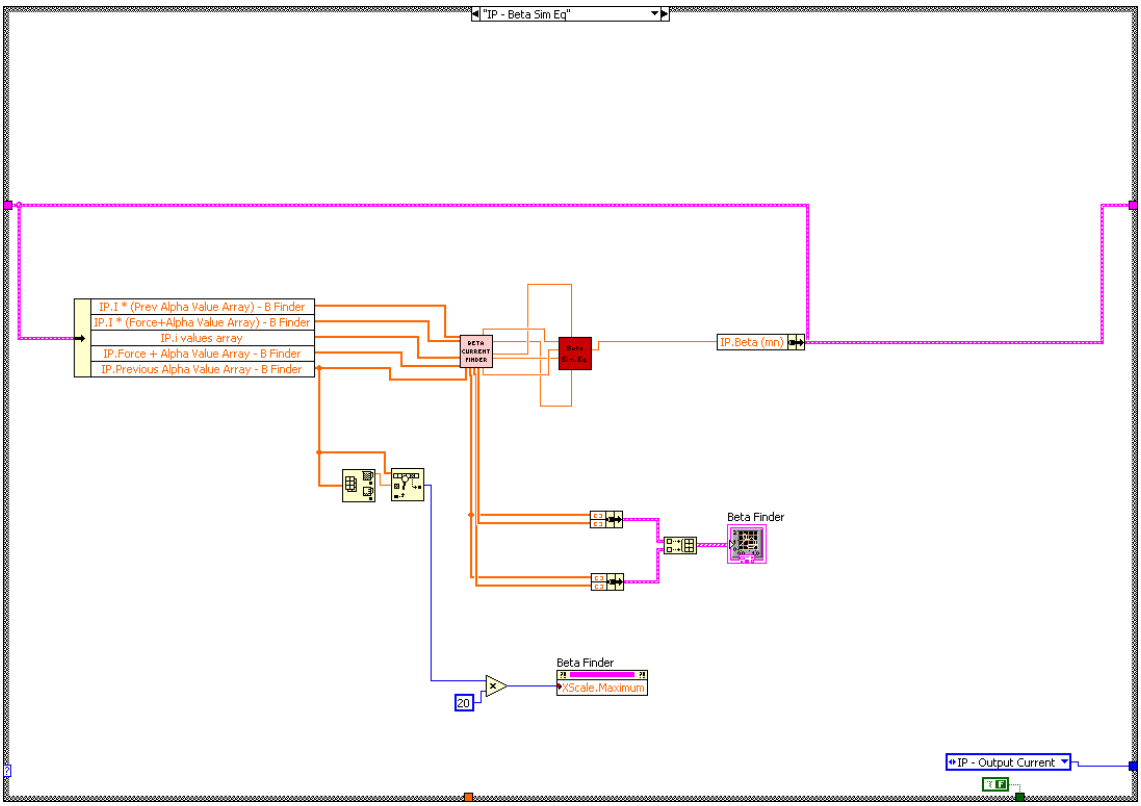

State 20 – Finalising Beta Output

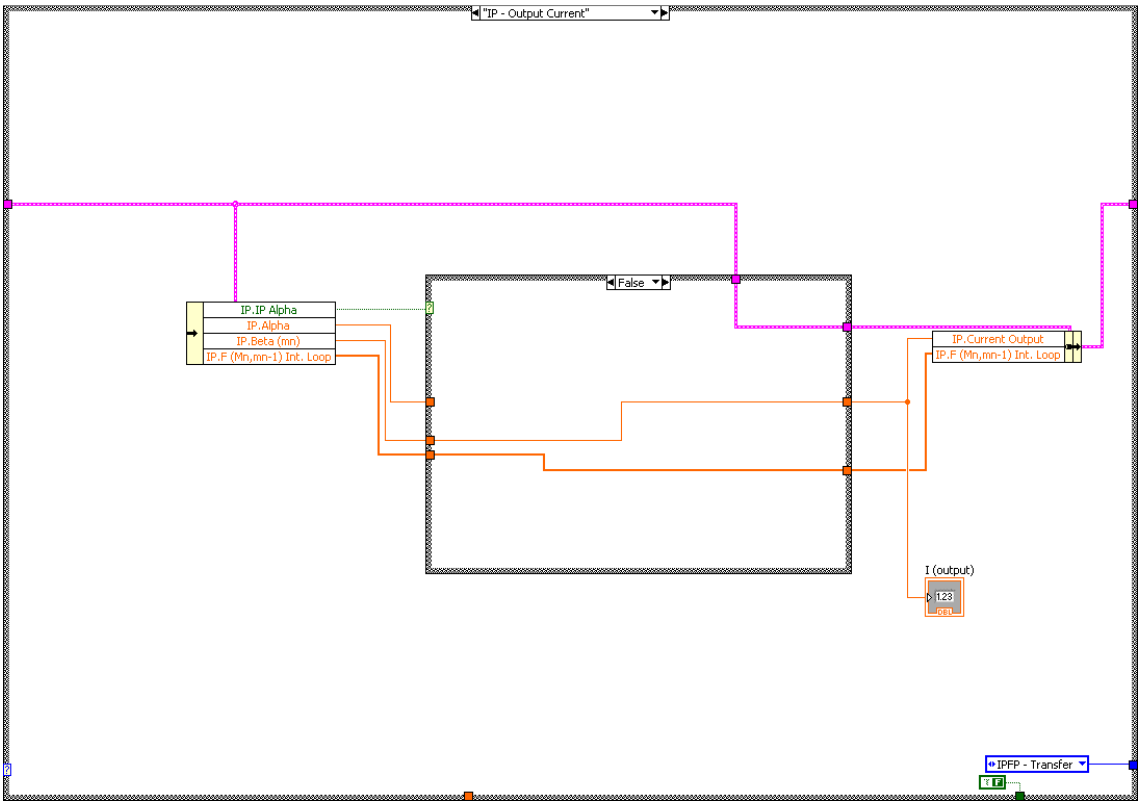

State 21 – Outputting Relevant Value

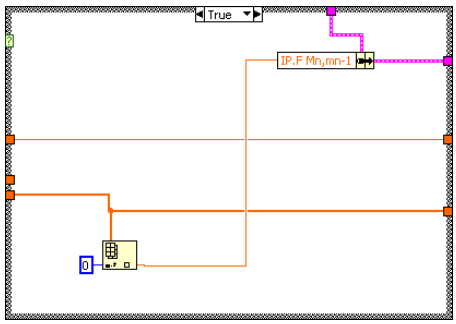

State 21 – Alternate State Sub-Routines

APPENDIX IV - Prosthetic Finger Dynamics Virtual Instrument

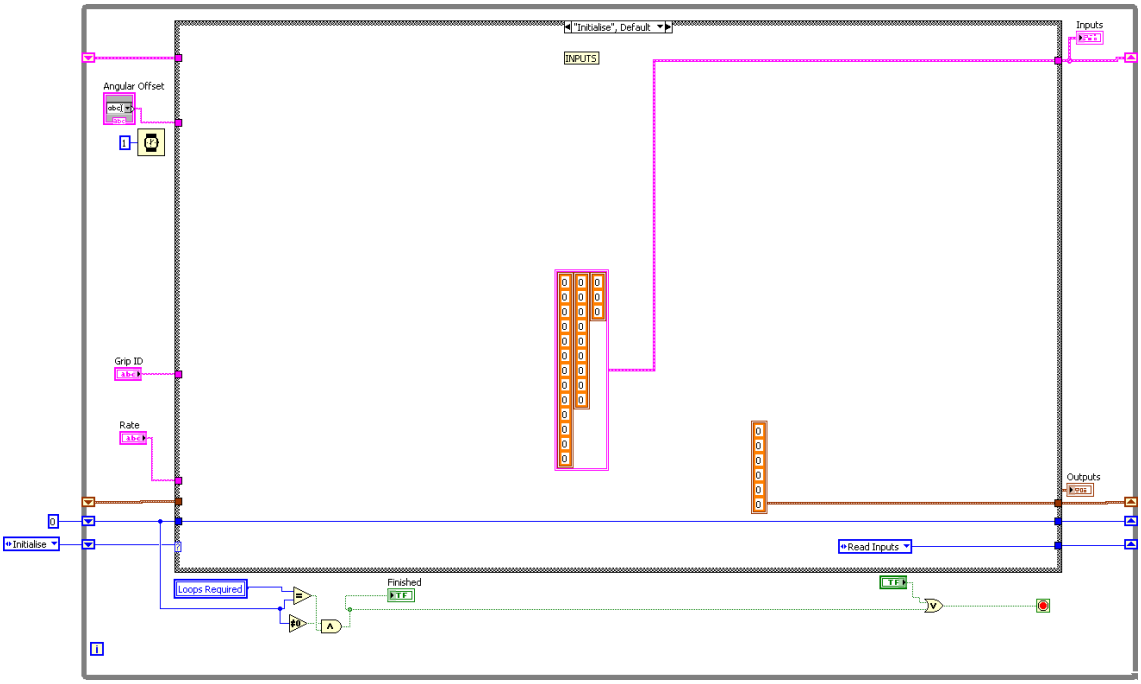

State Machine Setup

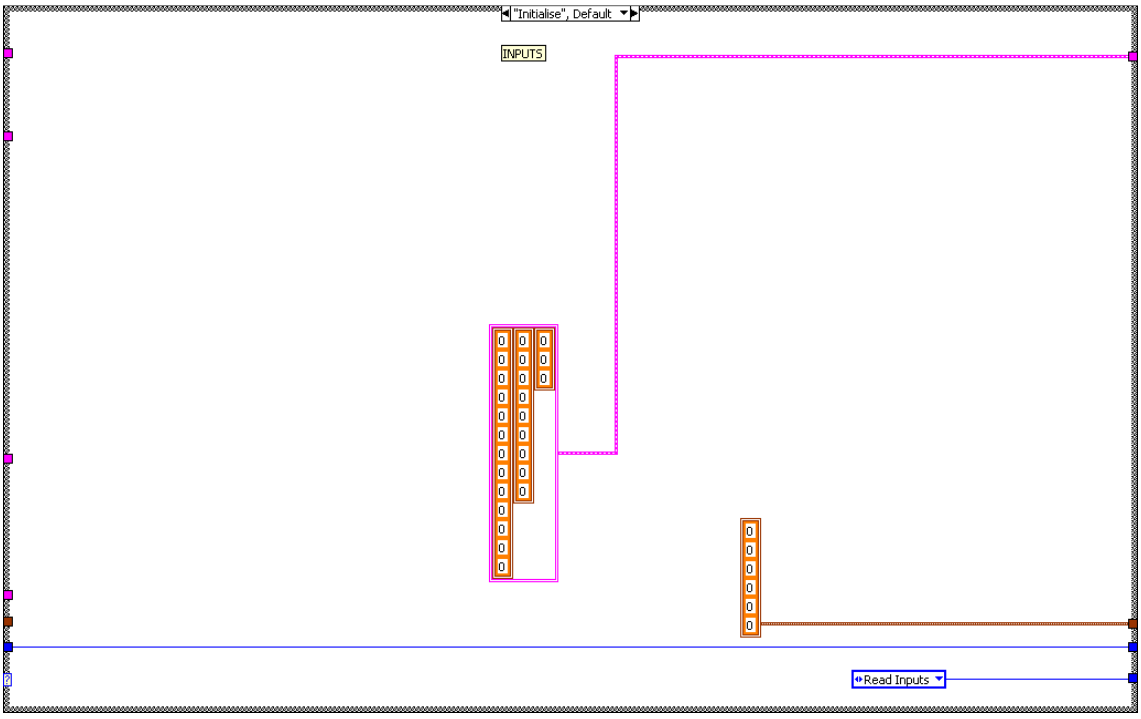

State 1 – Initialising Values

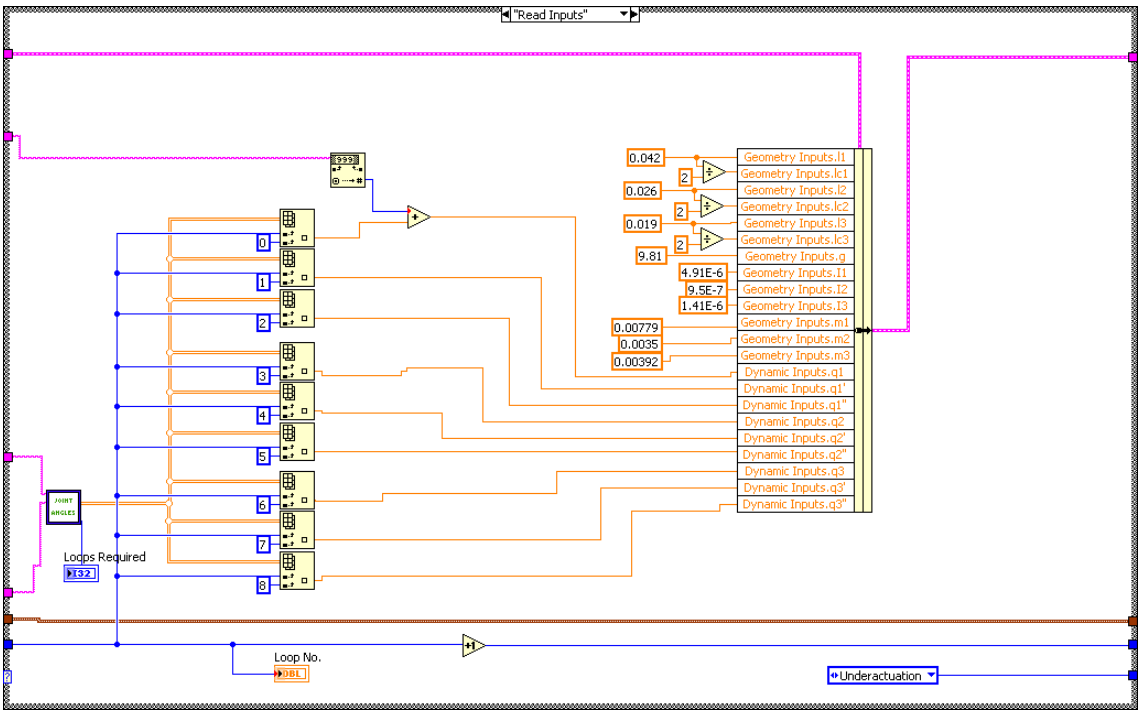

State 2 – Reading Inputs and Physical Characteristics

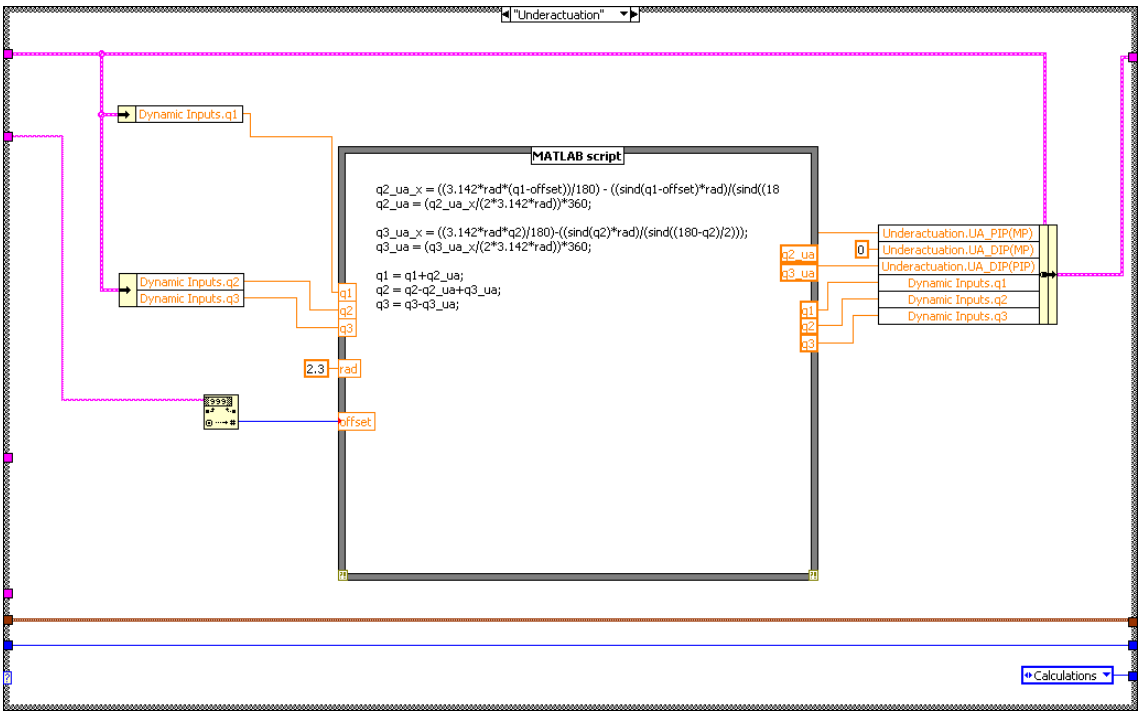

State 3 - Determining Underactuation Effects

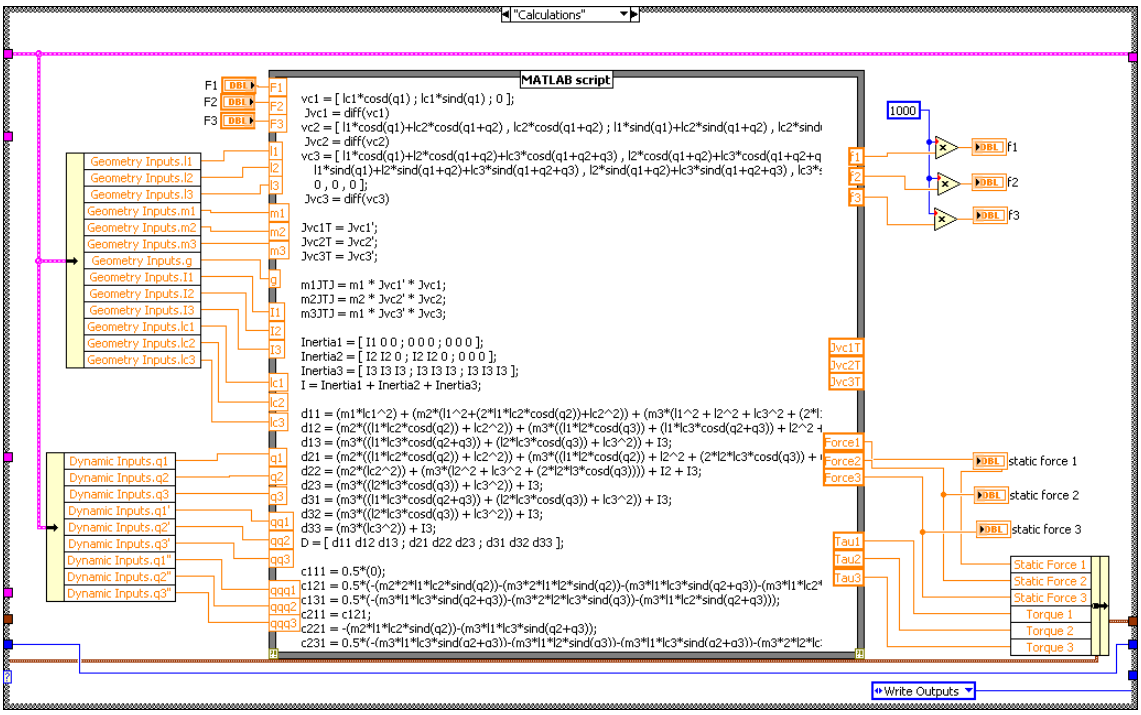

State 4 – Calculating Torque Requirements at Joints – (Code – Appendix V)

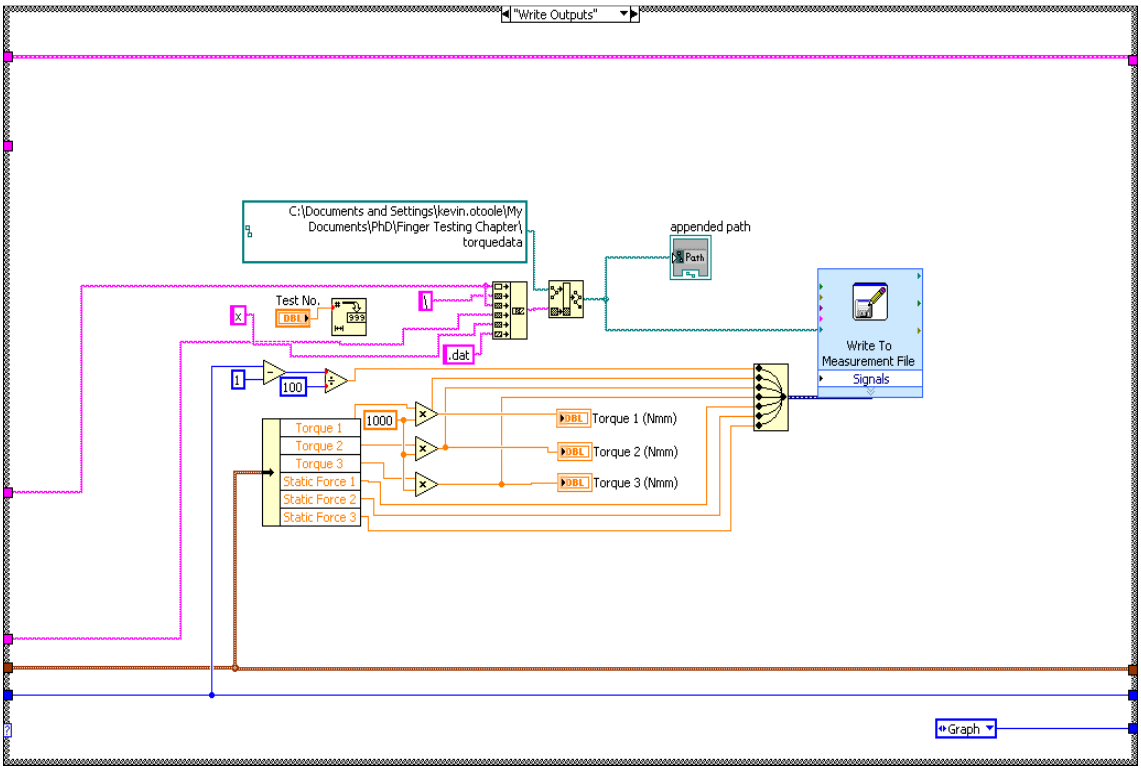

State 5 – Write Outputs to File

APPENDIX V - Experimental Profiles Matlab Code

```
%% Inputting Parameters

 prompt = {'Grip Type (1=Cylindrical 2=Tip 3=Lateral 4=Fully closed) ',

        'Grip Speed (1=Slow 2=Medium 3=Fast) ',

        'Finger Joint (1=MP, 2=PIP, 3=DIP) ',

        'Applied Rig Mass (1-10N) '};

name = 'Grip Test Setup';

numlines = 1;

def = {'1' ,'1' ,'1' ,'1'};

answer = inputdlg(prompt,name,numlines,def);



a1 = answer(1);

a2 = answer(2);

a3 = answer(3);

a4 = answer(4);



a1 = cell2mat(a1);

a1 = str2double(a1);



a2 = cell2mat(a2);

a2 = str2double(a2);
```

```
a3 = cell2mat(a3);

a3 = str2double(a3);


a4 = cell2mat(a4);

a4 = str2double(a4);


% setting data for answer 1 (Grip Type)

if a1==1;

   param1 = char('f3');

elseif a1==2;

   param1 = char('f4');

elseif a1==3;

   param1 = char('f5');

elseif a1==4;

   param1 = char('f6');

end


% setting data for answer 2 (Grip Speed)

if a2==1;

   param2 = char('slow');
```

```
elseif a2==2;
   param2 = char('medium');
elseif a2==3;
   param2 = char('fast');
end

% setting data for answer 3 (Joint Type)
if a3==1;
   param3 = char('j0t');
elseif a3==2;
   param3 = char('j1t');
elseif a3==3;
   param3 = char('j2t');
end

% setting data for answer 3 (Rig Mass)
param4 = a4;
 clear a1 a2 a4 answer def mass numlines prompt name


%% Loading Variables
```

```
% string parts for filepath generation

gripdata = (param1);

torquedata = (param1);

speed = (param2);

slash = char('\');

joint = (param3);

ending = char ('.dat');

pathbase1 = char('(path address)');

pathbase2 = char('(path address)');


% gripdata filepath

path1 = strcat(pathbase1,gripdata,slash,speed,slash,joint,ending);

% torquedata filepath

path2 = strcat(pathbase2,torquedata,slash,torquedata,speed,ending);

% variable name for use in file

 angle = load (path1);

torque = load (path2);


%% Determining Relevant Variables

mass = (param4);%(N) %select from dropdown menu

time = torque(:,1);
```

```
q = angle(1:length(time),1);

 x = (2.3*pi*q)/180;


%determining the correct column to extract from torque array

      y = joint(2);

      y = str2double(y);

 if y == 0

       z = 5;

      elseif y == 1

       z = 6;

      elseif y == 2

       z = 7;

end


F = torque(:,z);

       clear y z

W = -F.*x;

 Wdisp = W/mass;

 rig_x = x+Wdisp;

 %% Accounting for Gearing

 % gearing decreases the amount of displacement needed, but increases the
```

```
% mass required

 gear1 = 1;

 gear2 = 1.6;

 gear3 = 1.3;

if a3 == 1

        gear = gear1;

    elseif a3 == 2

        gear = gear2;

    elseif a3 == 3

        gear = gear3;

end

rig_x = rig_x/gear;

mass_required = param4*gear


%% profile plotting

 profile_data = [x,Wdisp];

profile_plot = max(profile_data,[],2);


figure(1)

cla

plot (time,x)
```

```
hold on

plot (time,Wdisp,'black')

plot (time,profile_plot,'--r','LineWidth',2)


maximum = (max(profile_plot))


%% saving rig_x profile to dat file

savepathbase = char('(save path address)');

save1 = strcat (savepathbase,torquedata,slash,speed,joint,ending);

 save (save1, 'rig_x', '-ascii')

 clear gripdata torquedata speed slash ending pathbase1 pathbase2 path1 path2
save1 savepathbase param1 param2 param3 param4

clear gear1 gear2 gear3 mass a3
```

APPENDIX VI - Dynamics Calculation Matlab Code

```
%% Determining Jacobians

vc1 = [ lc1*cosd(q1) ; lc1*sind(q1) ; 0 ];

 Jvc1 = diff(vc1)

vc2 = [ l1*cosd(q1)+lc2*cosd(q1+q2) , lc2*cosd(q1+q2) ;
l1*sind(q1)+lc2*sind(q1+q2) , lc2*sind(q1+q2) ; 0 , 0 ];

 Jvc2 = diff(vc2)

vc3 = [ l1*cosd(q1)+l2*cosd(q1+q2)+lc3*cosd(q1+q2+q3) ,
l2*cosd(q1+q2)+lc3*cosd(q1+q2+q3) , lc3*cosd(q1+q2+q3) ;

   l1*sind(q1)+l2*sind(q1+q2)+lc3*sind(q1+q2+q3) ,
l2*sind(q1+q2)+lc3*sind(q1+q2+q3) , lc3*sind(q1+q2+q3) ;

   0 , 0 , 0 ];

 Jvc3 = diff(vc3)


Jvc1T = Jvc1';

Jvc2T = Jvc2';

Jvc3T = Jvc3';


%% Determining Inertia Matrix

m1JTJ = m1 * Jvc1' * Jvc1;

m2JTJ = m2 * Jvc2' * Jvc2;

m3JTJ = m1 * Jvc3' * Jvc3;
```

```
Inertia1 = [ I1 0 0 ; 0 0 0 ; 0 0 0 ];

Inertia2 = [ I2 I2 0 ; I2 I2 0 ; 0 0 0 ];

Inertia3 = [ I3 I3 I3 ; I3 I3 I3 ; I3 I3 I3 ];

I = Inertia1 + Inertia2 + Inertia3;


d11 = (m1*lc1^2) + (m2*(l1^2+(2*l1*lc2*cosd(q2))+lc2^2)) + (m3*(l1^2 +
l2^2 + lc3^2 + (2*l1*l2*cosd(q2)) + (l1*lc3*cosd(q2+q3)) + (2*l2*lc3*cosd(q3))
+ (l1*lc2*cosd(q2+q3)))) + I1 + I2 + I3;

d12 = (m2*((l1*lc2*cosd(q2)) + lc2^2)) + (m3*((l1*l2*cosd(q3)) +
(l1*lc3*cosd(q2+q3)) + l2^2 + lc3^2 + (2*l2*lc3*cosd(q3)))) + I2 + I3;

d13 = (m3*((l1*lc3*cosd(q2+q3)) + (l2*lc3*cosd(q3)) + lc3^2)) + I3;

d21 = (m2*((l1*lc2*cosd(q2)) + lc2^2)) + (m3*((l1*l2*cosd(q2)) + l2^2 +
(2*l2*lc3*cosd(q3)) + (l1*lc3*cosd(q2+q3)) + lc3^2)) + I2 + I3;

d22 = (m2*(lc2^2)) + (m3*(l2^2 + lc3^2 + (2*l2*l3*cosd(q3)))) + I2 + I3;

d23 = (m3*((l2*lc3*cosd(q3)) + lc3^2)) + I3;

d31 = (m3*((l1*lc3*cosd(q2+q3)) + (l2*lc3*cosd(q3)) + lc3^2)) + I3;

d32 = (m3*((l2*lc3*cosd(q3)) + lc3^2)) + I3;

d33 = (m3*(lc3^2)) + I3;

D = [ d11 d12 d13 ; d21 d22 d23 ; d31 d32 d33 ];


%% Christoffel Symbols

 c111 = 0.5*(0);
```

```
c121 = 0.5*(-(m2*2*l1*lc2*sind(q2))-(m3*2*l1*l2*sind(q2))-
(m3*l1*lc3*sind(q2+q3))-(m3*l1*lc2*sind(q2+q3)));

c131 = 0.5*(-(m3*l1*lc3*sind(q2+q3))-(m3*2*l2*lc3*sind(q3))-
(m3*l1*lc2*sind(q2+q3)));

c211 = c121;

c221 = -(m2*l1*lc2*sind(q2))-(m3*l1*lc3*sind(q2+q3));

c231 = 0.5*(-(m3*l1*lc3*sind(q2+q3))-(m3*l1*l2*sind(q3))-
(m3*l1*lc3*sind(q2+q3))-(m3*2*l2*lc3*sind(q3)));

c311 = 0.5*(-(m3*l1*lc3*sind(q2+q3))-(m3*2*l2*lc3*sind(q3))-
(m3*l1*lc2*sind(q2+q3)));

c321 = 0.5*(-(m3*l1*l2*sind(q3))-(m3*l1*lc3*sind(q2+q3))-
(m3*2*l2*lc3*sind(q2+q3))-(m3*l1*lc3*sind(q2+q3)));

c331 = -(m3*l1*lc3*sind(q2+q3))-(m3*l2*lc3*sind(q3));


c112 = -0.5*(-(m2*2*l1*lc2*sind(q2))-(m3*2*l1*l2*sind(q2))-
(m3*l1*lc3*sind(q2+q3))-(m3*l1*lc2*sind(q2+q3)));

c122 = 0.5*(-(m2*l1*lc2*sind(q2))-(m3*l1*l2*sind(q2))-
(m3*l1*lc3*sind(q2+q3))+(m2*l1*lc2*sind(q2))+(m3*l1*lc3*sind(q2+q3)));

c132 = 0.5*(-(m3*2*l2*lc3*sind(q3))-
(m3*l1*lc3*sind(q2+q3))+(m3*l1*lc3*sind(q2+q3)));

c212 = 0.5*(0);

c222 = 0.5*(0);

c232 = 0.5*(-(m3*2*l2*l3*sind(q3)));

c312 = 0.5*(-(m3*2*l2*lc3*sind(q3))-
(m3*l1*lc3*sind(q2+q3))+(m3*l1*lc3*sind(q2+q3)));
```

```
c322 = 0.5*(-2*m3*l2*l3*sind(q3));

c332 = 0.5*(-(m3*l2*lc3*sind(q3)));


c113 = -0.5*(-(m3*l1*lc3*sind(q2+q3))-(m3*2*l2*lc3*sind(q3))-
(m3*l1*lc2*sind(q2+q3)));

c123 = 0.5*(-
(m3*l1*lc3*sind(q2+q3))+(m3*l1*l2*sind(q3))+(m3*l1*lc3*sind(q2+q3))+(m3
*2*l2*lc3*sind(q3)));

c133 = 0.5*(-(m3*l1*lc3*sind(q2+q3))-
(m3*l2*lc3*sind(q3))+(m3*l1*lc3*sind(q2+q3))+(m3*l2*lc3*sind(q3)));

c213 = 0.5*(-
(m3*l1*lc3*sind(q2+q3))+(m3*2*l2*lc3*sind(q3))+(m3*l1*lc3*sind(q2+q3)));

c223 = 0.5*(-(m3*2*l2*l3*sind(q3)));

c233 = 0.5*(0);

c313 = 0.5*(0);

c323 = 0.5*(0);

c333 = 0.5*(0);


%% Potential Energy

 p1 = m1*g*lc1*sind(q1);

p2 = m2*g*lc2*sind(q1+q2) + m2*g*l1*sind(q1);

p3 = m3*g*lc3*sind(q1+q2+q3) + m3*g*l2*sind(q1+q2) + m3*g*l1*sind(q1);

P = p1+p2+p3;
```

```
%% Gravity

g1 =
m1*g*lc1*cosd(q1)+m2*g*lc2*cosd(q1+q2)+m2*g*l1*cosd(q1)+m3*g*lc3*cosd
(q1+q2+q3)+m3*g*l2*cosd(q1+q2)+m3*g*l1*cosd(q1);

g2 =
m2*g*lc2*cosd(q1+q2)+m3*g*lc3*cosd(q1+q2+q3)+m3*g*l2*cosd(q1+q2);

g3 = m3*g*lc3*cosd(q1+q2+q3);

G = [g1 g2 g3]; %gravity vector


%% Joint Torque Values

 Tau1 = (d11*qqq1)+(d12*qqq2)+(d13*qqq3) +
(c111*qq1^2)+(c221*qq2^2)+(c331*qq3^2)+(c121*qq1*qq2)+(c131*qq1*qq3
)+(c211*qq2*qq1)+(c231*qq2*qq3)+(c311*qq3*qq1)+(c321*qq3*qq2) + g1;

Tau2 = (d21*qqq1)+(d22*qqq2)+(d23*qqq3) +
(c112*qq1^2)+(c222*qq2^2)+(c332*qq3^2)+(c122*qq1*qq2)+(c132*qq1*qq3
)+(c212*qq2*qq1)+(c232*qq2*qq3)+(c312*qq3*qq1)+(c322*qq3*qq2) + g2;

Tau3 = (d31*qqq1)+(d32*qqq2)+(d33*qqq3) +
(c113*qq1^2)+(c223*qq2^2)+(c333*qq3^2)+(c123*qq1*qq2)+(c133*qq1*qq3
)+(c213*qq2*qq1)+(c233*qq2*qq3)+(c313*qq3*qq1)+(c323*qq3*qq2) + g3;
```